NASA Technical Memorandum 88210

Top-Mounted Inlet Performance for a V/STOL Fighter/Attack Aircraft Configuration

Donald B. Smeltzer

January 1987

National Aeronautics and
Space Administration

NASA Technical Memorandum 88210

Top-Mounted Inlet Performance for a V/STOL Fighter/Attack Aircraft Configuration

Donald B. Smeltzer, Ames Research Center, Moffett Field, California

January 1987

National Aeronautics and
Space Administration

Ames Research Center
Moffett Field, California 94035

NOMENCLATURE

AR	wing aspect ratio
DISTL	left duct distortion at the compressor face (PTMAX-PTMIN)/PT2L
DISTR	right duct distortion at the compressor face (PTMAX-PTMIN)/PT2R
DIST1L	distortion at the left ramp rake station, (PTMAX-PTMIN)/PT1L
DIST1R	distortion at the right ramp rake station, (PTMAX-PTMIN)/PT1R
DPTLL	flow-field distortion for the left duct, (PTMAX-PTMIN)/PTLL
DPTLR	flow-field distortion for the right duct, (PTMAX-PTMIN)/PTLR
EARL	left duct airflow ratio (1.0 = design condition)
EARR	right duct airflow ratio (1.0 = design condition)
FRP	fuselage reference plane
LE-W	wing leading edge flap deflection angle (deg)
MACH	freestream Mach number
P	pressure
PTLL	flow-field pitot-pressure recovery, left duct
PTLR	flow-field pitot-pressure recovery, right duct
PTMAX	maximum measured pitot or total pressure for a single rake tube
PTMIN	minimum measured pitot or total pressure for a single rake tube
PTO	freestream total pressure
PT1L	pitot-pressure recovery at the left ramp rake station
PT1R	pitot-pressure recovery at the right ramp rake station
PT2L	left duct total-pressure recovery at the compressor face
PT2R	right duct total-pressure recovery at the compressor face
TE-W	wing trailing edge flap deflection angle (deg)

α	angle of attack
β	angle of sideslip
Γ	dihedral angle
Λ	aspect ratio

SUMMARY

Inlet flow-field and internal performance data were obtained for a 0.095-scale model of a vertical/short take-off and landing fighter/attack aircraft configuration with twin top-mounted inlets. The model was tested in the Ames Research Center 11- by 11-Foot Transonic and 9- by 7-Foot Supersonic Wind Tunnels. The effects on the flow field of inlet location, canopy-dorsal integration, wing leading-edge extension (LEX) planform area, variable incidence canards, and wing leading- and trailing-edge flap-deflections were measured. A brief discussion of the results is presented; a more thorough analysis is presented elsewhere.

Tests were conducted at Mach numbers from 0.6 to 2.0 and at angles of attack and sideslip up to 27° and 12°, respectively. Reynolds number was held constant at 9.8×10^6 per meter. Total pressure measurements were obtained in the inlet flow field just upstream from the inlet lip. For the subsonic/transonic testing (M = 0.6-1.2), inlet performance data were obtained from total and static pressure measurements at the compressor face. These data were obtained over a range of inlet mass flows. For the supersonic testing (M = 1.6 and 2.0), inlet performance data were obtained from total pressure measurements at the inlet throat. Supersonic data were obtained only for the maximum mass-flow condition.

INTRODUCTION

Recent vertical/short take-off and landing (V/STOL) fighter/attack aircraft technology studies (e.g., ref. 1) have shown that configurations with top-mounted inlets have significant potential advantages over configurations with more conventionally mounted inlets. Among these advantages are reduced ingestion of hot gases and debris, and better weapons integration. However, certain problem areas have been identified such as the ingestion of (1) distorted flows at high angles of attack, (2) vortices from a canard or wing leading-edge extension (LEX), and (3) low-energy boundary layers. These advantages and problem areas are discussed, and top inlet performance is compared with the performance of three conventionally mounted inlets in reference 2.

The twin-engine top-mounted inlet configuration identified in reference 1 was based on a detailed aerodynamic analysis by Northrop Corporation in a program jointly sponsored by Ames Research Center and the David Taylor Naval Ship Research and Development Center (ref. 3). An aerodynamic force model of this configuration was constructed and tested in the Ames wind tunnels. The model had flow-through ducts with limited pressure instrumentation in the throat. The test results

(ref. 4) indicated reasonably good performance, so a more detailed inlet pressure test was planned to measure both the inlet flow-field and compressor-face performance. Similar results were obtained in earlier tests (refs. 5 and 6), but were confined only to flow field surveys or to very low speed (M = 0.25).

The aerodynamic force model from reference 3 was modified for the inlet performance testing. Instrumentation was added to measure the inlet flow-field properties and the inlet internal performance. Remotely controlled mass-flow control plugs were added and the ducts were modified so that they could be positioned at three fuselage stations. Tests were conducted in the 11- by 11-Foot Transonic and 9- by 7-Foot Supersonic Wind Tunnels at the Ames Research Center. The test matrix included Mach numbers from 0.6 to 2.0 and angles of attack and sideslip up to 27° and 12°, respectively. Reynolds number was held constant at 9.8×10^6 per meter. The effects of inlet location, canopy-dorsal integration, LEX planform area, variable incidence canards, and wing leading- and trailing-edge-flap deflections were determined.

A brief discussion of the results is presented; a more thorough analysis is presented in references 7, 8, and 9.

MODEL AND INSTRUMENTATION

The 0.095-scale aerodynamic force model described in reference 3 was modified for the inlet performance tests. A photograph of the model is shown in figure 1 and a rear view, highlighting the mass-flow control plugs, is shown in figure 2. The model had a conventional sting with a dummy balance for attachment to the wind tunnel support system. The mass-flow control plugs were remotely actuated and included linear position indicators. Calibrations performed prior to the wind tunnel test correlated the physical position of these plugs with inlet mass flow.

A layout of the model is shown in figure 3. The plan view shows the wing leading- and trailing-edge flaps. These flaps could be manually deflected to angles of up to 30°. The plan view also shows the three locations where the inlet could be positioned as a function of projected wing-root chord. These three positions are designated on the profile view and on the plotted results as FWD, MID, and AFT.

Figure 4(a) shows the canopy-off mold line. This might be considered a reduced canopy configuration because there is still an aft-facing slope to the dorsal. Figure 4(b) shows the LEX planform options. The standard LEX had the largest planform area, while the alternative LEX reduced the area by 40%. With the LEX removed, the wing leading edge continued inboard to the fuselage juncture. Figure 4(c) shows the variable incidence canards. The canard had a 20° dihedral angle and could be manually deflected up to ±20° incidence.

Subsonic/transonic testing instrumentation is shown in figures 5(a) and 5(b). Figure 5(a) shows the external flow field and duct instrumentation. The external flow-field rake had 10 five-hole cone probes and 35 total pressure probes. Note

that a cross section of this rake relative to one duct is shown. Each duct was instrumented with a 3 × 3 matrix of static pressure taps on the ramp and four centerline duct statics as shown. In addition, the right duct was instrumented with eight diffuser statics.

Compressor-face instrumentation is shown in figure 5(b). Six combination Kulite dynamic/total pressure probes, twelve total pressure probes, and 4 static pressure taps were installed in each duct. Each total pressure probe was located at the centroid of equal areas.

Supersonic testing special instrumentation is shown in figure 6. A portion of the inlet cowl was removed and a rake with 25 total pressure tubes was located on the ramp of each duct. This "clipped" cowl caused the terminal shock wave to be positioned behind this rake. A measure of the supersonic performance was obtained in this way because the inlets had no boundary layer bleed system; hence, measurements at the compressor face would not be characteristic of a supersonic inlet with a typical bleed system.

CALIBRATIONS

The mass-flow control plug assemblies at the duct exit were calibrated at Northrop. Mass flow was determined as a function of duct-to-throat pressure ratio by using a bellmouth and a vacuum sphere with a calibrated orifice. The mass flow was also correlated with the flow control plug position. Data were obtained at two stagnation pressures and the results were converted to corrected weight flow.

The five-hole cone probes on the flow-field rake were calibrated in the 6- by 6-Foot Supersonic Wind Tunnel at Ames Research Center. Data were obtained at Mach numbers 0.4 to 2.0 and angles of attack from -2° to 20°. The rake was installed both upright and inverted, and was rolled ±90°. From this procedure, local Mach number and angles of attack and sideslip were determined as a function of differential pressure coefficient.

TEST PROCEDURE

The test variables for each configuration were Mach number, angle of attack, angle of sideslip, and inlet mass flow. Reynolds number was held constant at 9.8×10^6 per meter. The model configurations and test variables are shown in figure 7. For each configuration, the principal point-to-point variable was angle of attack; while the angle of sideslip, Mach number, and mass flow were held constant. For selected configurations, point-to-point mass flow variations were obtained at constant angle of attack, angle of sideslip, and Mach number. For other selected configurations, the flow field rake was installed and data were obtained for point-to-point variations in angle of attack or inlet mass flow.

DATA REDUCTION

All internal static and total pressure measurements were reduced to a pressure ratio of the form P/PTO. The total pressure recovery shown in most figures is the sum of the individual pressure ratios divided by the number of pressures measured. The distortion presented is the conventional maximum minus minimum total pressure recovery from individual probes divided by the average total pressure recovery. Corrected weight flow was computed using measured pressures and temperatures and the duct calibration data.

The pressure tubes on the flow field rake were located both inside and outside the inlet highlight area. Therefore, the computed values of pressure recovery and distortion were area weighted so that the computed results reflected the performance within the inlet stream tube for maximum mass flow.

Other distortion parameters were computed such as radial, circumferential, average minus minimum distortion, and turbulence measurements. These quantities are not presented in this report, but some of the measurements are presented in reference 7. In addition, local Mach number and angle of attack and sideslip were computed from the cone probe measurements, and some of these results are presented in reference 7.

RESULTS

The plotted results are presented in figures 8-13. Each figure is plotted on the same scales. The results are identified at the top of each page, except for Mach number which is generally indicated below the figure title. A brief description of the results shown on each figure is given below.

Figures 8(a) to 8(jj) show inlet performance as a function of inlet air flow ratio (1.0 equals design airflow for a candidate engine). Each page shows results for one configuration, one Mach number (either 0.6, 0.9, or 1.2), two angles of attack (0° and a high angle), and either 0° or 12° angle of sideslip.

Figures 9(a) to 9(hh) present inlet performance as a function of angle of attack. The results are for design airflow conditions which correspond to a value of 1.0 on the abscissa of figure 8. Each page shows results for one configuration, one Mach number (either 0.6, 0.9, or 1.2), and angles of sideslip of 0°, 4°, 8°, and 12°. Note that left inlet results are not shown for many configurations because the airflow was incorrectly set (ratio > 1.0); thus, pressure recovery was too low and distortion was too high.

Figures 10(a) to 10(vv) compare inlet performance for various configurations as a function of angle of attack. Performance is shown at Mach numbers of 0.6, 0.9, and 1.2 for maximum engine airflow conditions. Again, some results for the left duct are not presented for the reason previously stated.

Figures 11(a) to 11(gg) show the total pressure recovery and distortion of the flow field entering each inlet as a function of angle of attack. Each page shows results at 0°, 4°, 8°, and 12° angle of sideslip for one configuration and Mach number. Data are included at Mach numbers of 0.6, 0.9, 1.2, 1.6, and 2.0.

Figures 12(a) to 12(p) show total pressure recovery and distortion at the ramp rake station as a function of angle of attack. Each page shows results for one configuration, at angles of sideslip of 0°, 4°, and 8°, and for one Mach number (1.6 or 2.0). Recall that at supersonic Mach numbers, the "clipped" cowl configuration (fig. 5(c)) was used.

Figures 13(a) to 13(x) compare total pressure recovery and distortion at the ramp rake station for different configurations as a function of angle of attack. All configurations used the "clipped" cowl (fig. 6). Each page shows results for a Mach number of either 1.6 or 2.0 and for a sideslip angle of 0°, 4°, or 8°.

DISCUSSION

Inlet flow field and compressor-face performance data were obtained for a model of a fighter/attack aircraft configuration with twin top-mounted inlets. Some of the important results and the supporting data are discussed herein. For many of the results only right or windward inlet performance data are shown. The complete results (both inlets) for the mid inlet location (figs. 9(d)-9(f)) show symmetrical performance at 0° angle of sideslip, and generally larger losses in pressure recovery and larger increases in distortion for the right (or windward) inlet at angles of sideslip other than 0°. Therefore, the discussion of the configurations that follows reflects probable symmetrical performance at 0° sideslip angle and, generally, the worst trends at non-zero sideslip.

For purposes of this discussion, distortion was considered to be the most important parameter. A value of 20% or less was considered to be acceptable; that is, it would not result in possible engine stall. Pressure recovery is also important, however, since reduced pressure recovery results in either increased fuel flow at a constant thrust or the inability to perform a maneuver if sufficient thrust is not available.

Subsonic/Transonic Performance

Inlet location- Inlet pressure recovery and distortion were measured with the inlets located at three fuselage stations: 30%, 44%, and 70% of projected wing-root chord. Results were obtained at Mach numbers of 0.6, 0.9, and 1.2 at angles of attack and sideslip up to 27° and 12°, respectively. Inlet airflow was varied at certain selected conditions. For airflow ratios of 1.0 or less, inlet location had little effect on the performance at Mach numbers 0.6 and 0.9 (figs. 8(a)-8(i)); while at Mach number 1.2, the performance was better with the inlets at the MID

location. At higher airflow ratios (>1.0) there were large decreases in pressure recovery, and distortion was generally unacceptably high (>20%).

Inlet location effects were investigated further by varying the angle of attack while the airflow ratio was held constant at 1.0. Performance results were obtained at different sideslip angles. There were large decreases in pressure recovery for all inlet locations at angles of attack greater than 15° and angles of sideslip of 8° and 12° (figs. 9(a)-9(i)). Also, distortion was unacceptably high (>20%) for many attitude/Mach number combinations. Overall, high distortion occurred less frequently at Mach numbers 0.6 and 0.9 with the MID-inlet configuration than with the forward or aft configurations. At Mach number 1.2, there were numerous instances of high distortion for all inlet locations.

The comparison of results from the three inlet locations generally shows small differences in performance at 0° sideslip angle (figs. 10(a)-10(c)). A similar comparison at 4° sideslip angle showed a greater performance variation. Moreover, distortion becomes unacceptably high at Mach number 1.2 (figs. 10(m)-10(o)). At 8° angle of sideslip, inlet performance varied less with changes in location than at 4° (figs. 10(y)-10(aa)). Note that pressure recovery is considerably higher at Mach number 1.2 and high angles with the inlet aft (fig. 10(aa)). At 12° angle of sideslip, pressure recovery was very low and distortion high for some conditions (figs. 10(kk)-10(mm)).

Overall, the inlet location results are mixed, no location was clearly better in terms of higher pressure recovery and lower distortion. The MID location was selected for the investigation of other configuration variables because of limits to the available test time.

Canopy dorsal integration- Data obtained with the inlet at the mid location show a slight drop in pressure recovery between about 4° and 15° angle of attack; most pronounced at 0° sideslip angle (figs. 9(d)-9(f)). This was thought to be, at least partially, a result of canopy-dorsal integration. To investigate this premise, a canopy-off or reduced canopy configuration was tested (fig. 4(a)). Note that this reduced canopy configuration has a dorsal with a downward slope; this would tend to promote local flow acceleration supersonically.

The canopy on/off results are compared at 0°, 4°, 8°, and 12° sideslip angle in figures 10(g)-10(i), 10(s)-10(u), 10(ee)-10(gg), and 10(qq)-10(ss), respectively. Pressure recovery was generally higher when the canopy was removed. However, distortion was higher, particularly at 12° angle of sideslip (figs. 10(qq)-10(ss)). Overall, when the canopy was removed there were more combinations of angle of attack/angle of sideslip in which distortion was unacceptably high (>20%).

Wing plan- Wing leading-edge extensions (LEX) have been shown to produce a vortex system which helps to counteract upper fuselage flow separation (refs. 1 and 4). Since this is an important consideration with top mounted inlets, two LEX configurations and a LEX-removed configuration were tested (fig. 4(b)). Note that the alternate LEX had 60% of the planform area of the standard LEX.

Pressure recovery was higher and distortion was lower when either LEX was installed (figs. 10(d)-10(f)). The standard LEX appeared to control flow separation to a higher angle of attack since pressure recovery was slightly higher and distortion lower at the higher angles. However, the alternate LEX did control separation compared to the LEX-off results. At 4° angle of sideslip, the results were similar. The standard LEX was better than the alternate LEX which, in turn, is considerably better than LEX-off (figs. 10(p)-10(r)). However, at Mach number 1.2, distortion was high for all configurations. At 8° angle of sideslip, a LEX is still beneficial; distortion is generally less than 20% for either LEX configuration (figs. 10(bb)-10(dd)). At 12° angle of sideslip, the performance with either LEX was, again, better than with the LEX removed (figs. 10(nn)-10(pp)). At Mach number 1.2, however, pressure recovery was low and distortion was generally high for all configurations. Overall, inlet performance was generally better with the standard LEX; pressure recovery was higher and distortion lower. The standard LEX was, generally, most effective at the higher angles of attack.

Considerable inlet performance penalties were incurred with the standard LEX as the angle of sideslip was increased (figs. 9(d)-9(f)). Losses in pressure recovery and increases in distortion were generally greater for the right (windward) inlet. In particular, high distortion (>20%) could be a problem at Mach number 1.2. Distortion was generally less than 20% at 0° and 8° angle of sideslip, but at 4° it was greater than 20% for a considerable range of angle of attack. The inlet performance penalties were greater with the alternate LEX as the angle of sideslip was increased (figs. 9(j)-9(l)). The Mach number/angle of attack/angle of sideslip matrix where distortion was 20% or less was much smaller than for the standard LEX. When the LEX was removed, the inlet performance penalties increased considerably as the angle of sideslip was increased (figs. 9(m)-9(p)). At Mach numbers 0.9 and 1.2, distortion was nearly always greater than 20% at angles of sideslip other than 0°. Even at Mach number 0.6, distortion was occasionally greater than 20%; this was not the case for either LEX configuration.

Canard- Analysis indicated that the vortex system downstream from a canard with a dihedral angle would couple with the wing flow field for lift enhancement (fig. 4(c)). Furthermore, analysis also indicated that this canard would provide the same benefit as a LEX; in effect, it would control the upper fuselage flow separation at angle of attack.

The canard resulted in some inlet performance penalties relative to the standard LEX at 0° sideslip, significant only at Mach number 1.2 (figs. 10(j)-10(l)). At Mach number 1.2, pressure recovery decreased and distortion increased to greater than 20%. At 4° angle of sideslip there were recovery penalties with the canard at all Mach numbers (figs. 10(v)-10(x)). Distortion was generally higher at all Mach numbers, increasing to greater than 20% at Mach numbers 0.9 and 1.2. At 8° angle of sideslip, there were significant recovery losses for Mach numbers 0.6 and 0.9 with the canard (fig. 10(hh)-10(jj)). There was an unexplained increase in recovery at Mach number 1.2 and higher angles of attack, however. The canard caused distortion increases to greater than 20% at Mach numbers 0.9 and 1.2 and some angles of attack. At 12° angle of sideslip, the effects of the canard were mixed (figs. 10(tt)-

10(vv)). At Mach number 0.6, the canard resulted in a significant increase in pressure recovery at the higher angles of attack, a favorable result. Conversely, at Mach number 0.9 there was a large increase in distortion with the canard. At Mach number 1.2, the results with the canard were mixed; distortion decreased to less than 20% at some angles but, also, pressure recovery decreased.

Overall, the canard was not as beneficial as the LEX in controlling upper fuselage flow separation. Pressure recovery was generally, but not always, lower with the canard, and distortion was greater than 20% for larger portions of the Mach number/angle of attack/angle of sideslip test envelope.

Leading- and trailing-edge flaps- Since flaps are an integral part of most wing designs, it is important that deflected flaps not result in significant inlet performance penalties. The discussion will be confined to the effect of leading-edge-flap deflections since deflecting the trailing edge flaps did not affect inlet performance (figs. 9(ee) and 9(hh)).

Deflecting the leading-edge flaps 15° generally resulted in the same or slightly higher pressure recovery (figs. 9(d)-9(f) and 9(bb)-9(dd)). However, distortion increased to greater than 20% for some attitudes at Mach number 0.9 (fig. 9). Distortion also increased at Mach number 1.2 but the model attitudes where it was greater than 20% remained about the same (figs. 9(f) and 9(dd)). Greater flap deflections, to 30°, resulted in little or no change in pressure recovery (figs. 9(bb)-9(dd) and 9(ff)-9(hh)). (Neglect the trailing edge flap deflection of 30° on figs. 9(ff) and 9(hh), this did not affect inlet performance.) Moreover, the increased deflections did not signficantly affect the angle of attack/sideslip regions where distortion was greater than 20%.

In summary, deflecting leading-edge flaps either had no effect, or had a favorable effect on pressure recovery, but the Mach number/angle of attack/angle of sideslip regions where distortion was greater than 20% increased slightly.

Supersonic Performance

Inlet location- Inlet location effects were investigated at the supersonic Mach numbers of 1.6 and 2.0. At these Mach numbers, performance was measured near the inlet throat and should not be taken as the total inlet performance (see Model and Instrumentation section). At 0° angle of sideslip, both the right (windward) and left (leeward) inlet pressure recoveries were about the same or higher with the inlets aft (figs. 13(a) and 13(b)). (Note that the MID-inlet results are identified as baseline.) Moreover, distortion was considerably lower with the inlets aft; acceptably low (<20%) for the entire range of angles of attack at Mach number 1.6. At 4° angle of sideslip, the aft location was still better but the performance differences for the three locations were much less than at 0° (figs. 13(i) and 13(j)). At 8° angle of sideslip, the results were similar to those at 4°; the aft inlet location was better (figs. 13(q) and 13(r)).

In summary, locating the inlets aft resulted in the largest Mach number/angle of attack/angle of sideslip envelope where distortion was equal to, or less than, 20%. However, the MID location (baseline) was chosen for the investigation of other configuration variables so that a consistent set of data would be available for all Mach numbers. Note that these measurements were made near the inlet throat, not at the compressor face. It is expected that for an operational inlet, distortion at the compressor face would be lower than distortion near the throat.

At supersonic Mach numbers, there were losses in pressure recovery and increases in distortion for the right (windward) inlet as the angle of sideslip was increased (figs. 12(c) and 12(d), 12(g) and 12(h), and 12(i) and 12(j)). For the left (leeward) inlet, conversely, distortion generally decreased at the higher angles of attack as the angle of sideslip was increased. However, distortion was unacceptably high (>20%) for either or both inlets at most Mach number/angle of attack/angle of sideslip combinations.

Canopy dorsal integration- When the canopy was reduced in size, pressure recovery increased and distortion decreased. At 0° angle of sideslip, distortion decreased to acceptable levels (<20%) at all angles of attack (figs. 13(e) and 13(f)). At 4° angle of sideslip, pressure recovery was higher and distortion lower for the reduced canopy configuration; but distortion was still greater than 20% for the right (windward) inlet at the higher angles of attack (figs. 13(m) and 13(n)). The results at 8° angle of sideslip were similar to those at 4° except that with the reduced canopy, distortion was greater than 20% for a larger range of angles of attack (figs. 13(u) and 13(v)). Overall, the reduced canopy configuration resulted in a considerable increase in the Mach number/angle of attack/angle of sideslip envelope where distortion is acceptably low (<20%) (figs. 12(c) and 12(d) and 12(K) and 12(l)). The greatest reduction in distortion occurred for the left (leeward) inlet; while, for the windward inlet, distortion was often high at angles of sideslip other than 0°.

Wing plan- Pressure recovery was higher and distortion was lower for either LEX configuration than for LEX-off. At 0° angle of sideslip, the performance was similar for either LEX (figs. 13(c) and 13(d)). However, neither LEX was effective in reducing distortion to an acceptable level (<20%). At 4° angle of sideslip, either LEX was more effective than at 0° (figs. 13(k) and 13(l)). In particular, left (leeward) inlet distortion was reduced considerably at the higher angles of attack; conversely, distortion increased for this inlet at lower angles of attack, most apparent at Mach number 1.6. At 8° angle of sideslip, neither LEX was effective in reducing distortion from a high to an acceptable level (<20%) (figs. 13(s) and 13(t)). Overall, the results showed that the installation of a LEX resulted in increased inlet pressure recovery, but it reduced distortion to an acceptable level only over a limited range of test conditions.

Canard- The effects of the undeflected canard on inlet performance were investigated at supersonic Mach numbers. At 0° angle of sideslip, pressure recovery was slightly lower with the canard (figs. 13(g) and 13(h)). More importantly, however, distortion increased to greater than 20% at Mach number 1.6 and low angles of attack. At 4° angle of sideslip, the canard caused greater performance penalties

than at 0° (figs. 13(o) and 13(p)). Pressure recovery decreased and distortion increased to greater than 20% for the leeward inlet at all angles of attack. At 8° angle of sideslip, the most adverse effect of the canard was an increase in distortion at Mach number 1.6 and at higher angles of attack (figs. 13(w) and 13(x)). In summary, the overall effect of the canard was a general decrease in pressure recovery and reduction in the Mach number/angle of attack/angle of sideslip where distortion was less than 20%.

Flow field measurements- Total pressure recovery and distortion were measured using a rake mounted upstream from the inlet entrance (fig. 5(a)). Measurements were made during both subsonic/transonic (M = 0.6-1.2) and supersonic (M = 1.6 and 2.0) tests.

The transonic results are shown in figures 11(a)-11(u). A comparison of configurations generally shows the same trends in pressure recovery as did measurements at the compressor face. As an example, pressure recovery is higher for the standard LEX configuration than for LEX-off (figs. 11(a) and 11(c) and 11(g) and 11(i)). Distortion measurements, however, did not correlate well between the inlet entrance station and the compressor face. As an example, compare the distortion at the inlet entrance for the MID-inlet/standard LEX configuration (fig. 11(c)) with the distortion at the compressor face for the same configuration (fig. 9(d)). Distortion at the compressor face is low for all test conditions, even though the flow-field measurements indicate conditions where distortion is unacceptably high (>20%). Comparisons for other configurations often showed the same trend; high distortion measurements at the inlet entrance did not translate into high distortion at the compressor face.

The flow field measurement results at supersonic Mach numbers are shown in figures 11(v)-11(gg). These results showed high distortion for almost all configurations and test conditions. Flow field distortion measurements did not correlate well with measurements just downstream, at the ramp rake station. For instance, the low distortion measured for the left duct at the ramp rake station (fig. 12(c)) was not consistent with flow-field measurements (fig. 11(v)).

In summary, the results show that the measurement of pressure recovery in the flow field was not indicative of performance at the compressor face. Distortion measured in the flow field was not necessarily indicative of distortion at the compressor face, or even distortion at the ramp rake station (in the case of the supersonic results). For many configurations and test conditions, high distortion in the flow field was modulated to an acceptable level (<20%) at the compressor face or the ramp rake station.

CONCLUDING REMARKS

Inlet performance results were obtained for a wind tunnel model of a V/STOL fighter/attack aircraft configuration with twin-top mounted inlets. The effects of inlet location, canopy-dorsal integration, wing leading-edge extension

(LEX)/planform area, variable incidence canards, and wing leading- and trailing-edge-flap deflections were determined. The test conditions included Mach numbers from 0.6 to 2.0 and angles of attack and sideslip up to 27° an 12°, respectively.

At all Mach numbers and angles of attack and at 0° angle of sideslip, for at least one configuration (not the same configuration for all Mach numbers and angles), the pressure recovery was high and distortion acceptably low (<20%). Of those tested, the best configuration was the inlet located in the MID-position, with the standard LEX and the canopy reduced in size. Based on the results at Mach numbers 1.6 and 2.0, however, inlet performance might have been even better for that standard LEX/reduced-canopy configuration had the inlet been located aft.

At angles of sideslip other than 0°, pressure recovery was often low (<80%) and distortion often unacceptably high (>20%) for all configurations tested. These adverse effects were most pronounced for the windward inlet at the higher Mach numbers. However, at the higher Mach numbers, pressure recovery was generally higher and distortion lower with the inlet located aft.

The best prospects for performance improvements would appear likely from a canopy reconfiguration in conjunction with the inlet being moved downstream from the MID-position location used in this investigation. Even so, for the Mach number/ angle of attack/angle of sideslip envelope of this investigation, test conditions would probably occur in which distortion would be high for the windward inlet.

REFERENCES

1. Nelms W. P: Studies of Aerodynamic Technology for V/STOl Fighter/Attack Aircraft. AIAA Paper 78-1511, AIAA Aircraft Systems and Technology Conference, Los Angeles, CA, Aug. 21-23, 1978.

2. Williams, T. L.; and Hunt, B. L.: A Comparative Assessment of Top-Mounted and Conventional Inlet/Airframe Integrations. NASA CP-2162, Part 2, Tactical Aircraft Research and Technology Conference, NASA Langley Research Center, Hampton, VA, Oct. 21-23, 1980.

3. Gerhardt, H. A. et al.: Study of Aerodynamic Technology for V/STOl Fighter/Attack Aircraft - Vertical Attitude Concept. NASA CR-152131, 1978.

4. Nelms, W. P.; and Durston, D. A.: Preliminary Aerodynamic Characteristics of Several Advanced V/STOl Fighter/Attack Aircraft Concepts. SAE Paper 80-1178, SAE Aerospace Congress and Exposition, Los Angeles, CA, Oct. 13-16, 1980.

5. Rhoades, W. W.; and Surber, L. E.: Top Mounted Inlet Flow Field Testing for Future Fighter Aircraft. AIAA Paper 79-1147, AIAA/SAE/ASME 15th Joint Propulsion Conference, Las Vegas, NV, June 18-20, 1979.

6. Williams, T. L.; and Hunt, B. L.: Top Inlet Feasibility for Transonic Supersonic Fighter Aircraft Applications. AIAA Aircraft Systems Meeting, Anaheim, CA, Aug. 4-6, 1980.

7. Strasser T. E.: Study of Top Inlet Technology. NASA CR 177363, July 1985.

8. Williams, T. L.; Nelms, W. P.; and Smeltzer, D. B.: Top-Mounted Inlet System Feasibility for Transonic-Supersonic Fighter Aircraft. NASA TM 81292, May 1981. Also a paper presented at AGARD Symposium on "Aerodynamics of Power Plant Installation," Toulouse, France, May 11-14, 1981.

9. Smeltzer, D. B.; Nelms, W. P.; and Williams, T. L.: Airframe Effects on a Top-Mounted Inlet System for V/STOl Fighter Aircraft. AIAA/NASA Ames V/STOL Conference, Palo Alto, CA, Dec. 7-9, 1982, AIAA Paper 81-2631, pp. 1083-1087.

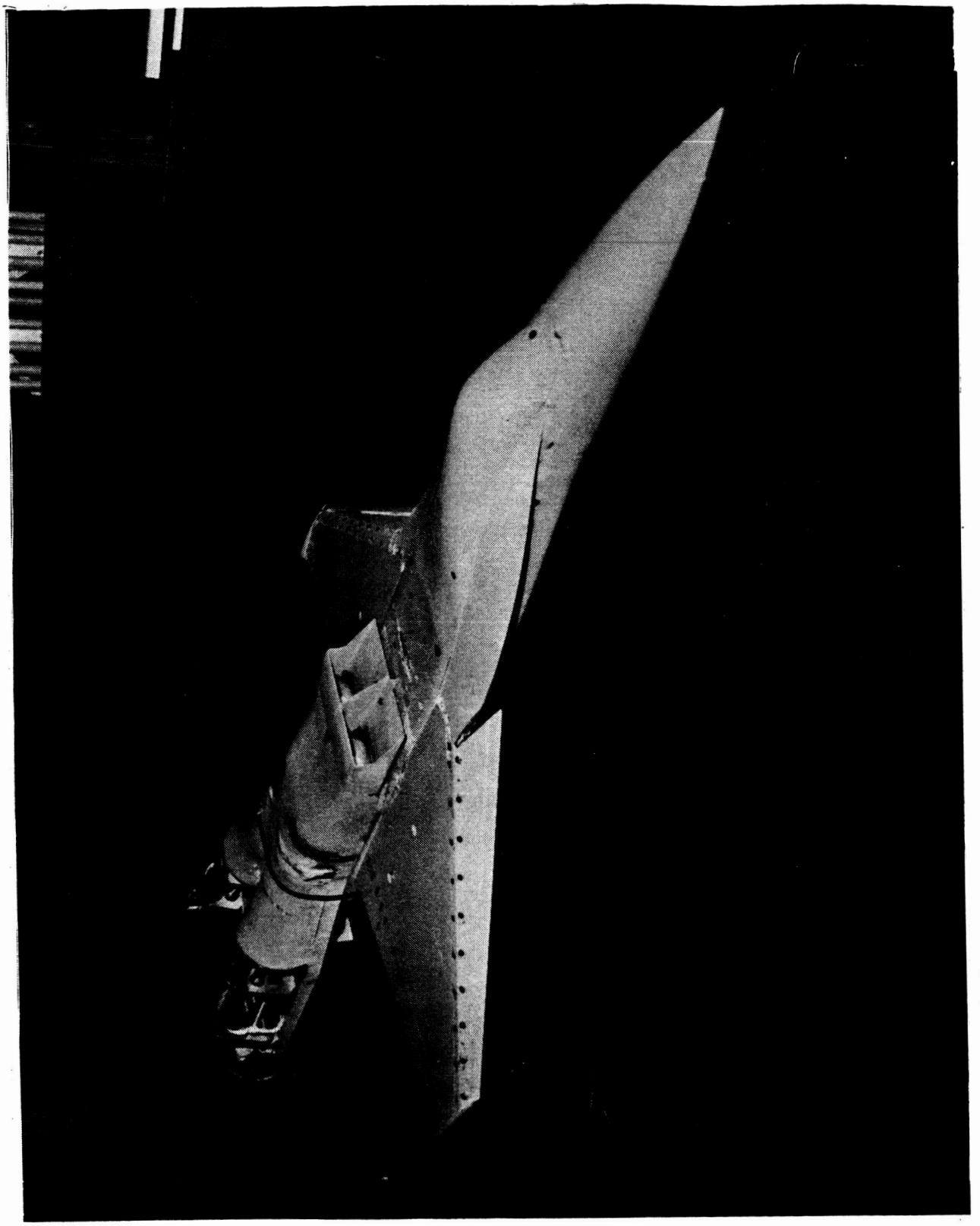

Figure 1.- Model mounted in the 11- by 11-Foot Wind Tunnel.

Figure 2.- Rear view of the model.

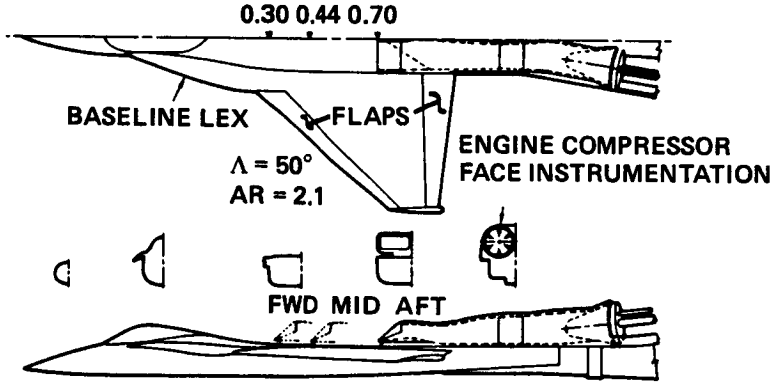

Figure 3.- Model layout.

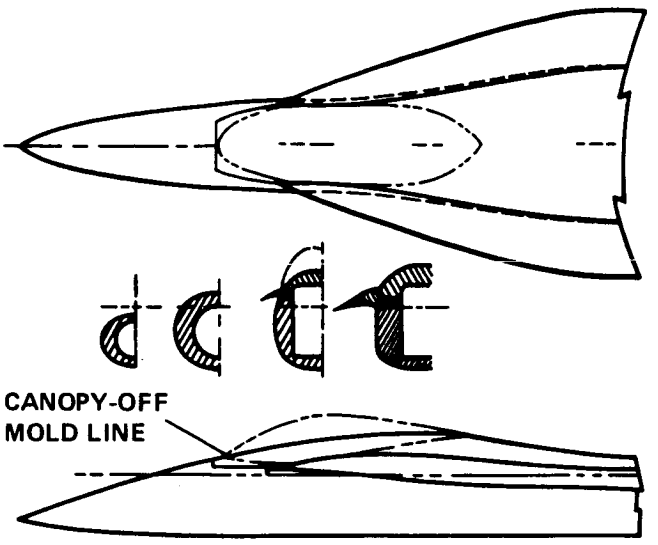

(a) CANOPY-OFF BLOCK

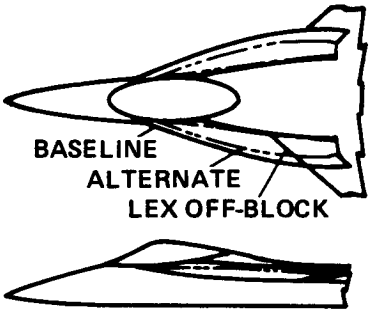

(b) WING LEADING-EDGE EXTENSION (LEX) PLANFORM OPTIONS

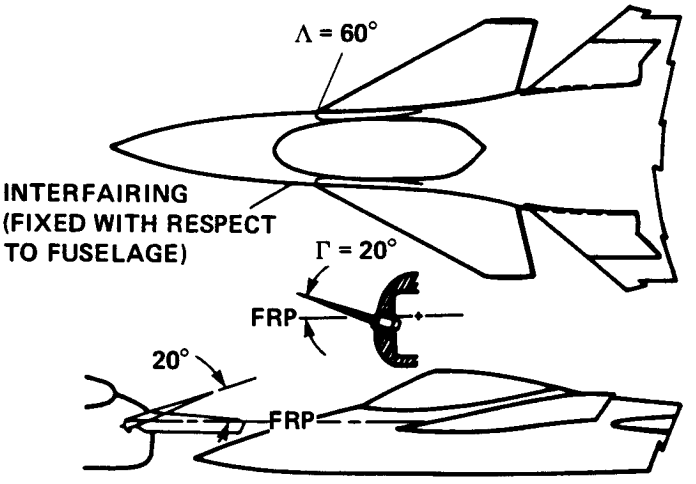

(c) CLOSE-COUPLED VARIABLE INCIDENCE CANARDS

Figure 4.- Model components.

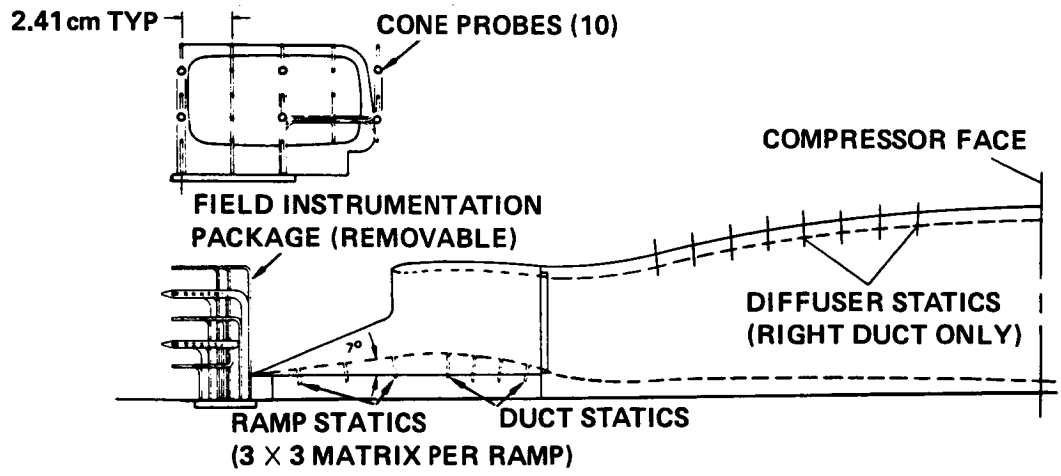

(a) EXTERNAL FLOW FIELD AND DUCT INSTRUMENTATION

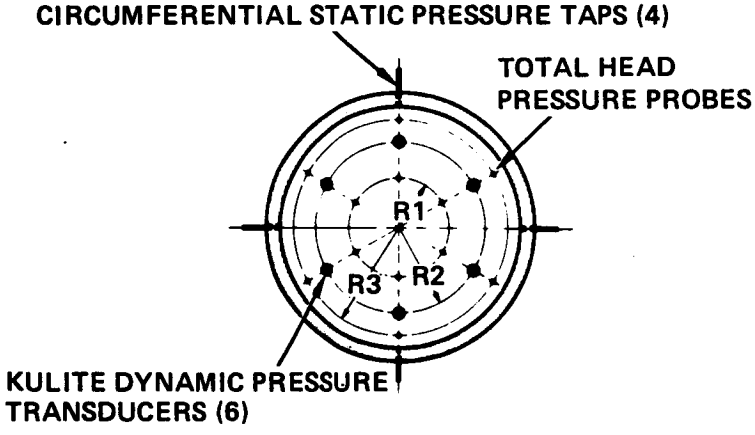

(b) COMPRESSOR-FACE INSTRUMENTATION

Figure 5.- Transonic test instrumentation.

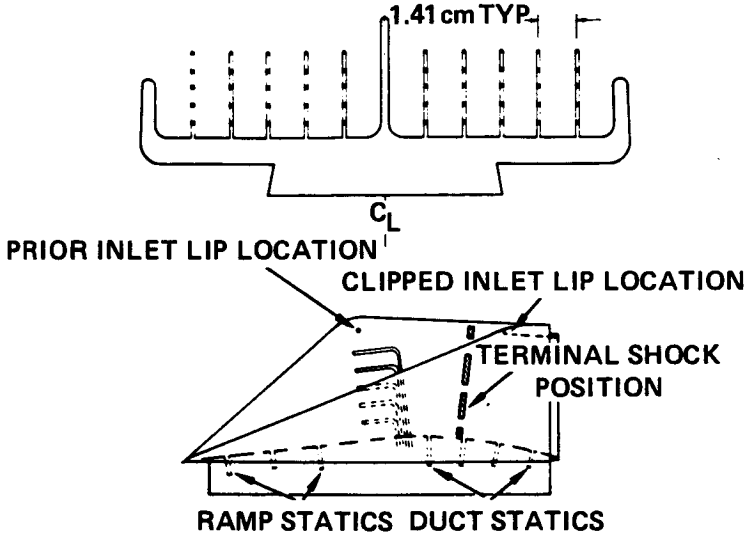

Figure 6.- Supersonic test instrumentation.

CONFIGURATION VARIABLE	FACILITY	INLET LOCATION	LEX	CANOPY	CANARD	DEFLECTIONS			MASS-FLOW SWEEP	FLOW FIELD RAKE
						CANARD	LEADING EDGE FLAP	TRAILING EDGE FLAP		
INLET LOCATION	11'&9×7	FWD	STANDARD	ON	OFF	–	0°	0°	YES	NO
	↓	MID	↓	↓	↓	–	↓	↓	↓	YES
	↓	AFT	↓	↓	↓	–	↓	↓	↓	NO
CANOPY	↓	MID	↓	OFF	↓	–	↓	↓	NO	YES
LEX	↓	↓	ALTERNATE	ON	↓	–	↓	↓	YES	↓
	↓	↓	OFF	↓	↓	–	↓	↓	↓	↓
CANARD	↓	↓	↓	↓	ON	0°	↓	↓	↓	↓
	↓	↓	↓	↓	↓	-10°	15°	↓	NO	↓
	11'	↓	↓	↓	↓	-25°	30°	↓	↓	↓
LEADING EDGE FLAPS	↓	↓	STANDARD	↓	OFF	–	15°	↓	↓	NO
	↓	↓	↓	↓	↓	–	30°	↓	↓	↓
L. & T. EDGE FLAPS	↓	↓	↓	↓	↓	–	30°	30°	↓	↓

MACH = 0.6, 0.9, & 1.2(11'); = 1.6 & 2.0 (9 × 7)
ALPHA ≈ -2° TO 27°(11'); = 0° TO 15° (9 × 7)
BETA = 0°, 4°, 8°, & 12° (11'); = 0°, 4°, & 8°(9 × 7)

Figure 7.- Model configurations and test variables.

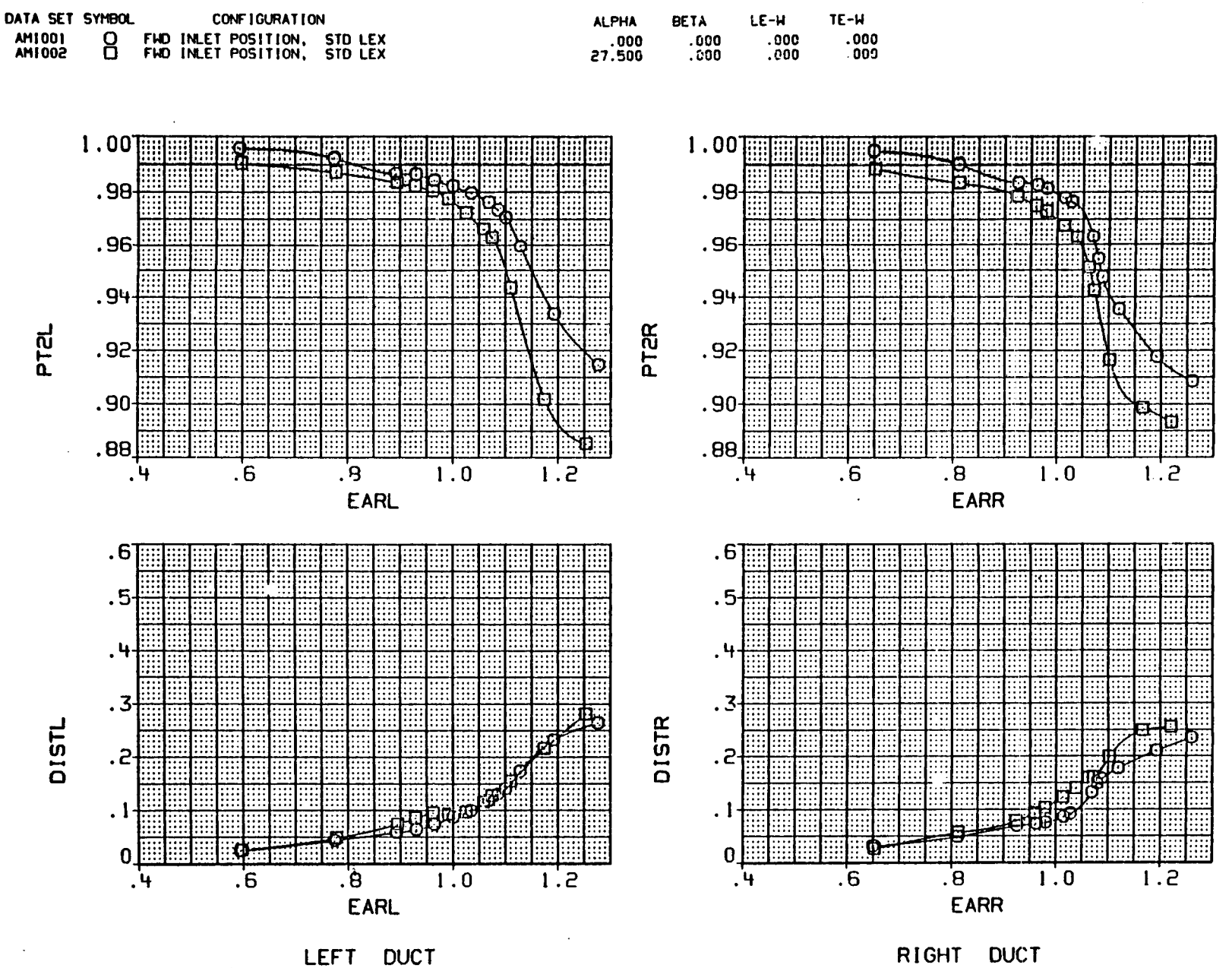

(a) Mach = 0.60.

Figure 8.- Effect of mass flow variations on inlet performance.

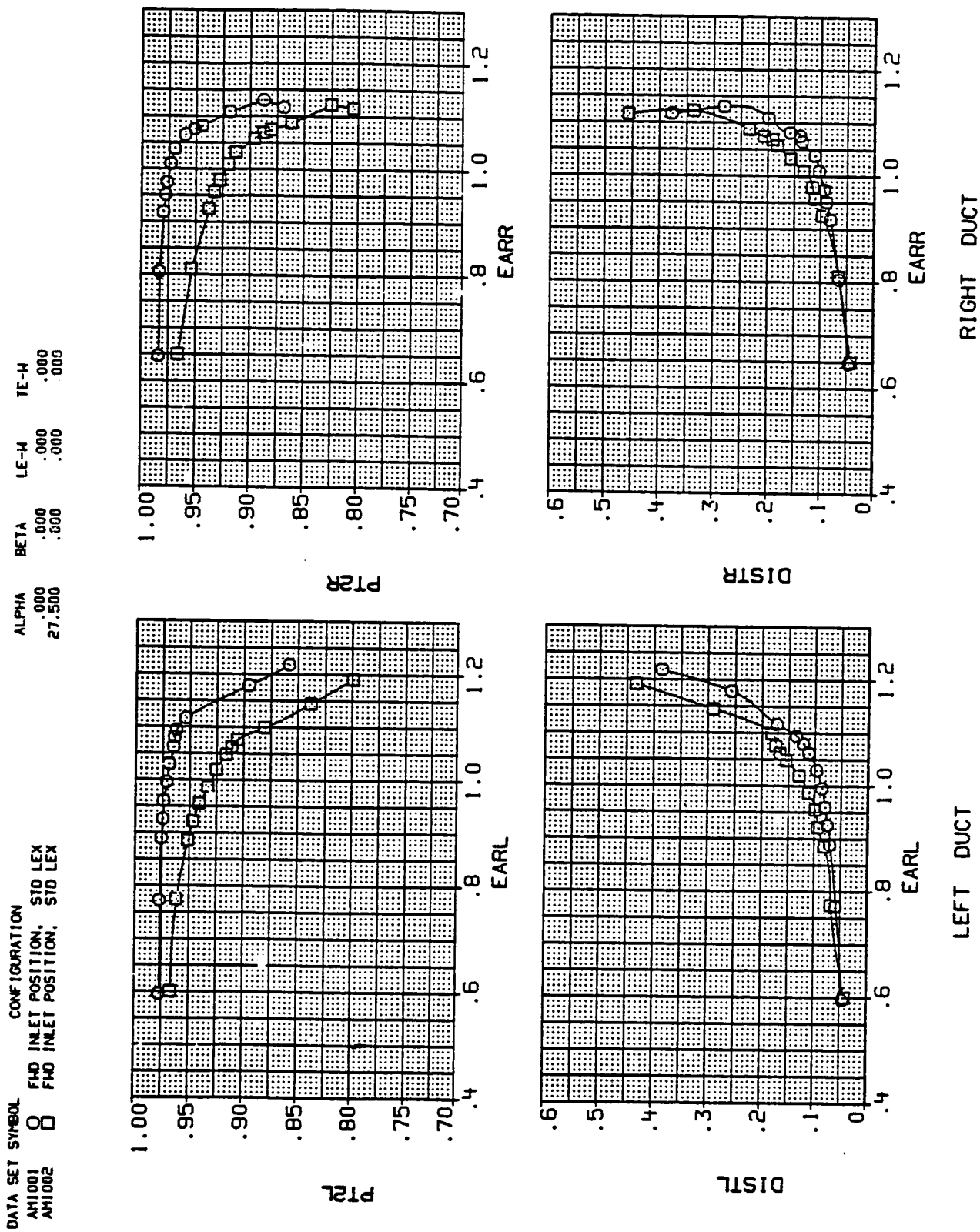

(b) Mach = 0.90.

Figure 8.- Continued.

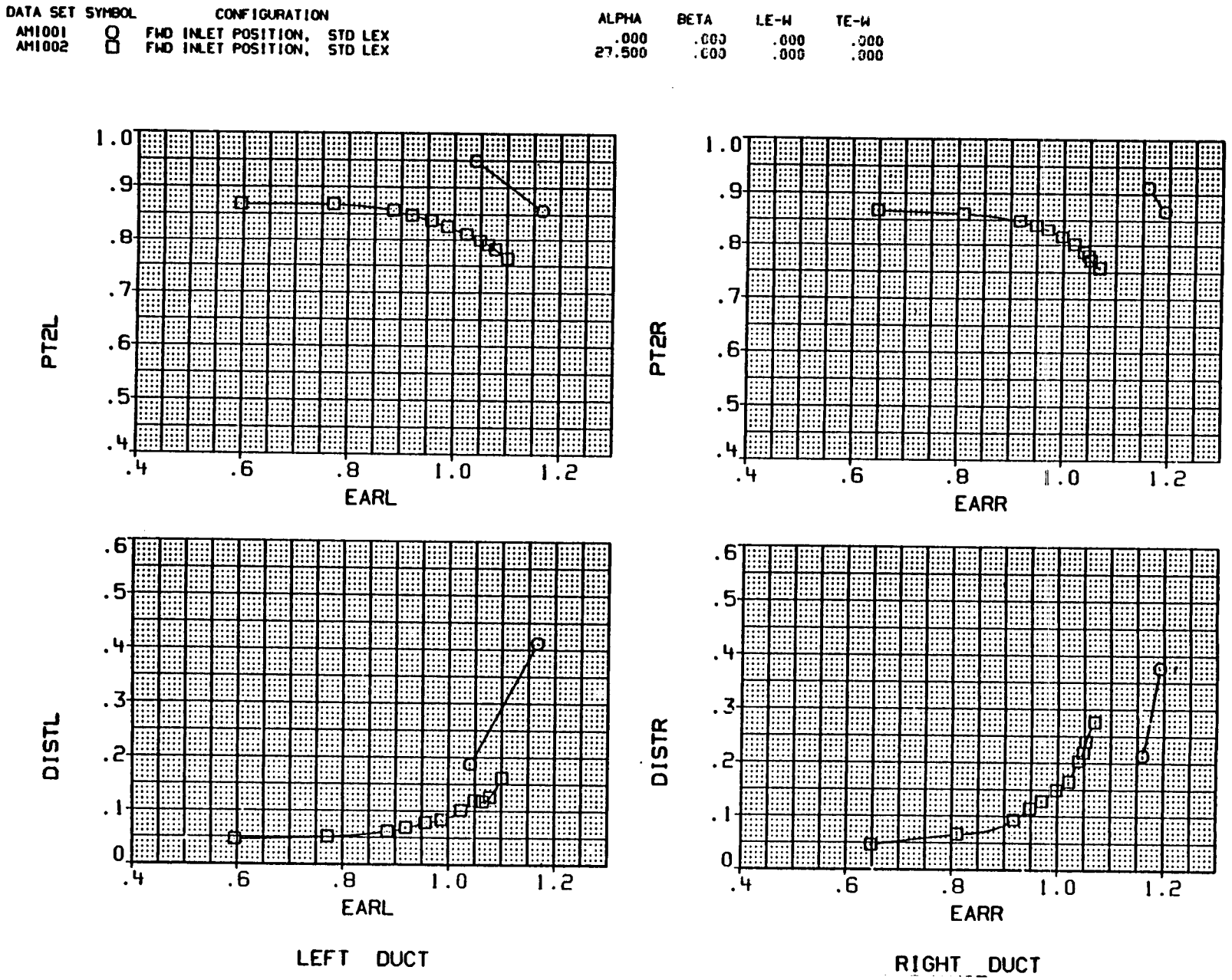

(c) Mach = 1.20.

Figure 8.- Continued.

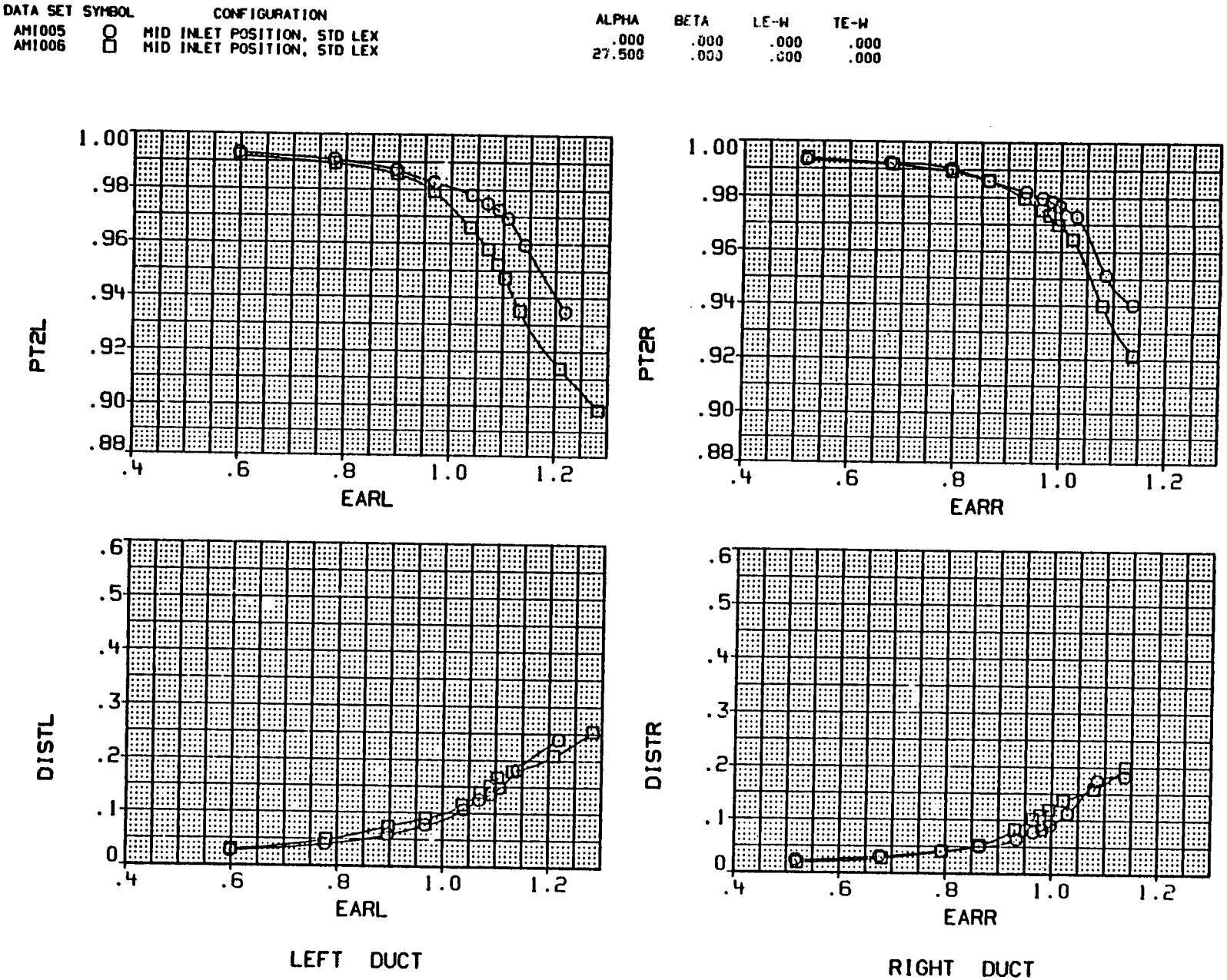

(d) Mach = 0.60.

Figure 8.- Continued.

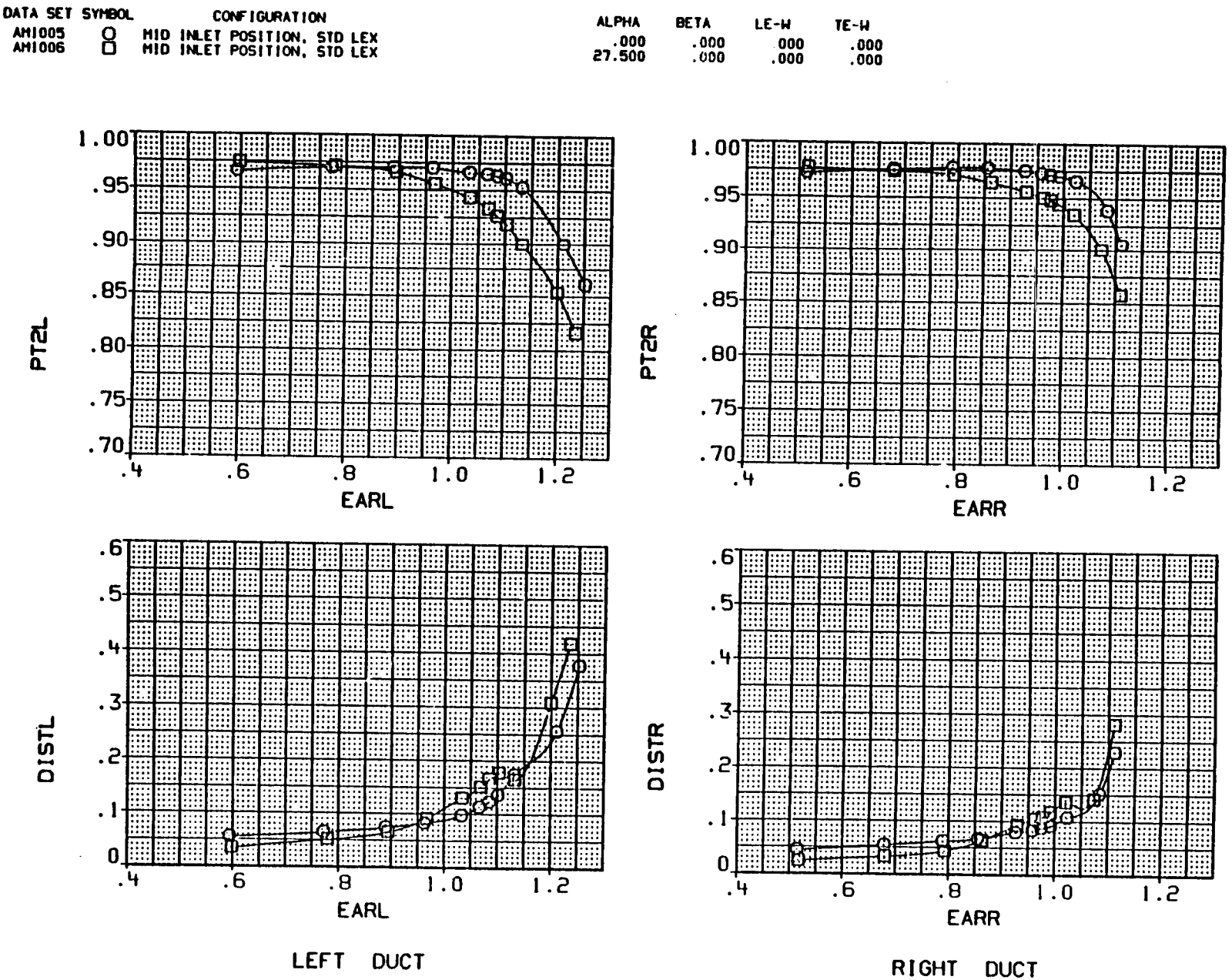

(e) Mach = 0.90.

Figure 8.- Continued.

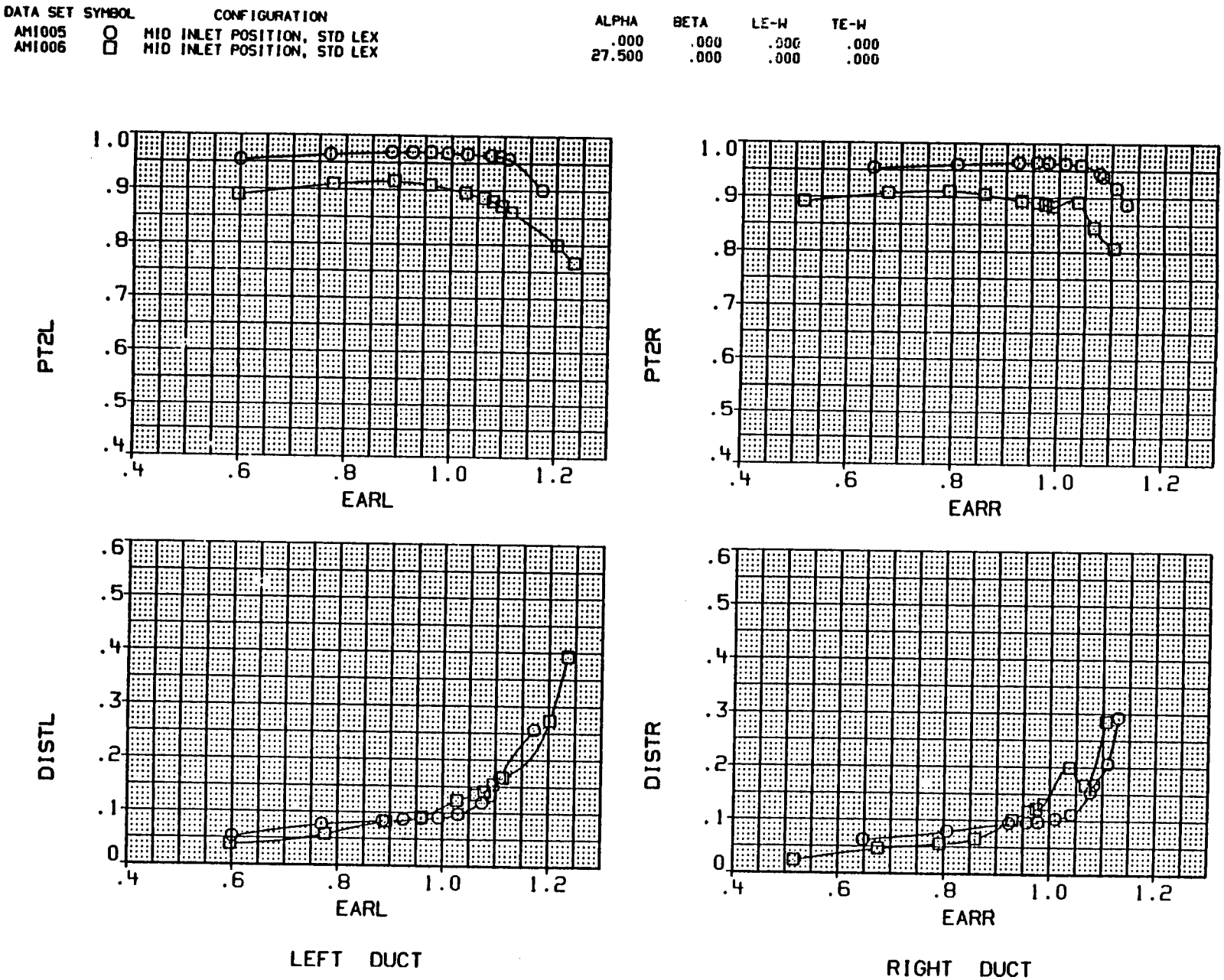

(f) Mach = 1.20.

Figure 8.- Continued.

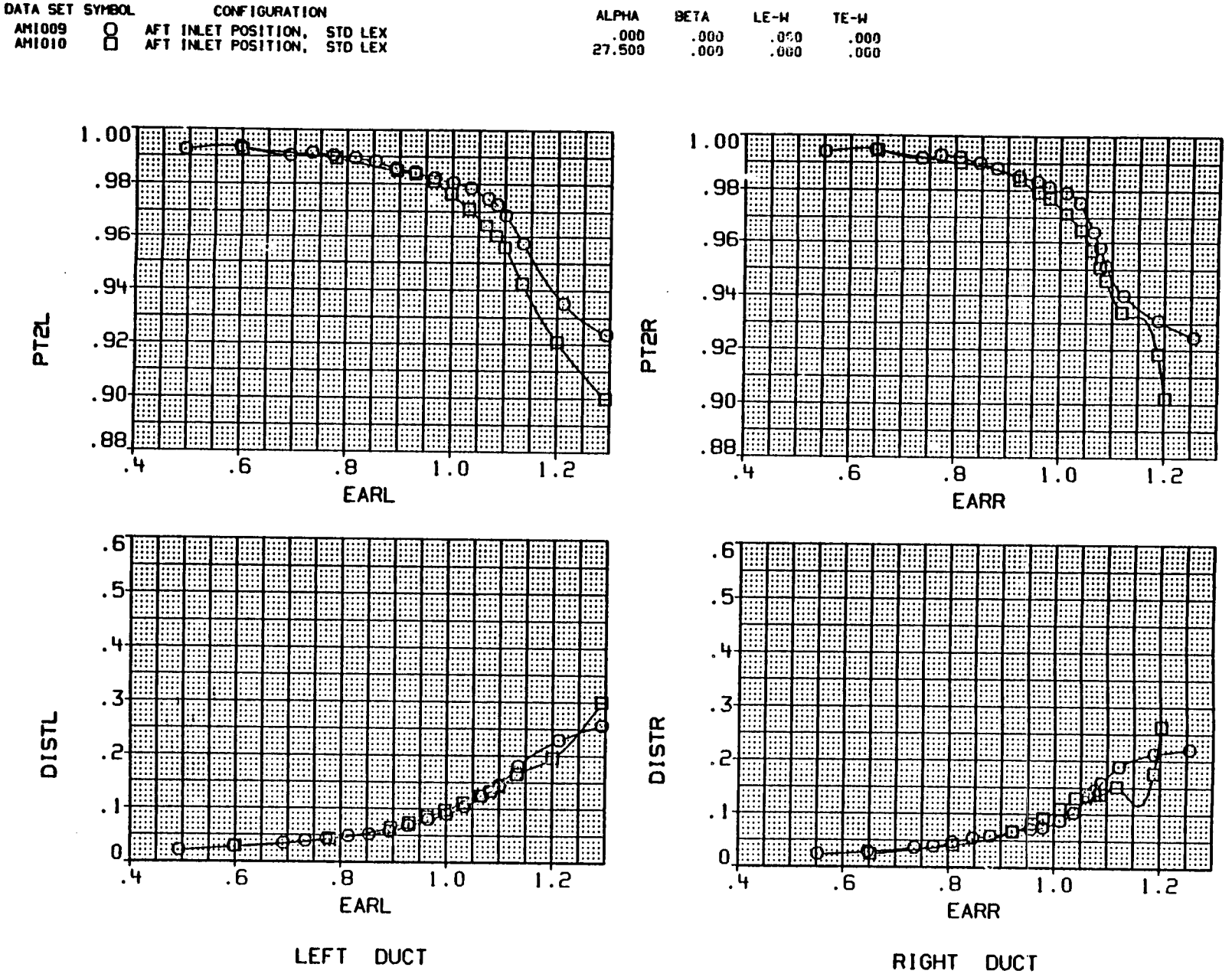

(g) Mach = 0.60.

Figure 8.- Continued.

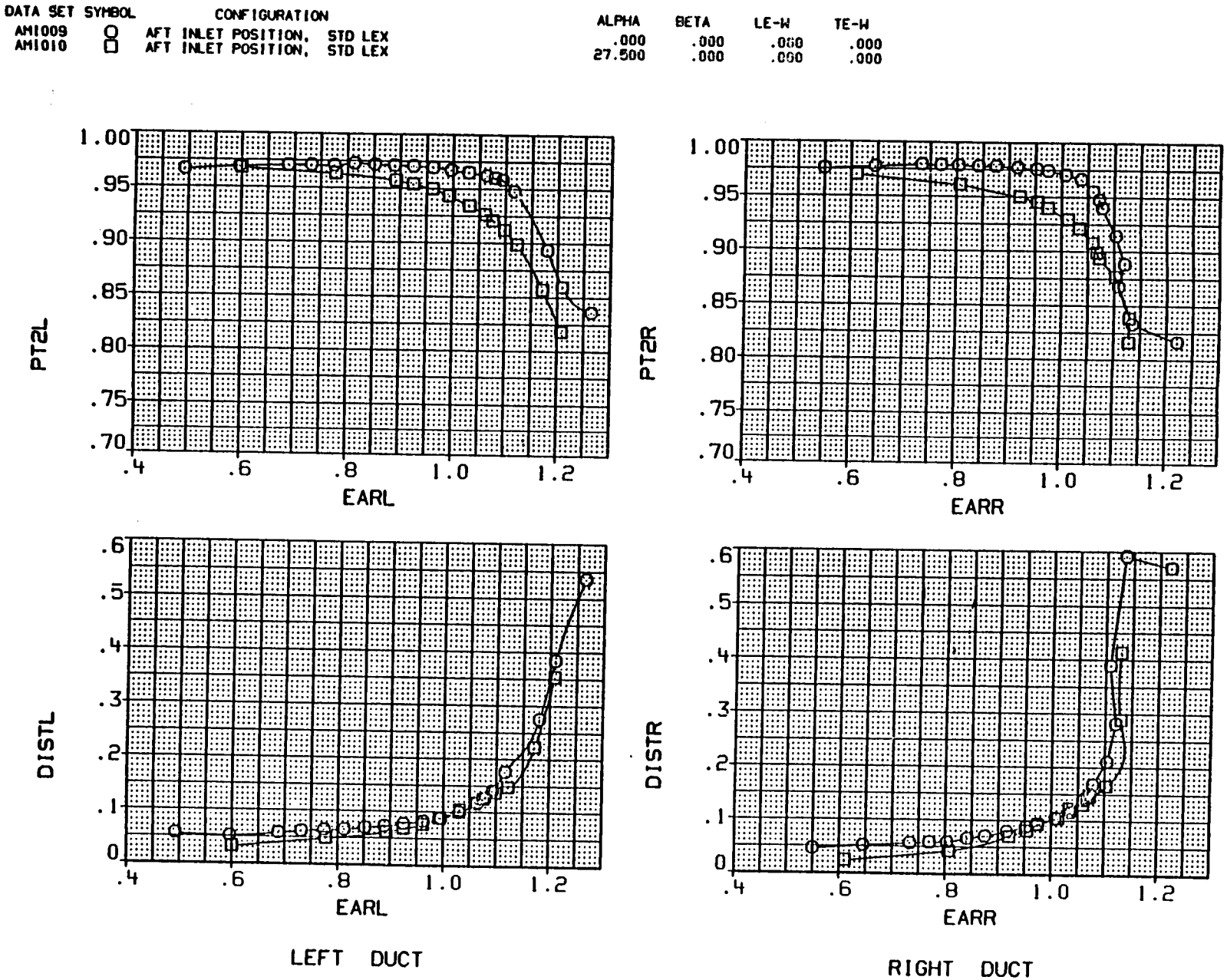

(h) Mach = 0.90.

Figure 8.- Continued.

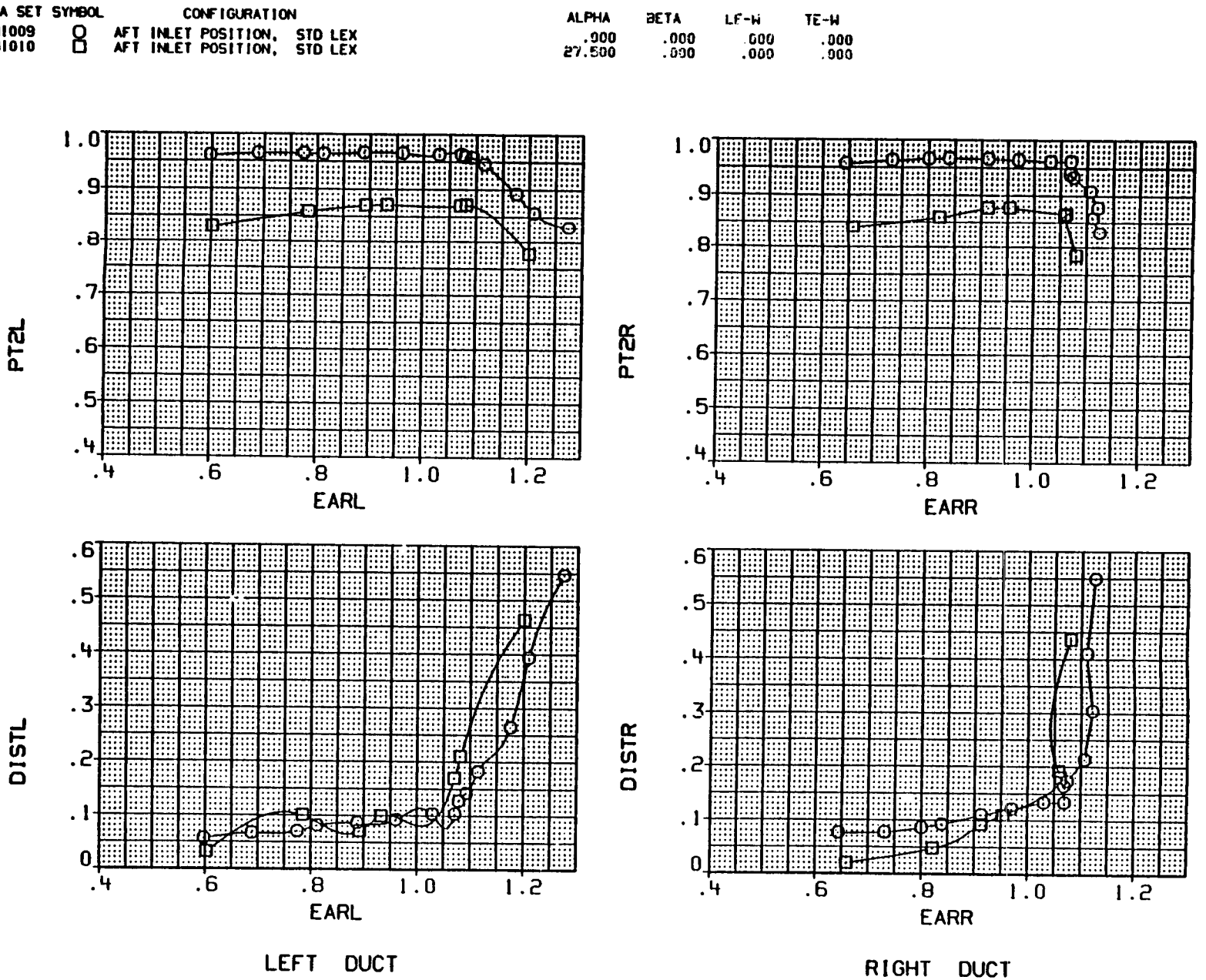

(i) Mach = 1.20.

Figure 8.- Continued.

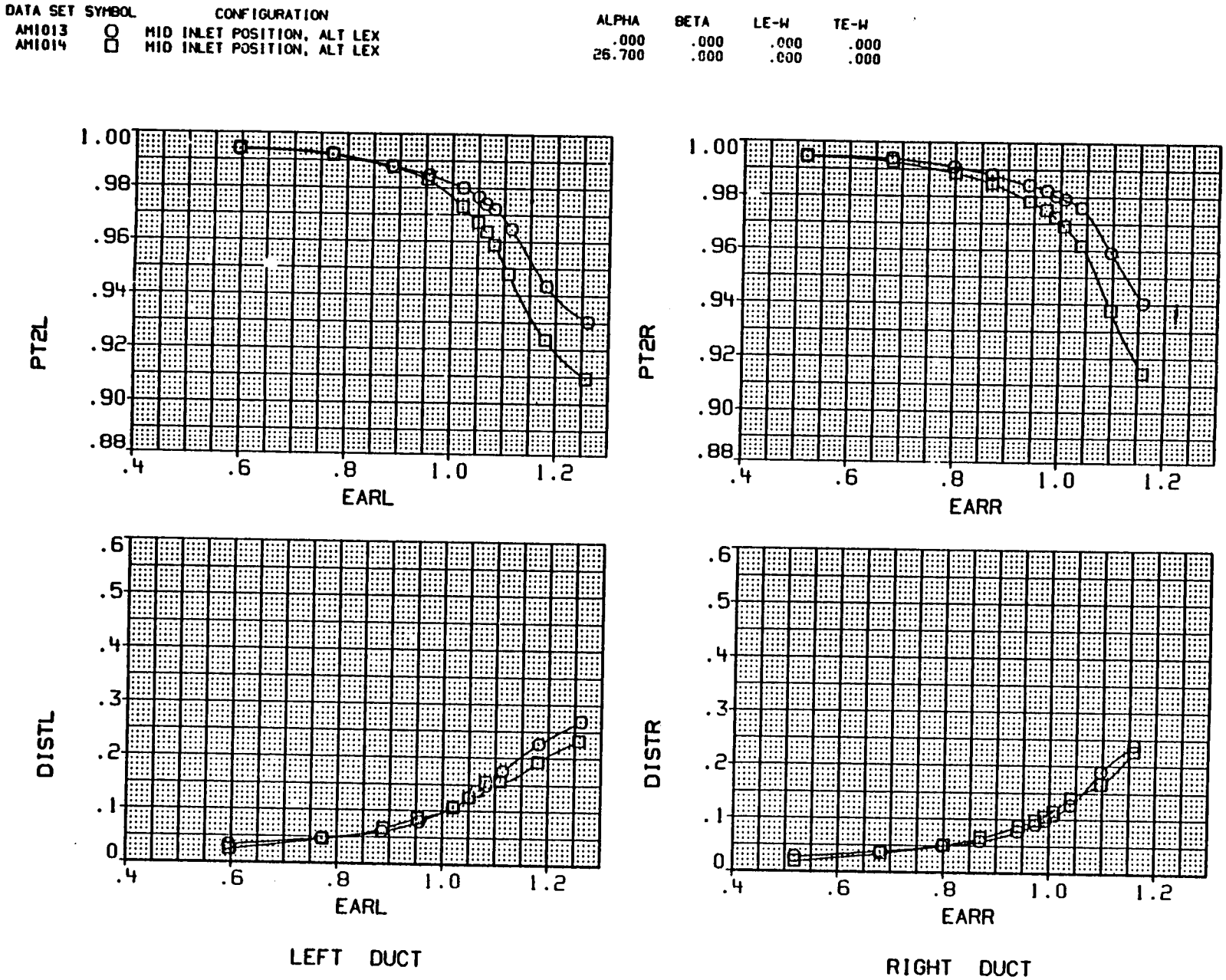

(j) Mach = 0.60.

Figure 8.- Continued.

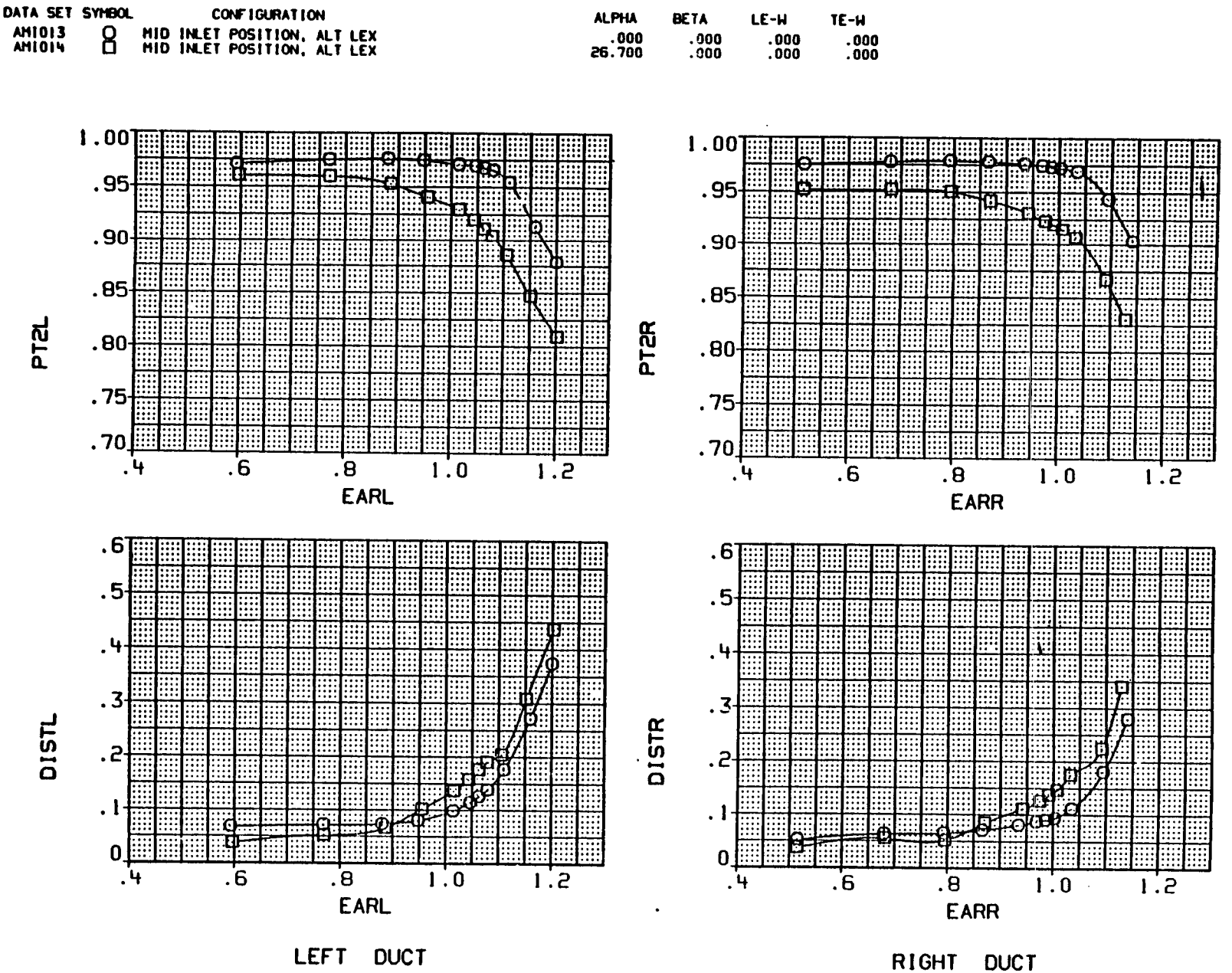

(k) Mach = 0.90.

Figure 8.- Continued.

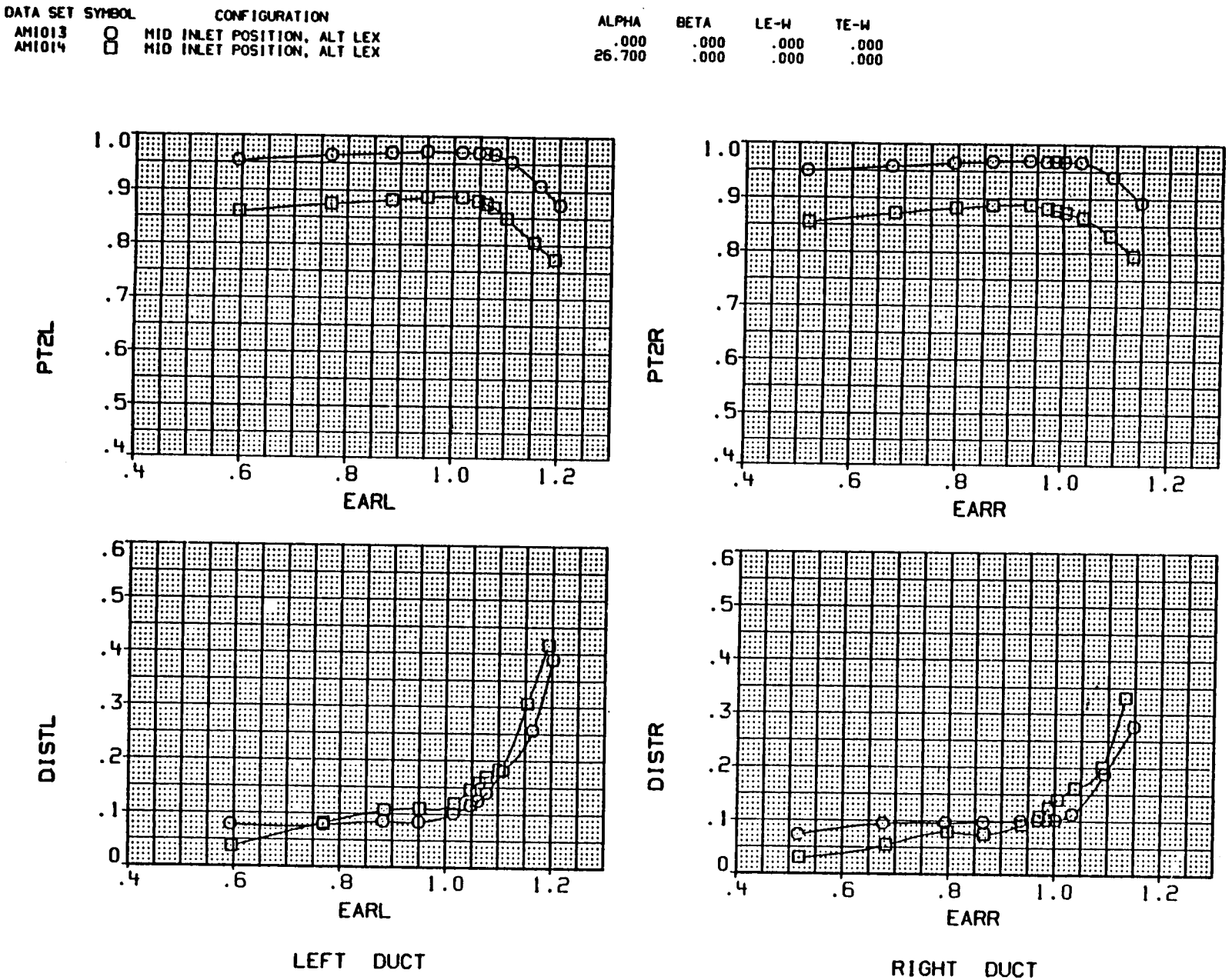

(1) Mach = 1.20.

Figure 8.- Continued.

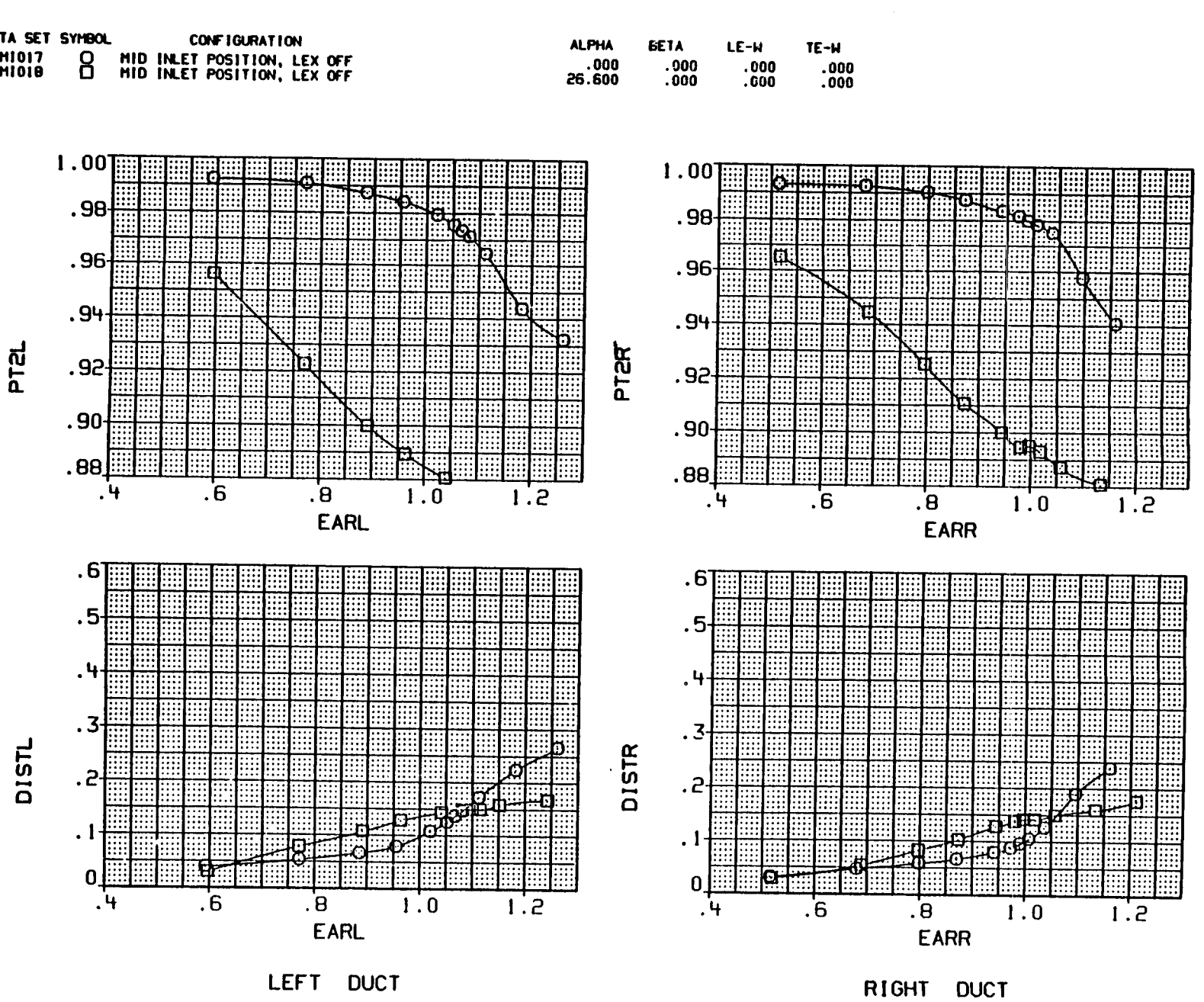

(m) Mach = 0.60.

Figure 8.- Continued.

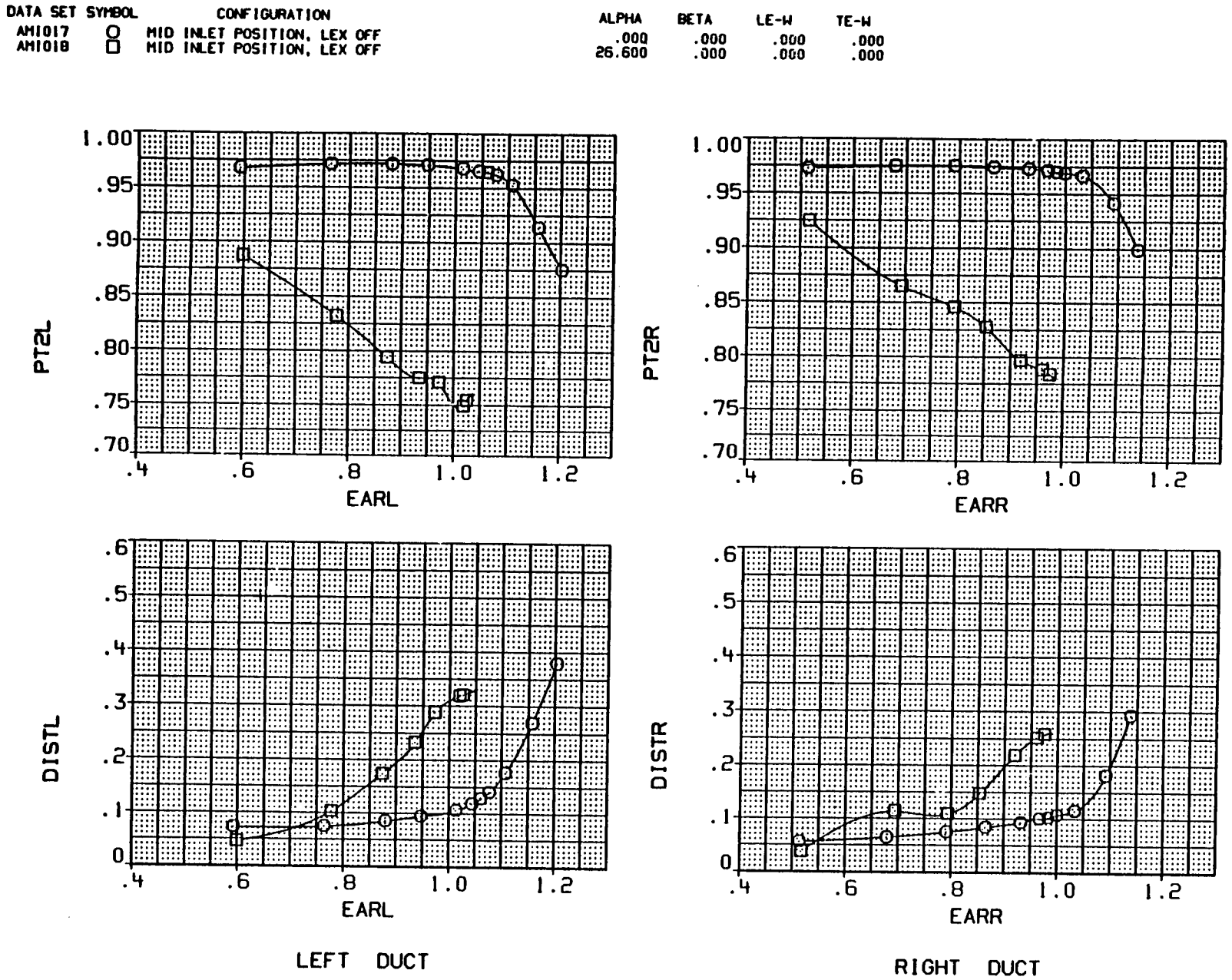

(n) Mach = 0.90.

Figure 8.- Continued.

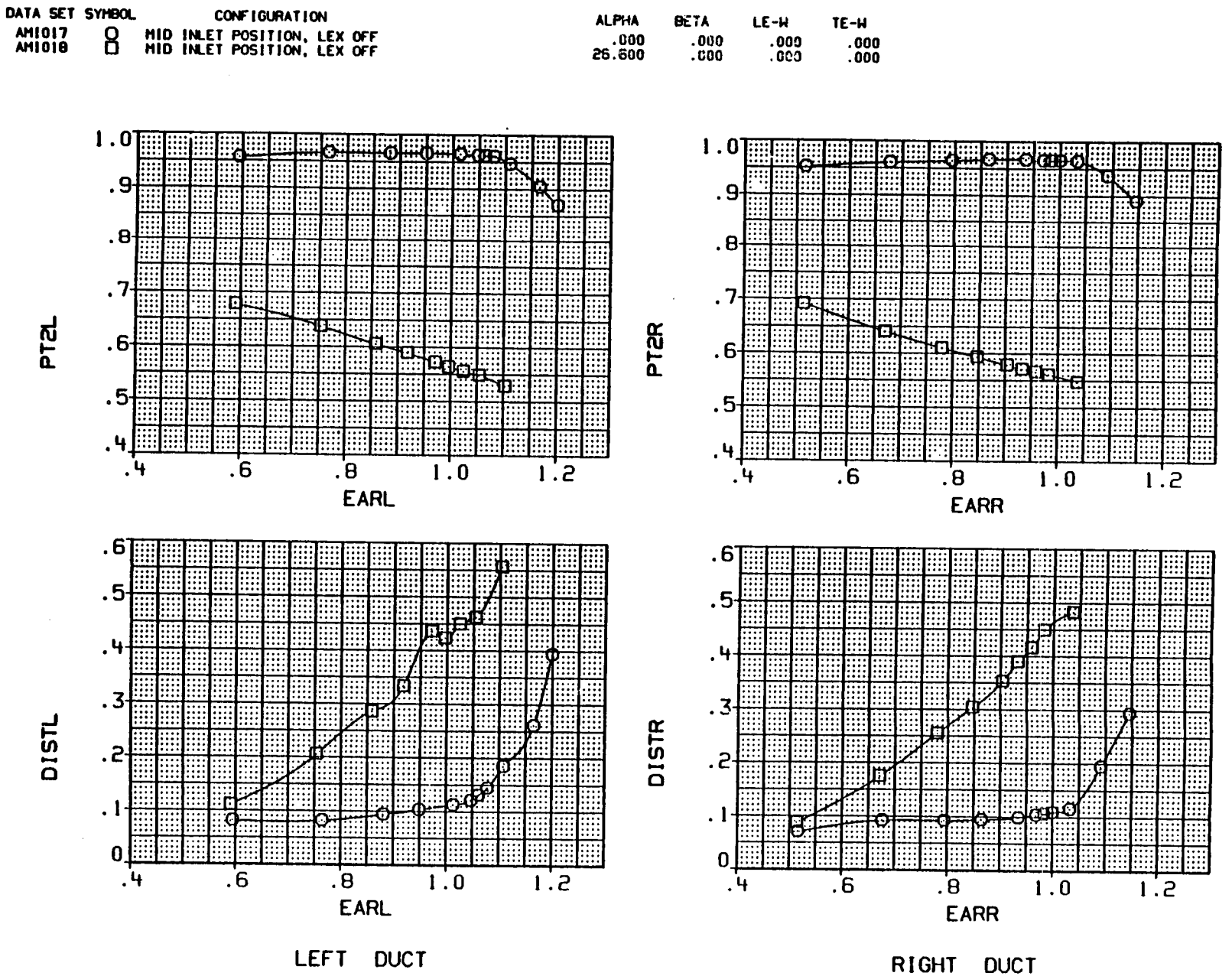

(o) Mach = 1.20.

Figure 8.- Continued.

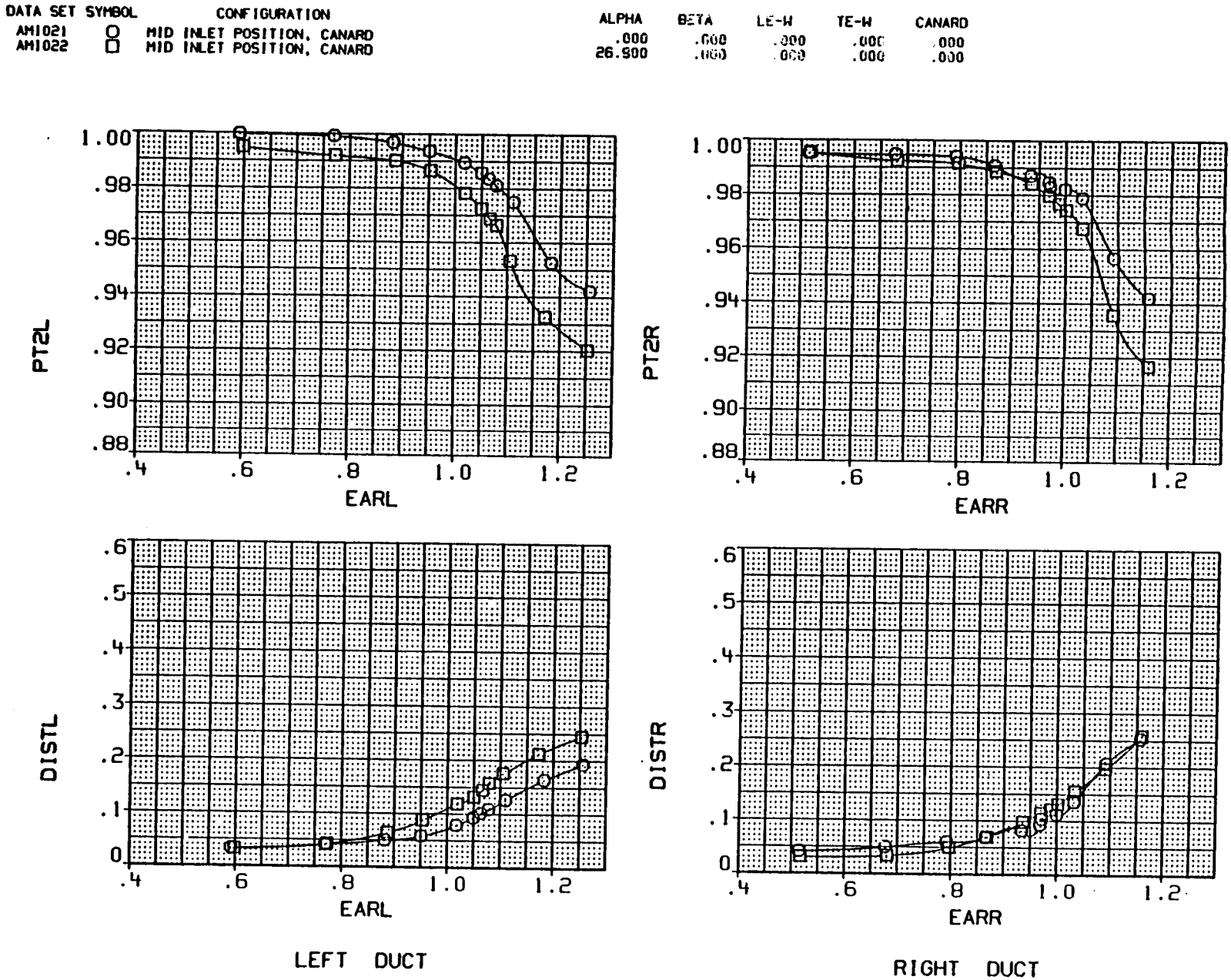

(p) Mach = 0.60.

Figure 8.- Continued.

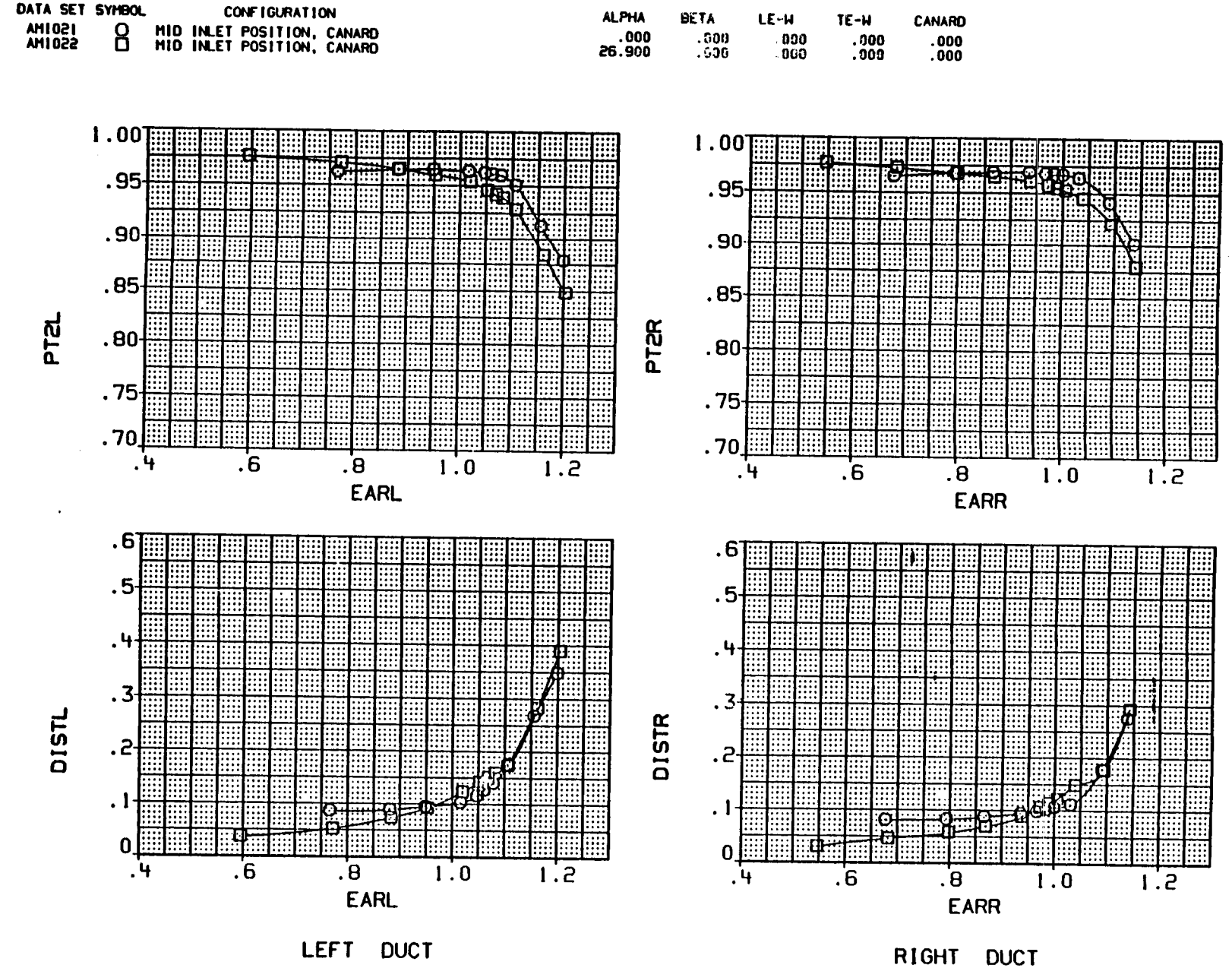

(q) Mach = 0.90.

Figure 8.- Continued.

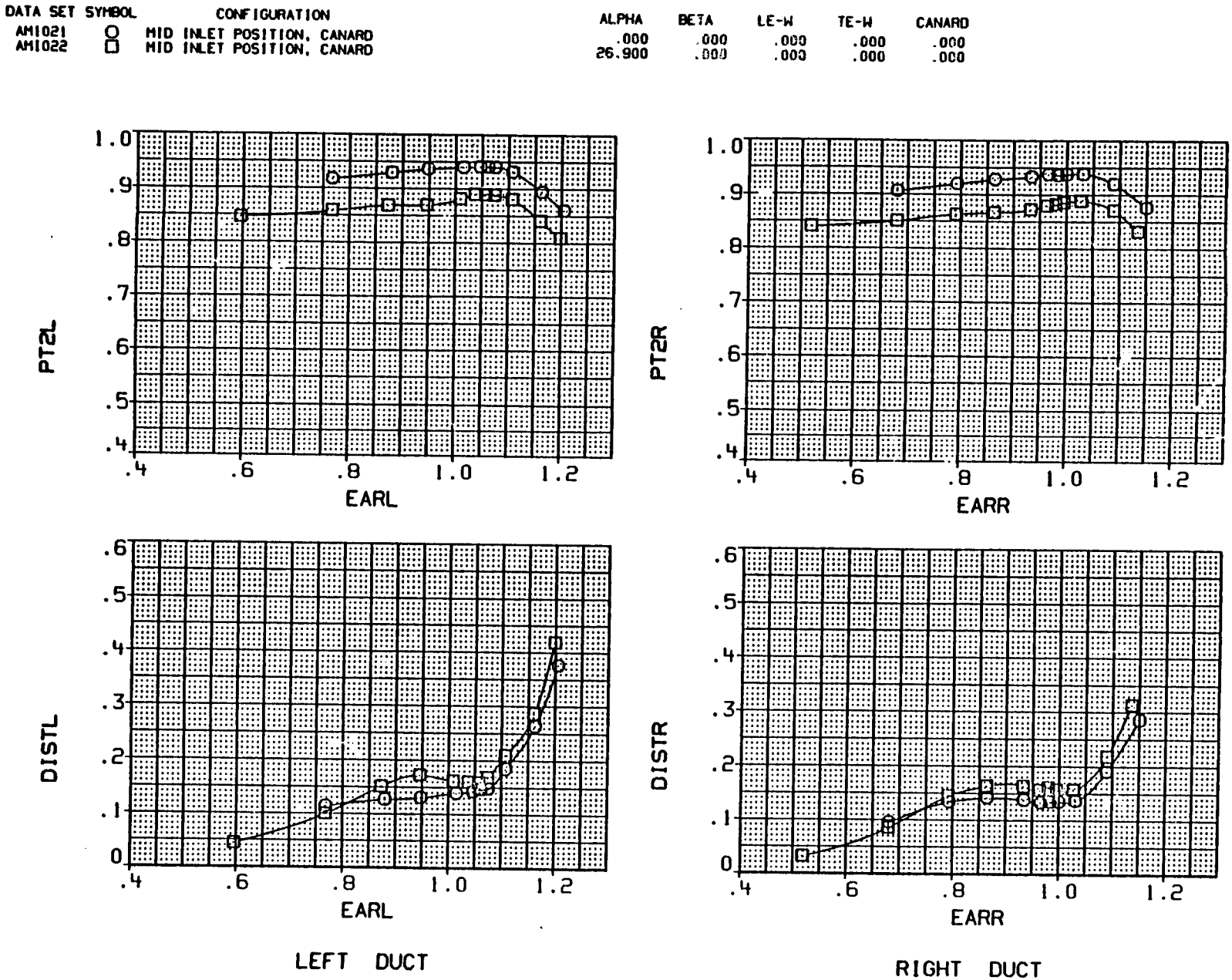

(r) Mach = 1.20.

Figure 8.- Continued.

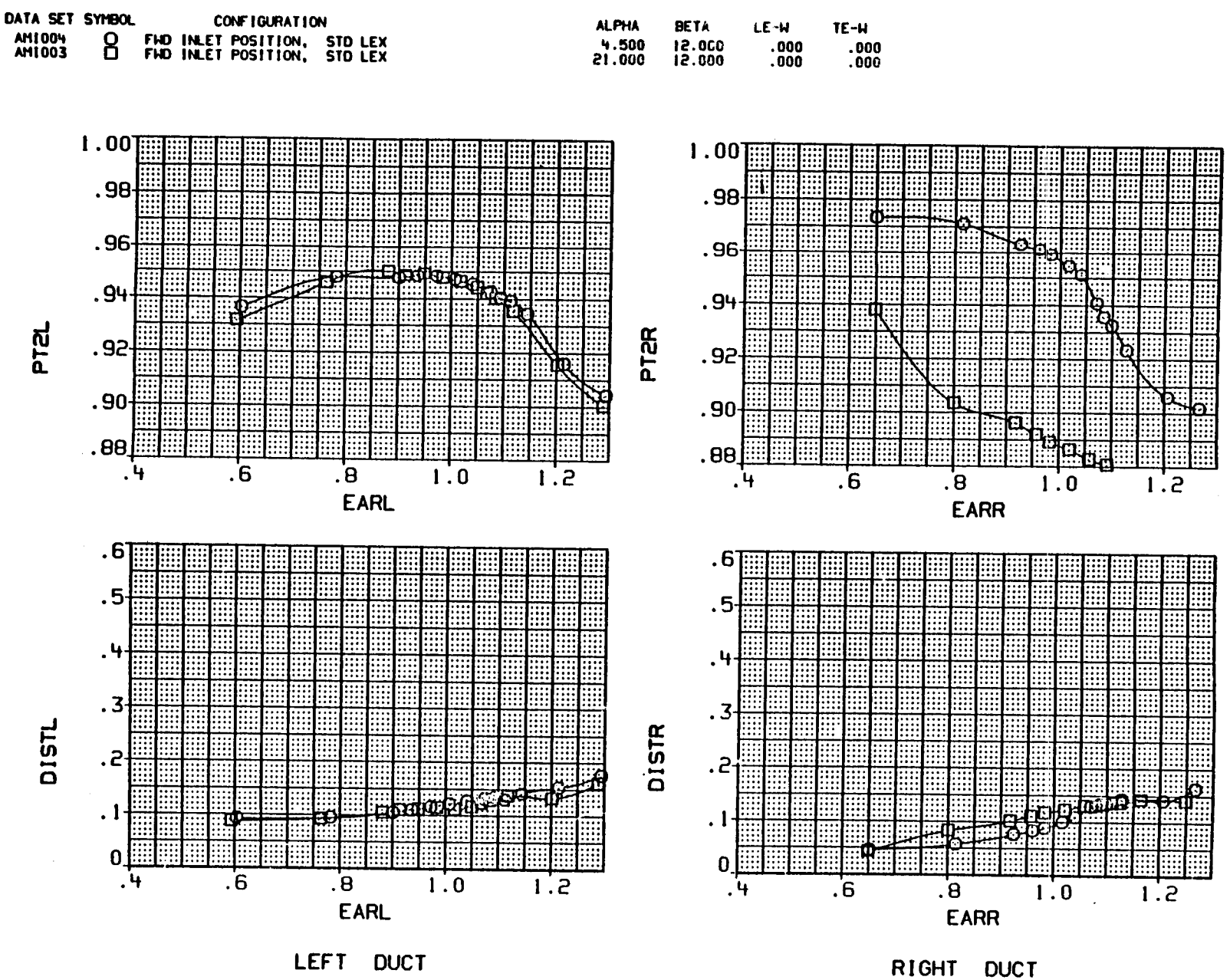

(s) Mach = 0.60.

Figure 8.- Continued.

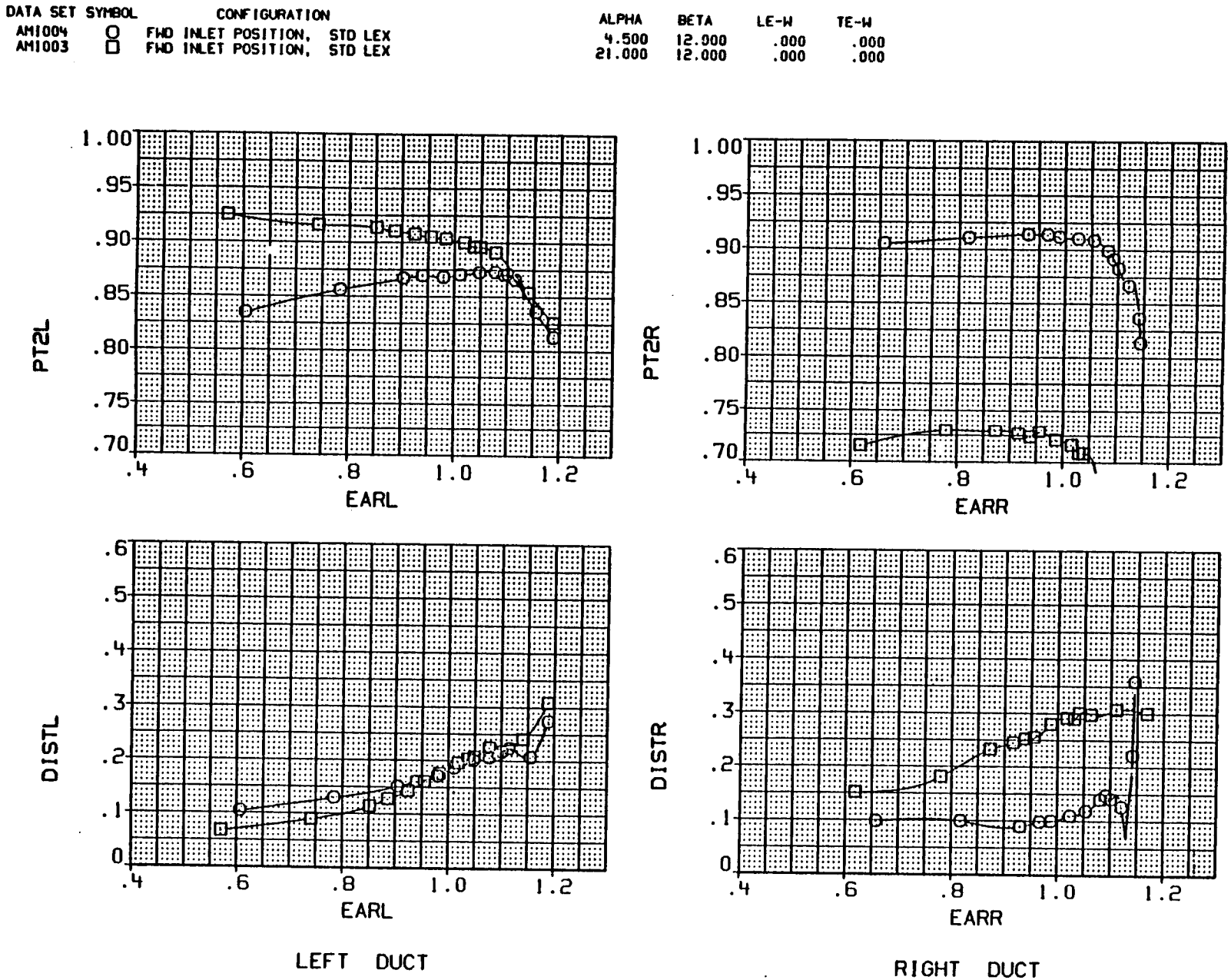

(t) Mach = 0.90.

Figure 8.- Continued.

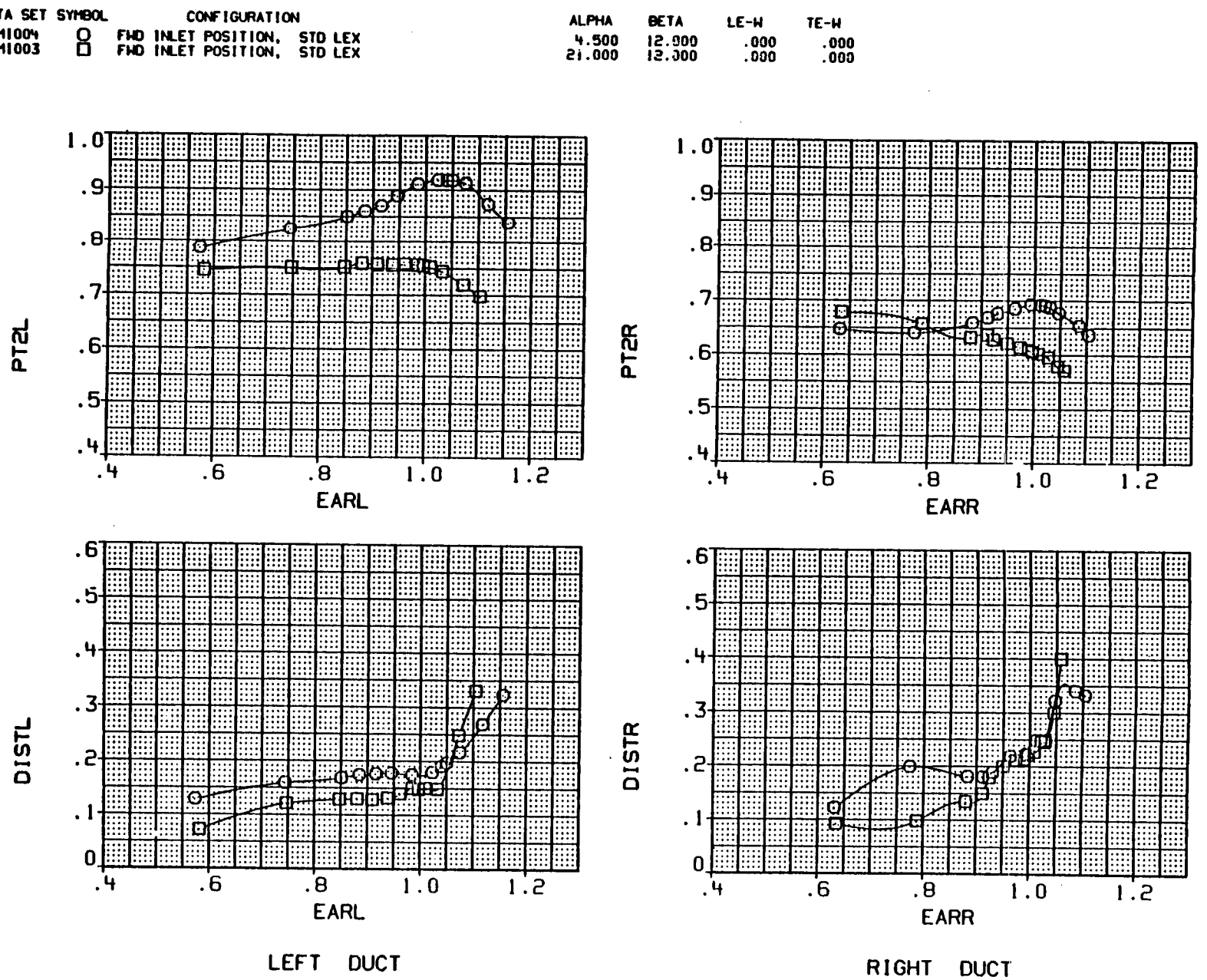

(u) Mach = 1.20.

Figure 8.- Continued.

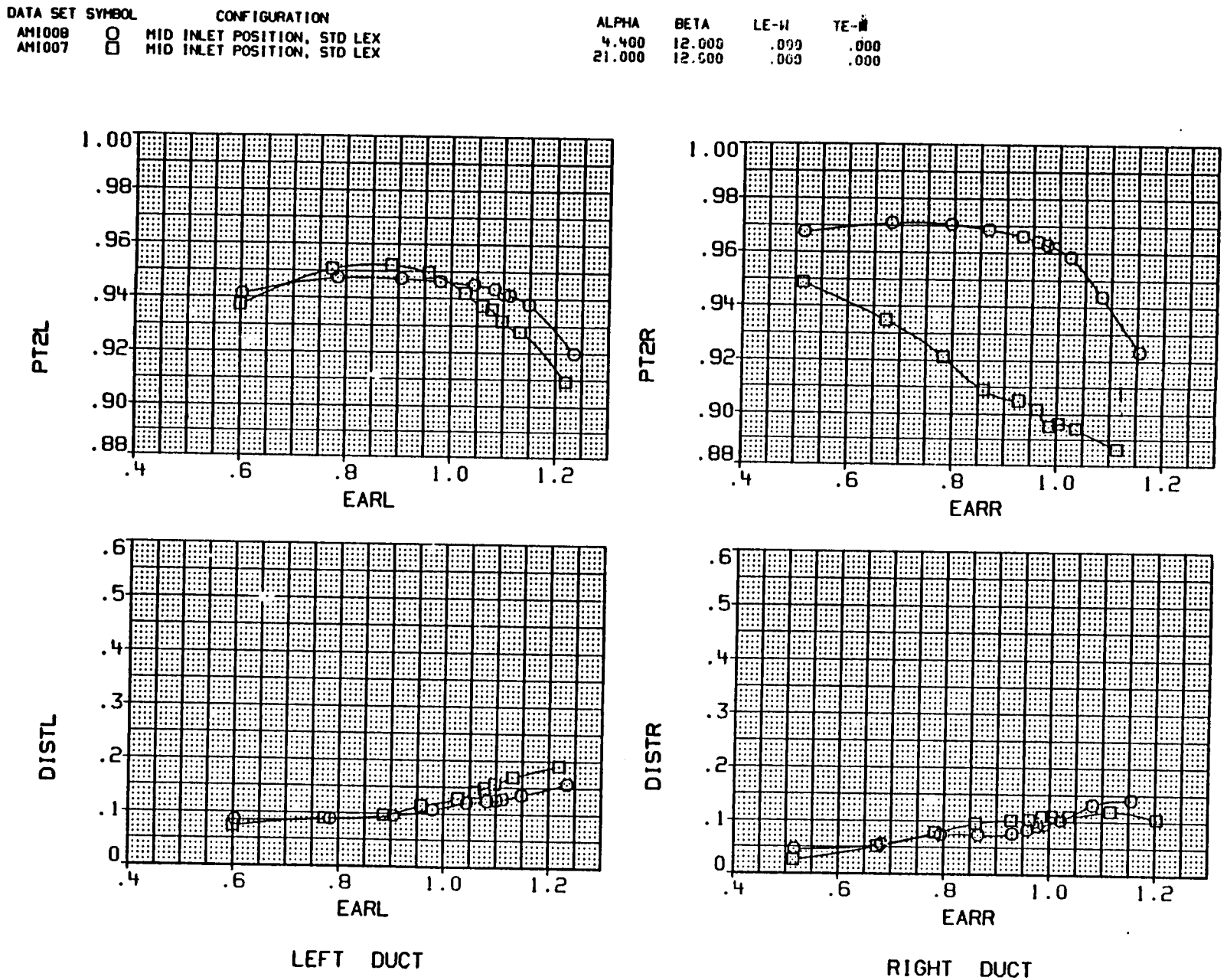

(v) Mach = 0.60.

Figure 8.- Continued.

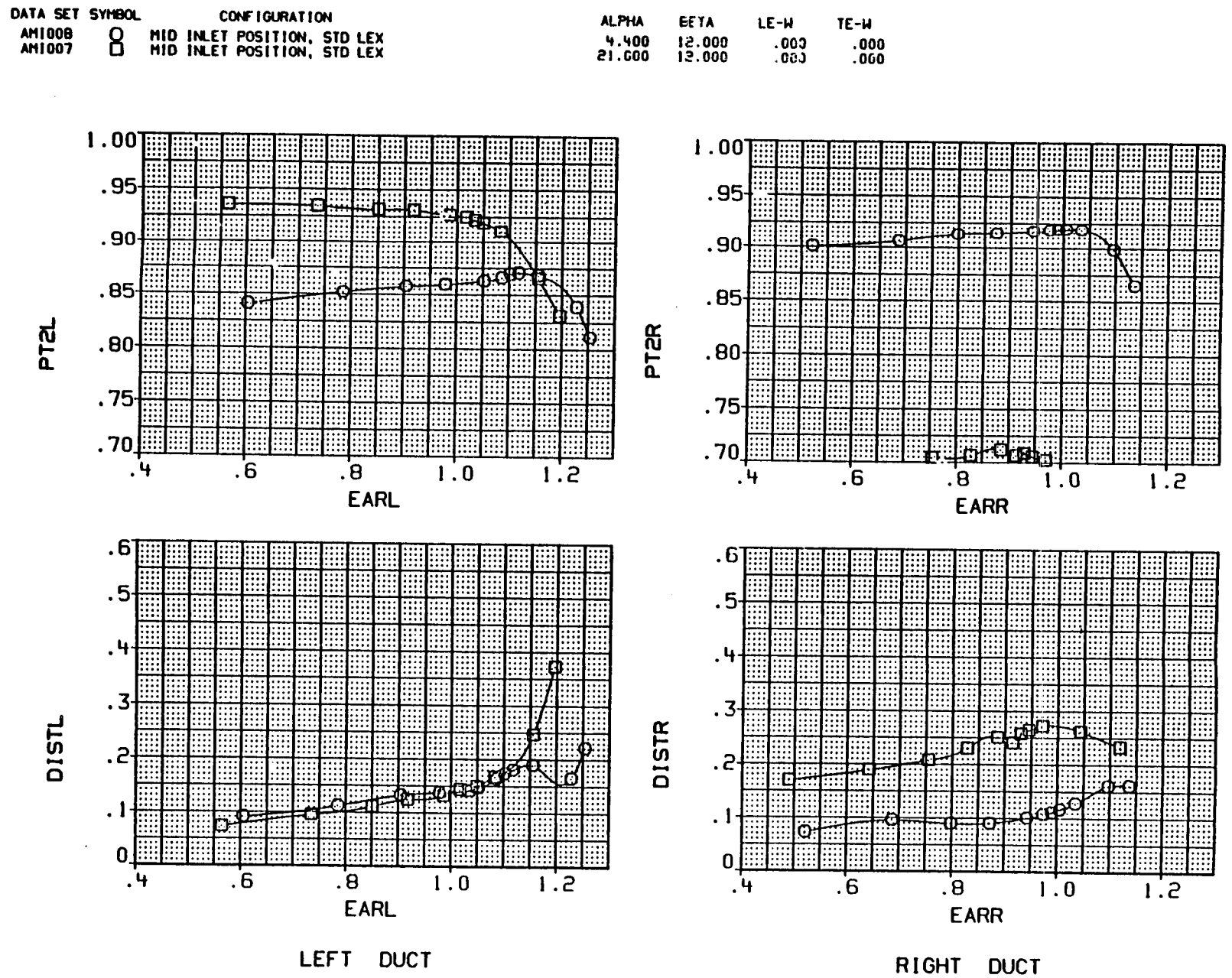

(w) Mach = 0.90.

Figure 8.- Continued.

DATA SET	SYMBOL	CONFIGURATION	ALPHA	BETA	LE-W	TE-W
AMI008	○	MID INLET POSITION, STD LEX	4.400	12.000	.000	.000
AMI007	□	MID INLET POSITION, STD LEX	21.000	12.000	.000	.000

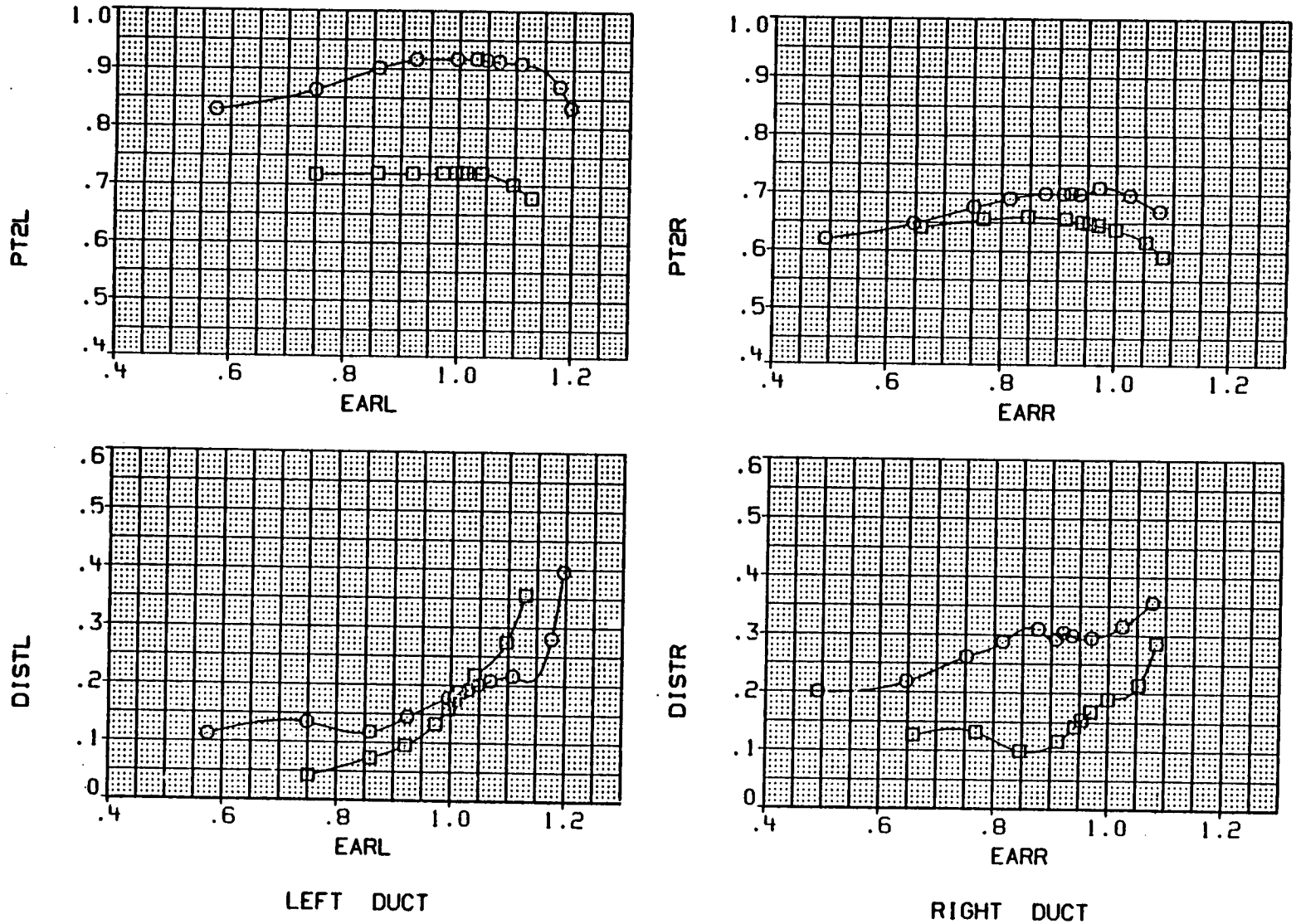

(x) Mach = 1.20.

Figure 8.- Continued.

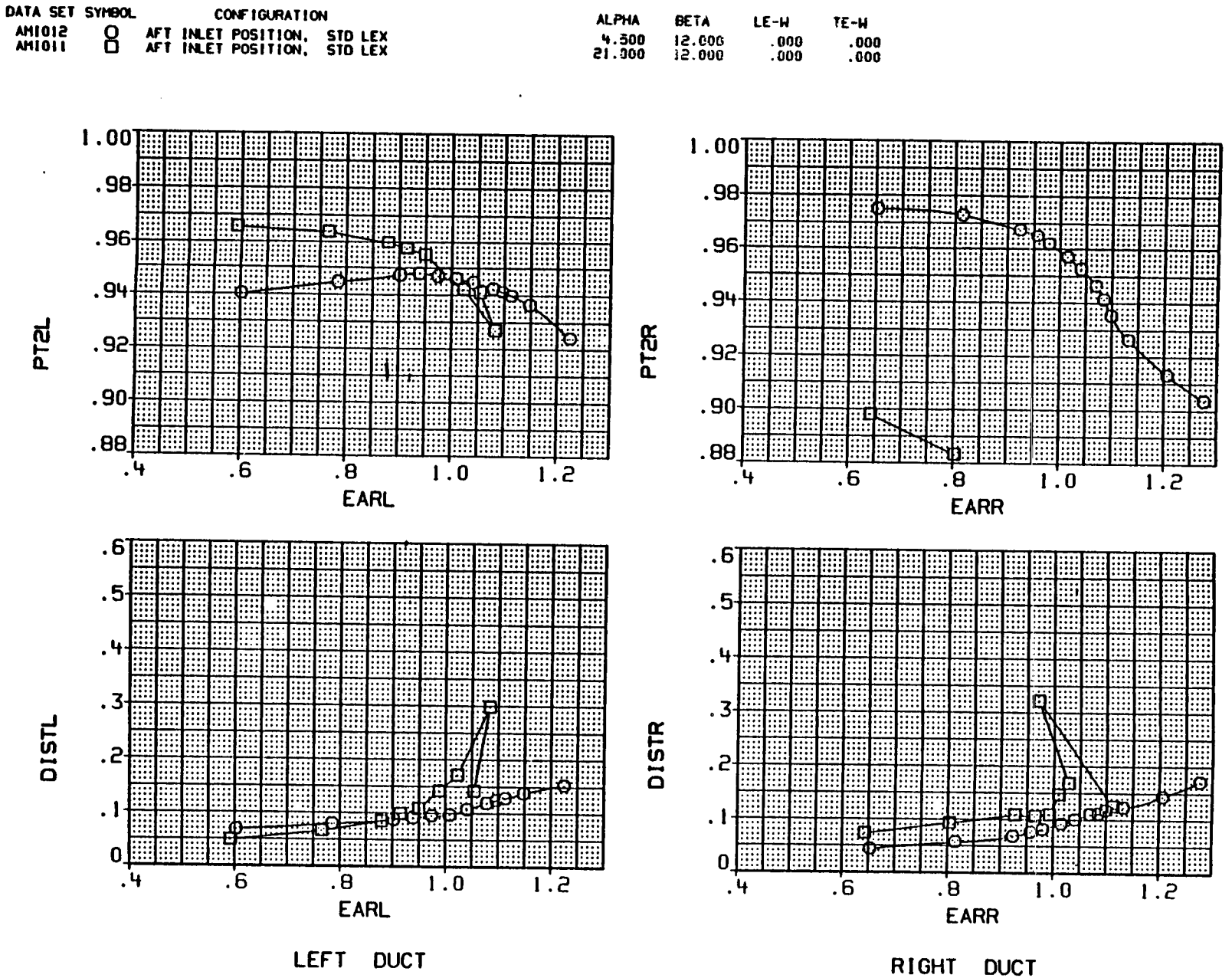

(y) Mach = 0.60.

Figure 8.- Continued.

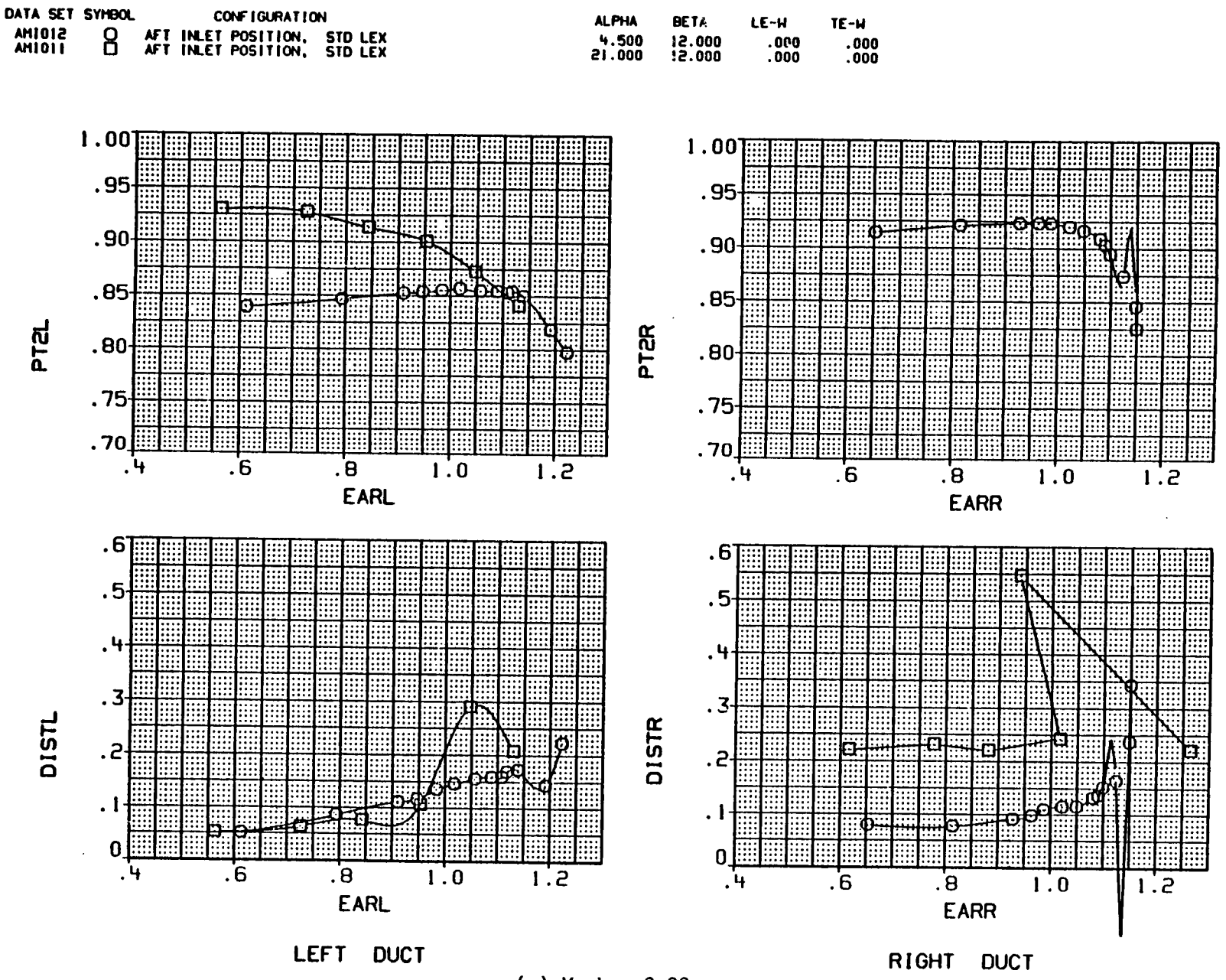

(z) Mach = 0.90.

Figure 8.- Continued.

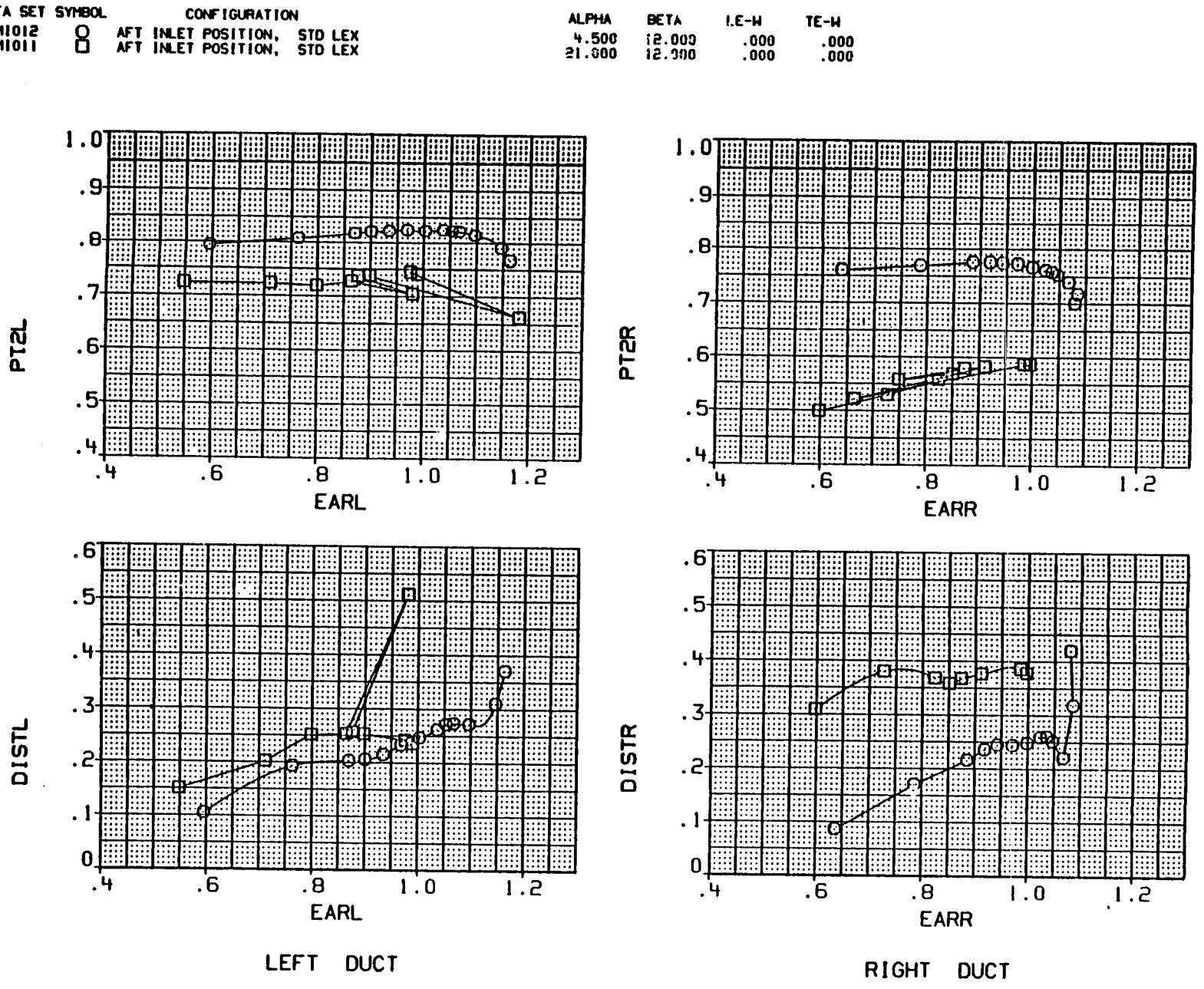

(aa) Mach = 1.20.

Figure 8.- Continued.

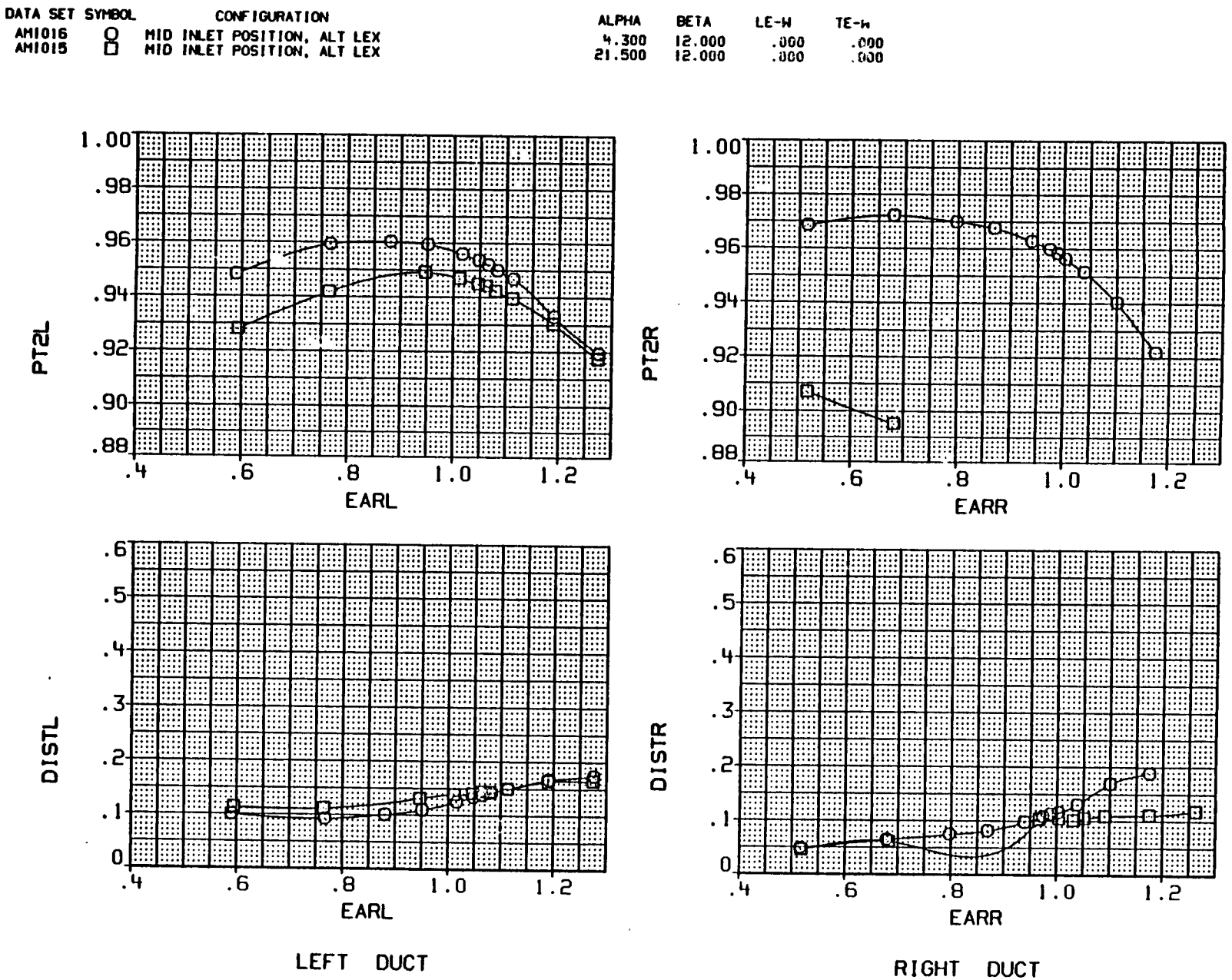

(bb) Mach = 0.60.

Figure 8.- Continued.

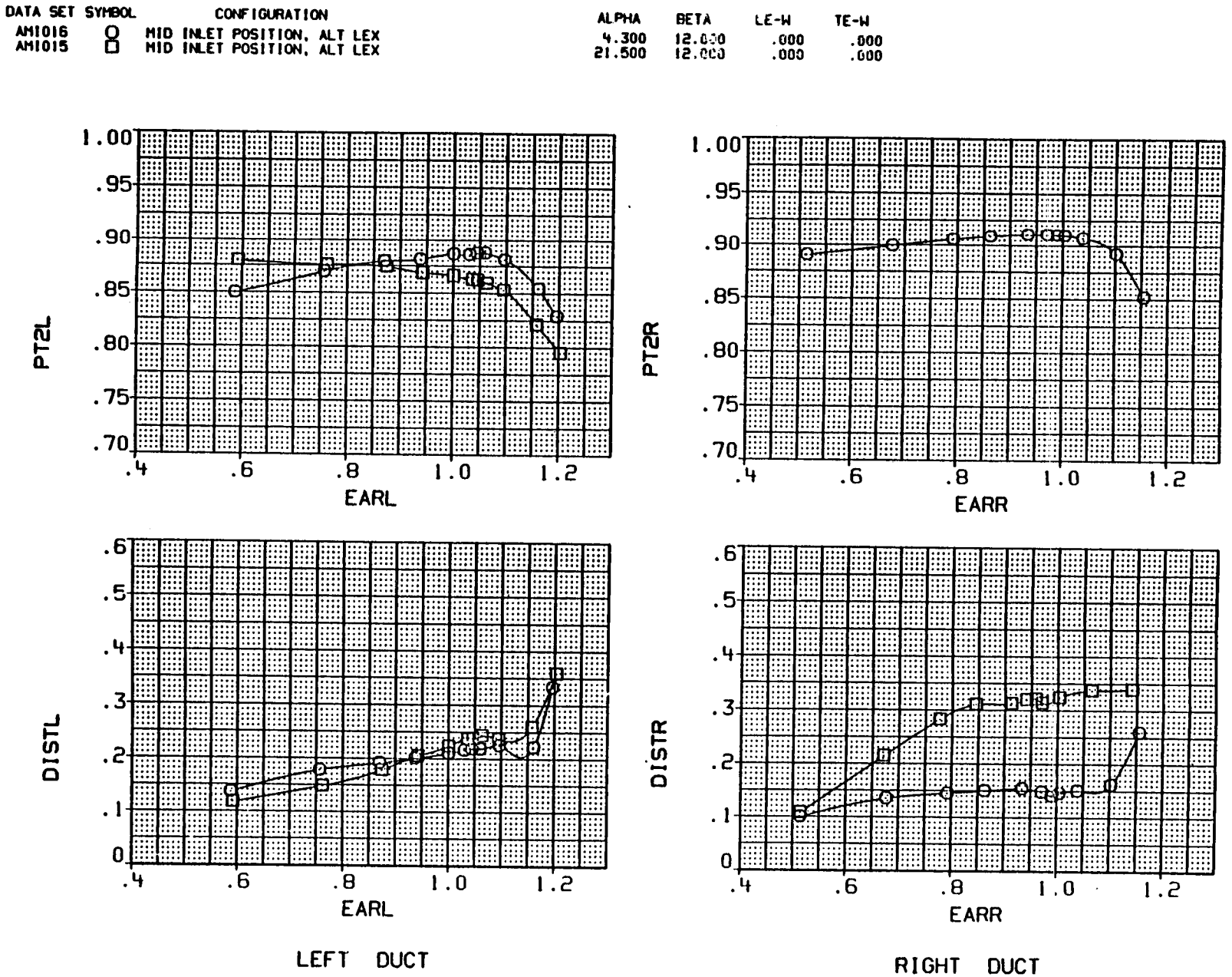

(cc) Mach = 0.90.

Figure 8.- Continued.

DATA SET	SYMBOL	CONFIGURATION
AM1016	○	MID INLET POSITION, ALT LEX
AM1015	□	MID INLET POSITION, ALT LEX

ALPHA	BETA	LE-W	TE-W
4.300	12.000	.000	.000
21.500	12.000	.000	.000

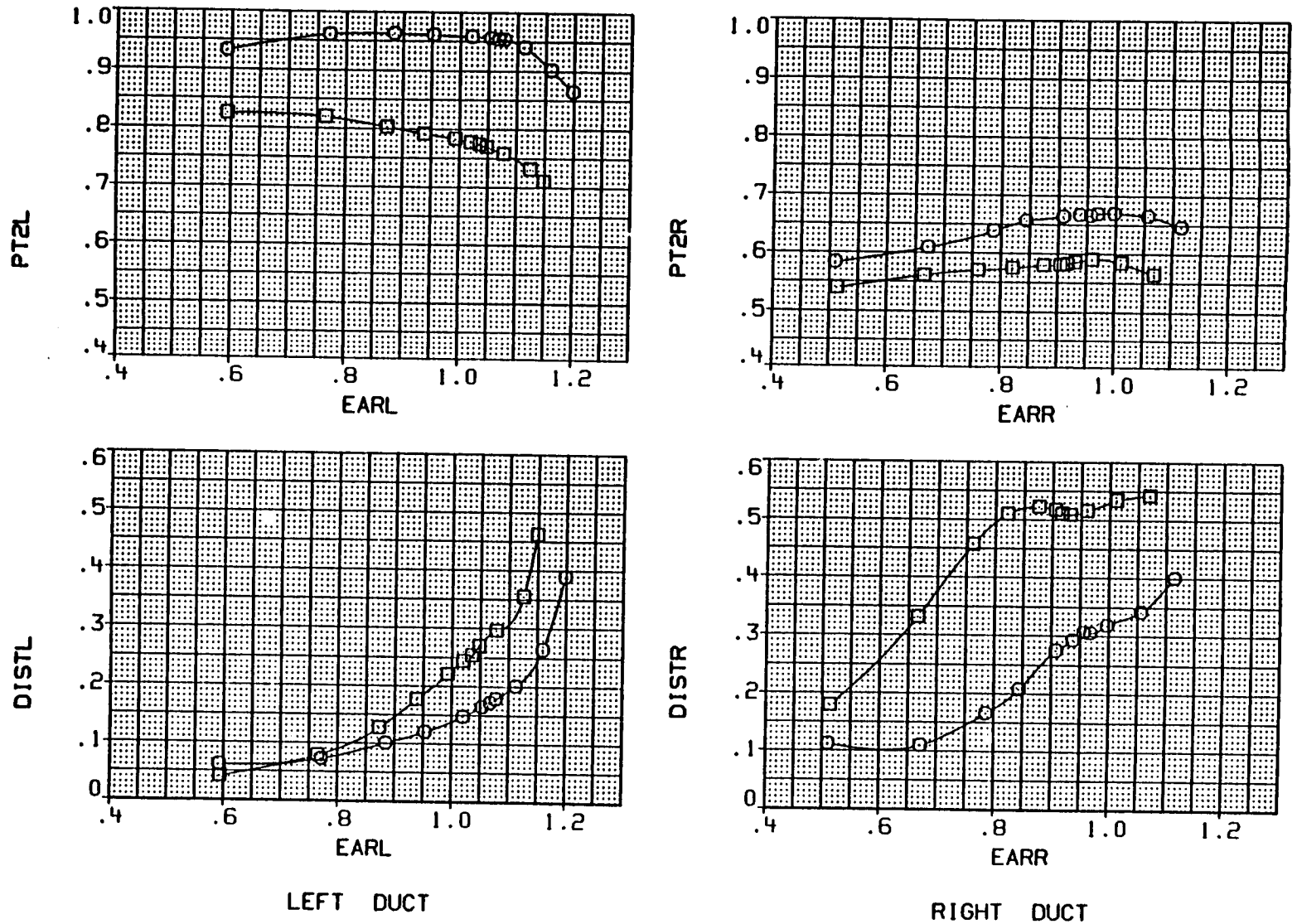

(dd) Mach = 1.20.

Figure 8.- Continued.

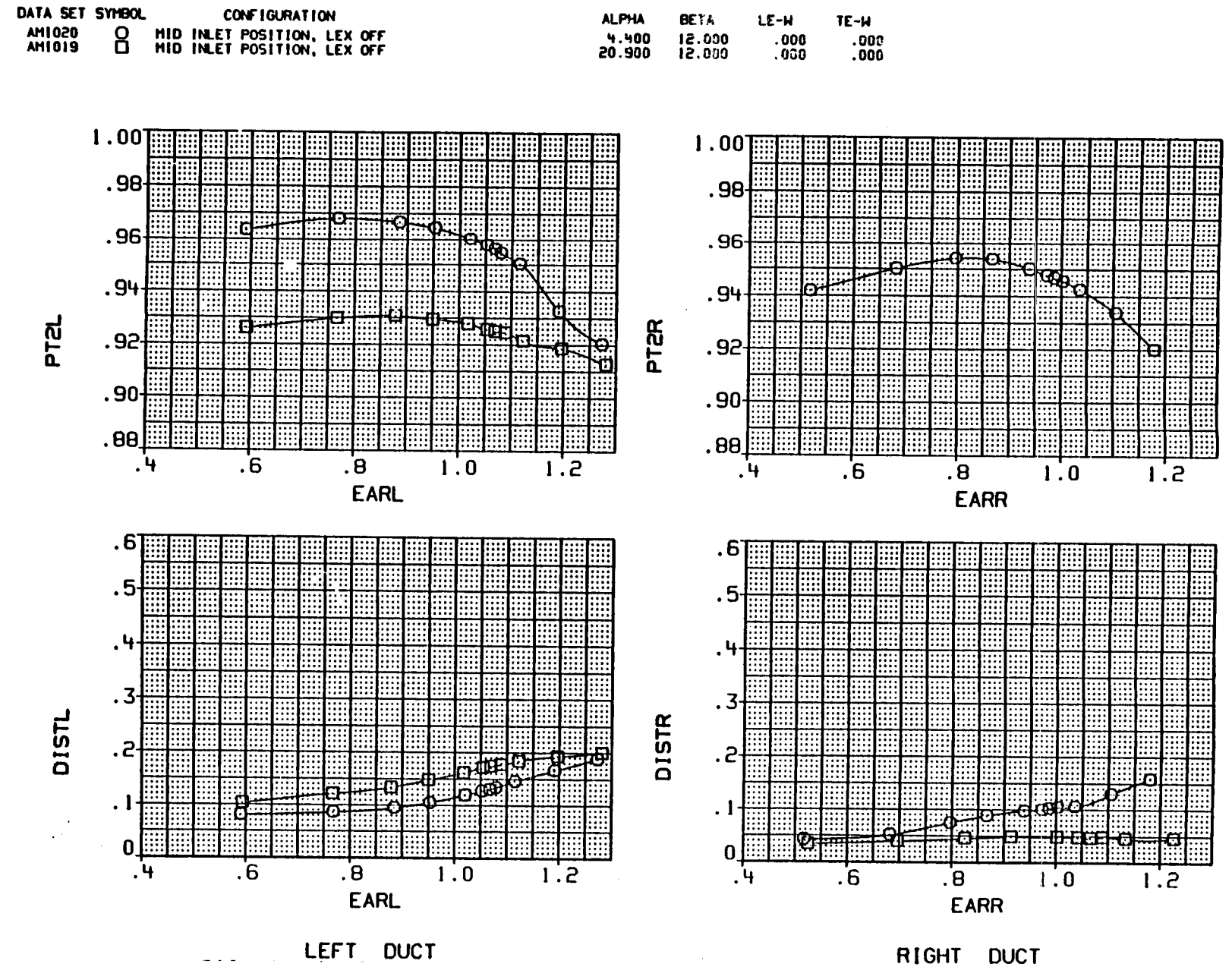

(ee) Mach = 0.60.

Figure 8.- Continued.

DATA SET	SYMBOL	CONFIGURATION	ALPHA	BETA	LE-W	TE-W
AM1020	○	MID INLET POSITION, LEX OFF	4.400	12.000	.000	.000
AM1019	□	MID INLET POSITION, LEX OFF	20.900	12.000	.000	.000

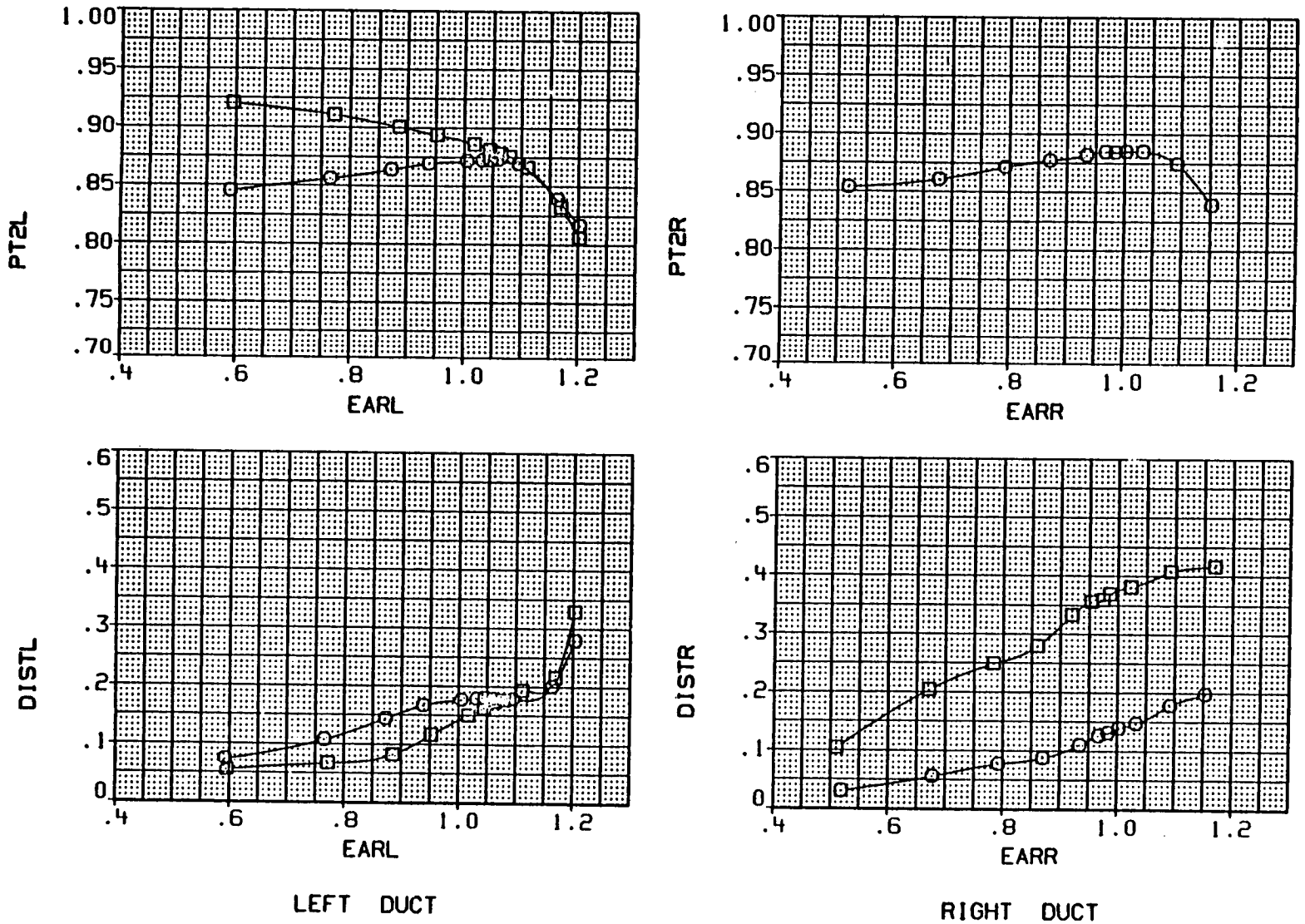

(ff) Mach = 0.90.

Figure 8.- Continued.

DATA SET	SYMBOL	CONFIGURATION	ALPHA	BETA	LE-H	TE-H
AM1020	○	MID INLET POSITION, LEX OFF	4.400	12.000	.000	.000
AM1019	□	MID INLET POSITION, LEX OFF	20.900	12.000	.000	.000

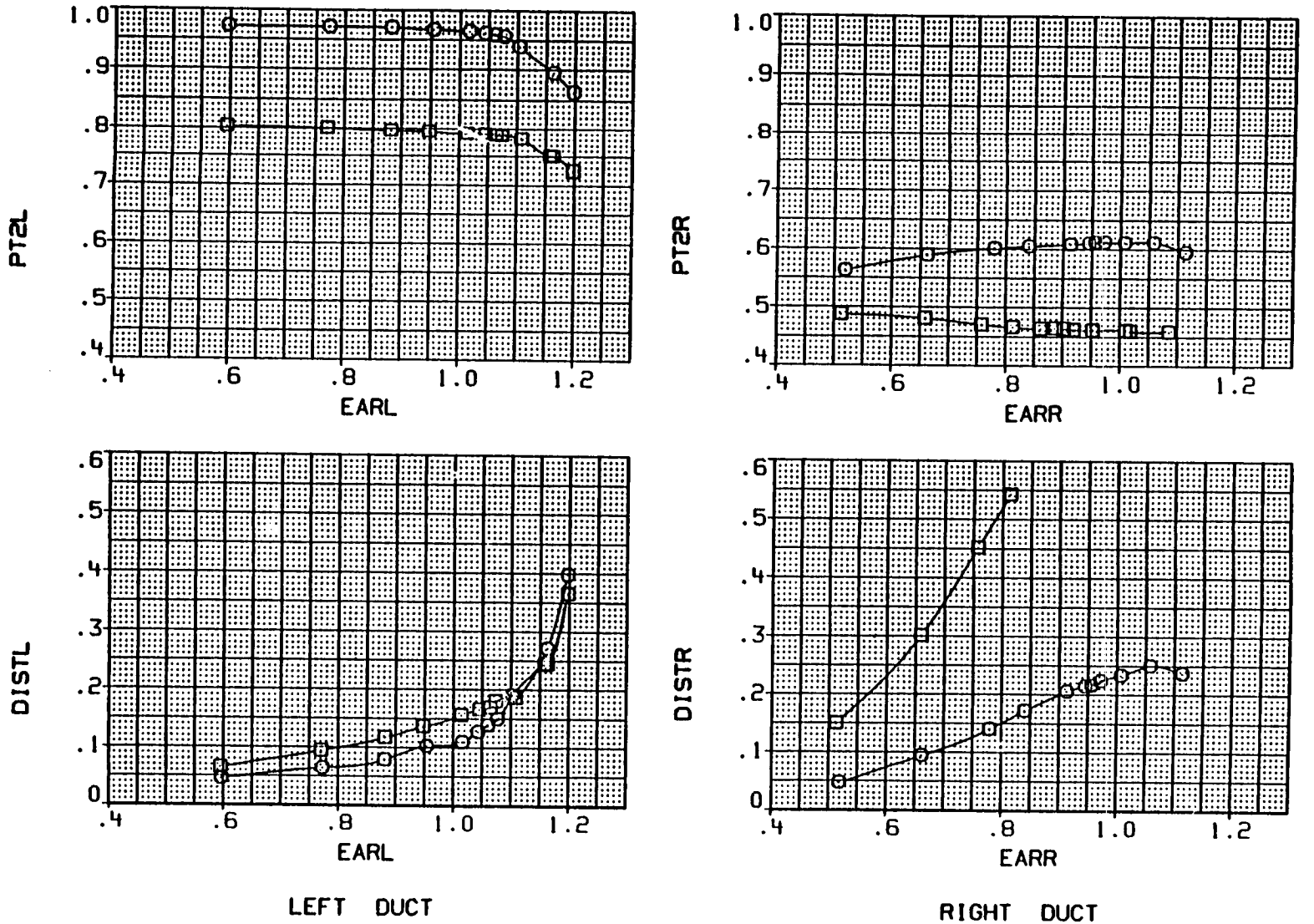

(gg) Mach = 1.20.

Figure 8.- Continued.

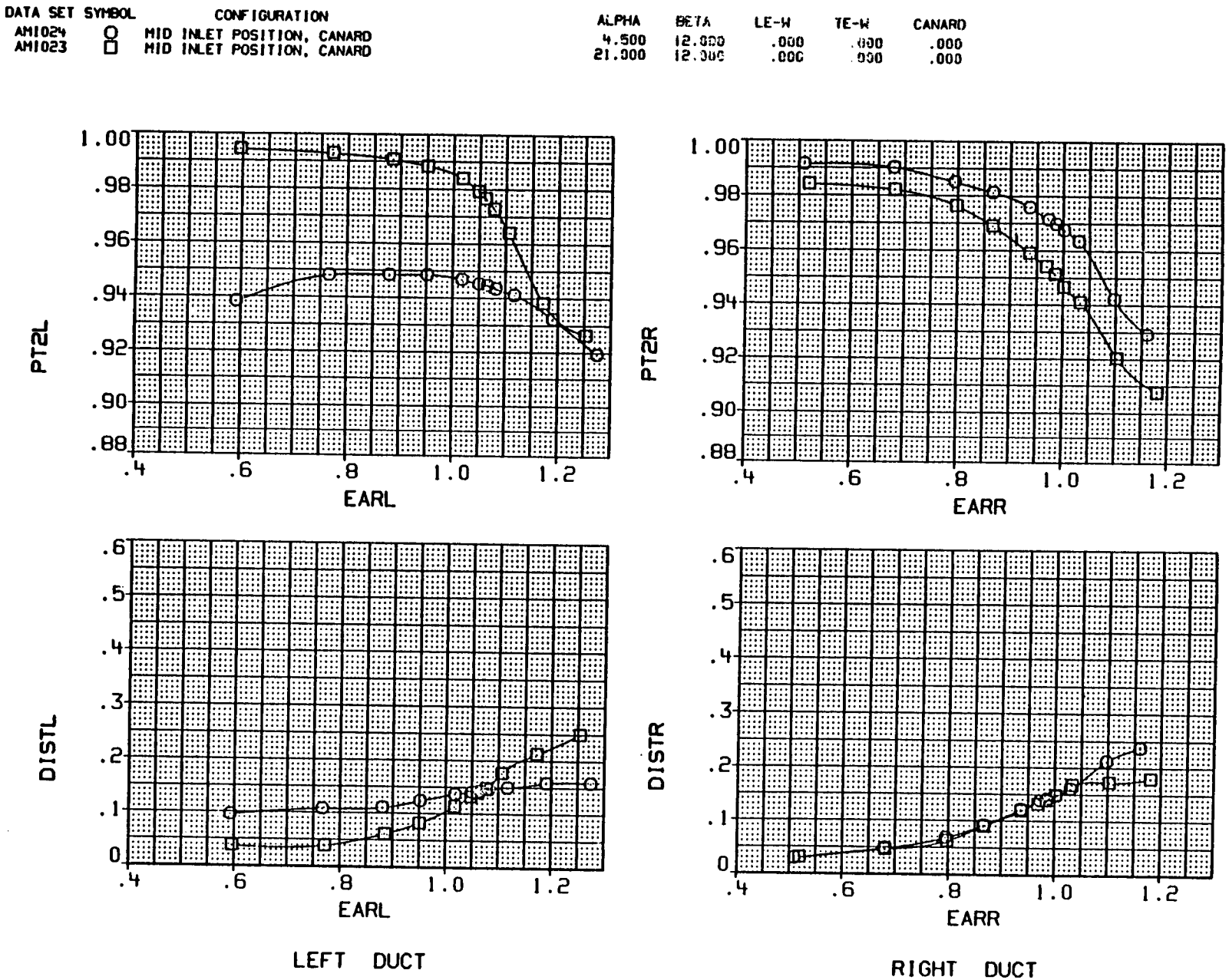

(hh) Mach = 0.60.

Figure 8.- Continued.

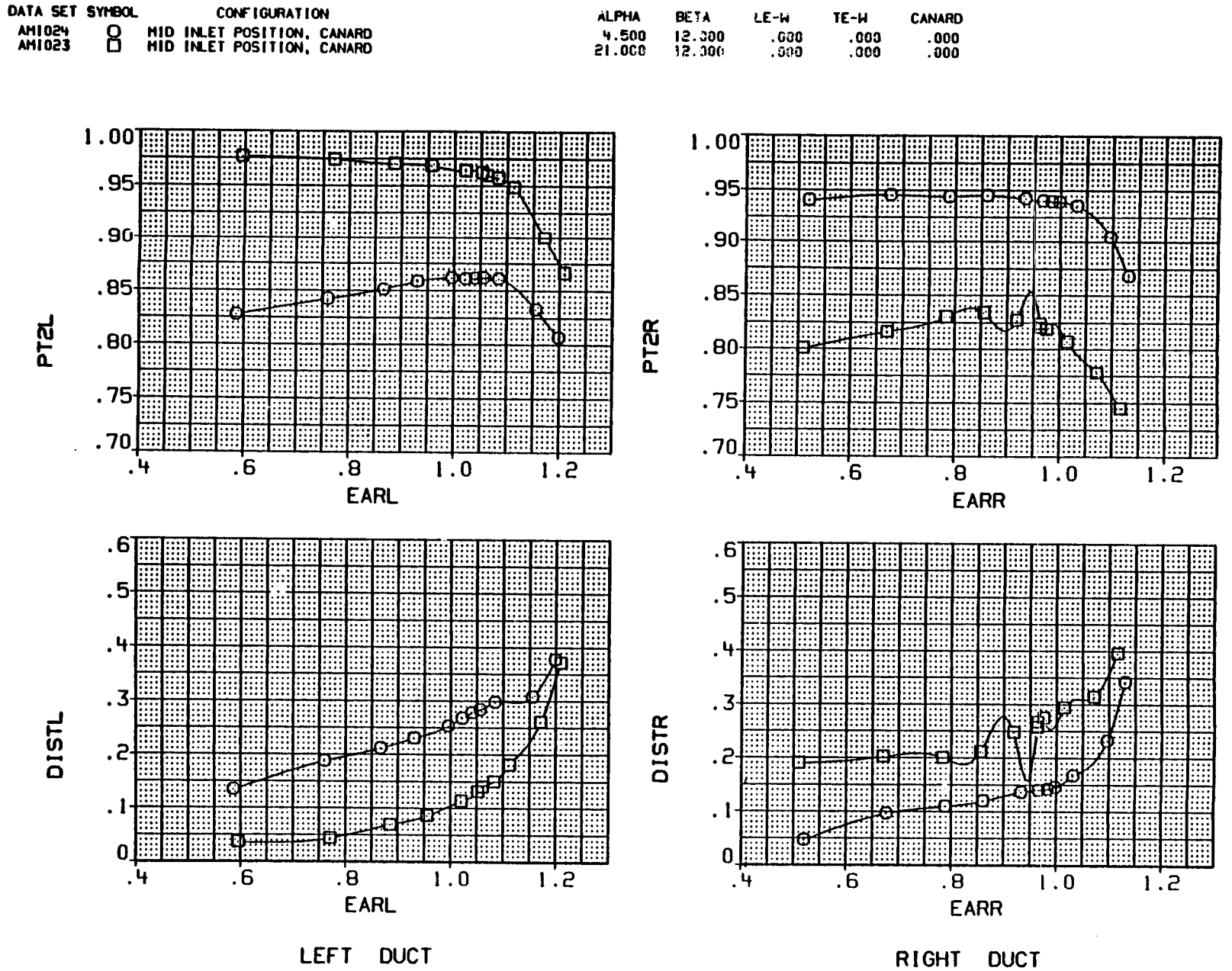

(ii) Mach = 0.90.

Figure 8.- Continued.

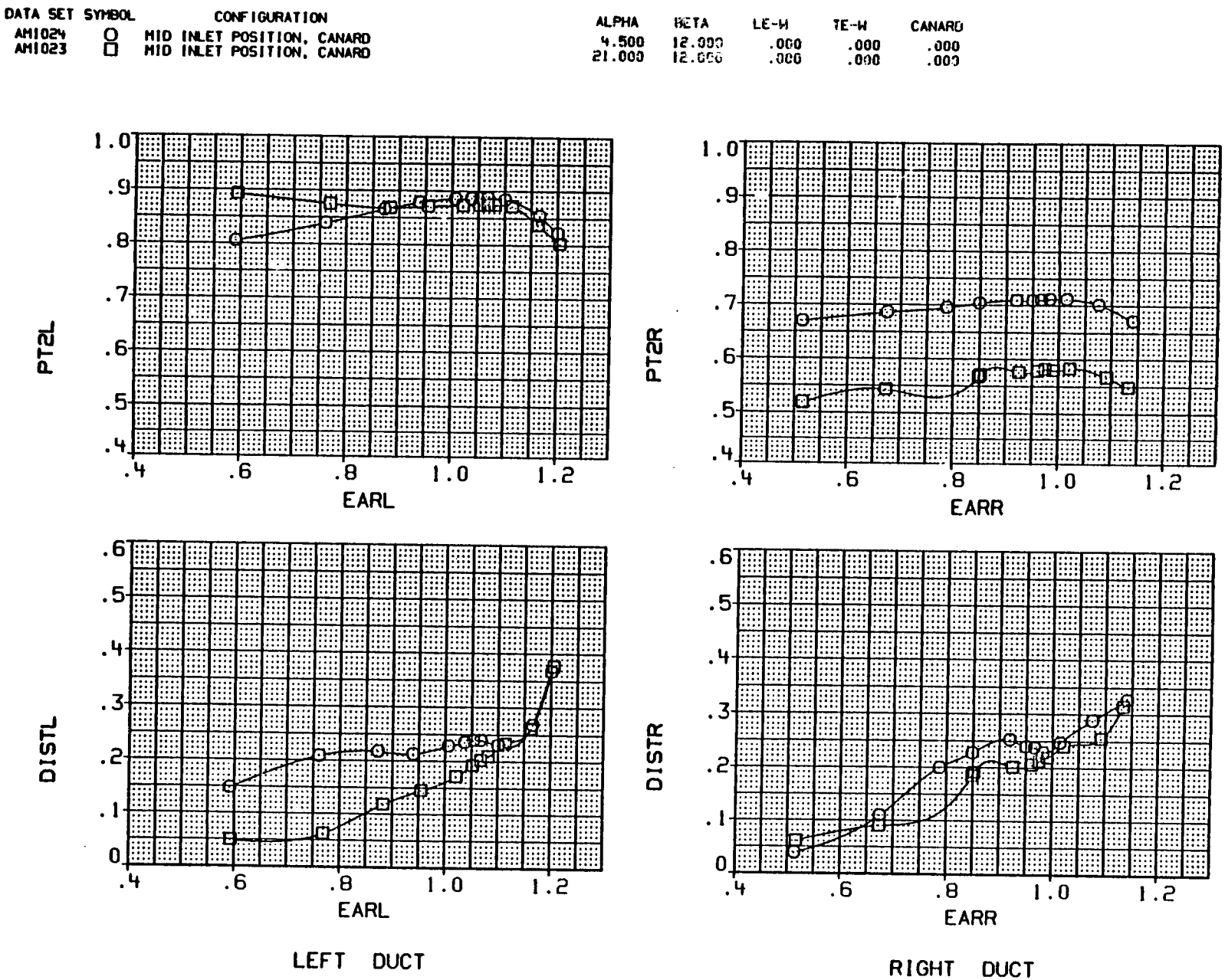

(jj) Mach = 1.20.

Figure 8.- Concluded.

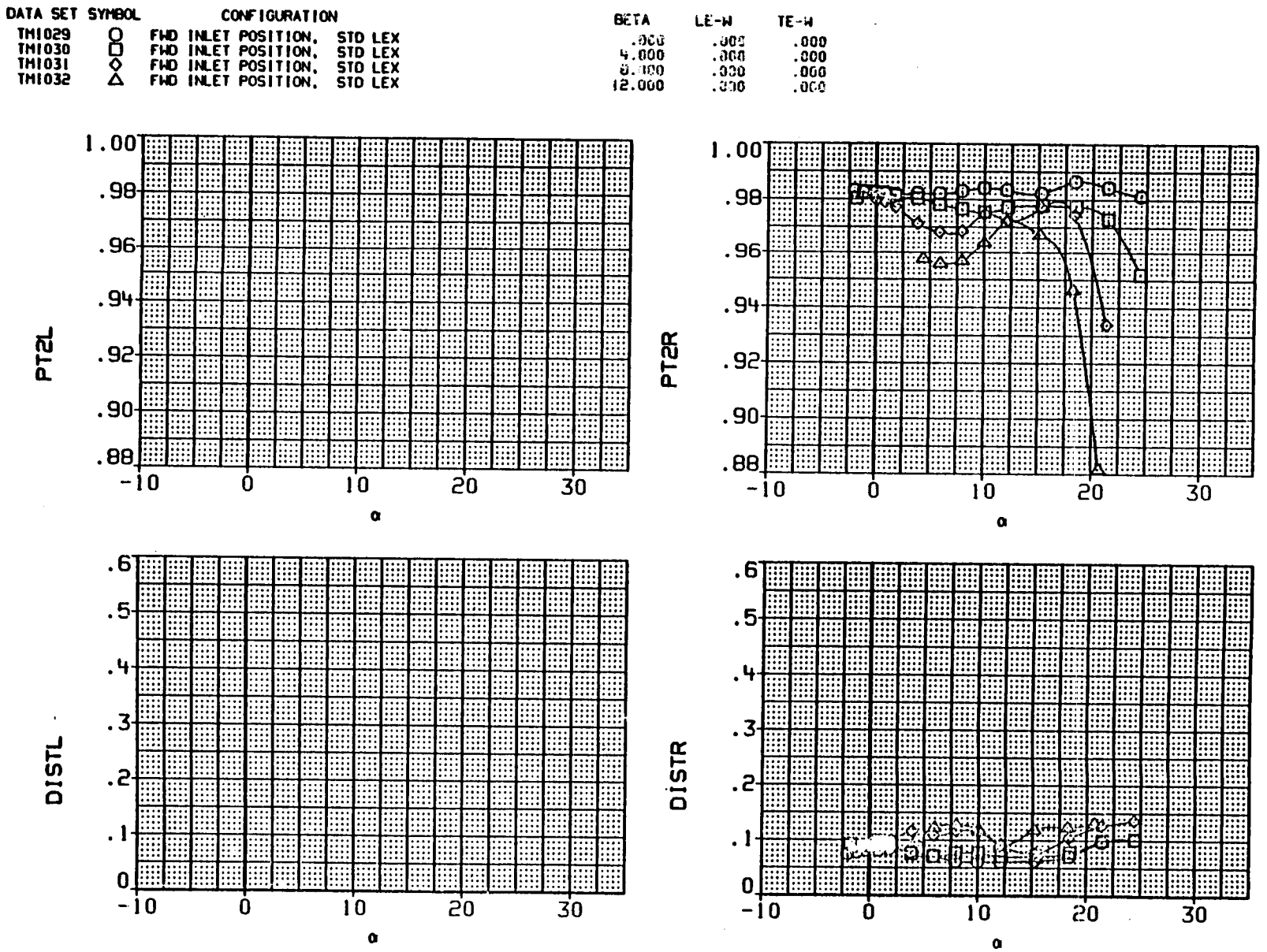

LEFT DUCT - MAX ENGINE AIRFLOW RIGHT DUCT - MAX ENGINE AIRFLOW

FIG. 9 - EFFECT OF ANGLE OF ATTACK ON INLET PERFORMANCE

37

(a) Mach = 0.60.

Figure 9.- Effect of angle of attack on inlet performance.

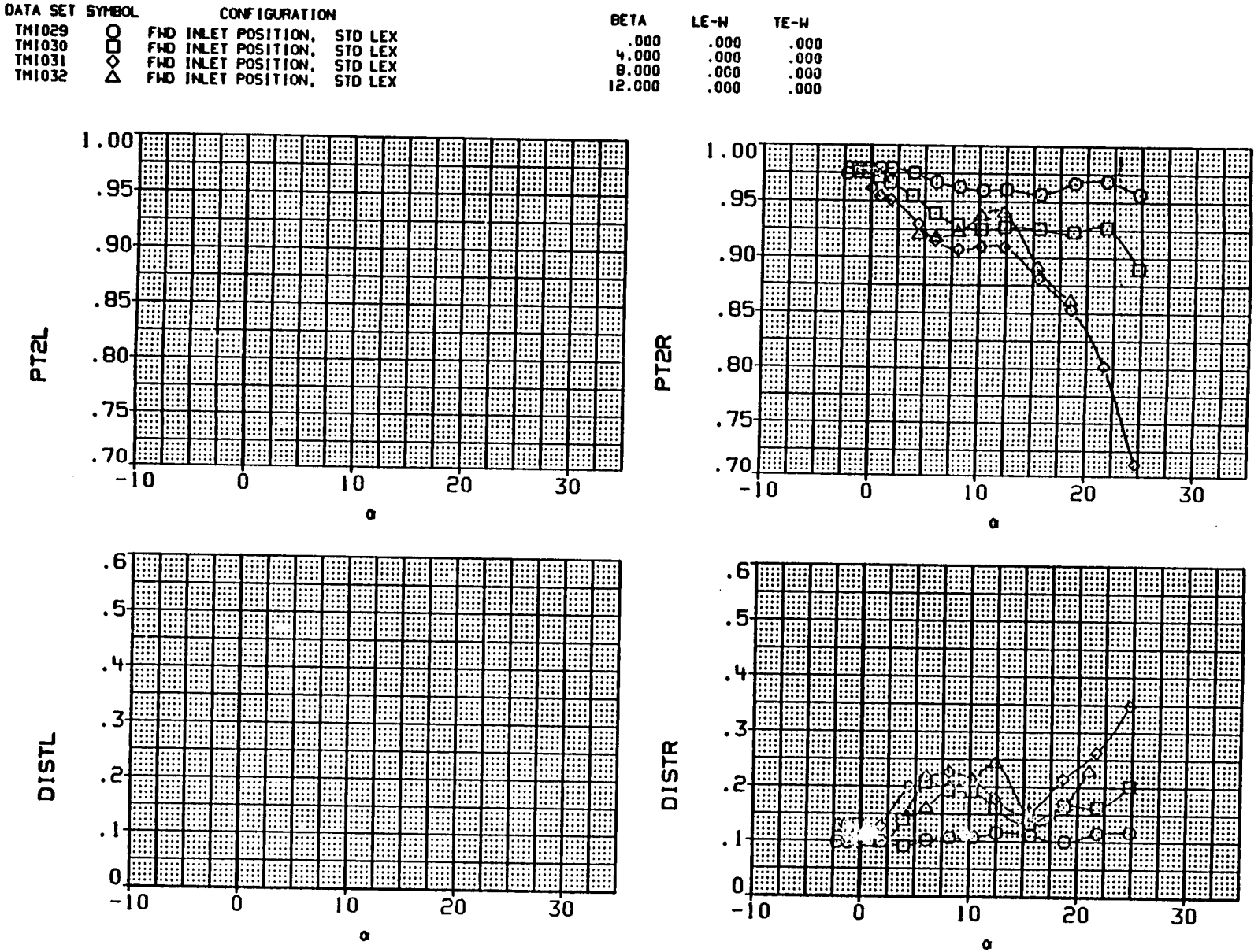

(b) Mach = 0.90.

Figure 9.- Continued.

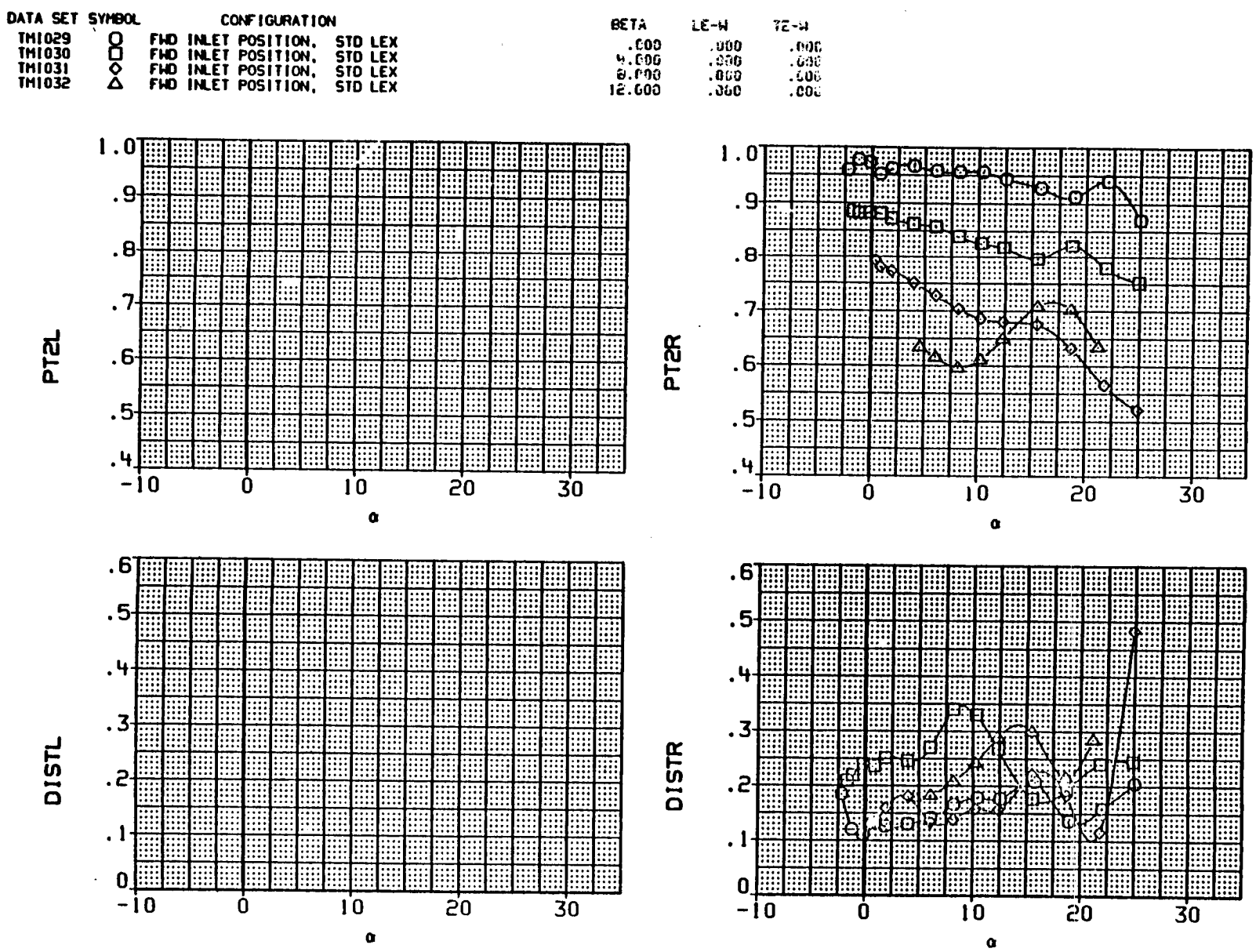

(c) Mach = 1.20.

Figure 9.- Continued.

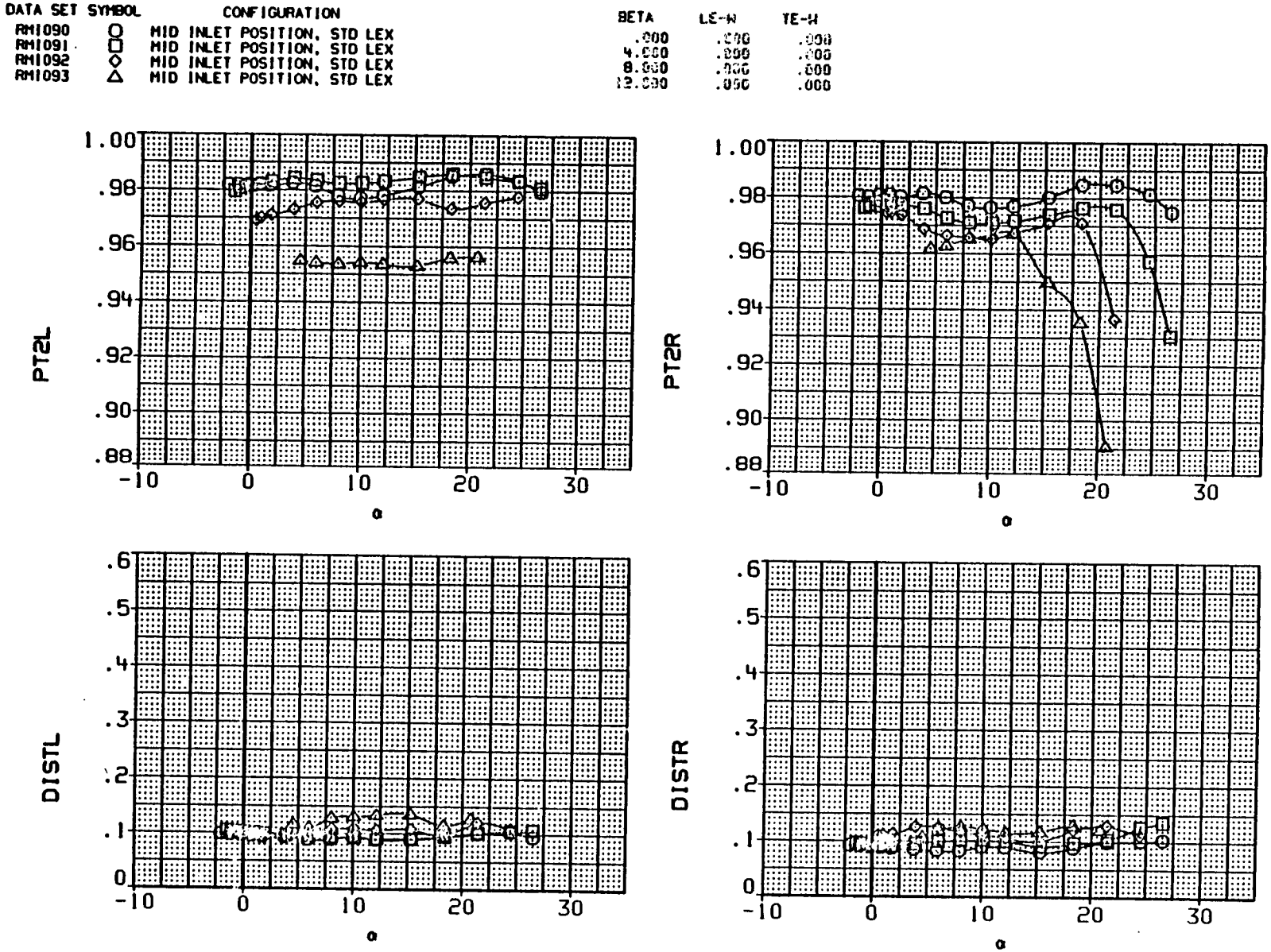

LEFT DUCT - MAX ENGINE AIRFLOW

RIGHT DUCT - MAX ENGINE AIRFLOW

(d) Mach = 0.60.

Figure 9.- Continued.

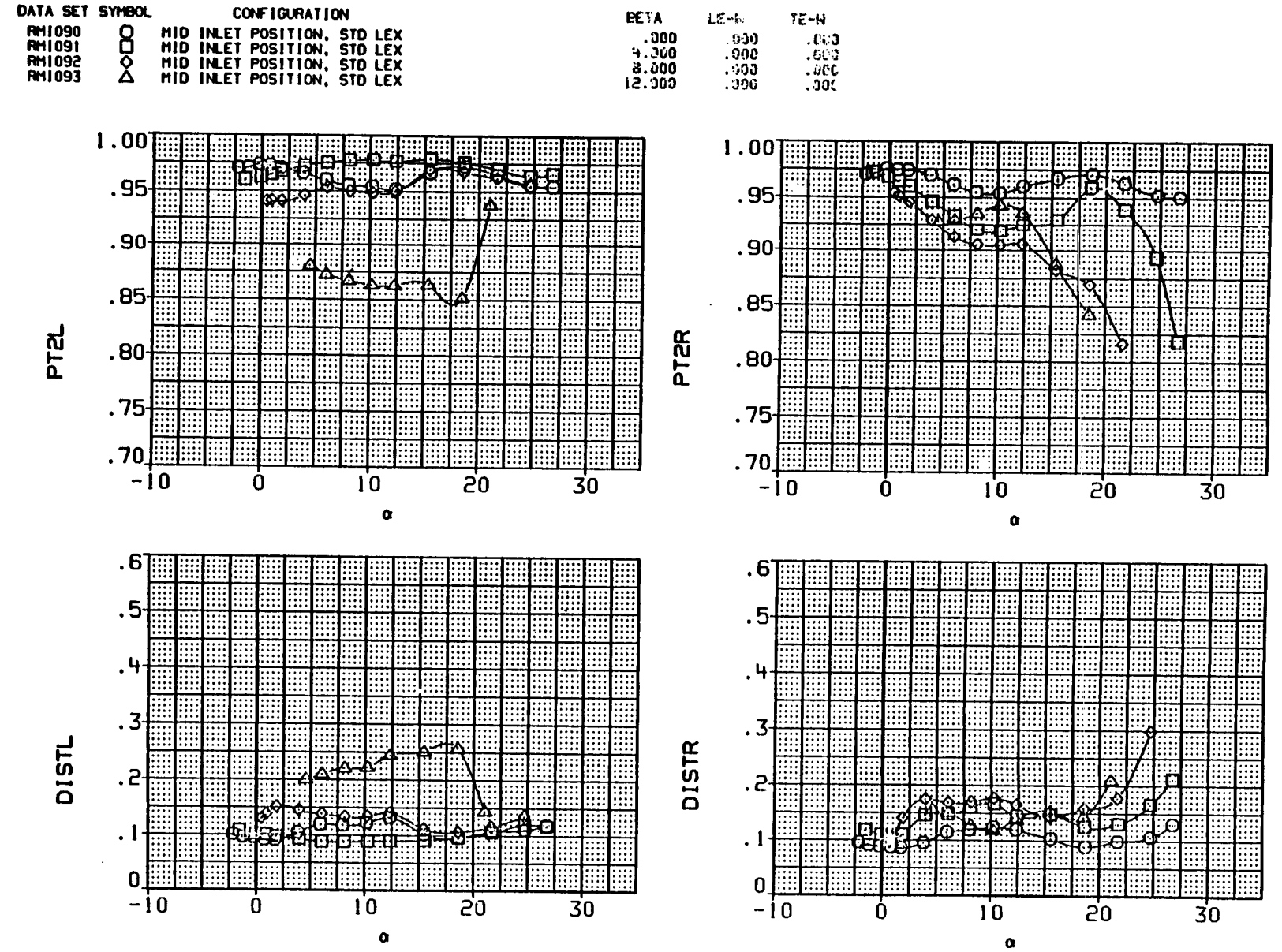

LEFT DUCT - MAX ENGINE AIRFLOW

RIGHT DUCT - MAX ENGINE AIRFLOW

(e) Mach = 0.90.

Figure 9.- Continued.

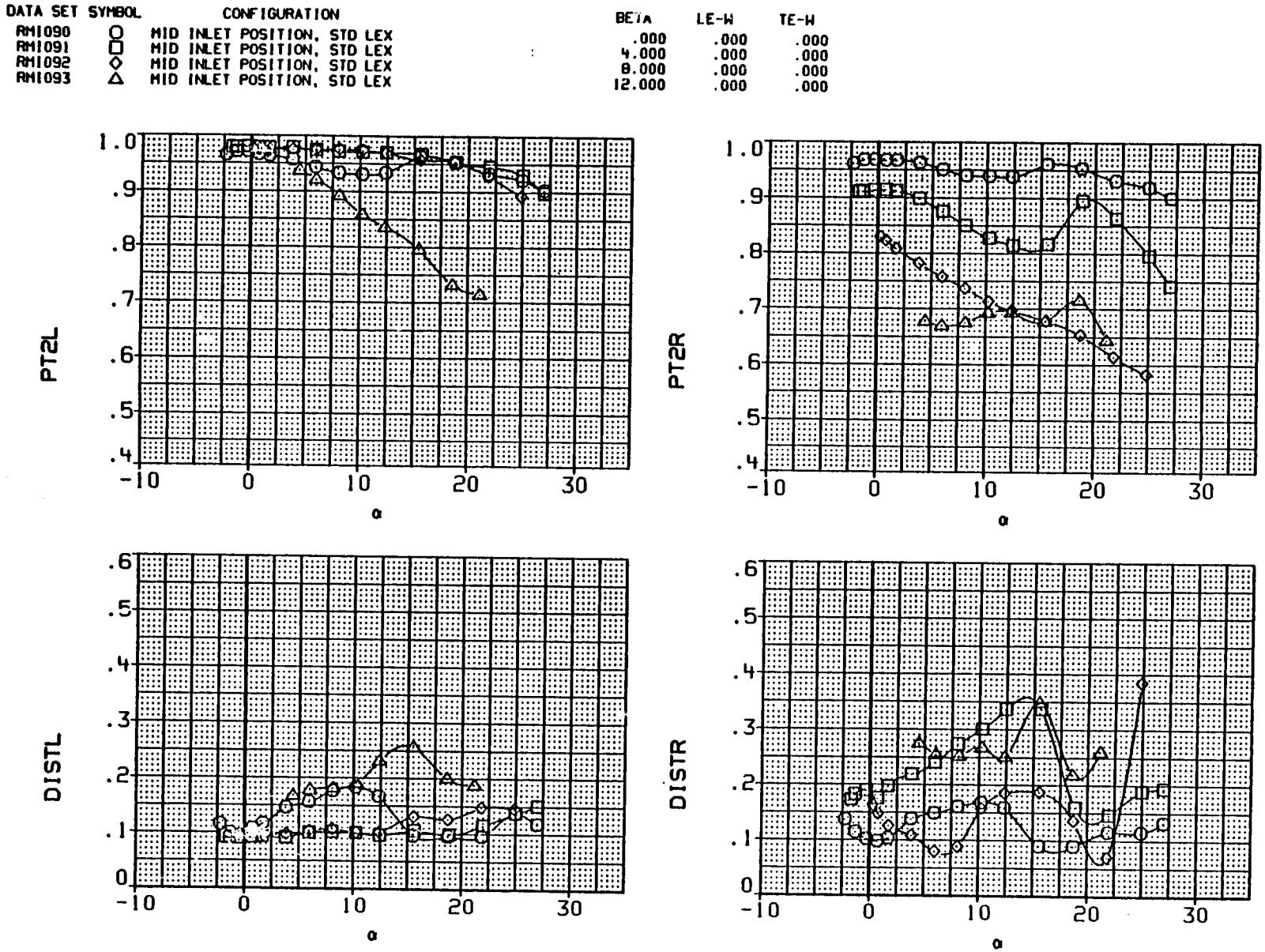

(f) Mach = 1.20.

Figure 9.- Continued.

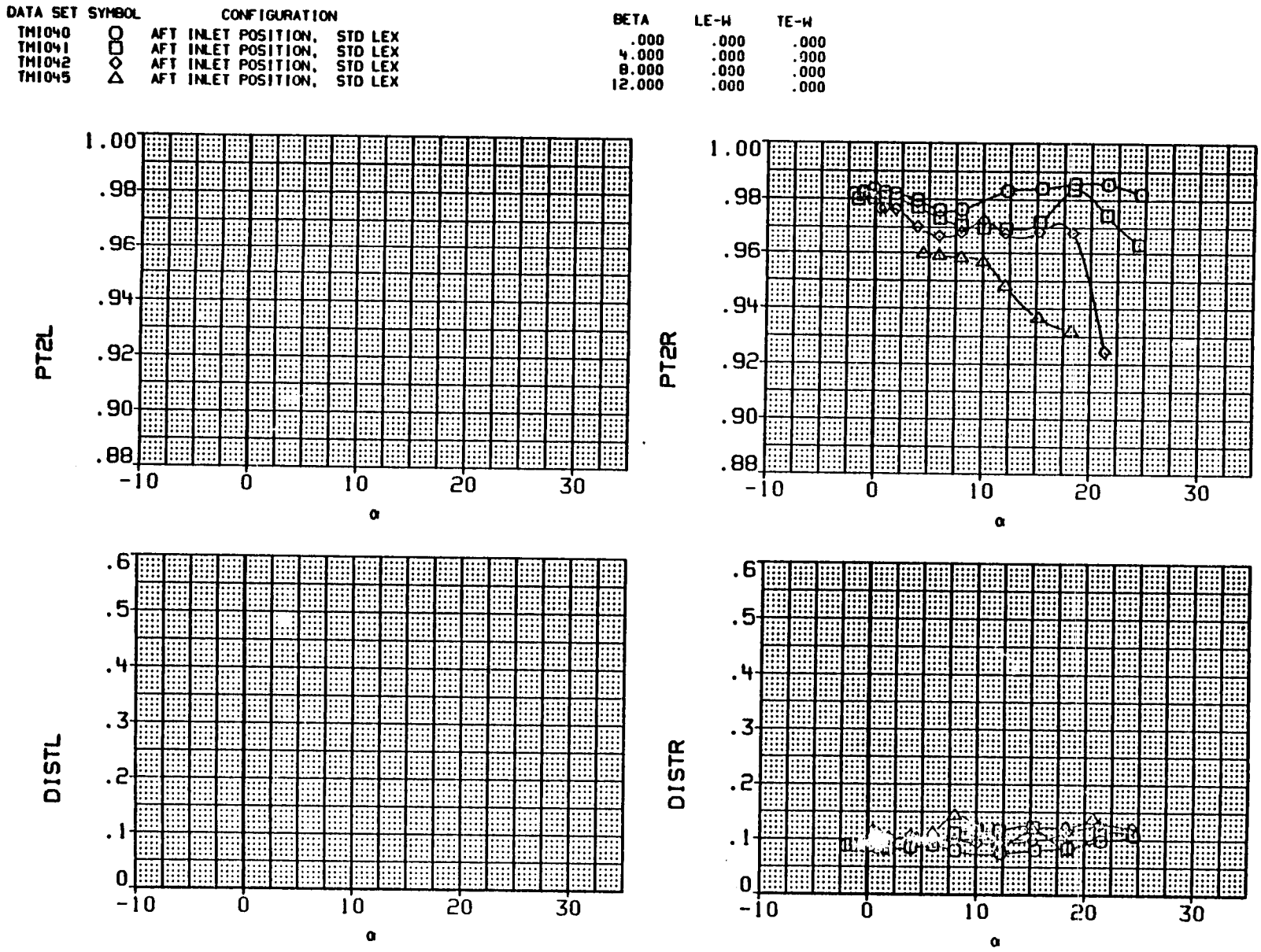

(g) Mach = 0.60.

Figure 9.- Continued.

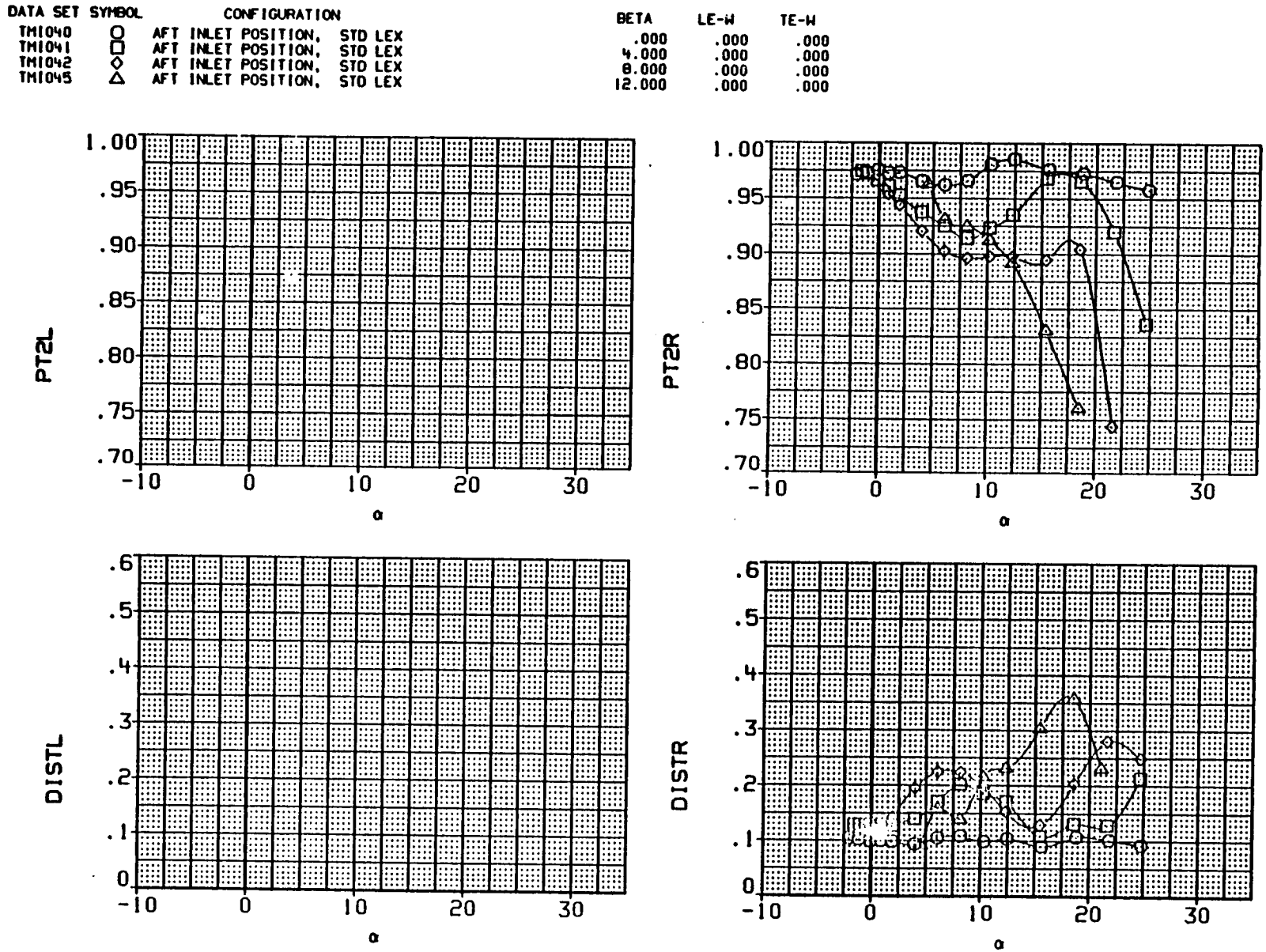

LEFT DUCT - MAX ENGINE AIRFLOW RIGHT DUCT - MAX ENGINE AIRFLOW

(h) Mach = 0.90.

Figure 9.- Continued.

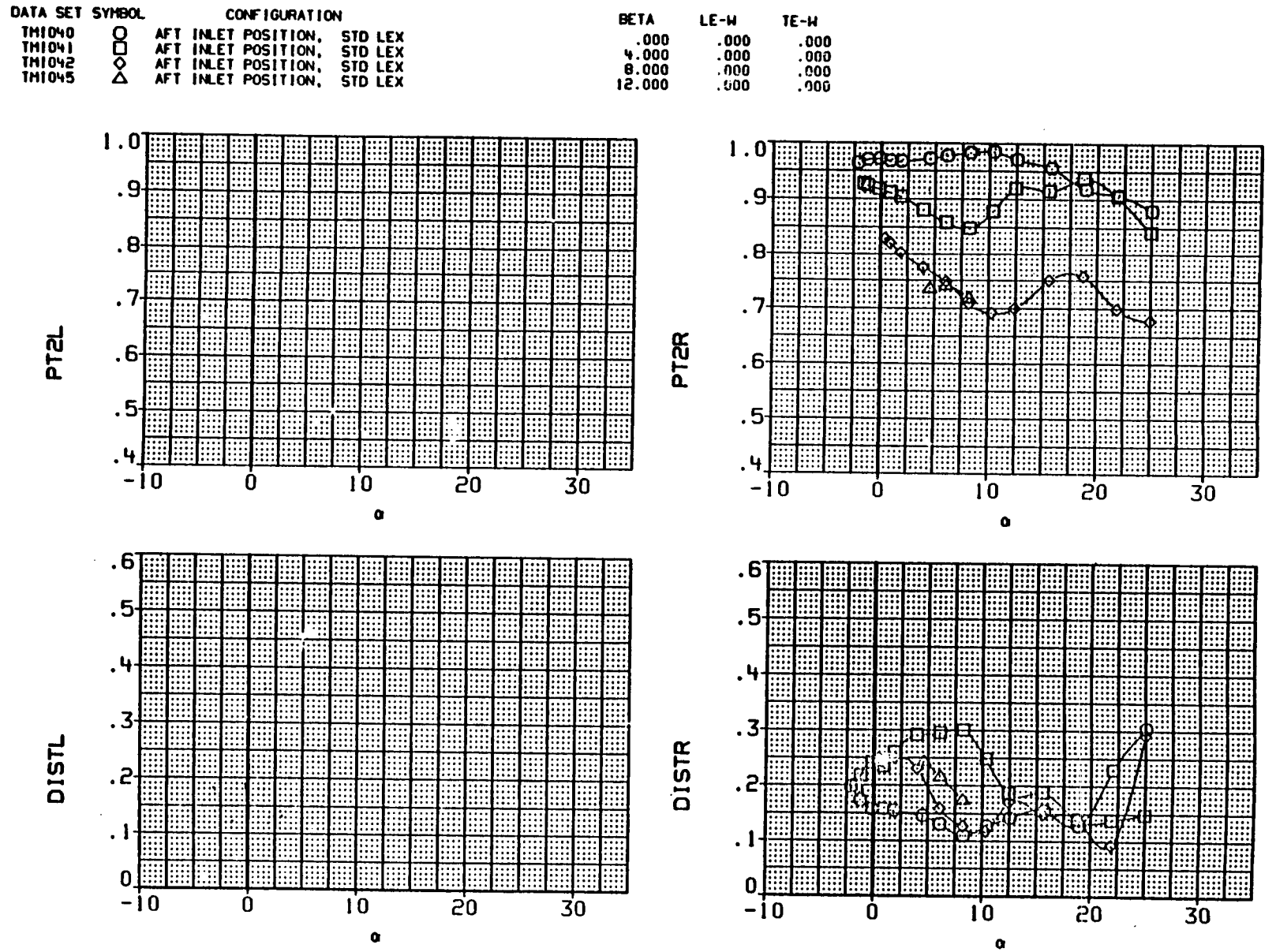

(i) Mach = 1.20.

Figure 9.- Continued.

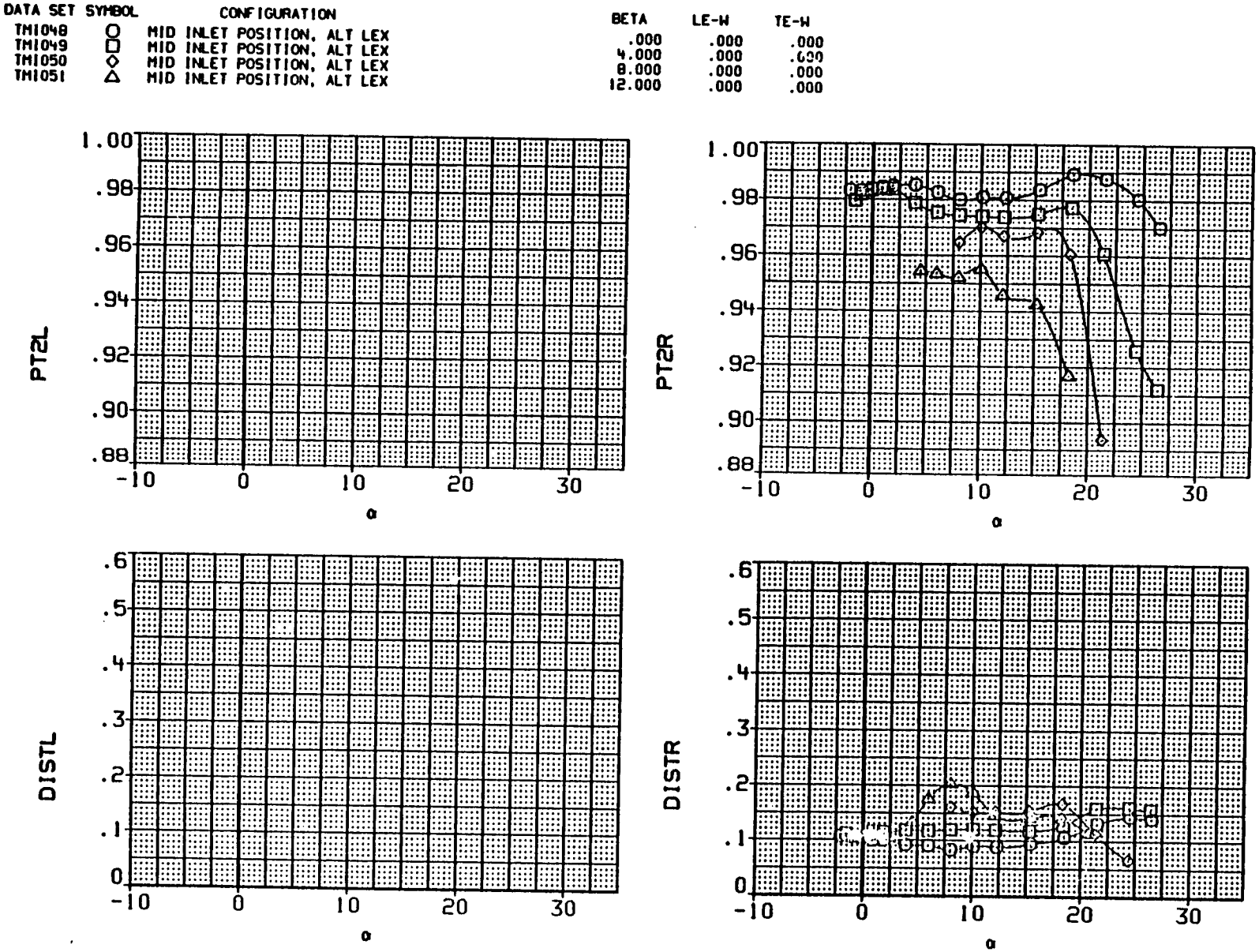

(j) Mach = 0.60.

Figure 9.- Continued.

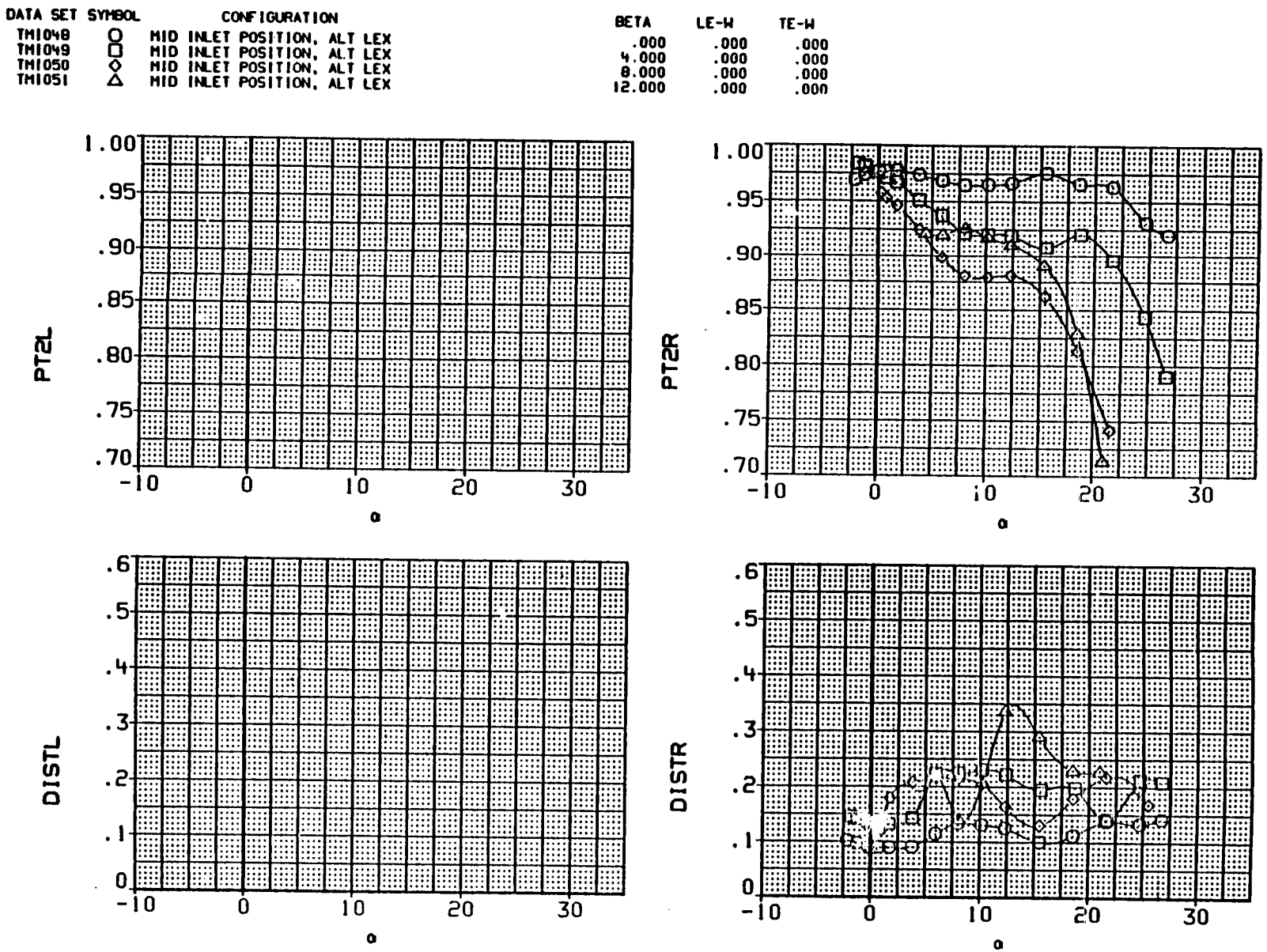

(k) Mach = 0.90.

Figure 9.- Continued.

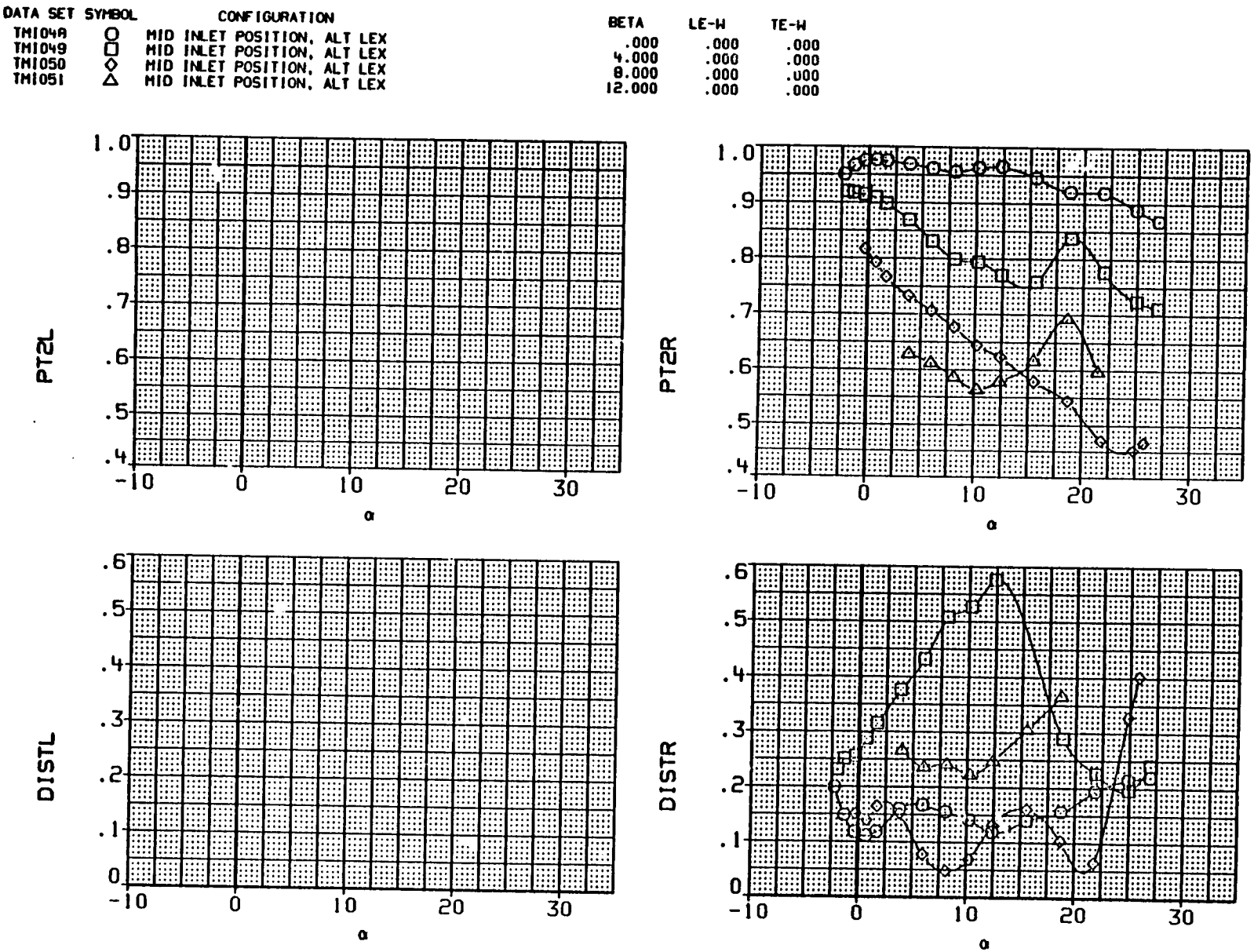

(1) Mach = 1.20.

Figure 9.- Continued.

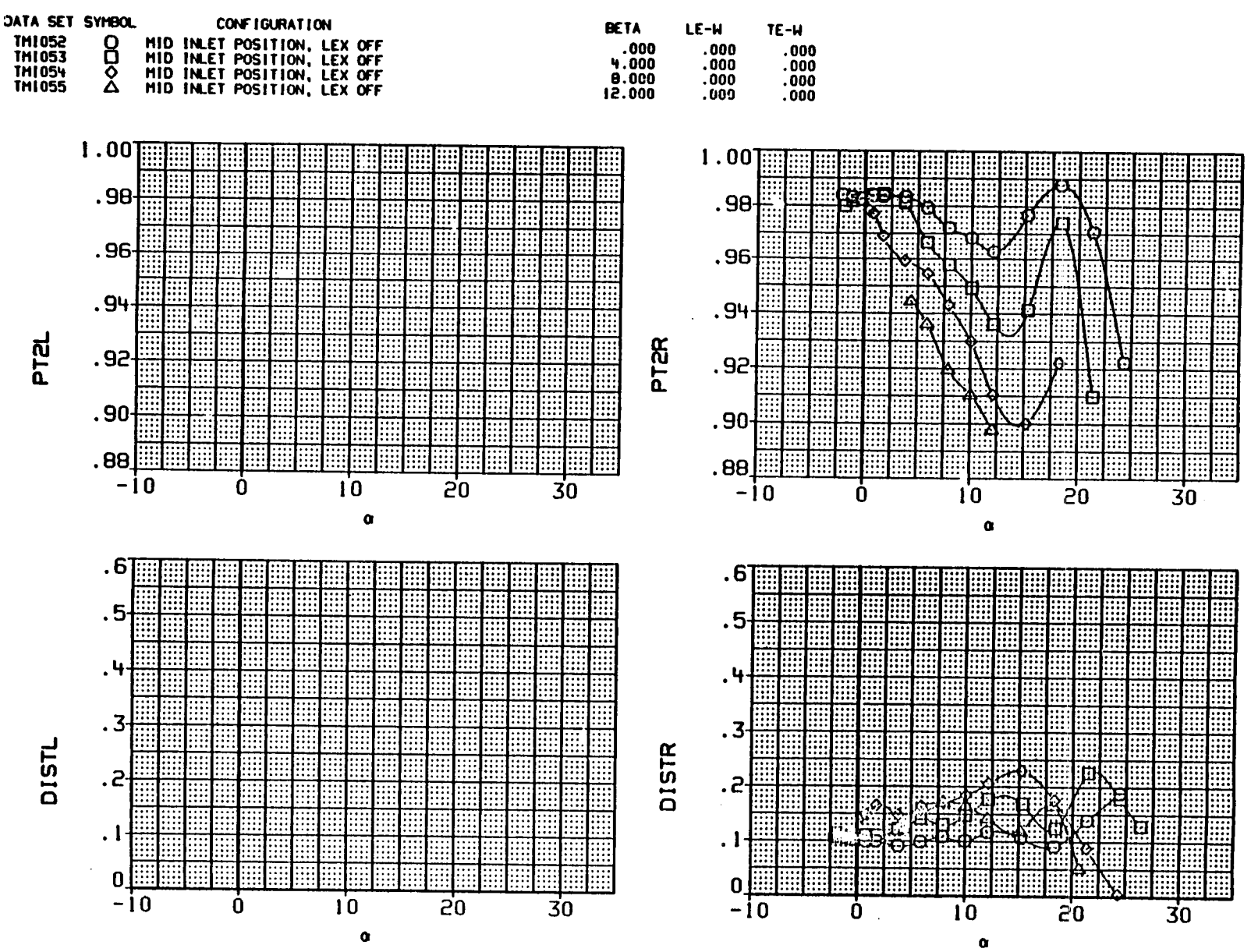

(m) Mach = 0.60.

Figure 9.- Continued.

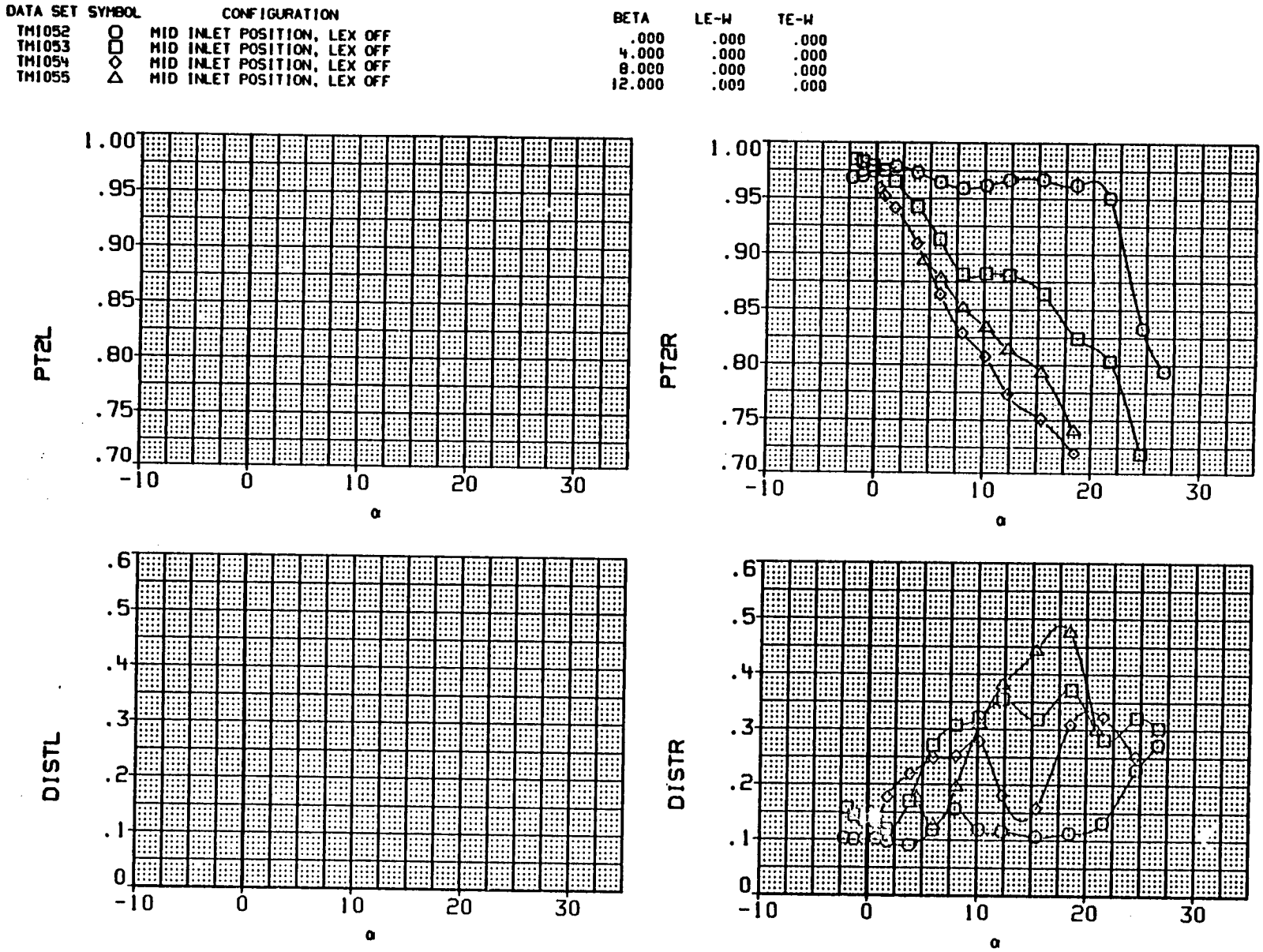

(n) Mach = 0.90.

Figure 9.- Continued.

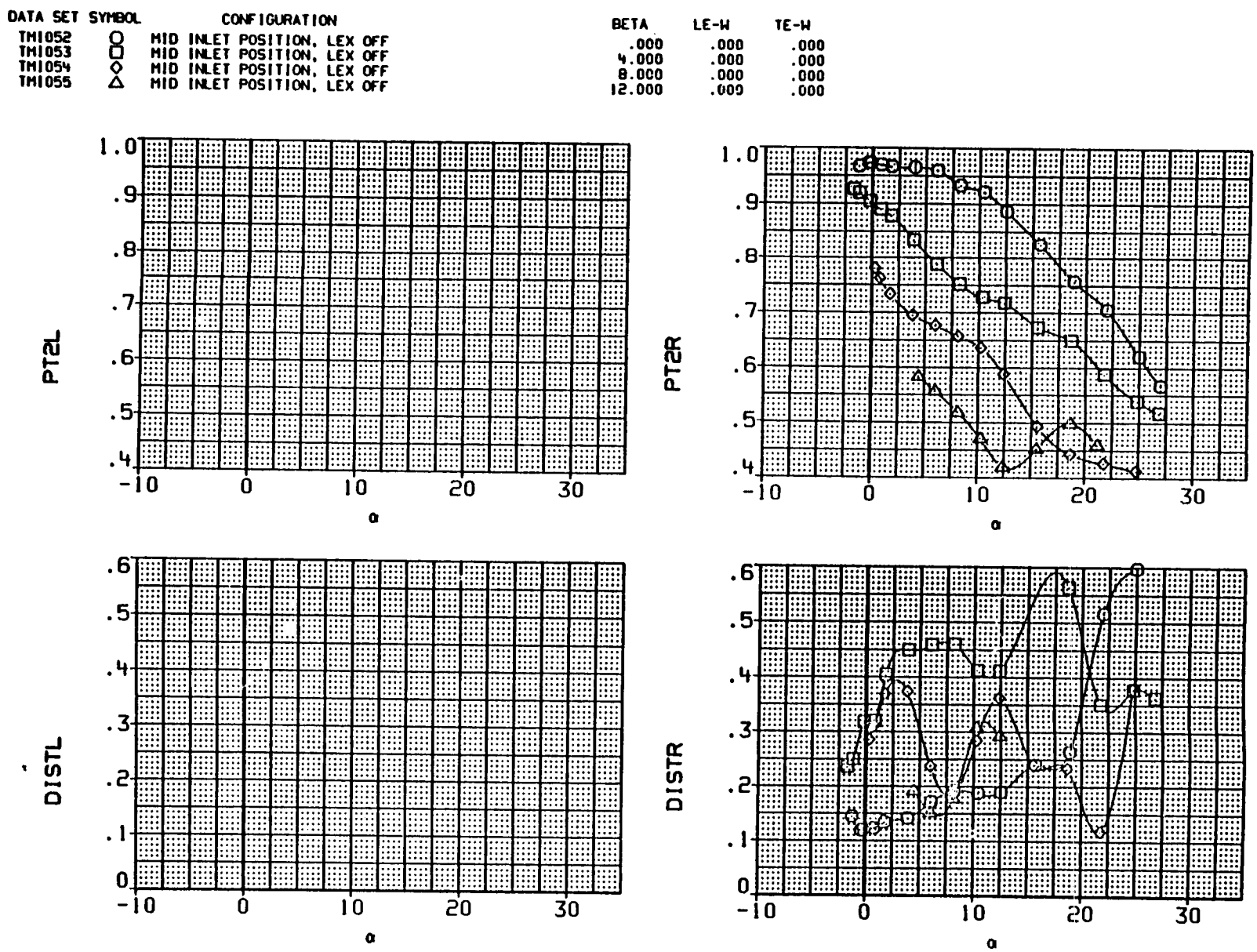

(o) Mach = 1.20.

Figure 9.- Continued.

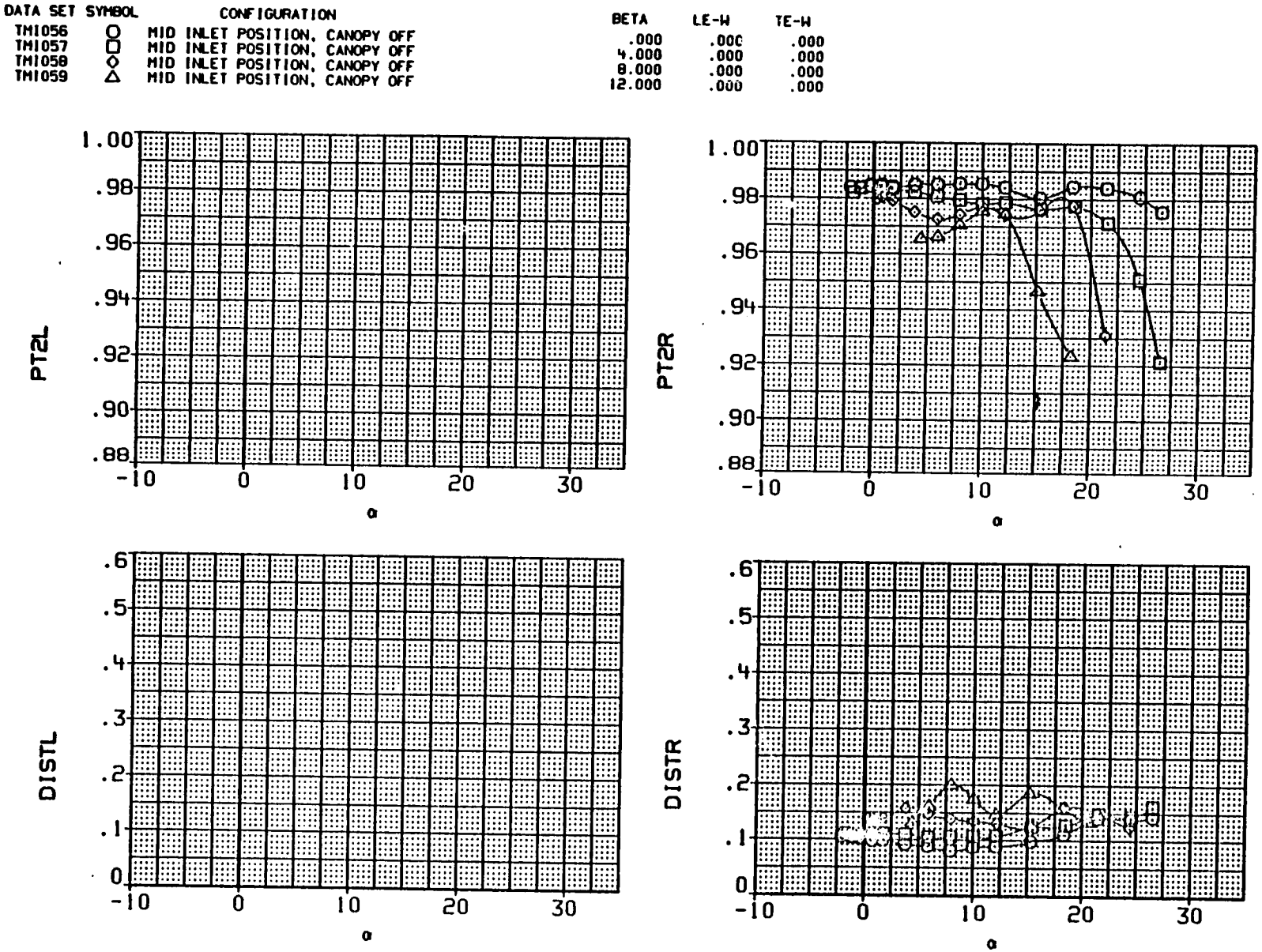

(p) Mach = 0.60.

Figure 9.- Continued.

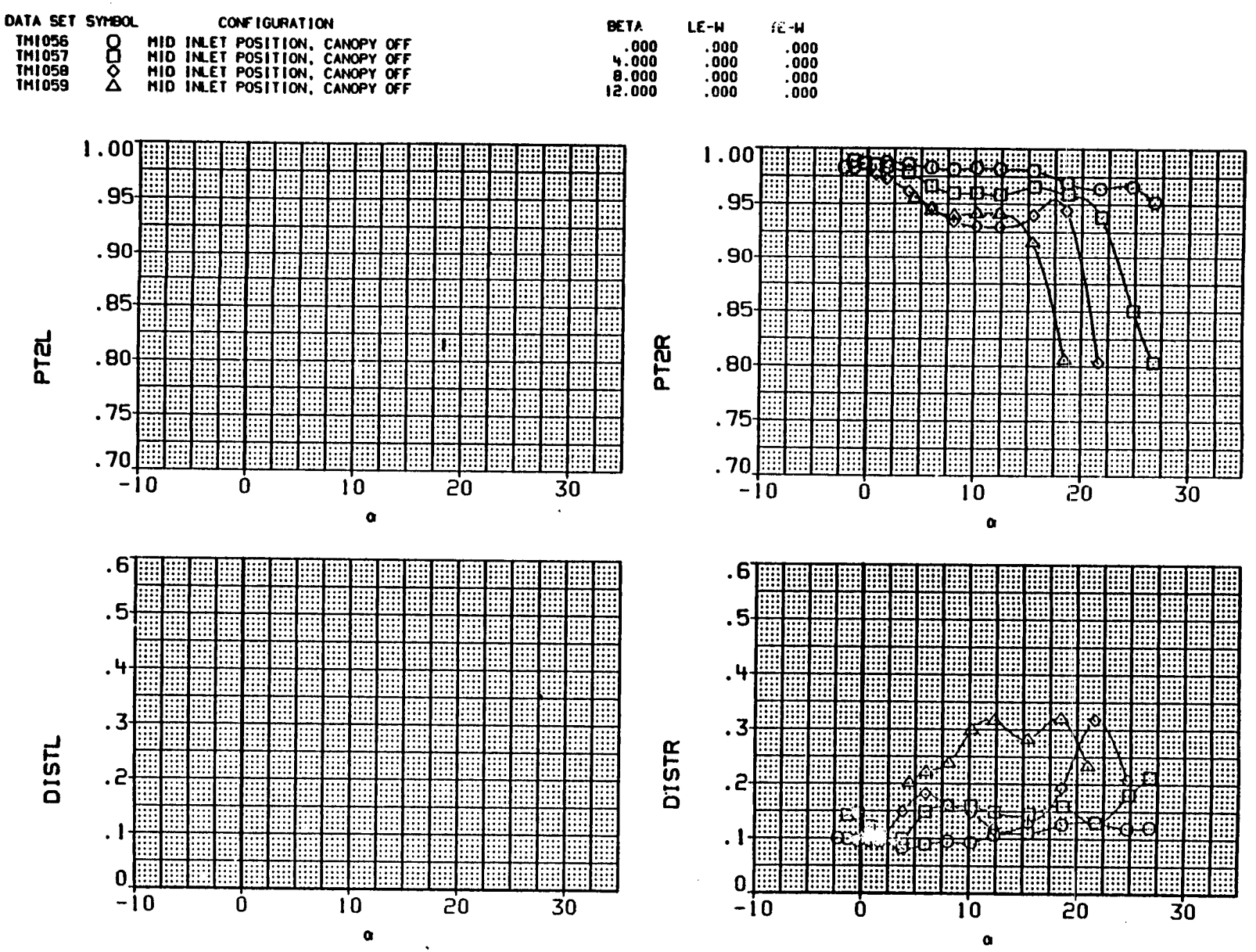

(q) Mach = 0.90.

Figure 9.- Continued.

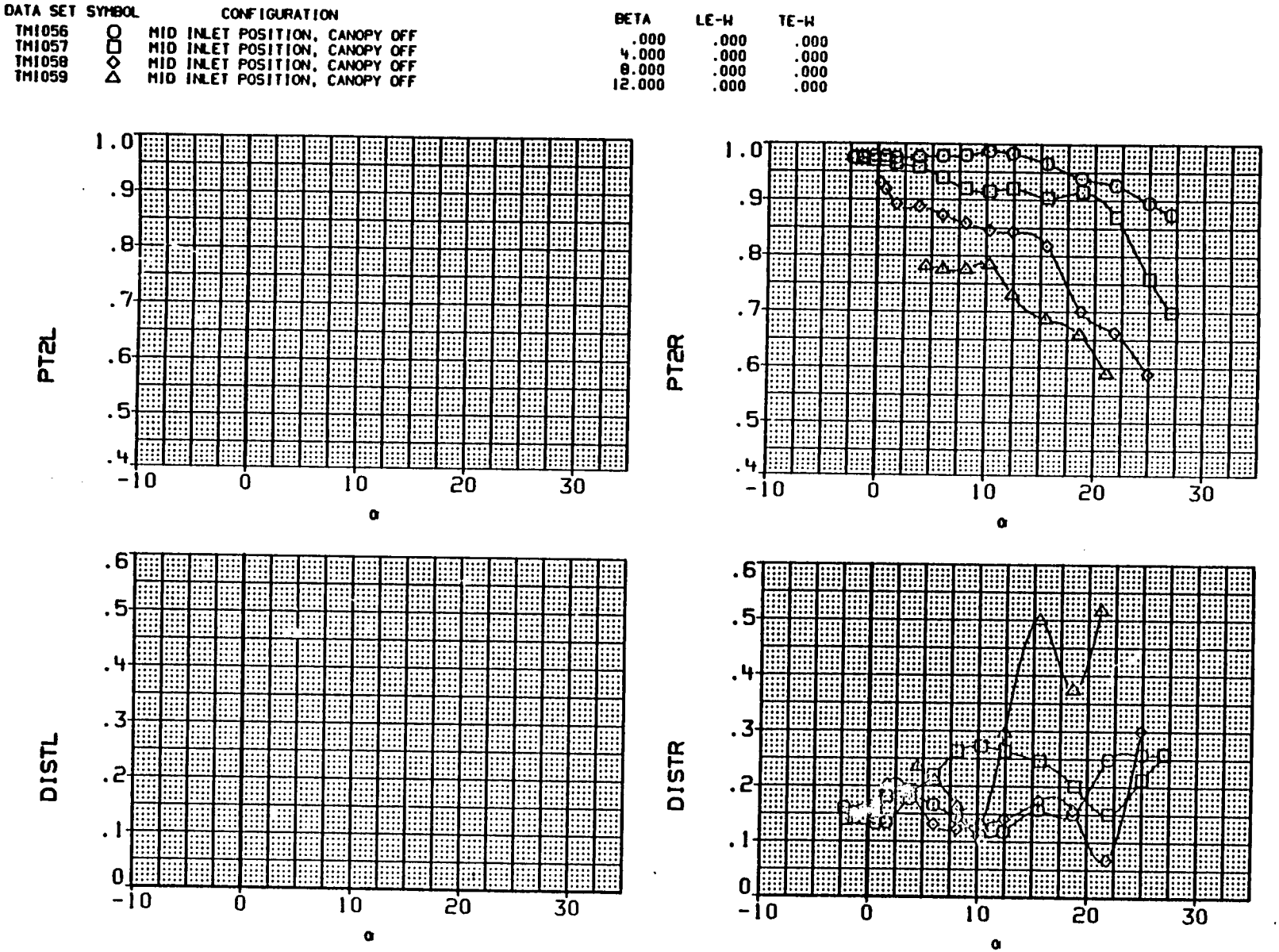

(r) Mach = 1.20.

Figure 9.- Continued.

DATA SET	SYMBOL	CONFIGURATION	BETA	LE-H	TE-H	CANARD
TM1060	○	MID INLET POSITION, CANARD	.000	.000	.000	.000
TM1061	□	MID INLET POSITION, CANARD	4.000	.000	.000	.000
TM1062	◇	MID INLET POSITION, CANARD	8.000	.000	.000	.000
TM1063	△	MID INLET POSITION, CANARD	12.000	.000	.000	.000

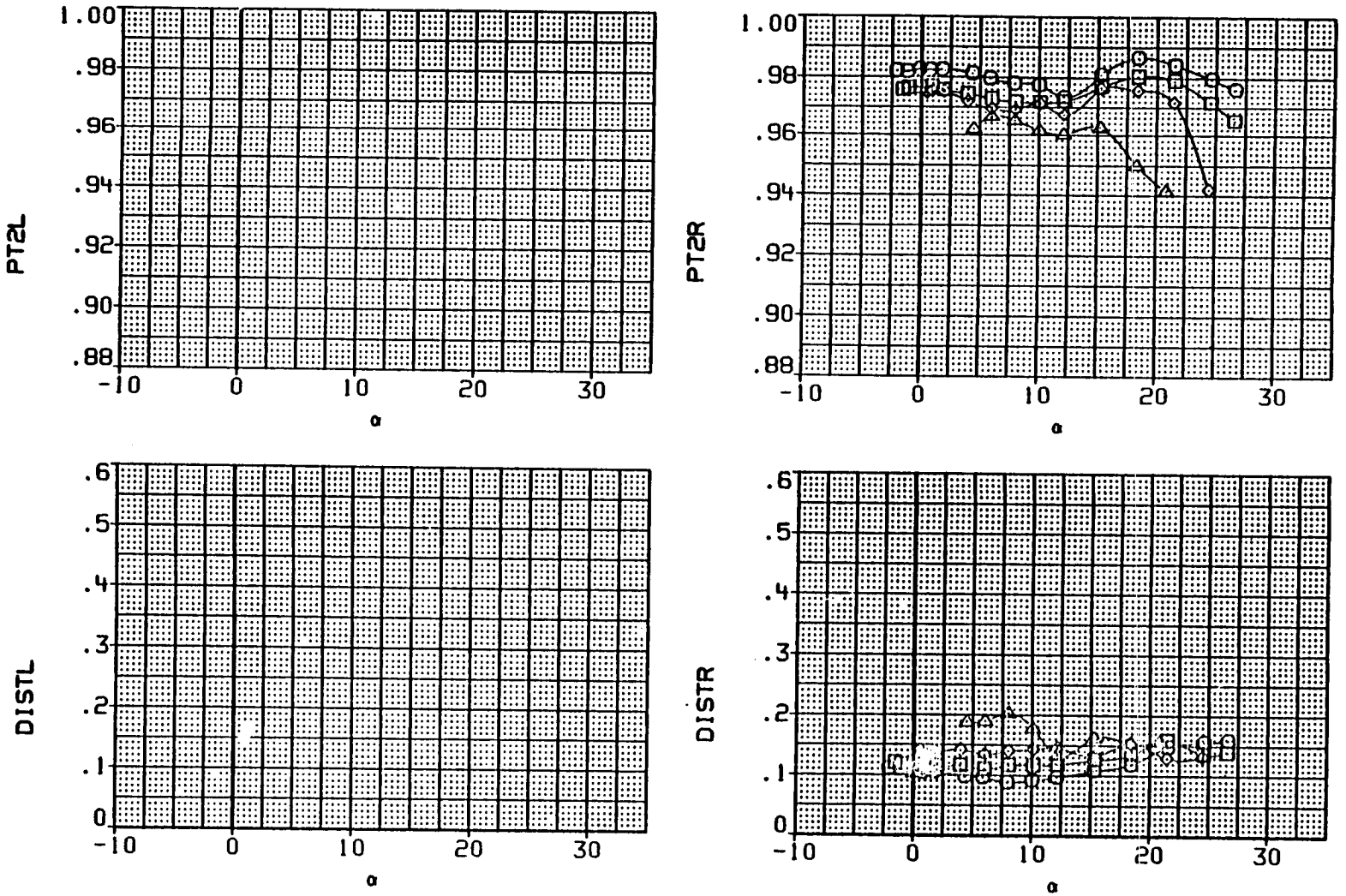

LEFT DUCT - MAX ENGINE AIRFLOW

RIGHT DUCT - MAX ENGINE AIRFLOW

(s) Mach = 0.60.

Figure 9.- Continued.

DATA SET	SYMBOL	CONFIGURATION
TM1060	○	MID INLET POSITION, CANARD
TM1061	□	MID INLET POSITION, CANARD
TM1062	◇	MID INLET POSITION, CANARD
TM1063	△	MID INLET POSITION, CANARD

BETA	LE-W	TE-W	CANARD
.000	.000	.000	.000
4.000	.000	.000	.000
8.000	.000	.000	.000
12.000	.000	.000	.000

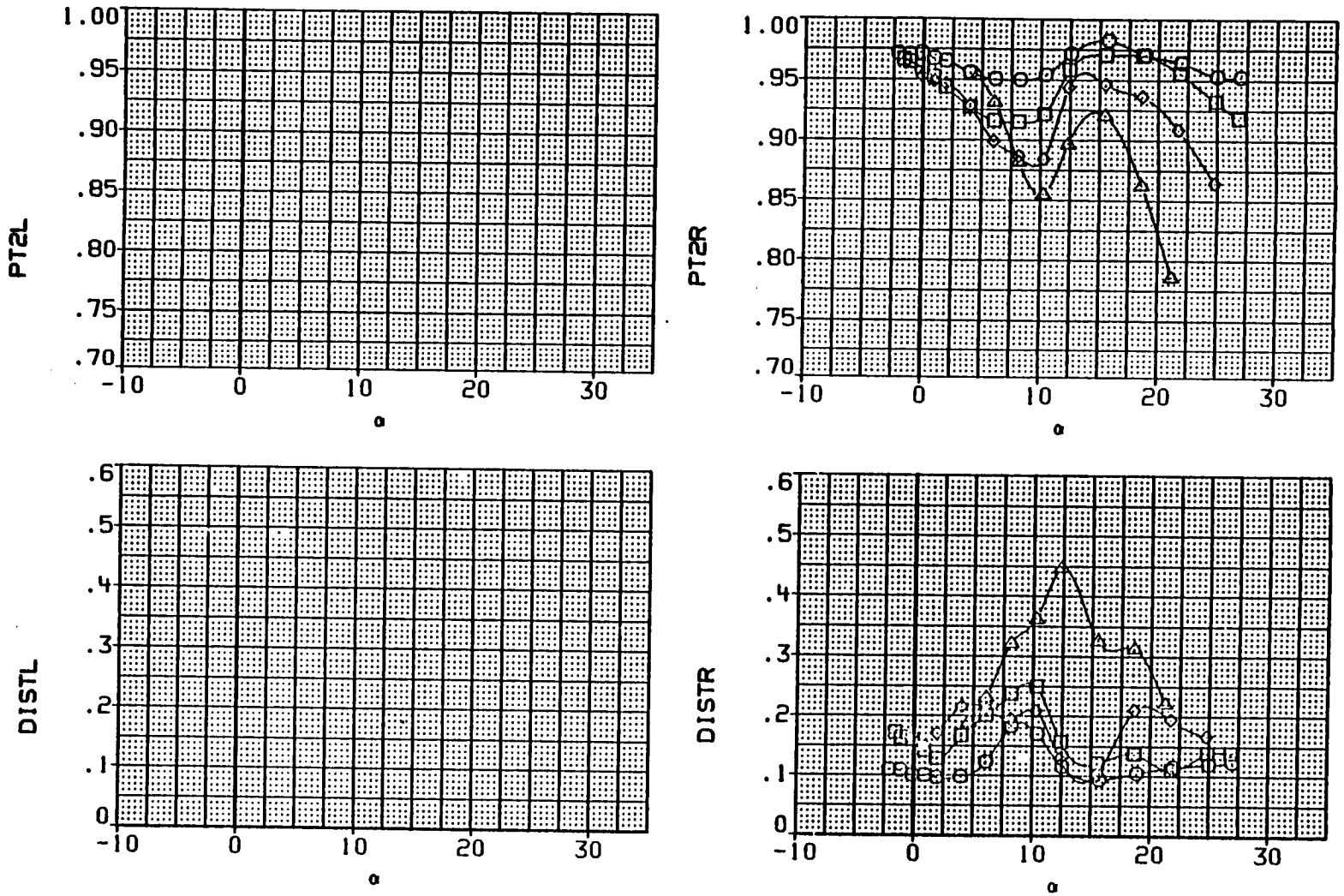

LEFT DUCT - MAX ENGINE AIRFLOW

RIGHT DUCT - MAX ENGINE AIRFLOW

(t) Mach = 0.90.

Figure 9.- Continued.

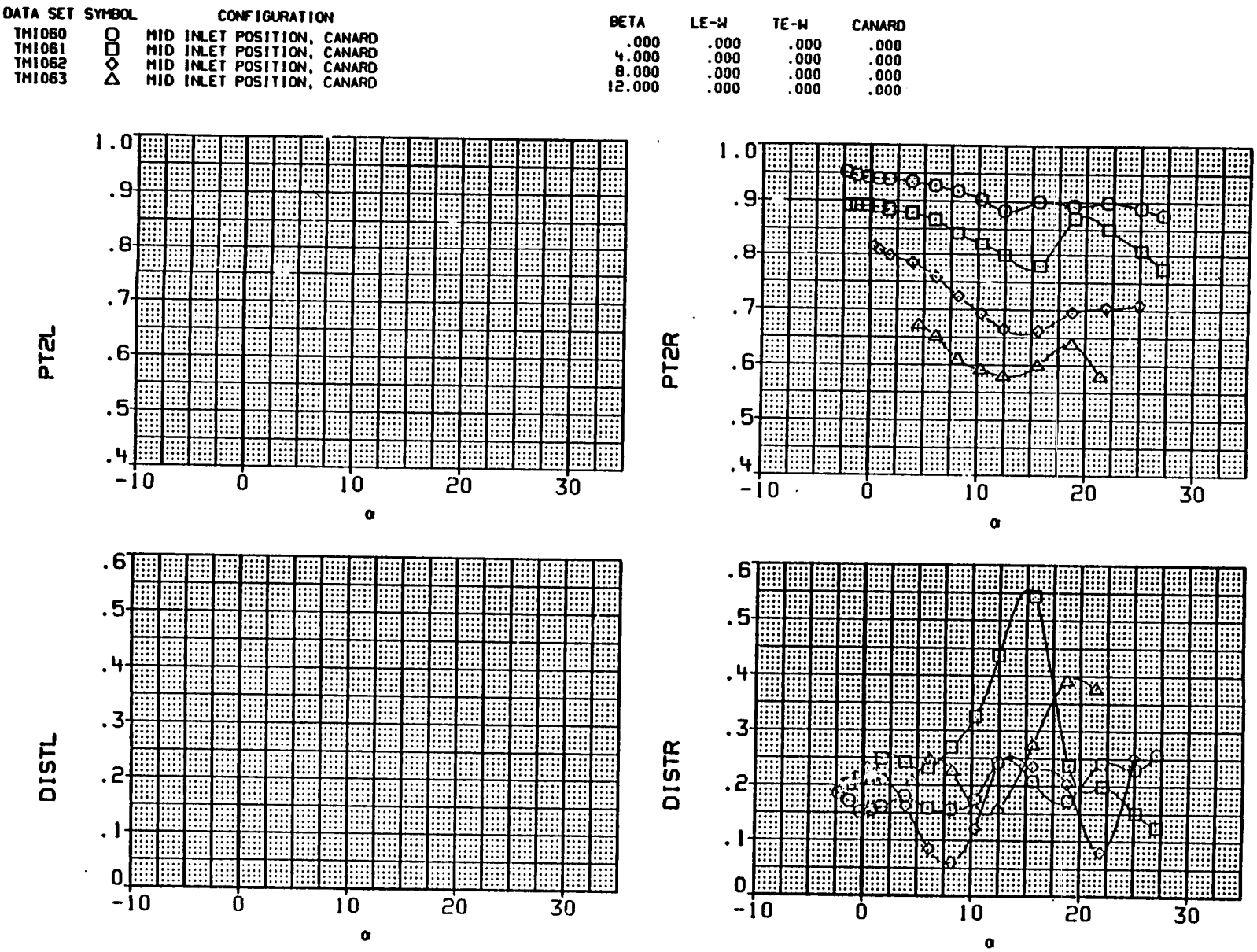

(u) Mach = 1.20.

Figure 9.- Continued.

DATA SET	SYMBOL	CONFIGURATION
TM1064	○	MID INLET POSITION, CANARD
TM1065	□	MID INLET POSITION, CANARD
TM1066	◇	MID INLET POSITION, CANARD
TM1067	△	MID INLET POSITION, CANARD

BETA	LE-W	TE-W	CANARD
.000	15.000	000	-10.000
4.000	15.000	.000	-10.000
8.000	15.000	.000	-10.000
12.000	15.000	.000	-10.000

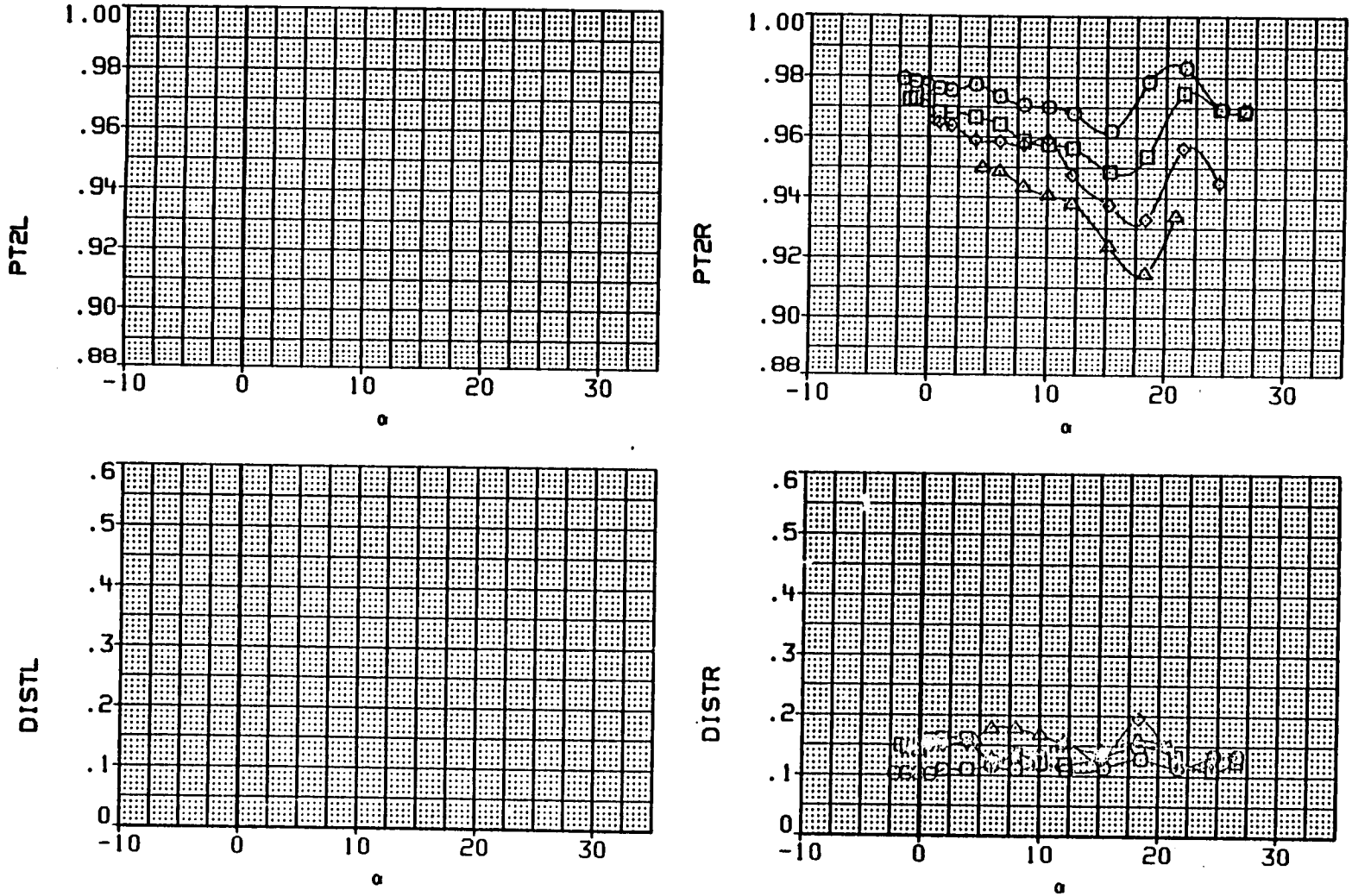

LEFT DUCT - MAX ENGINE AIRFLOW RIGHT DUCT - MAX ENGINE AIRFLOW

(v) Mach = 0.60.

Figure 9.- Continued.

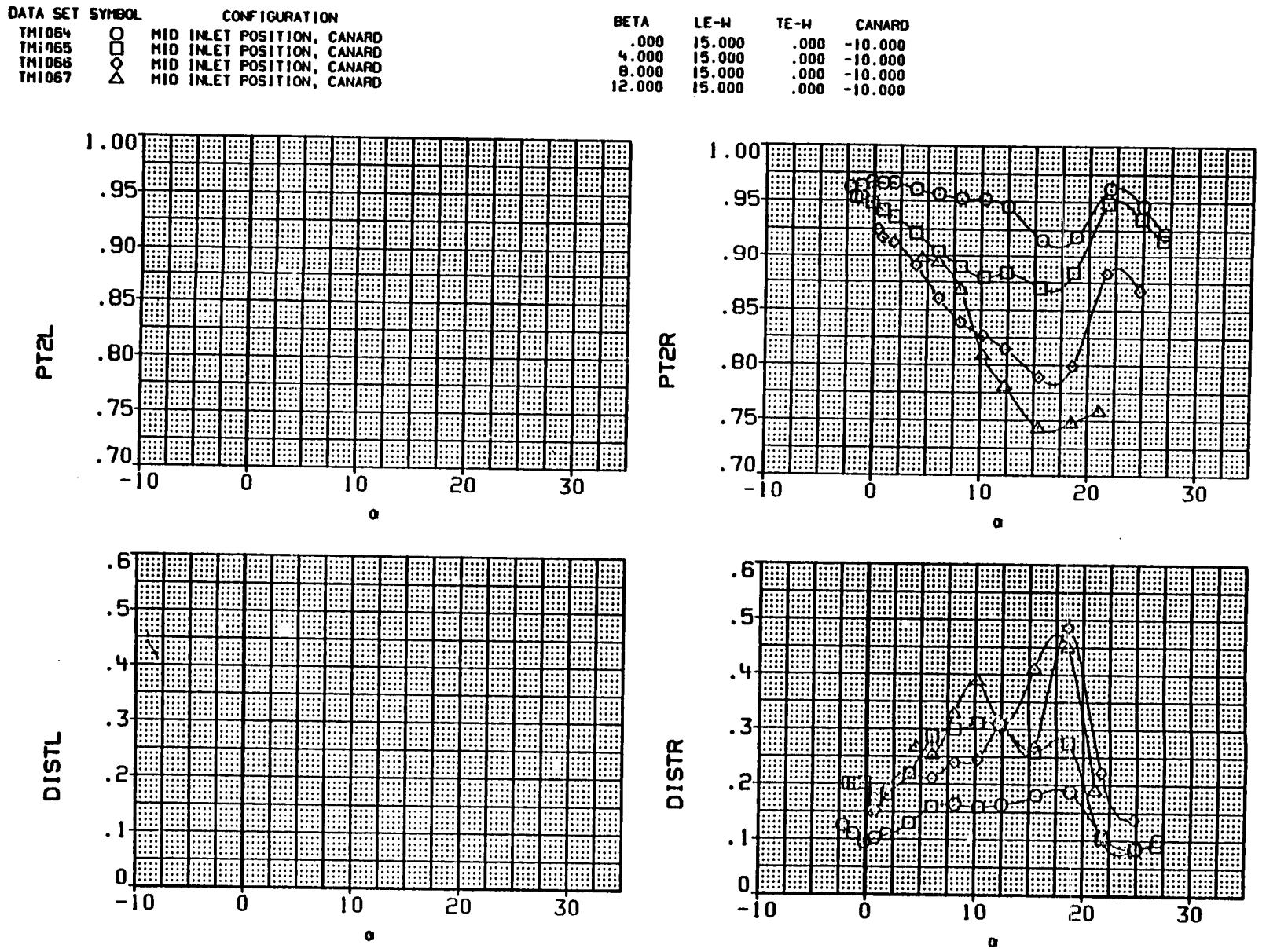

(w) Mach = 0.90.

Figure 9.- Continued.

DATA SET	SYMBOL	CONFIGURATION
TM1064	○	MID INLET POSITION, CANARD
TM1065	□	MID INLET POSITION, CANARD
TM1066	◇	MID INLET POSITION, CANARD
TM1067	△	MID INLET POSITION, CANARD

BETA	LE-W	TE-W	CANARD
.000	15.000	.000	-10.000
4.000	15.000	.000	-10.000
8.000	15.000	.000	-10.000
12.000	15.000	.000	-10.000

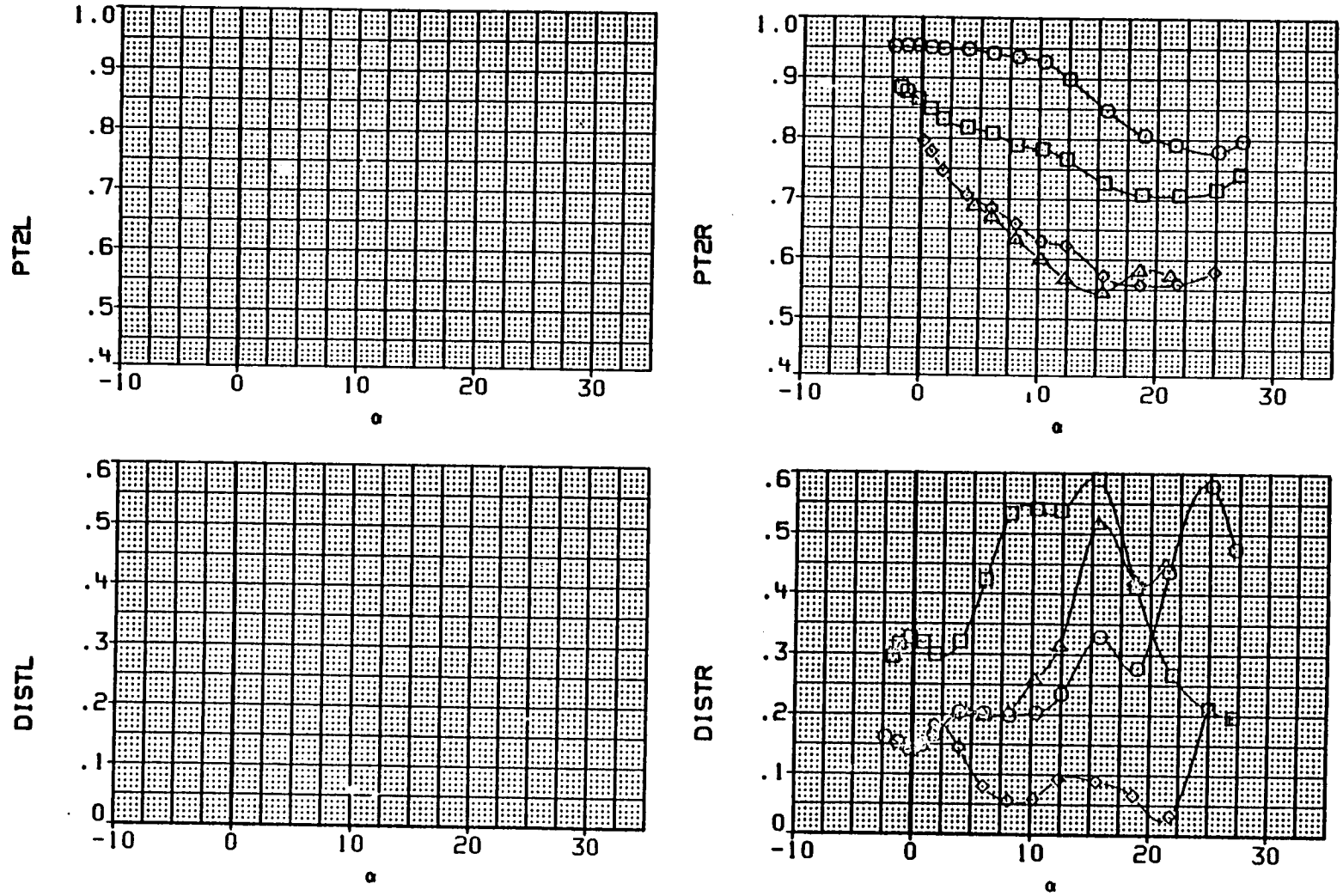

LEFT DUCT - MAX ENGINE AIRFLOW

RIGHT DUCT - MAX ENGINE AIRFLOW

(x) Mach = 1.20.

Figure 9.- Continued.

DATA SET	SYMBOL	CONFIGURATION	BETA	LE-W	TE-W	CANARD
TM1068	○	MID INLET POSITION, CANARD	.000	30.000	.000	-25.000
TM1069	□	MID INLET POSITION, CANARD	4.000	30.000	.000	-25.000
TM1070	◇	MID INLET POSITION, CANARD	8.000	30.000	.000	-25.000
TM1071	△	MID INLET POSITION, CANARD	12.000	30.000	.000	-25.000

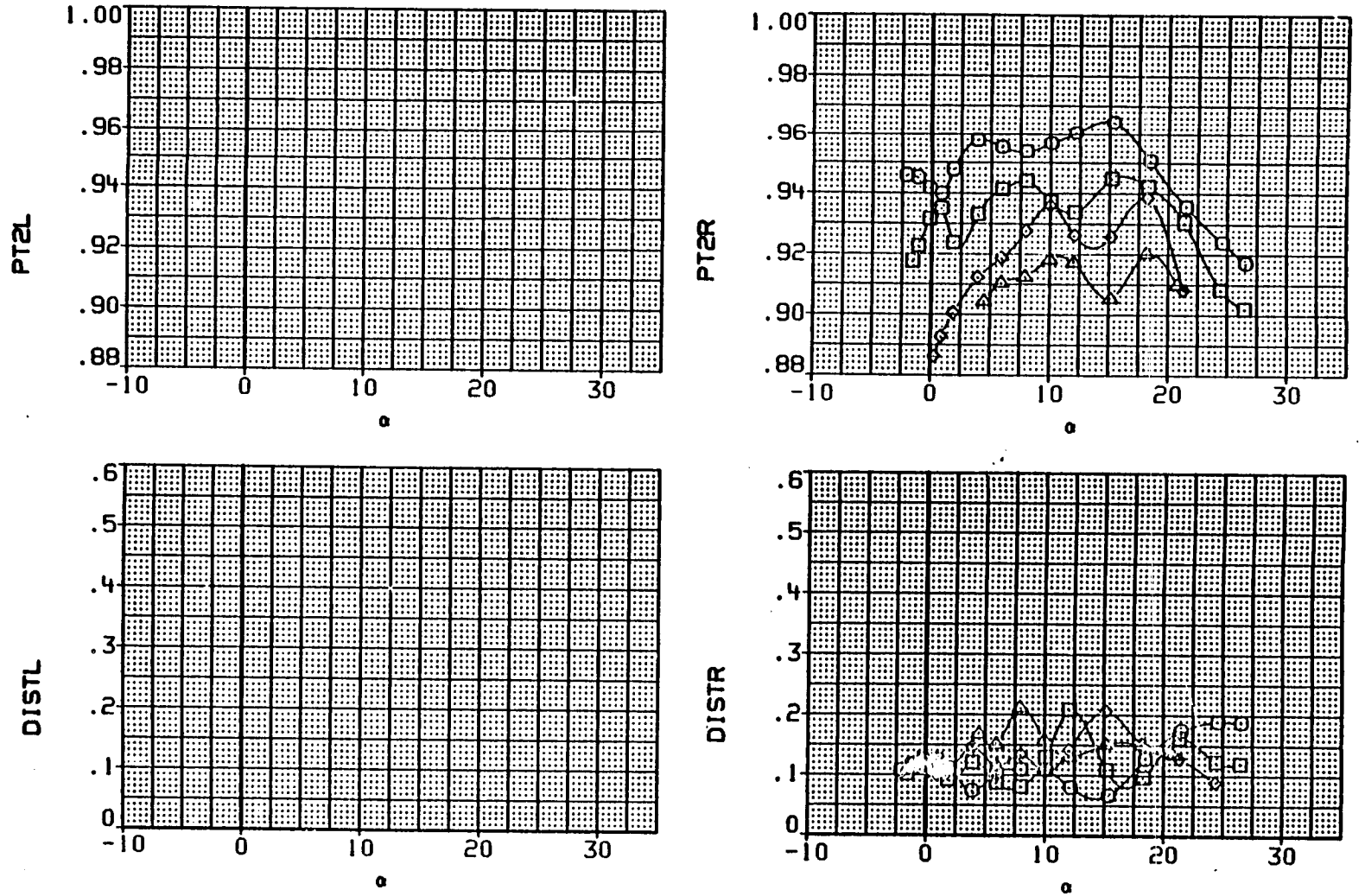

LEFT DUCT - MAX ENGINE AIRFLOW

RIGHT DUCT - MAX ENGINE AIRFLOW

(y) Mach = 0.60.

Figure 9.- Continued.

DATA SET	SYMBOL	CONFIGURATION
TM1068	○	MID INLET POSITION, CANARD
TM1069	□	MID INLET POSITION, CANARD
TM1070	◇	MID INLET POSITION, CANARD
TM1071	△	MID INLET POSITION, CANARD

BETA	LE-W	TE-W	CANARD
.000	30.000	.000	-25.000
4.000	30.000	.000	-25.000
8.000	30.000	.000	-25.000
12.000	30.000	.000	-25.000

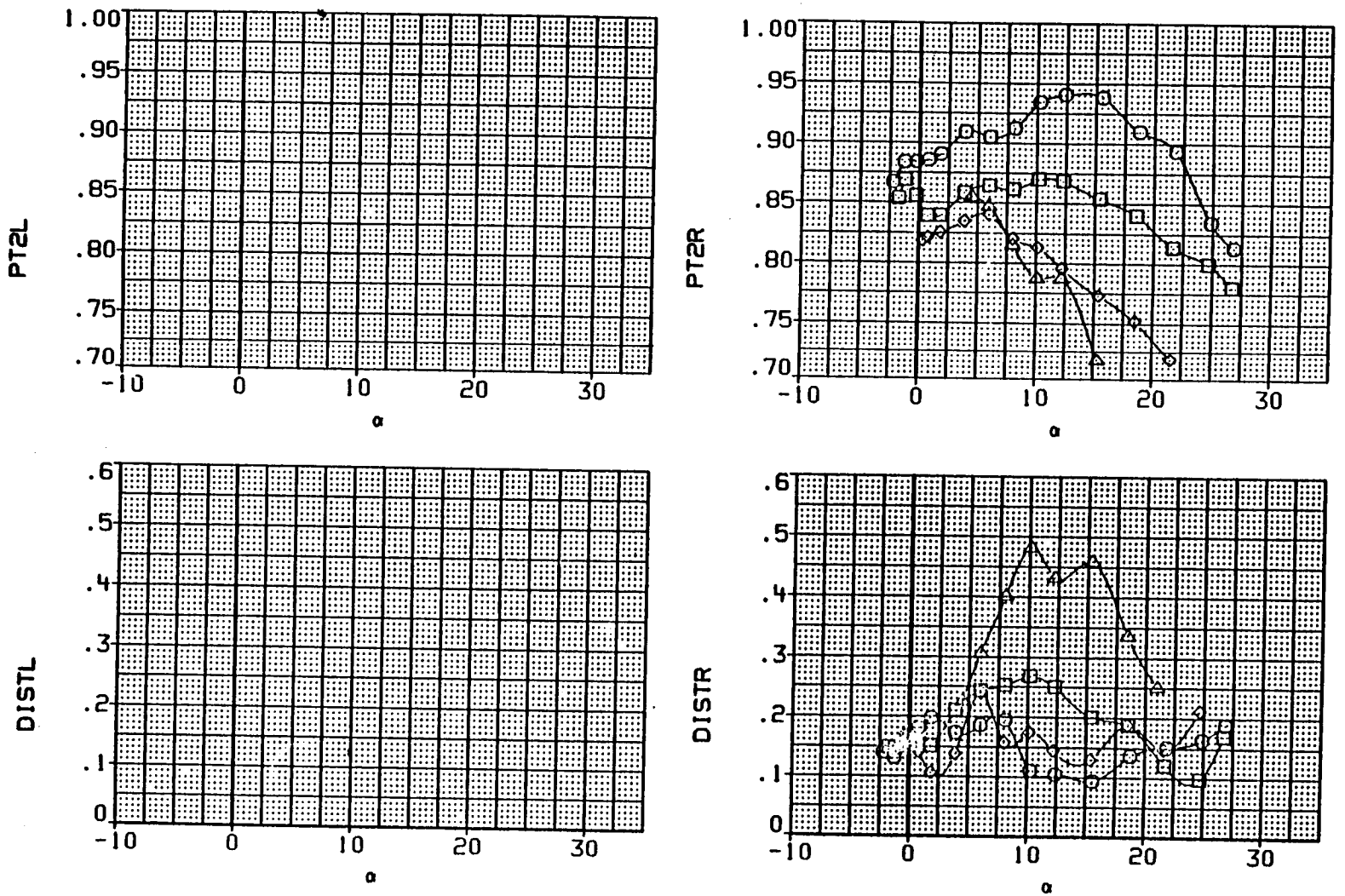

LEFT DUCT - MAX ENGINE AIRFLOW

RIGHT DUCT - MAX ENGINE AIRFLOW

(z) Mach = 0.90.

Figure 9.- Continued.

DATA SET	SYMBOL	CONFIGURATION
TM1068	○	MID INLET POSITION, CANARD
TM1069	□	MID INLET POSITION, CANARD
TM1070	◇	MID INLET POSITION, CANARD
TM1071	△	MID INLET POSITION, CANARD

BETA	LE-W	TE-W	CANARD
.000	30.000	.000	-25.000
4.000	30.000	.000	-25.000
8.000	30.000	.000	-25.000
12.000	30.000	.000	-25.000

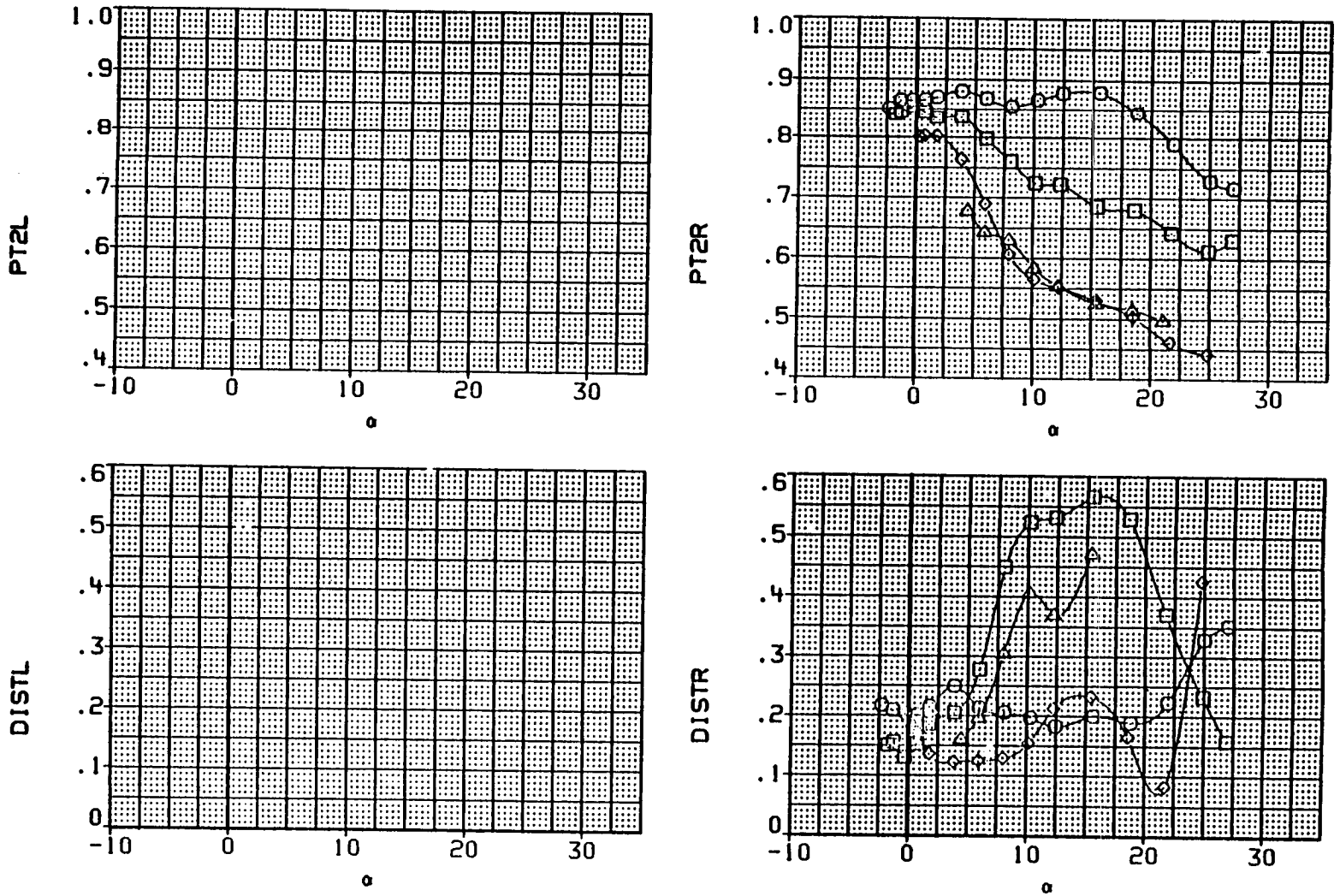

LEFT DUCT - MAX ENGINE AIRFLOW

RIGHT DUCT - MAX ENGINE AIRFLOW

(aa) Mach = 1.20.

Figure 9.- Continued.

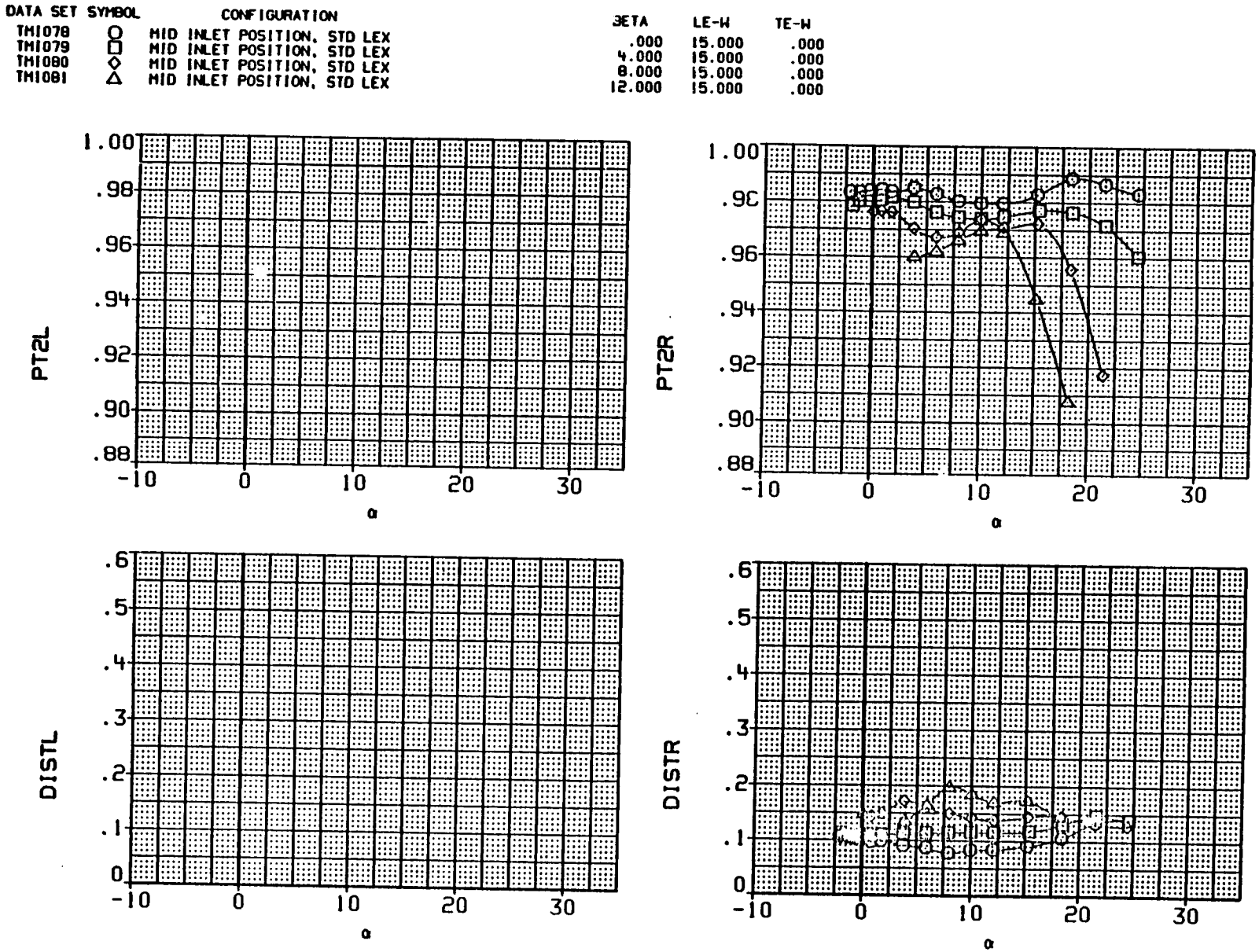

(bb) Mach = 0.60.

Figure 9.- Continued.

DATA SET	SYMBOL	CONFIGURATION
TM1078	○	MID INLET POSITION, STD LEX
TM1079	□	MID INLET POSITION, STD LEX
TM1080	◇	MID INLET POSITION, STD LEX
TM1081	△	MID INLET POSITION, STD LEX

BETA	LE-W	TE-W
.000	15.000	.000
4.000	15.000	.000
8.000	15.000	.000
12.000	15.000	.000

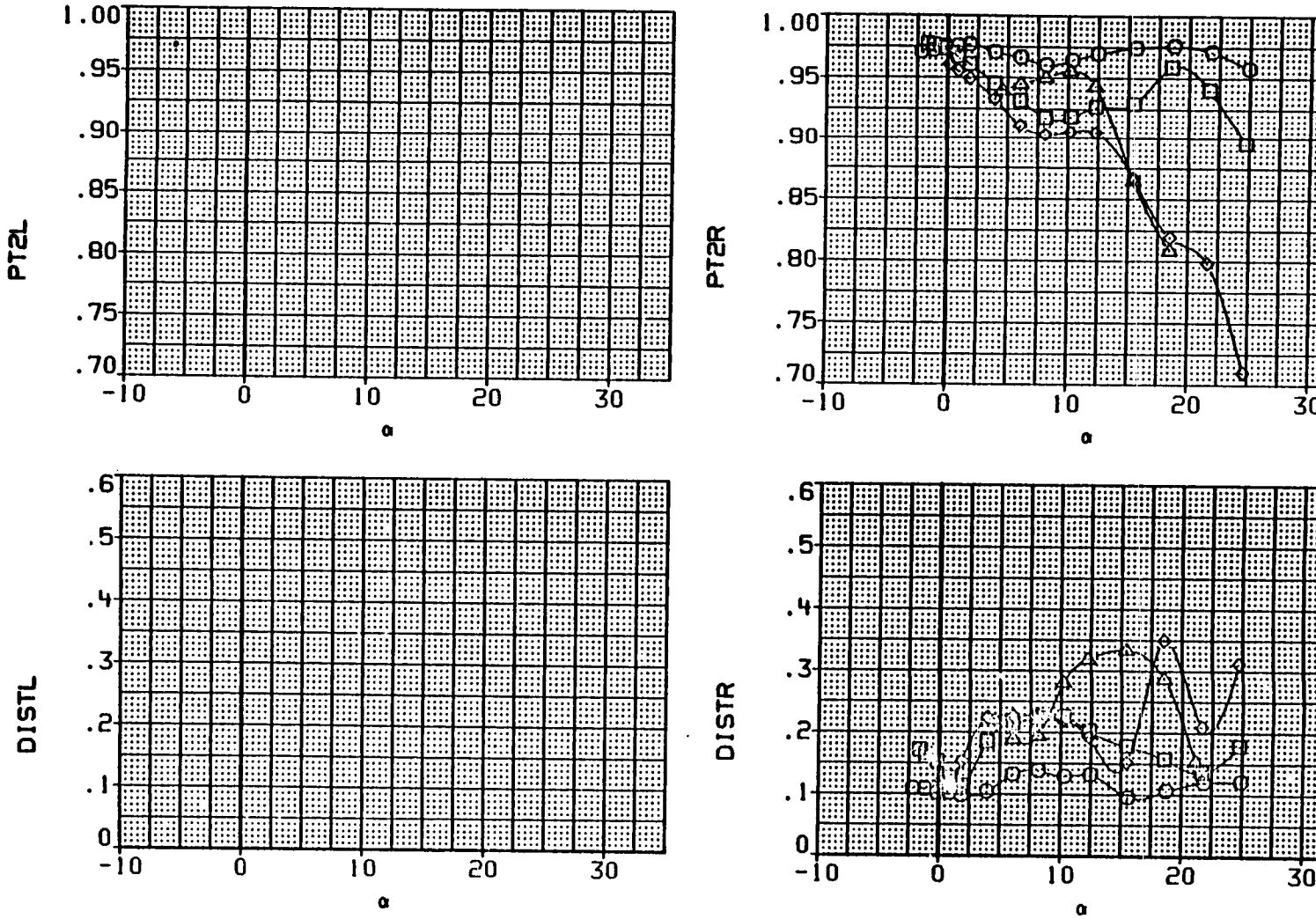

LEFT DUCT - MAX ENGINE AIRFLOW

RIGHT DUCT - MAX ENGINE AIRFLOW

(cc) Mach = 0.90.

Figure 9.- Continued.

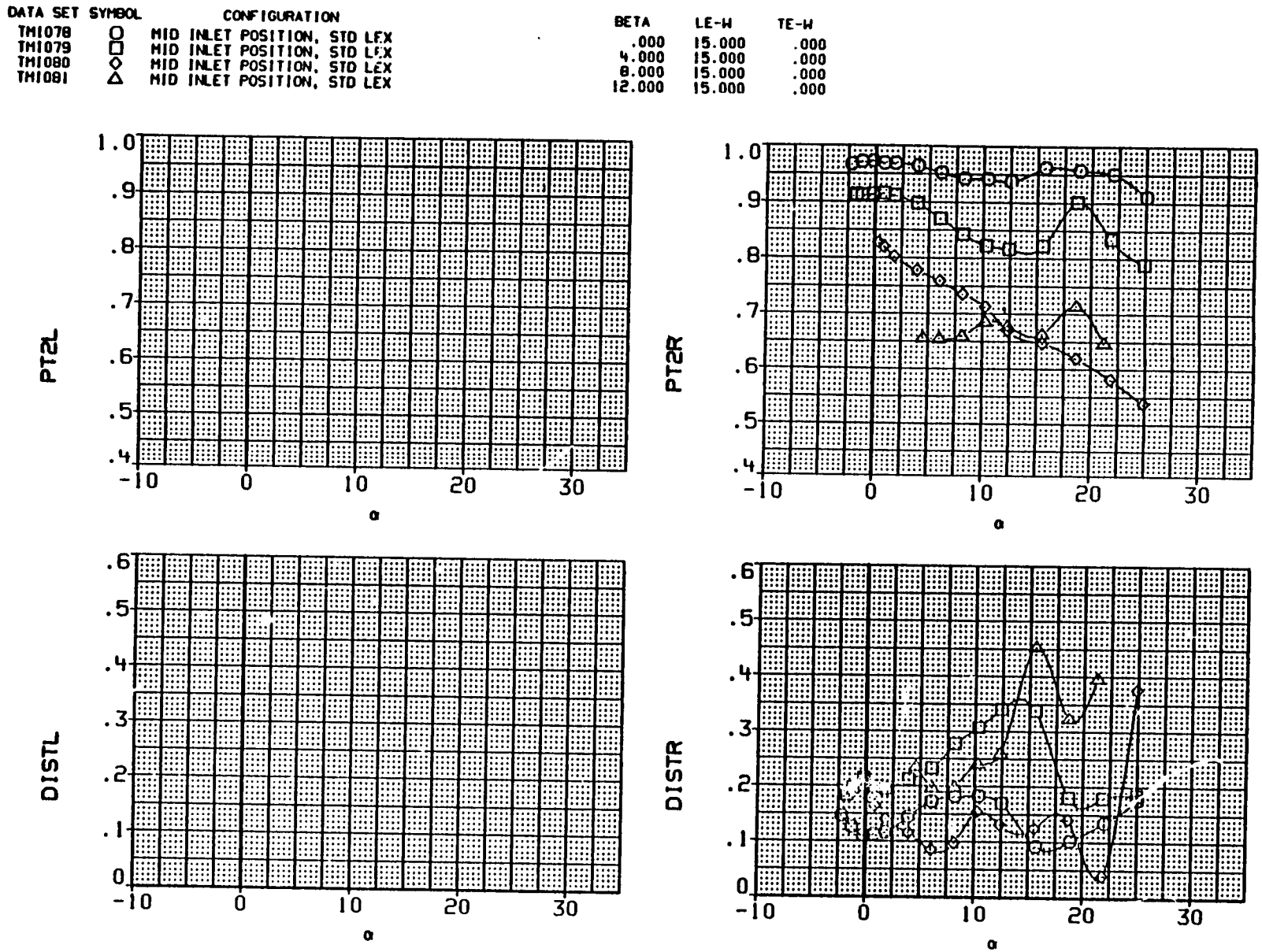

LEFT DUCT - MAX ENGINE AIRFLOW RIGHT DUCT - MAX ENGINE AIRFLOW

(dd) Mach = 1.20.

Figure 9.- Continued.

DATA SET	SYMBOL	CONFIGURATION
TM1082	○	MID INLET POSITION, STD LEX
TM1083	□	MID INLET POSITION, STD LEX
TM1084	◇	MID INLET POSITION, STD LEX

BETA	LE-W	TE-W
.000	30.000	.000
4.000	30.000	.000
8.000	30.000	.000

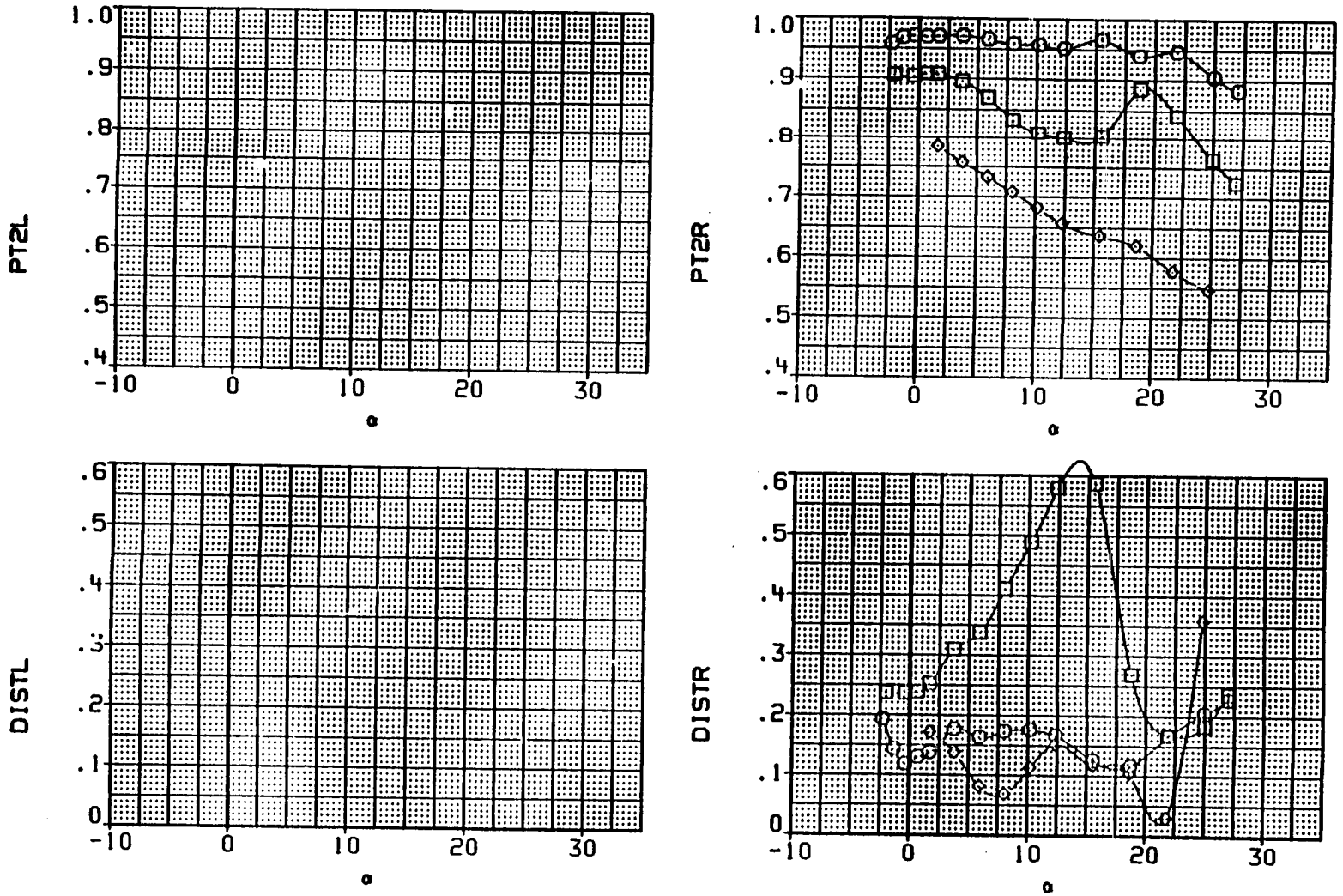

LEFT DUCT - MAX ENGINE AIRFLOW

RIGHT DUCT - MAX ENGINE AIRFLOW

(ee) Mach = 1.20.

Figure 9.- Continued.

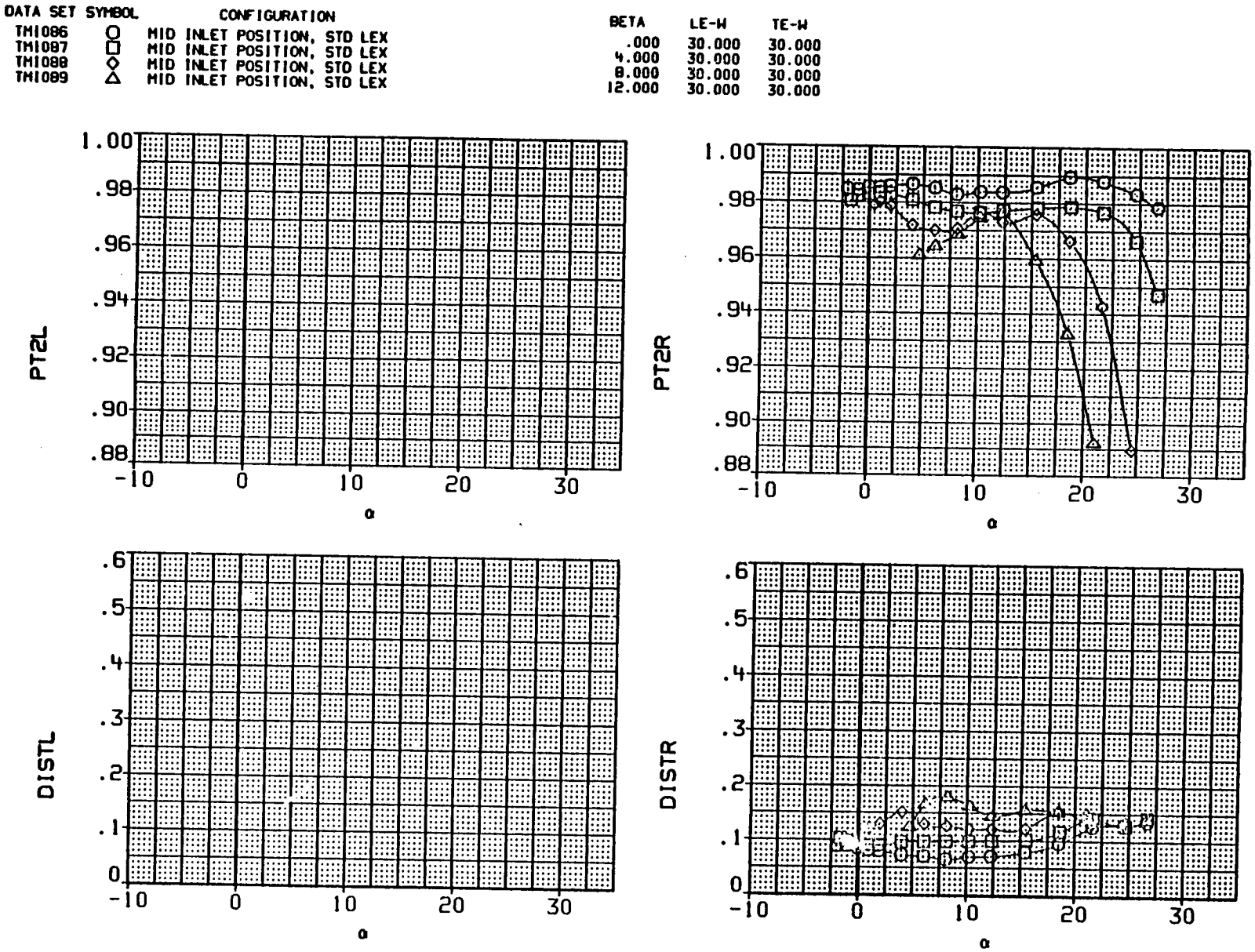

(ff) Mach = 0.60.

Figure 9.- Continued.

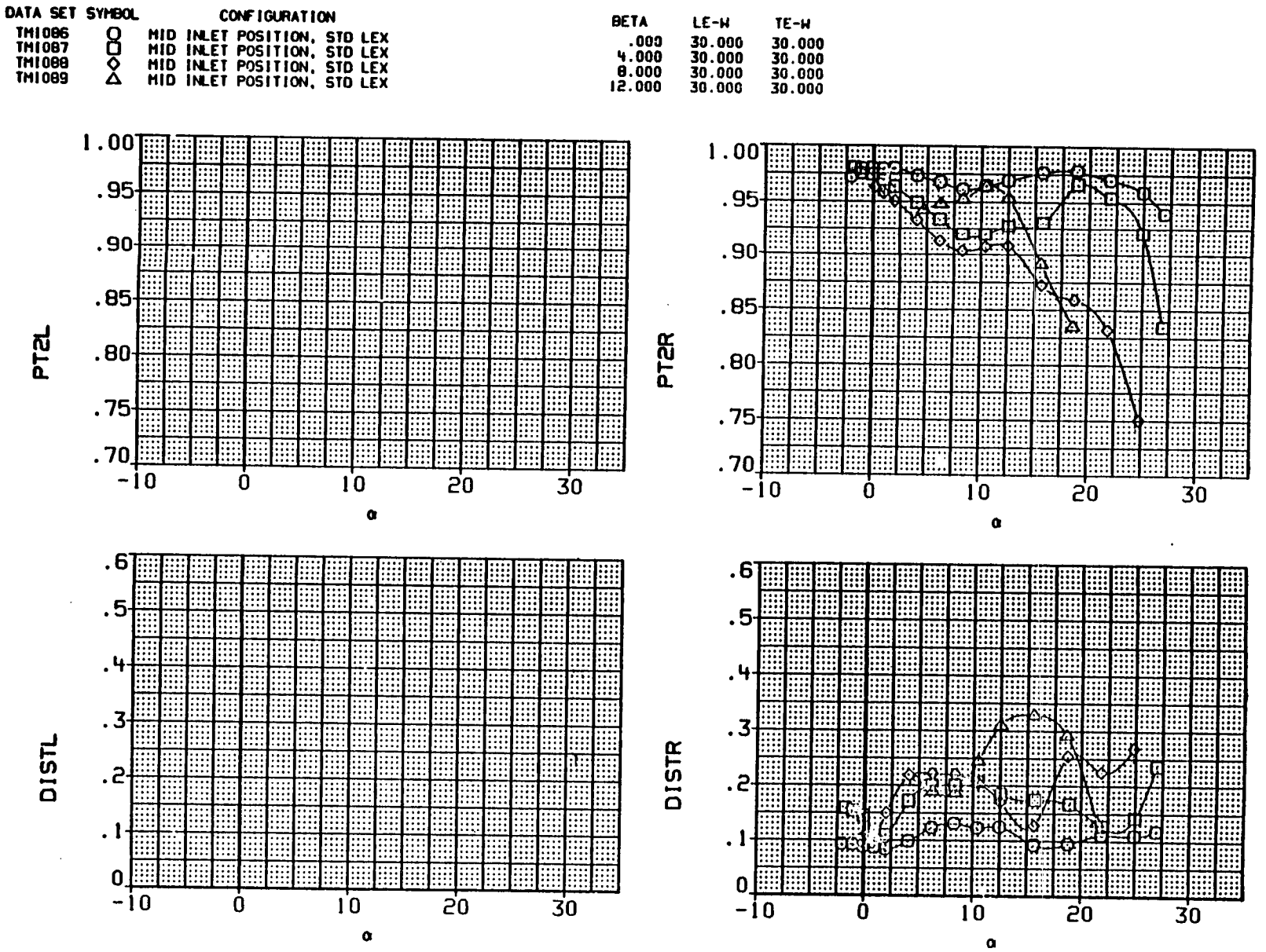

(gg) Mach = 0.90.

Figure 9.- Continued.

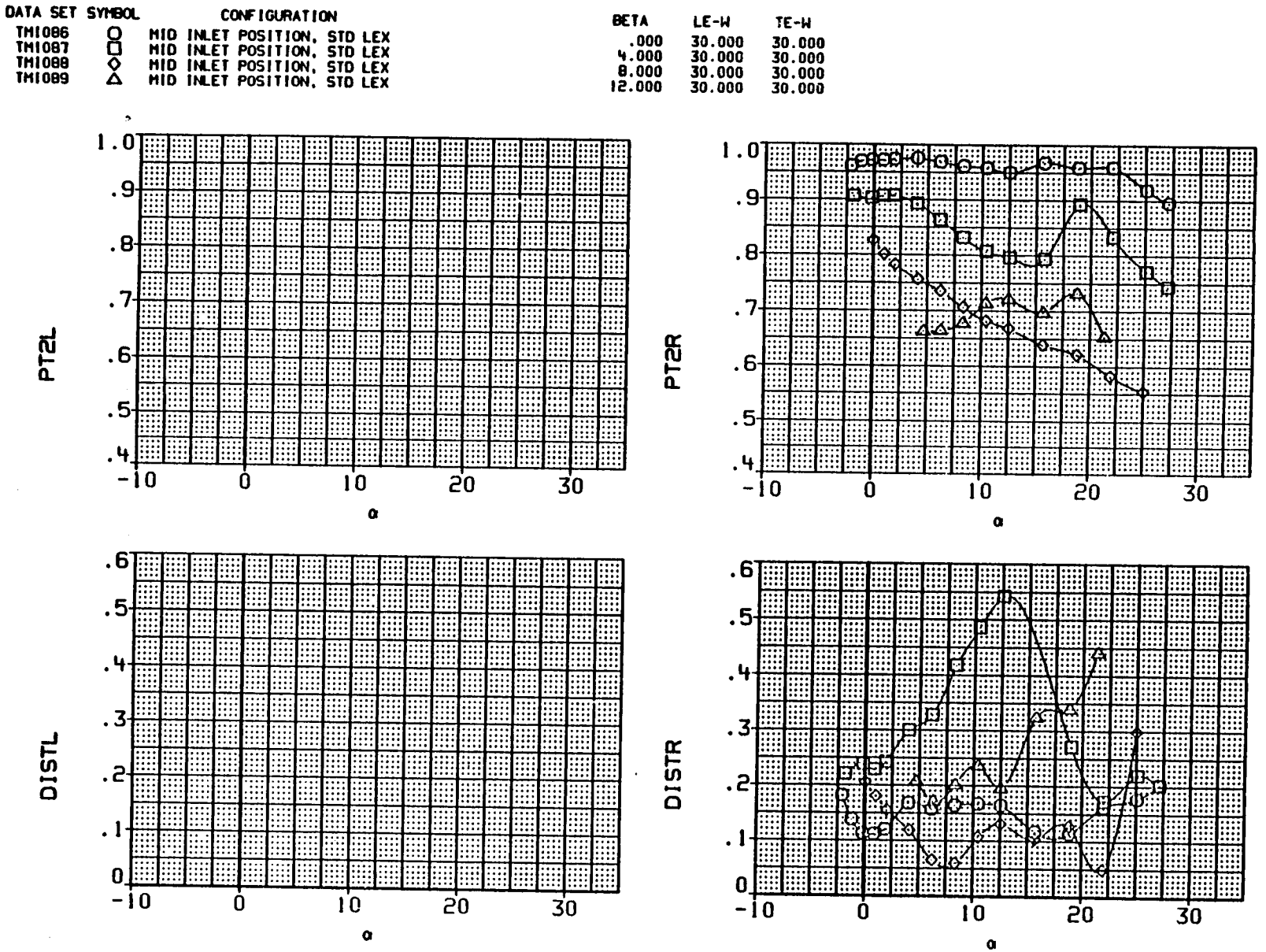

(hh) Mach = 1.20.

Figure 9.- Concluded.

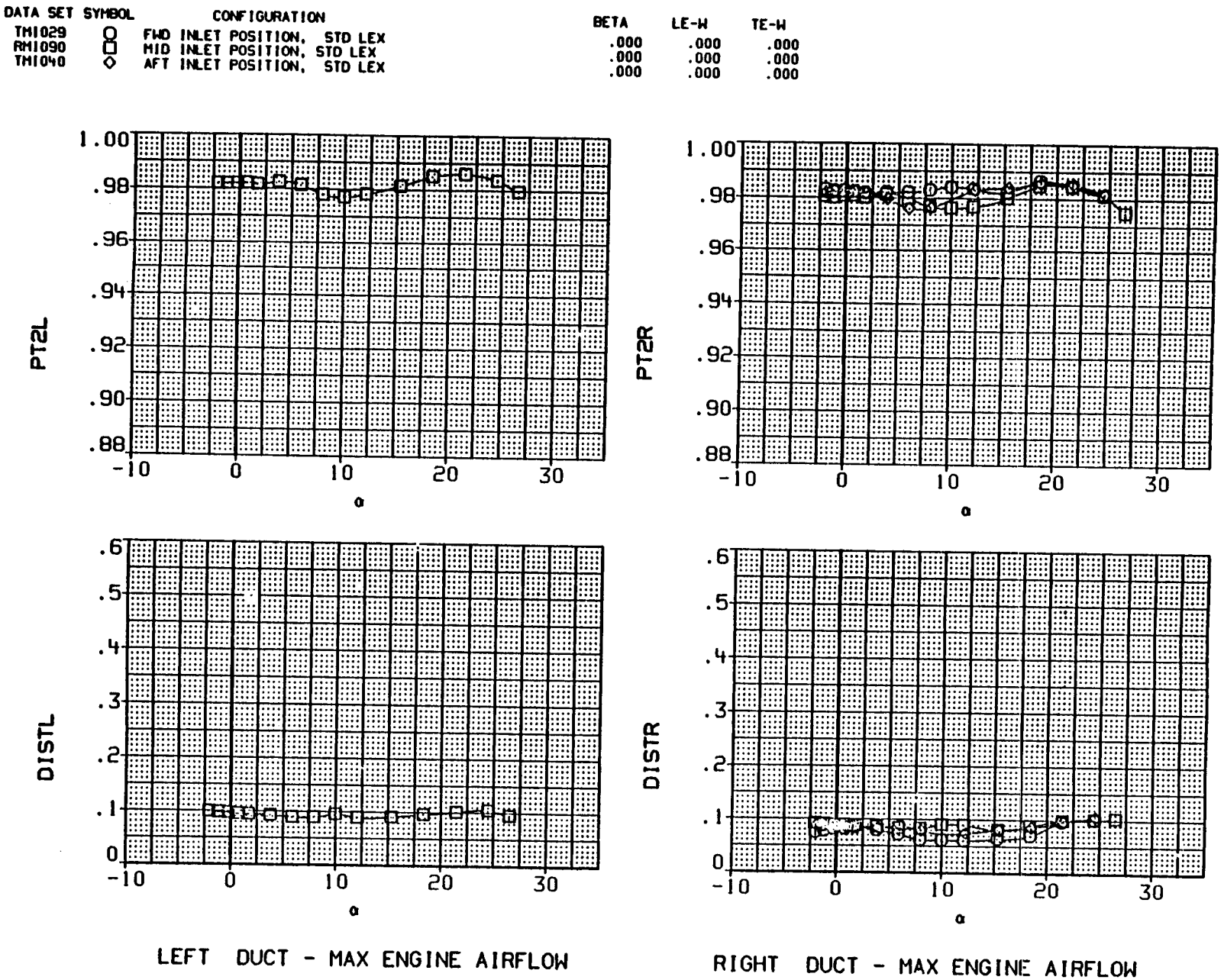

(a) Mach = 0.60.

Figure 10.- Comparisons of inlet performance for various configurations.

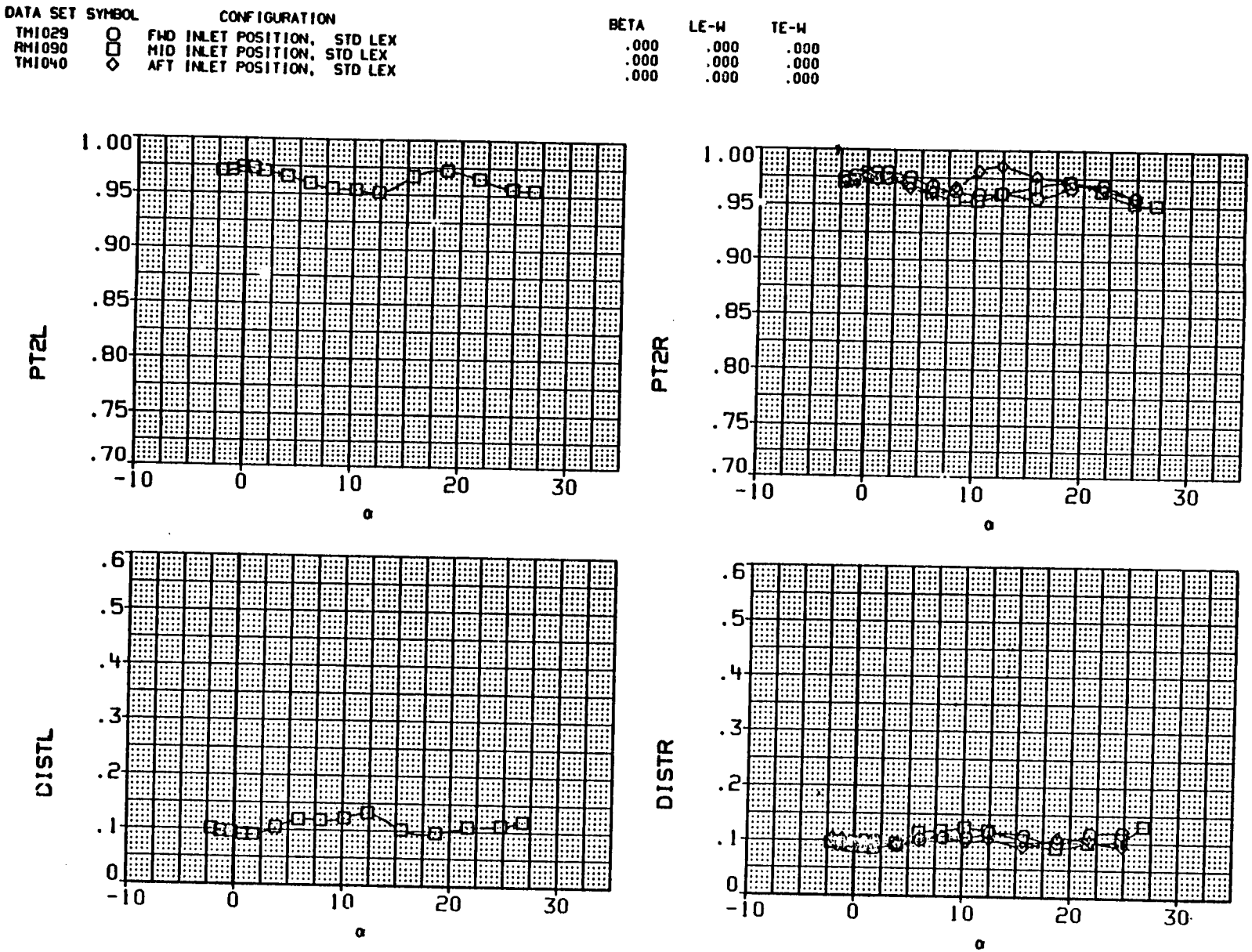

(b) Mach = 0.90.

Figure 10.- Continued.

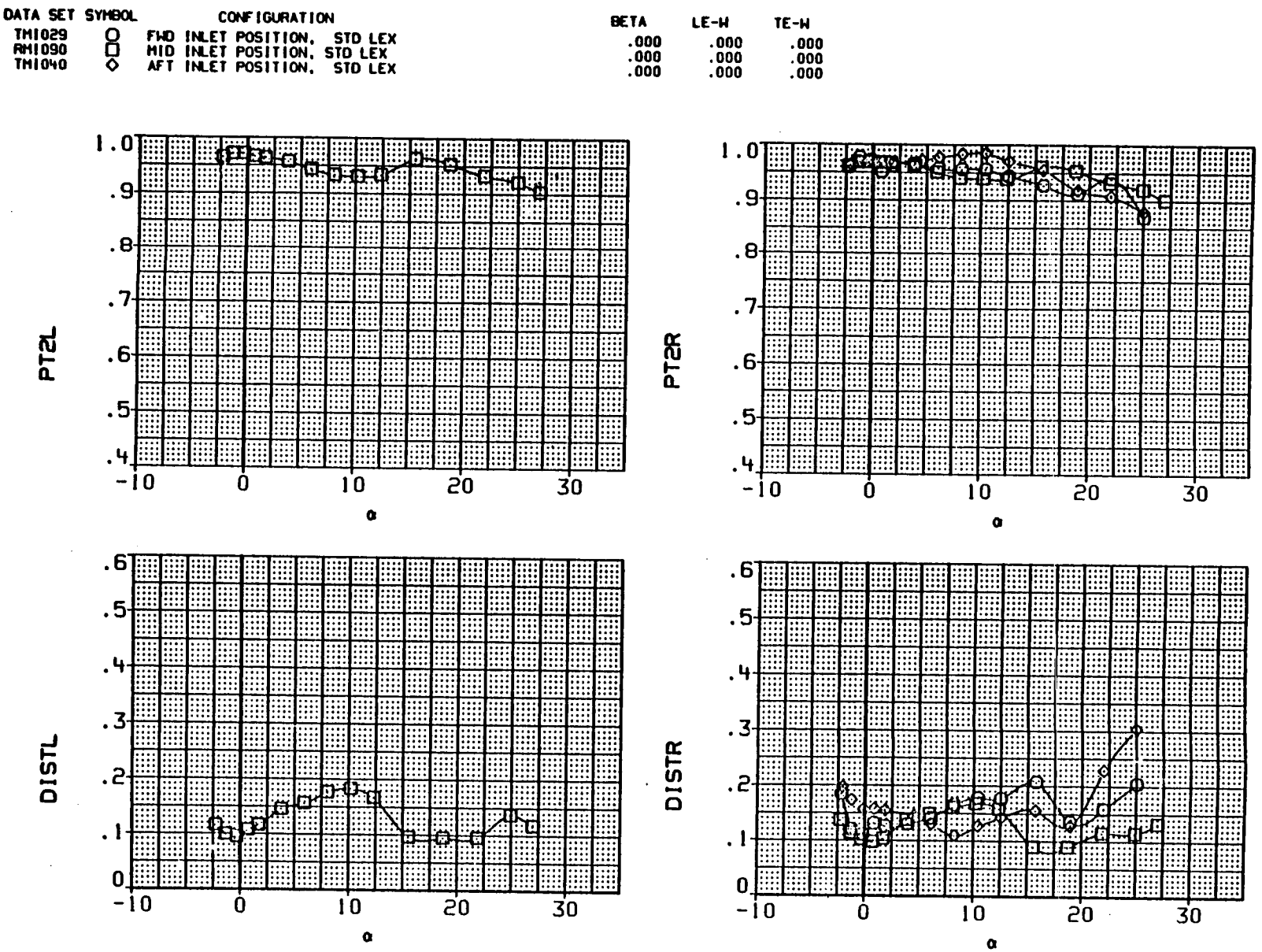

(c) Mach = 1.20.

Figure 10.- Continued.

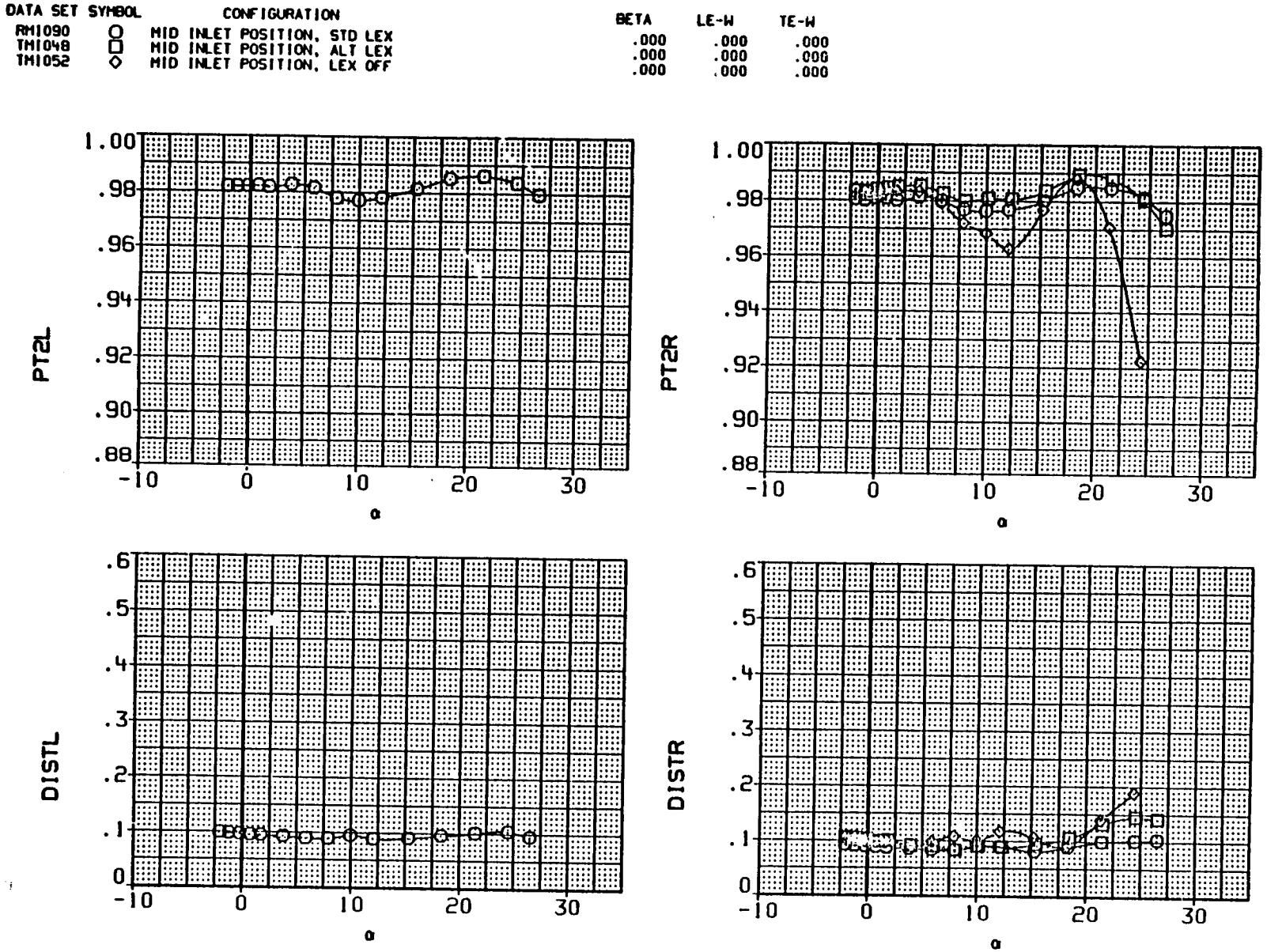

(d) Mach = 0.60.

Figure 10.- Continued.

DATA SET	SYMBOL	CONFIGURATION	BETA	LE-H	TE-H
RM1090	○	MID INLET POSITION, STD LEX	.000	.000	000
TM1048	□	MID INLET POSITION, ALT LEX	.000	.000	.000
TM1052	◇	MID INLET POSITION, LEX OFF	.000	.000	.000

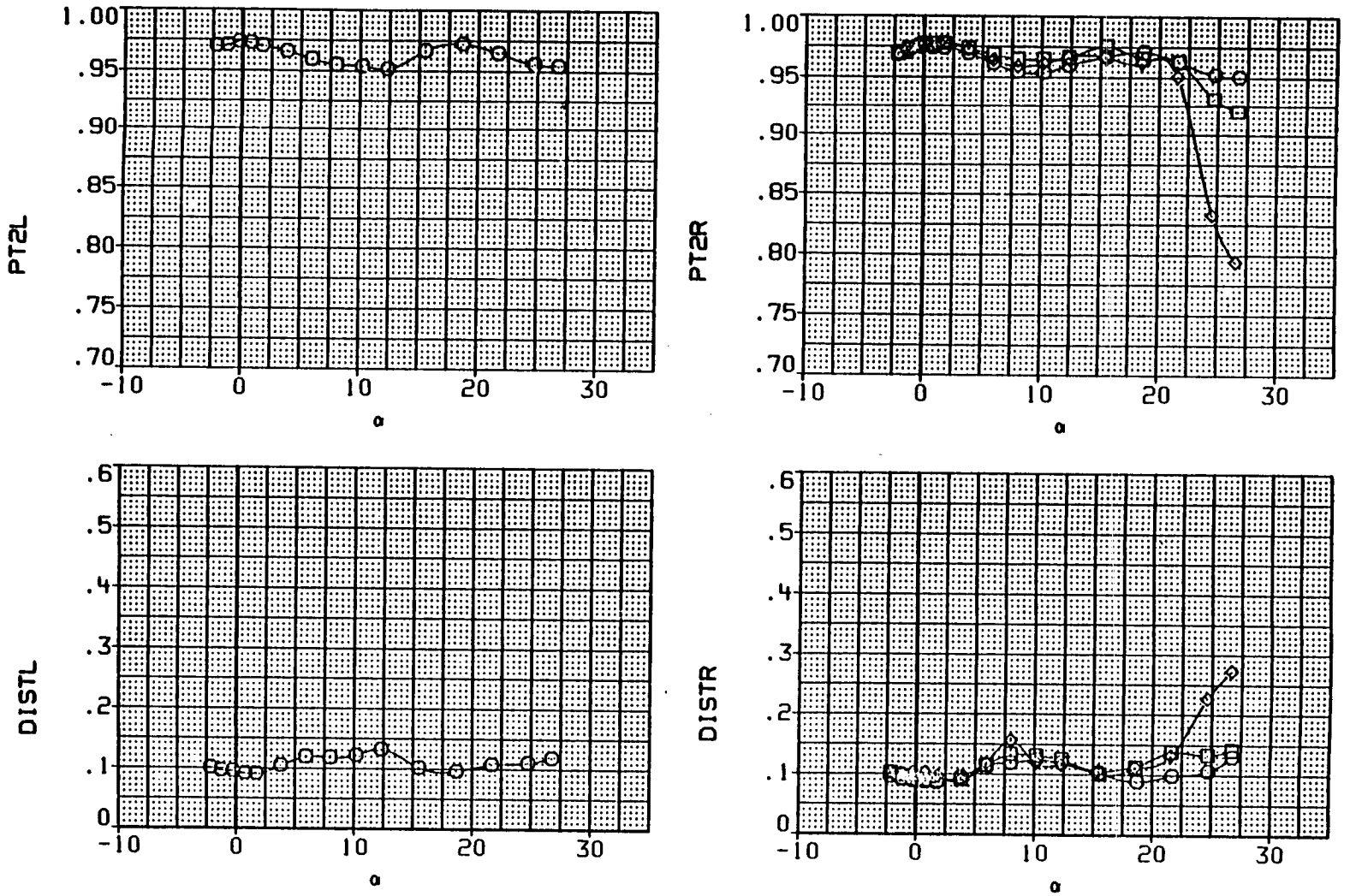

LEFT DUCT - MAX ENGINE AIRFLOW

RIGHT DUCT - MAX ENGINE AIRFLOW

(e) Mach = 0.90.

Figure 10.- Continued.

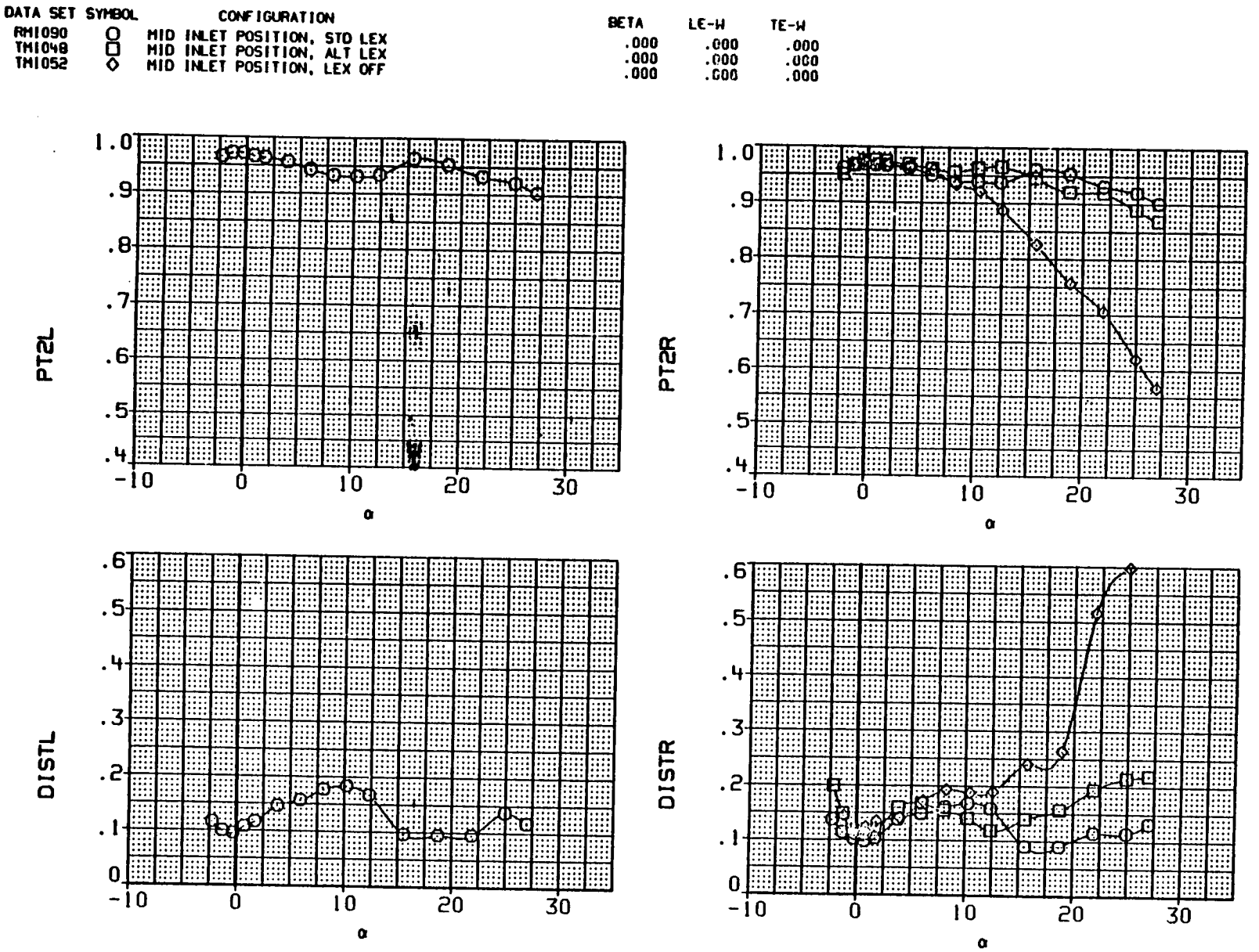

(f) Mach = 1.20.

Figure 10.- Continued.

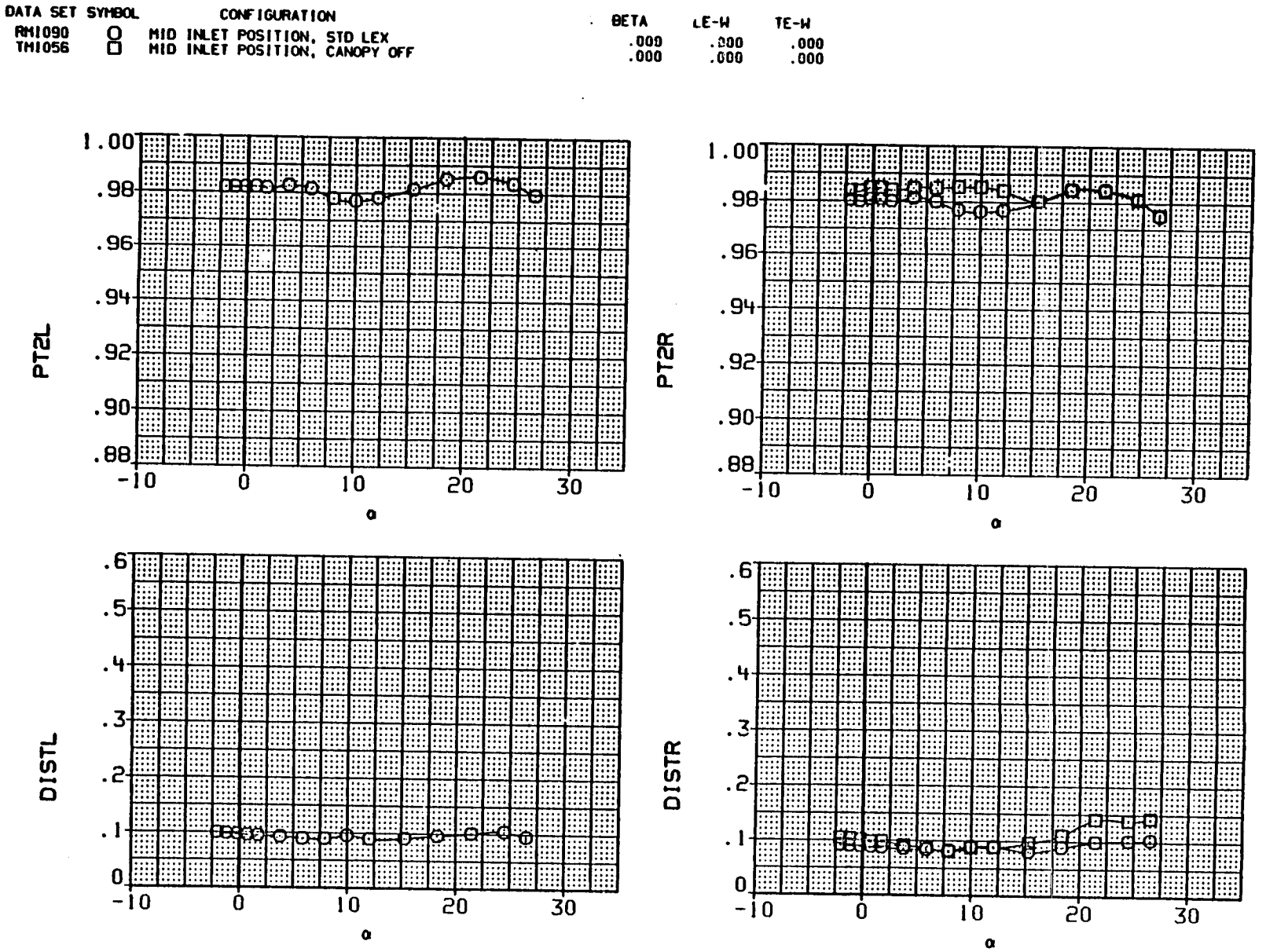

(g) Mach = 0.60.

Figure 10.- Continued.

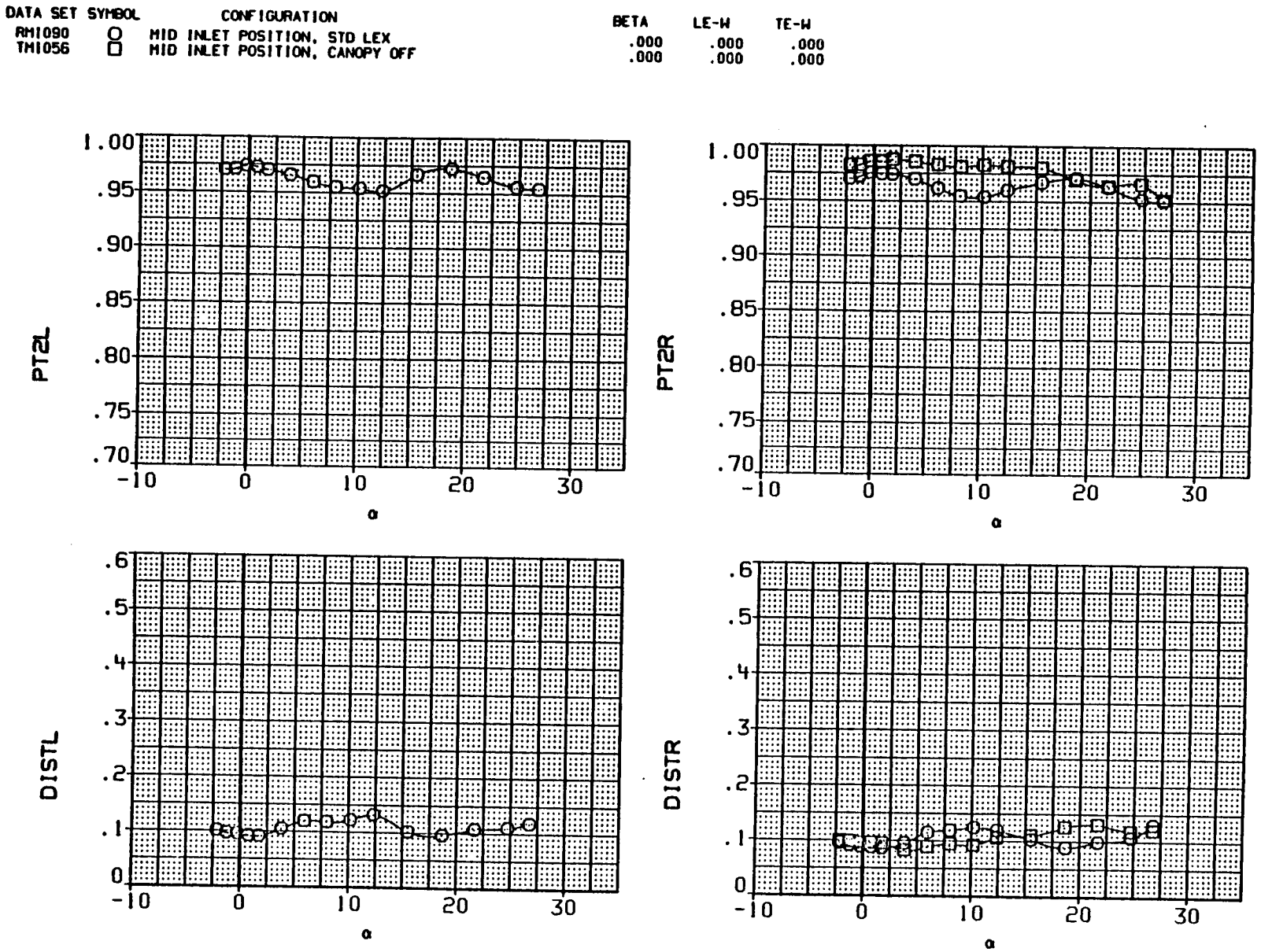

LEFT DUCT - MAX ENGINE AIRFLOW

RIGHT DUCT - MAX ENGINE AIRFLOW

(h) Mach = 0.90.

Figure 10.- Continued.

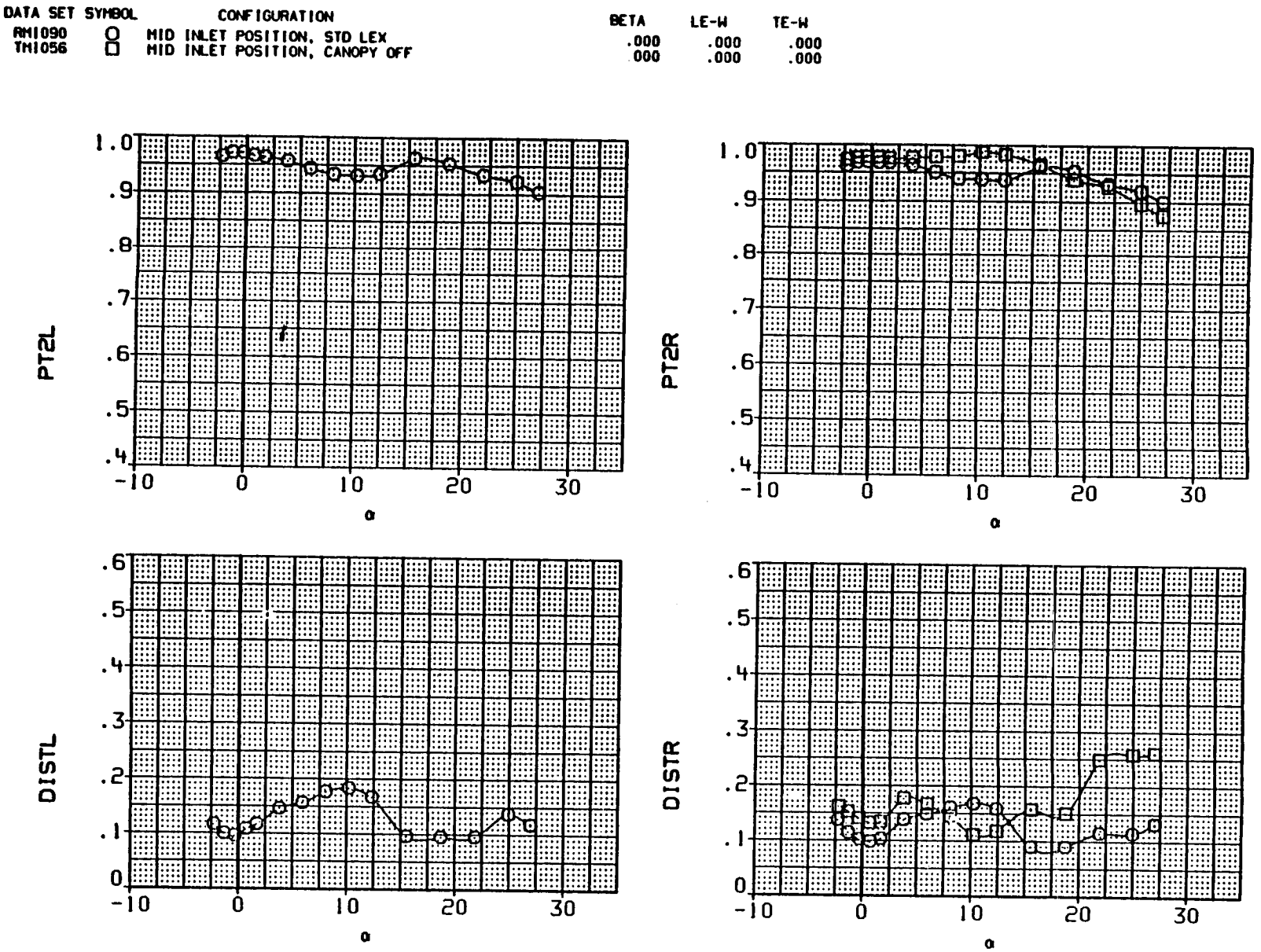

(i) Mach = 1.20.

Figure 10.- Continued.

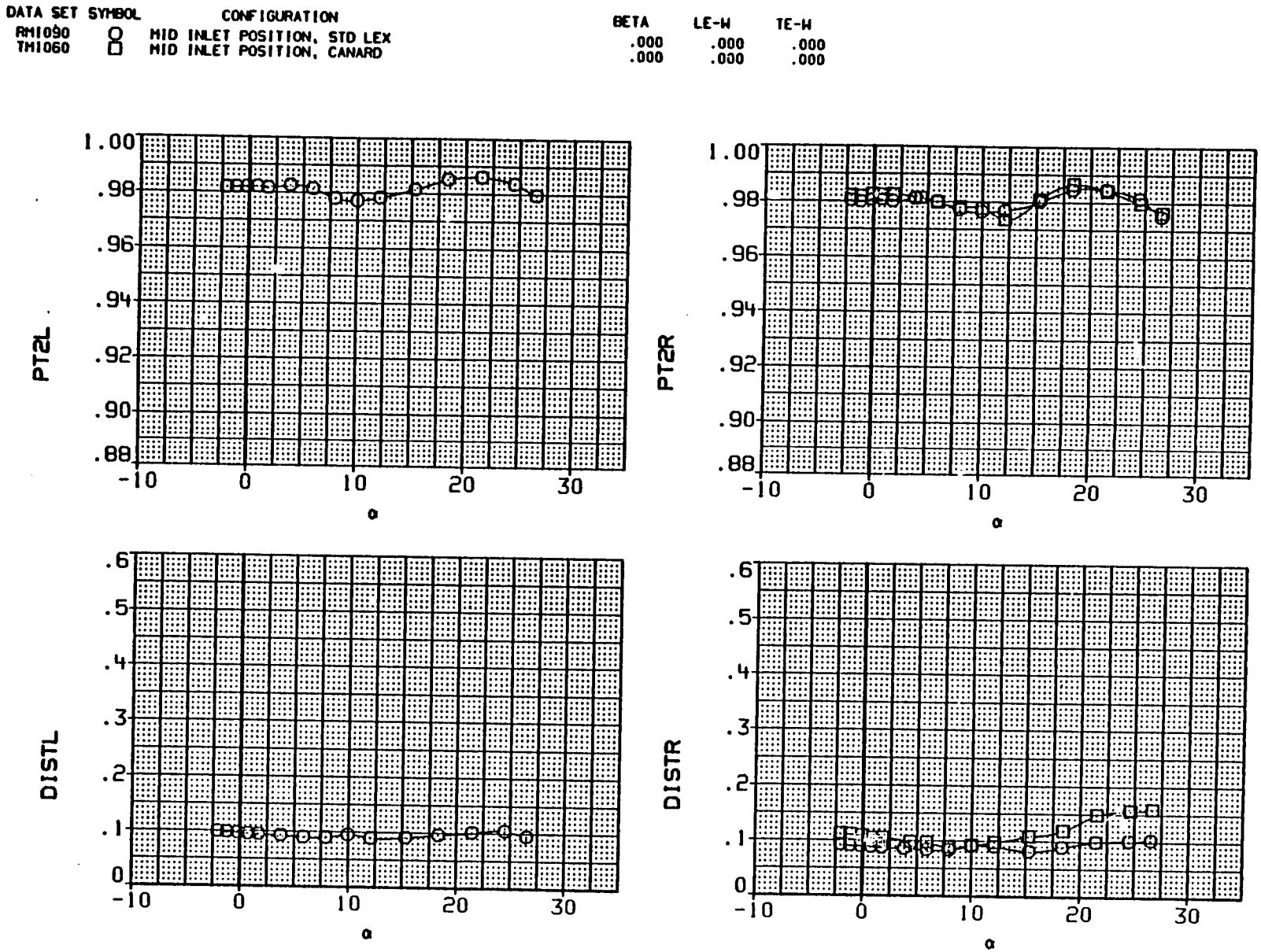

LEFT DUCT - MAX ENGINE AIRFLOW

RIGHT DUCT - MAX ENGINE AIRFLOW

(j) Mach = 0.60.

Figure 10.- Continued.

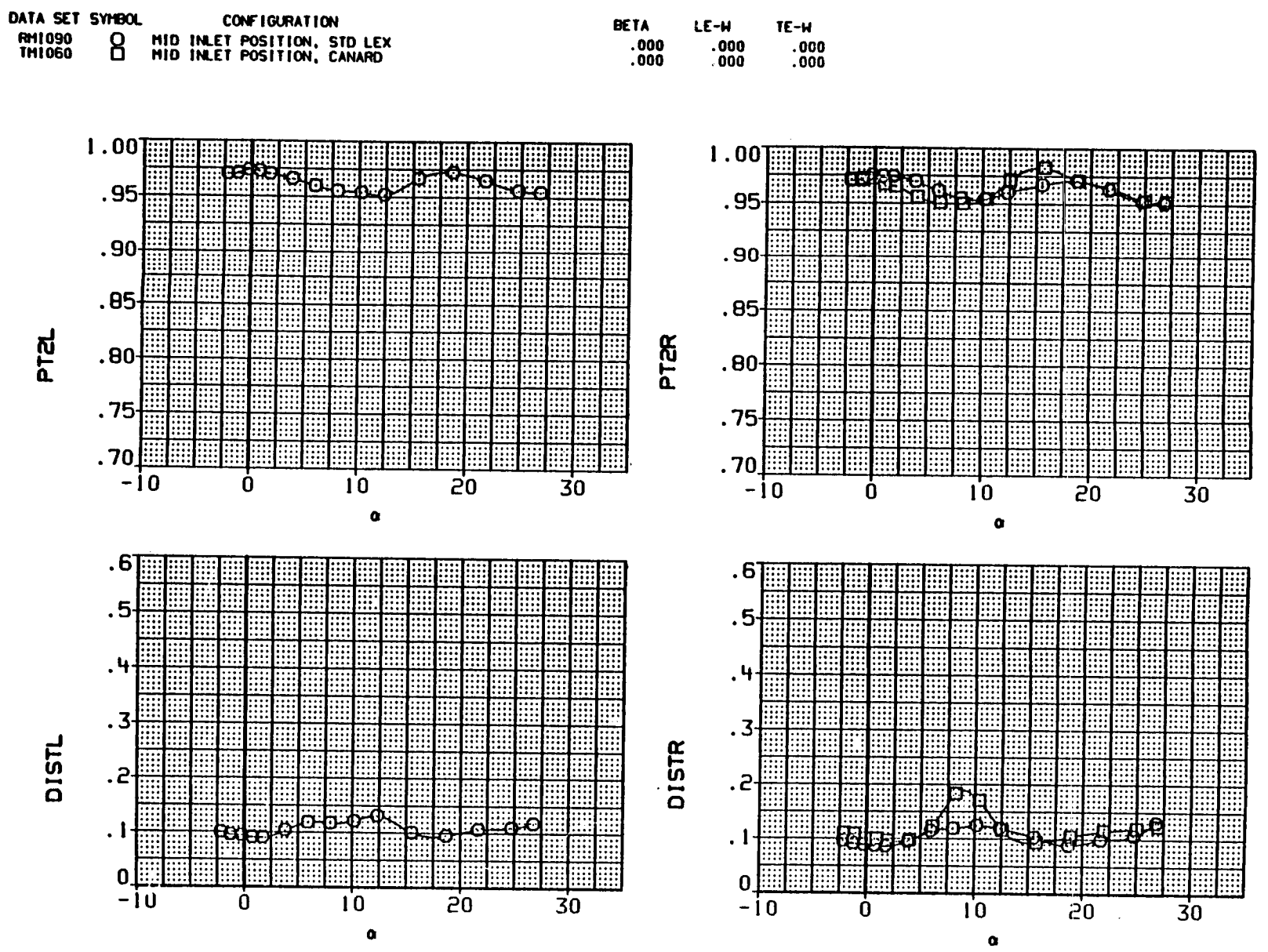

(k) Mach = 0.90.

Figure 10.- Continued.

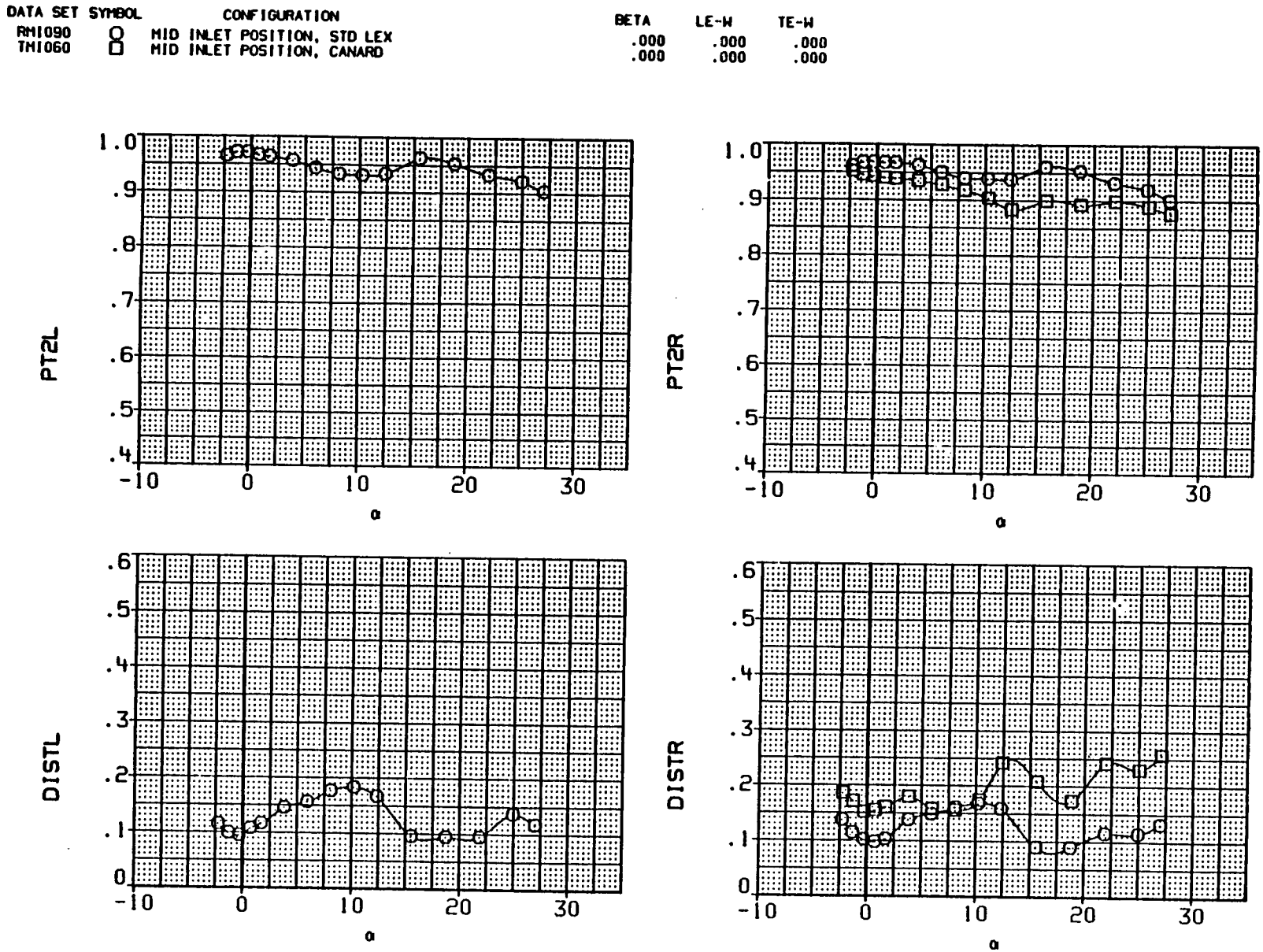

LEFT DUCT - MAX ENGINE AIRFLOW

RIGHT DUCT - MAX ENGINE AIRFLOW

(l) Mach = 1.20.

Figure 10.- Continued.

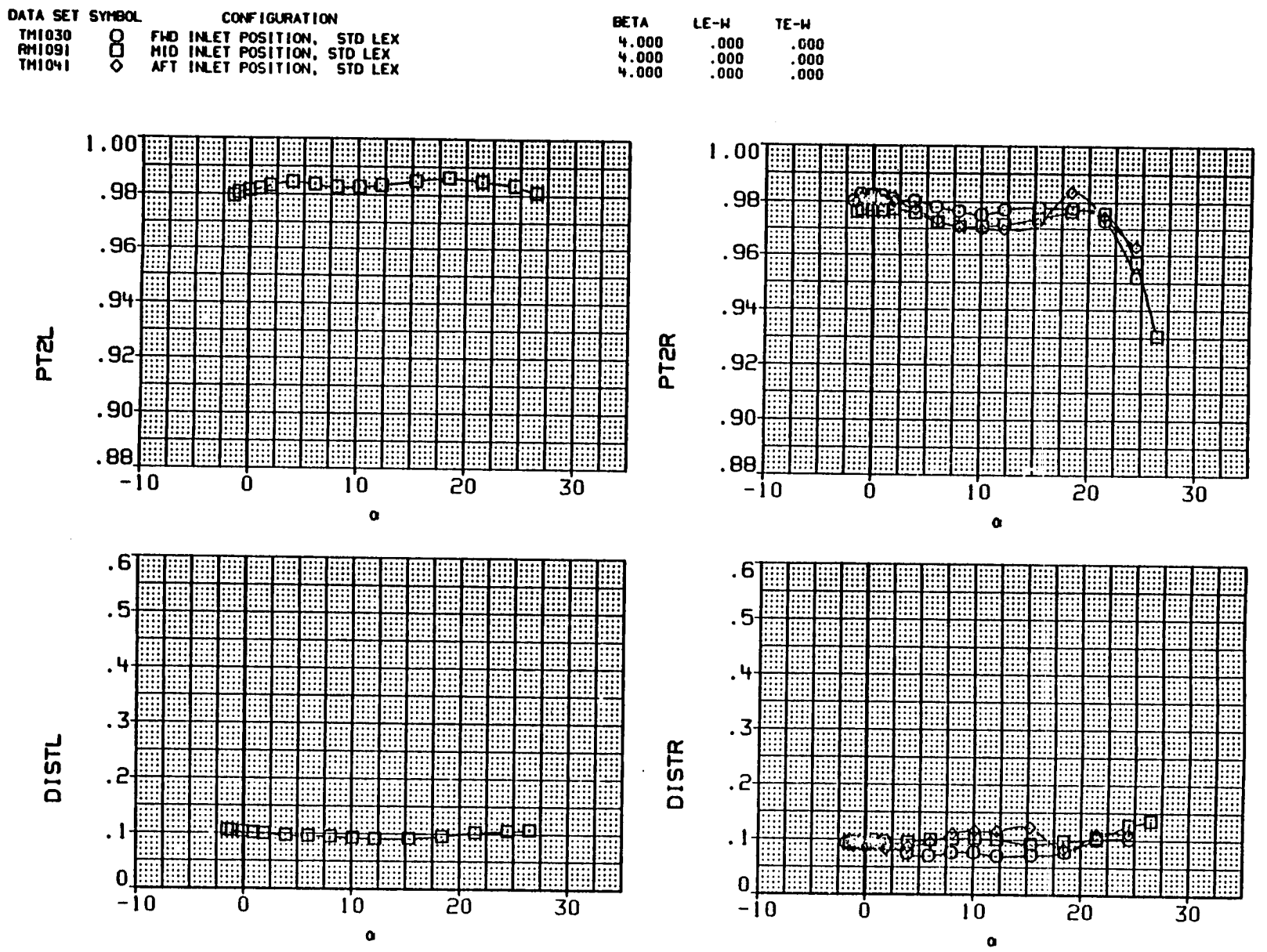

LEFT DUCT - MAX ENGINE AIRFLOW

RIGHT DUCT - MAX ENGINE AIRFLOW

(m) Mach = 0.60.

Figure 10.- Continued.

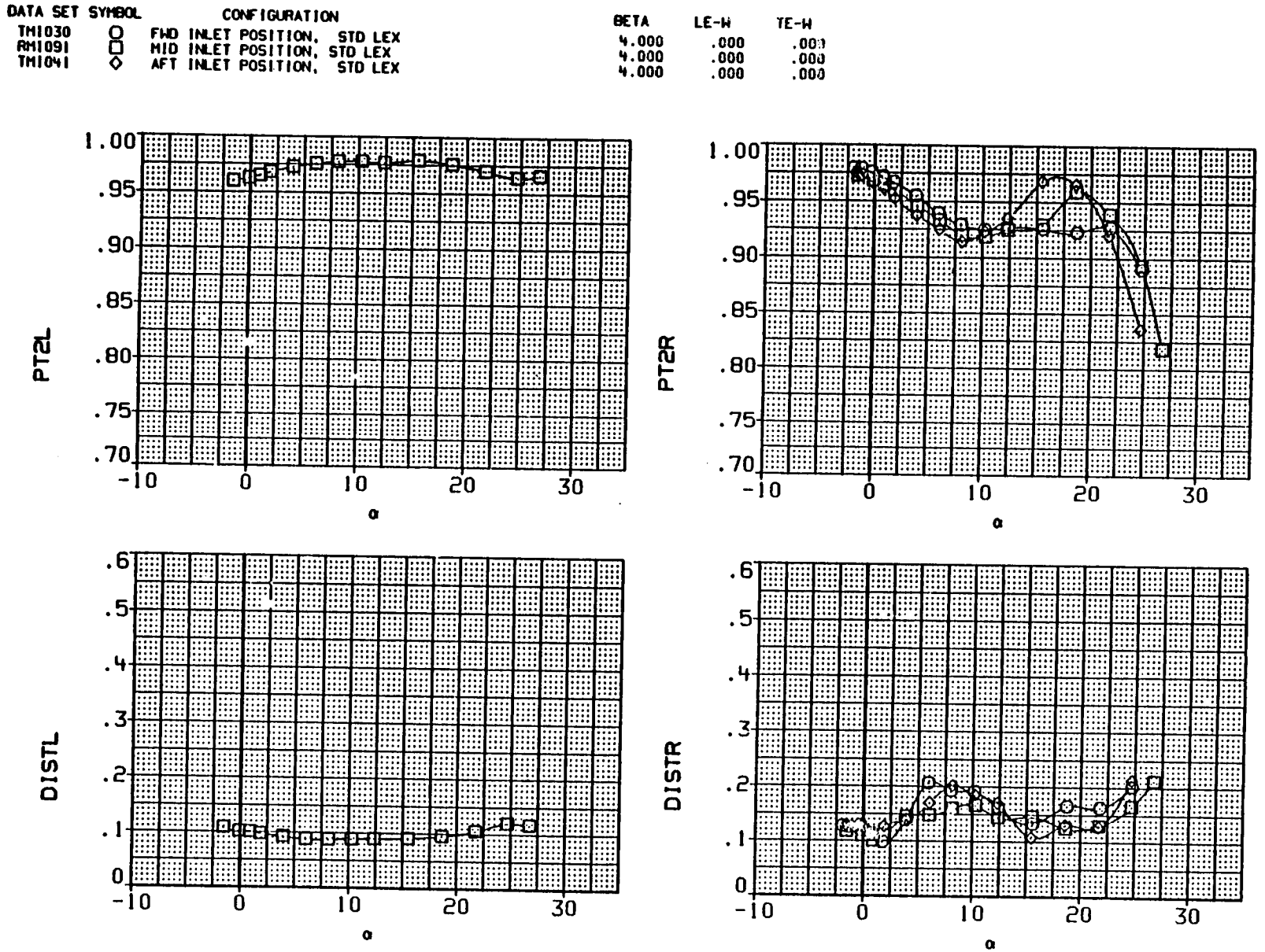

LEFT DUCT - MAX ENGINE AIRFLOW

RIGHT DUCT - MAX ENGINE AIRFLOW

(n) Mach = 0.90.

Figure 10.- Continued.

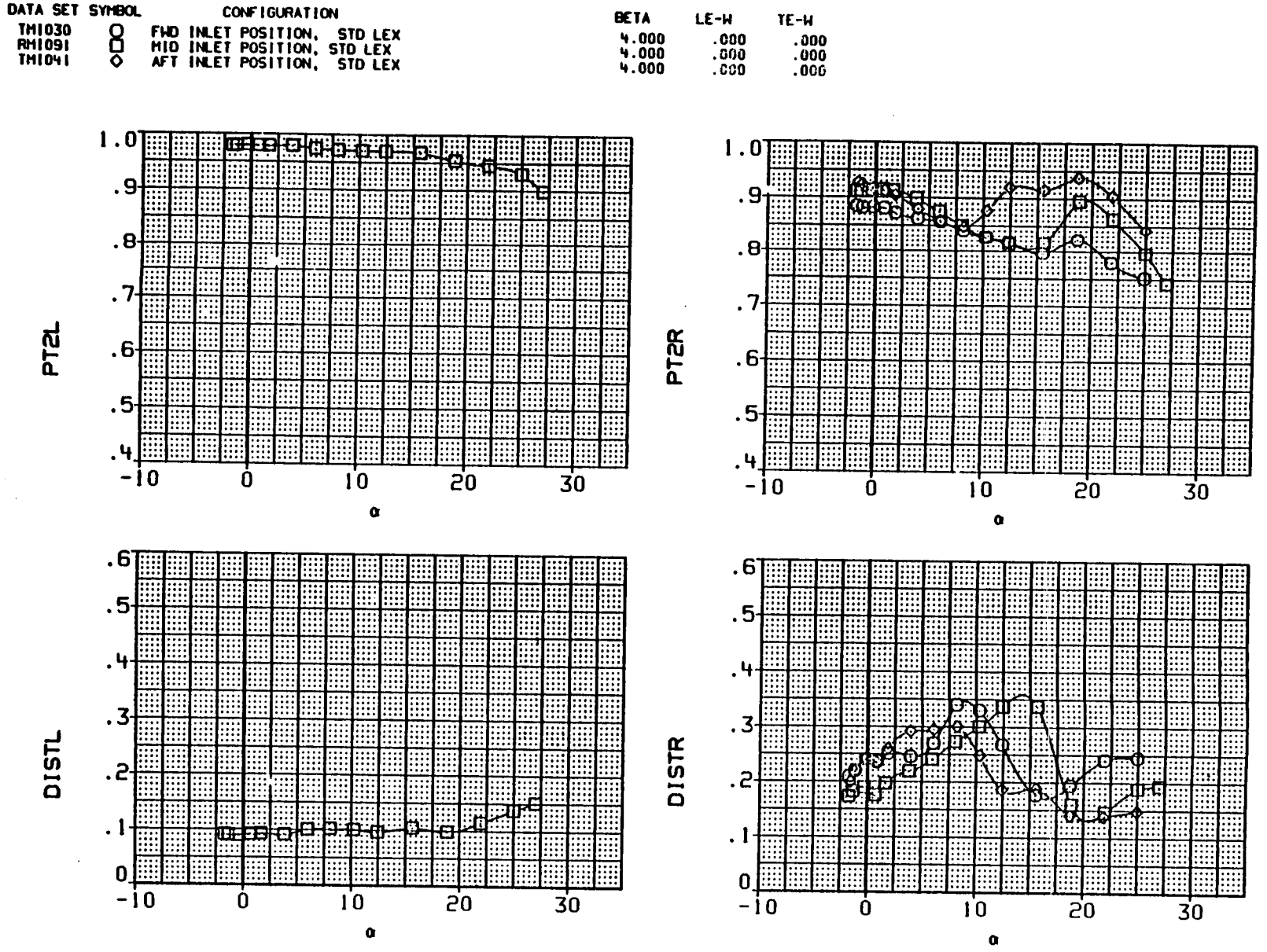

(o) Mach = 1.20.

Figure 10.- Continued.

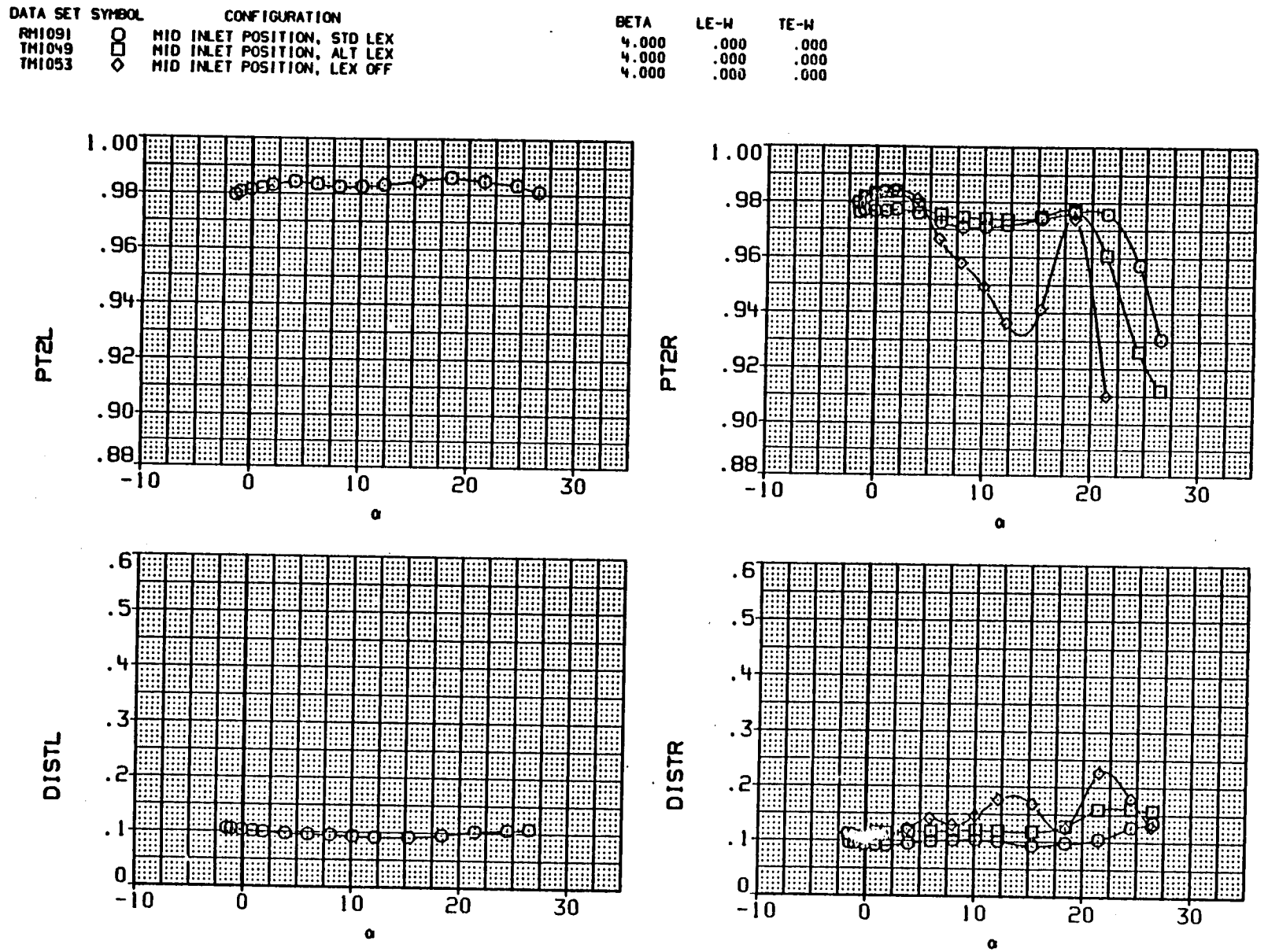

(p) Mach = 0.60.

Figure 10.- Continued.

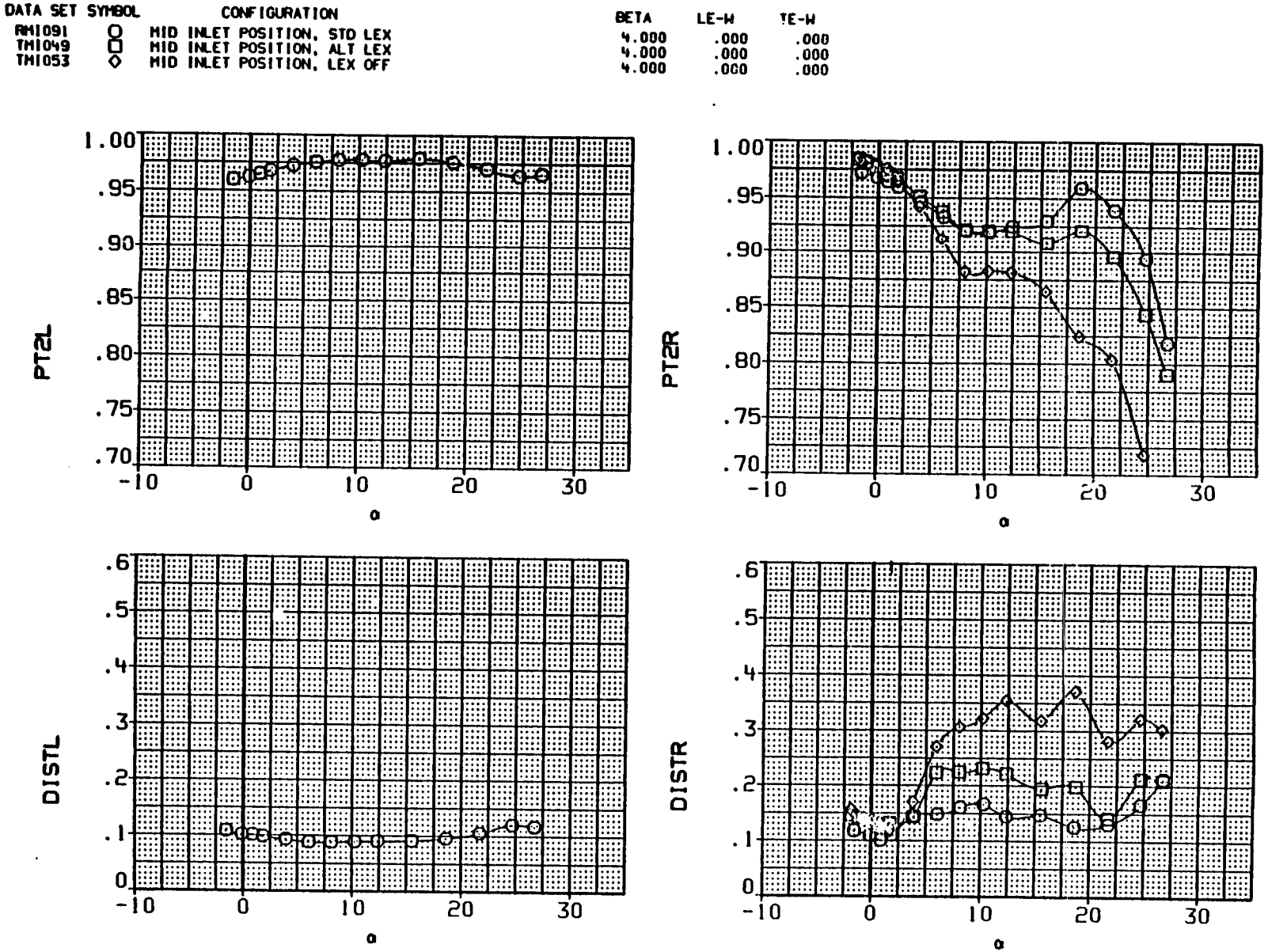

(q) Mach = 0.90.

Figure 10.- Continued.

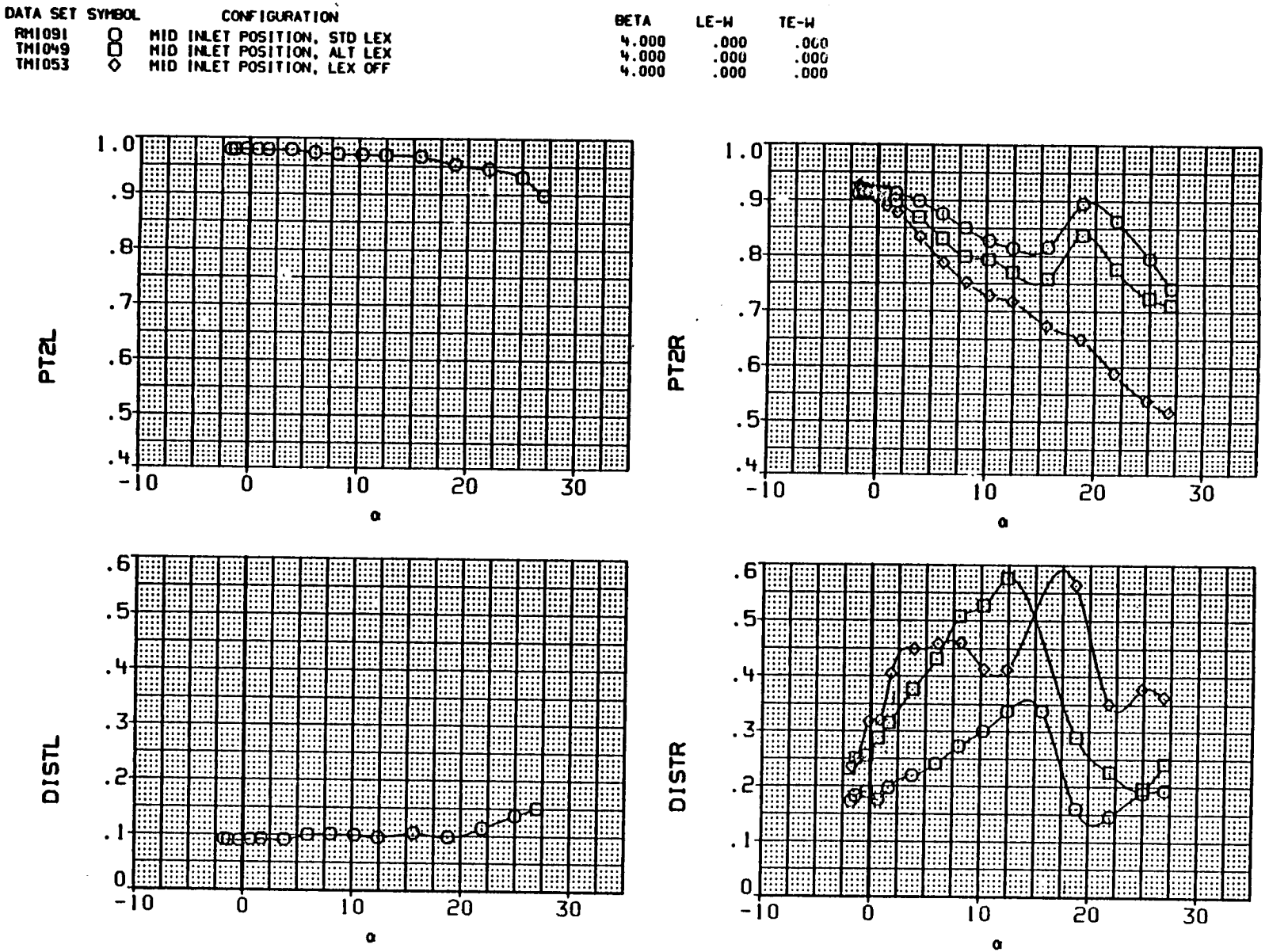

(r) Mach = 1.20.

Figure 10.- Continued.

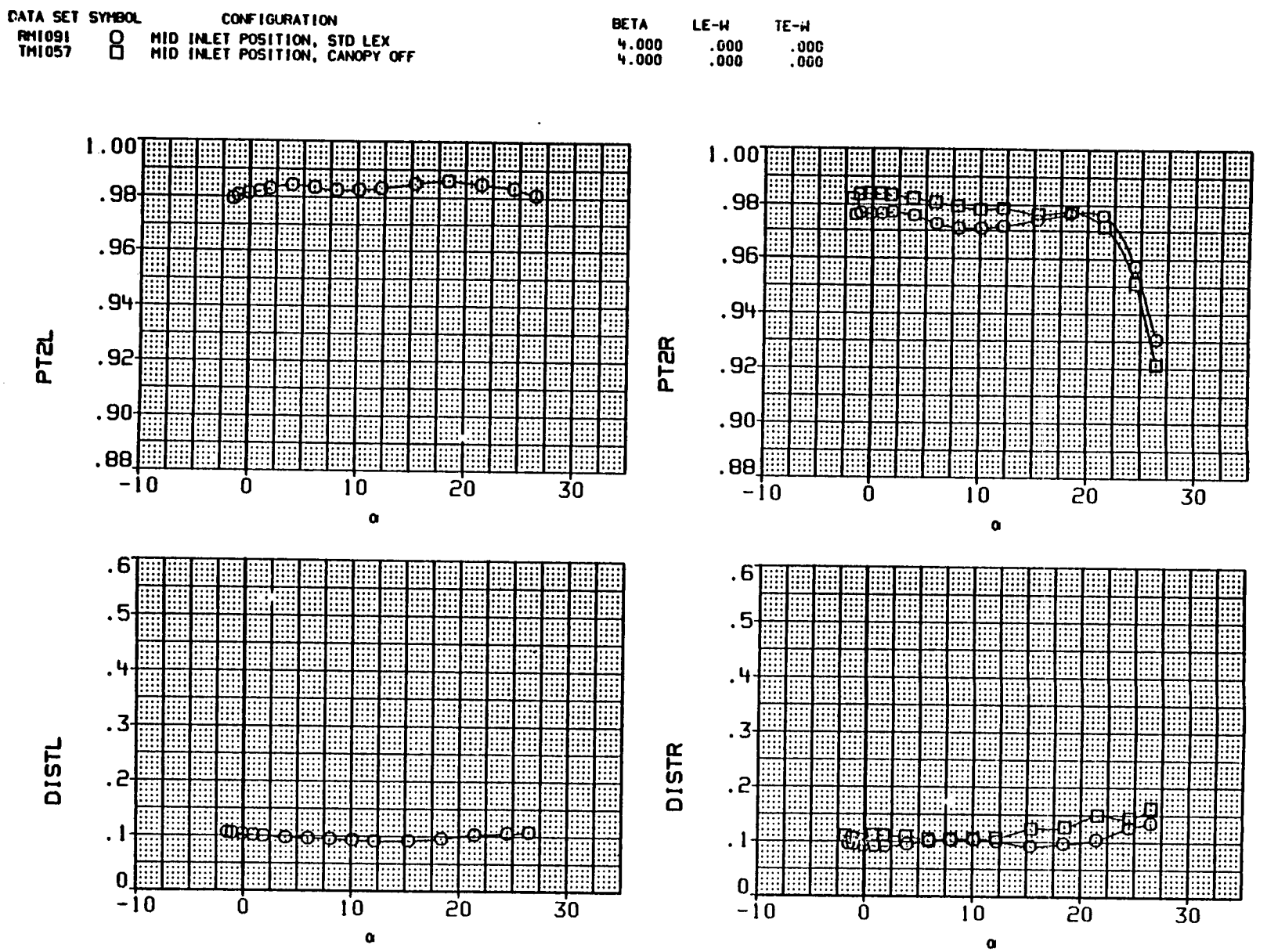

(s) Mach = 0.60.

Figure 10.- Continued.

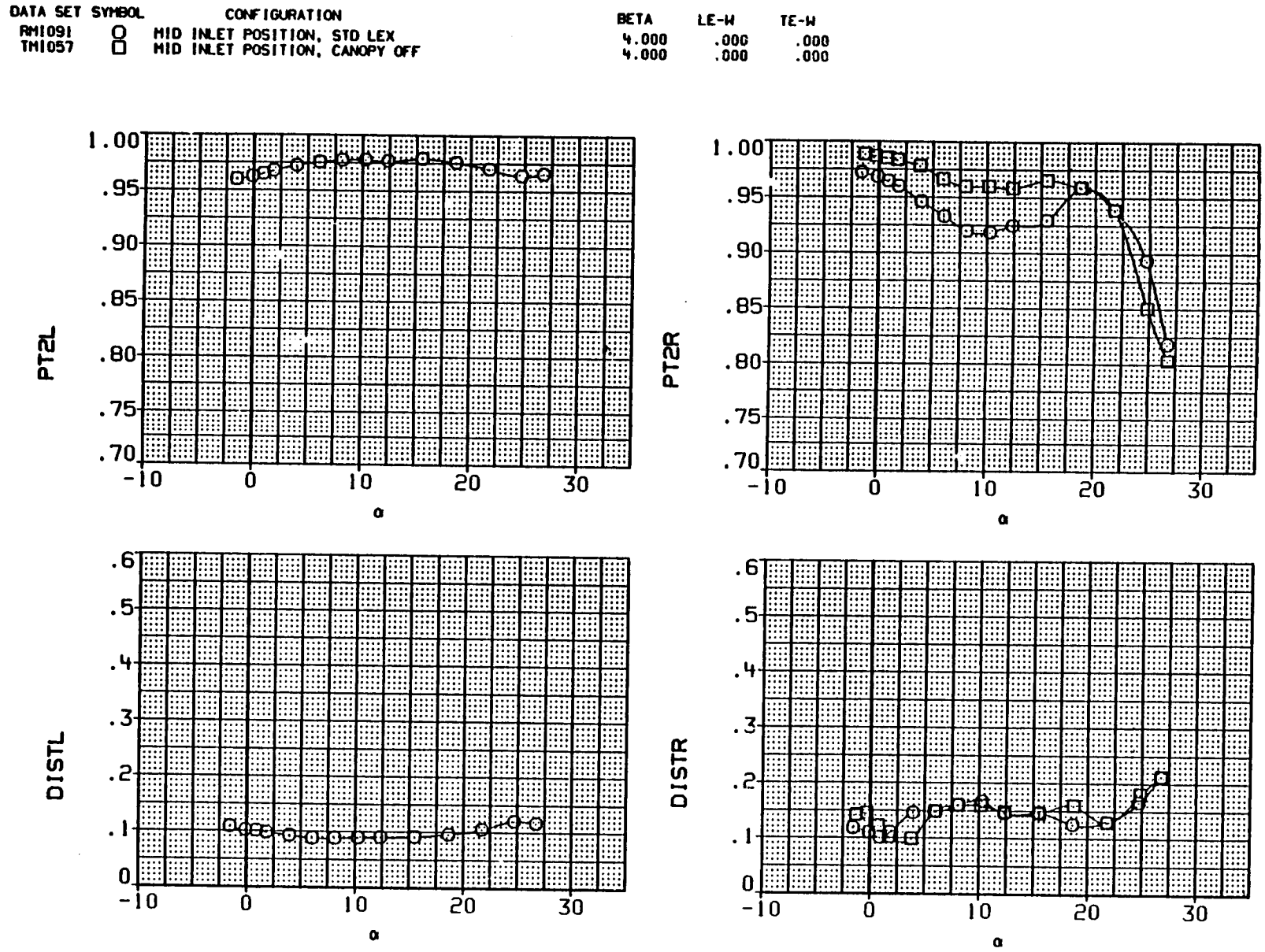

(t) Mach = 0.90.

Figure 10.- Continued.

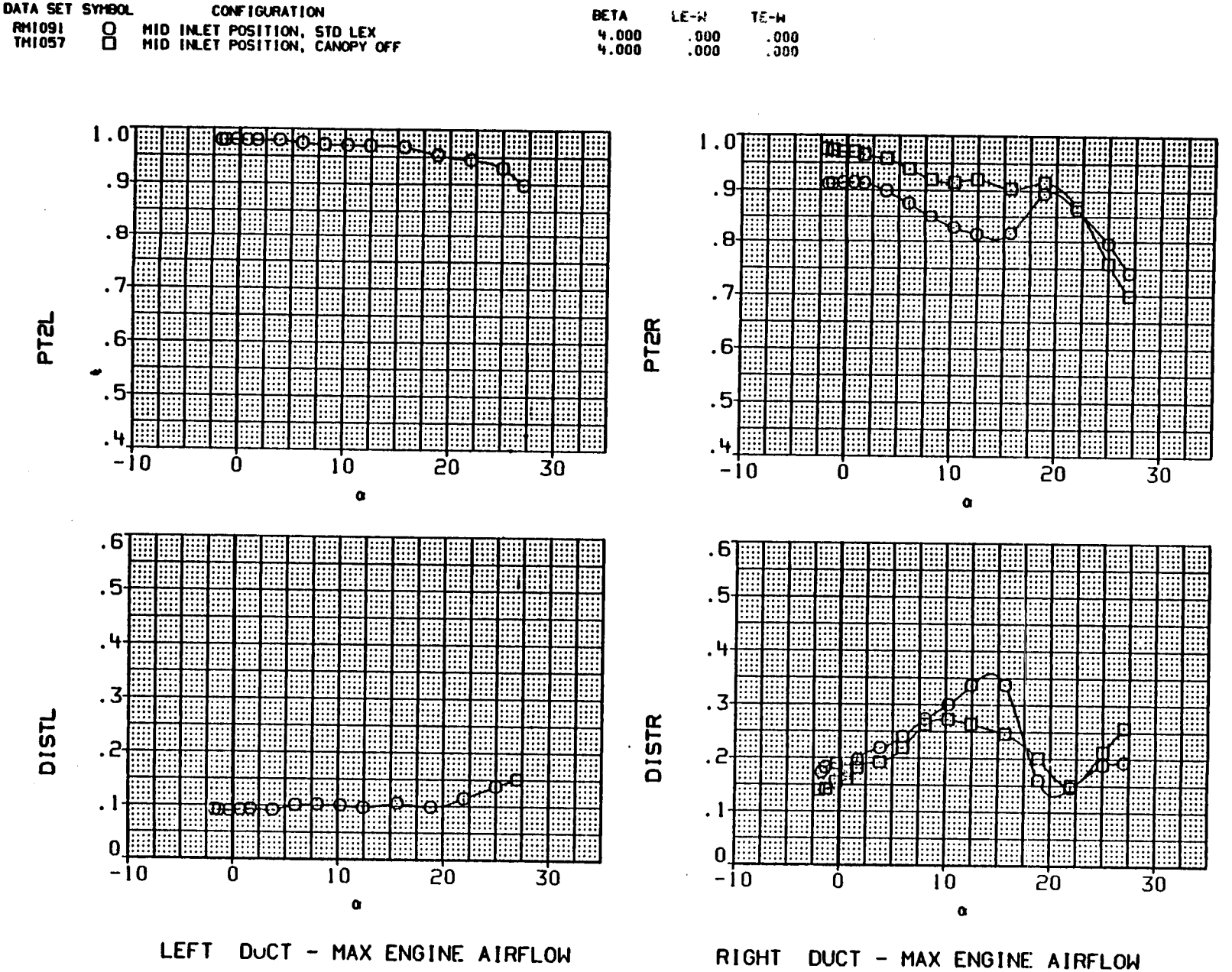

LEFT DUCT - MAX ENGINE AIRFLOW

RIGHT DUCT - MAX ENGINE AIRFLOW

(u) Mach = 1.20.

Figure 10.- Continued.

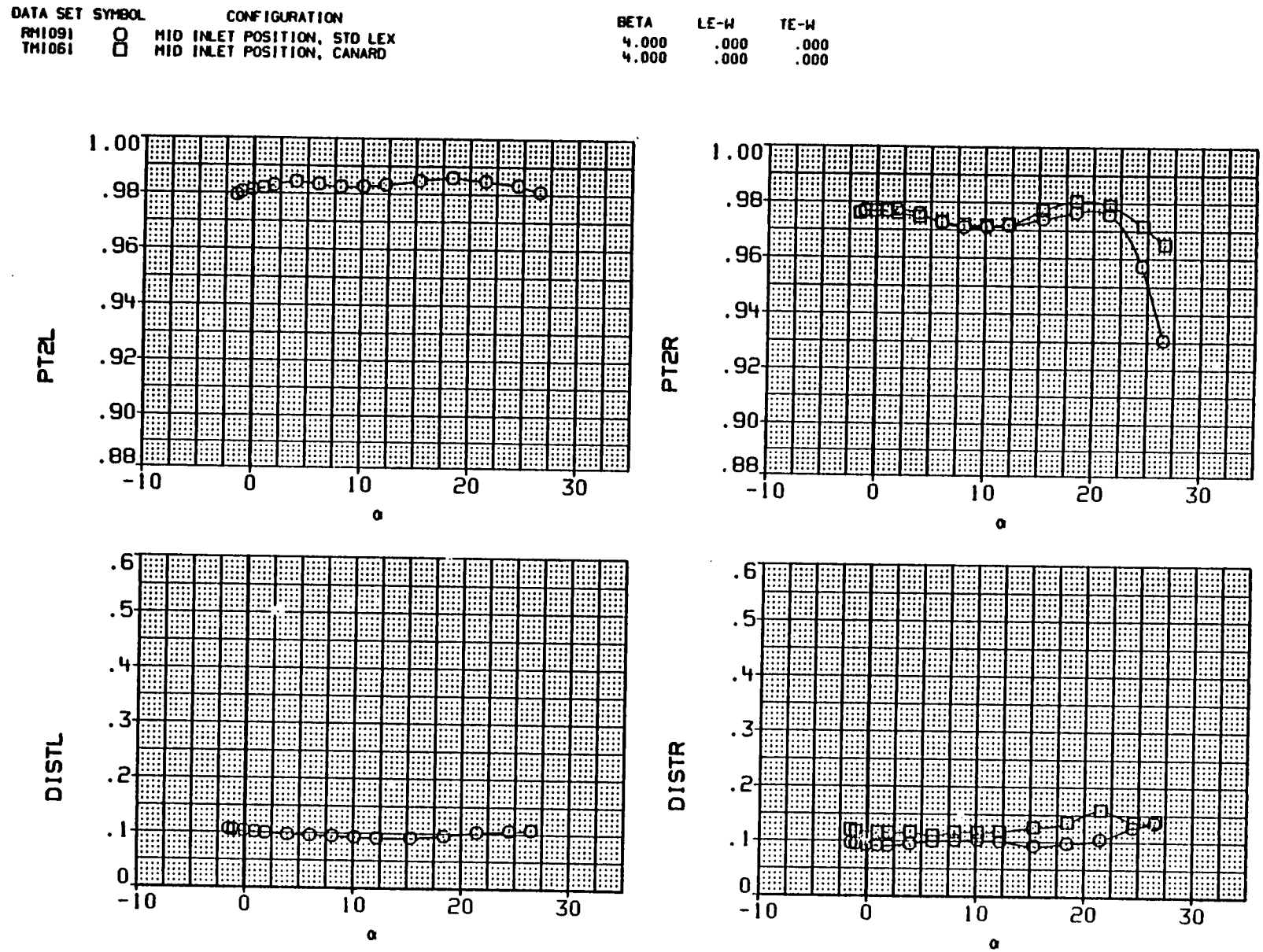

(v) Mach = 0.60.

Figure 10.- Continued.

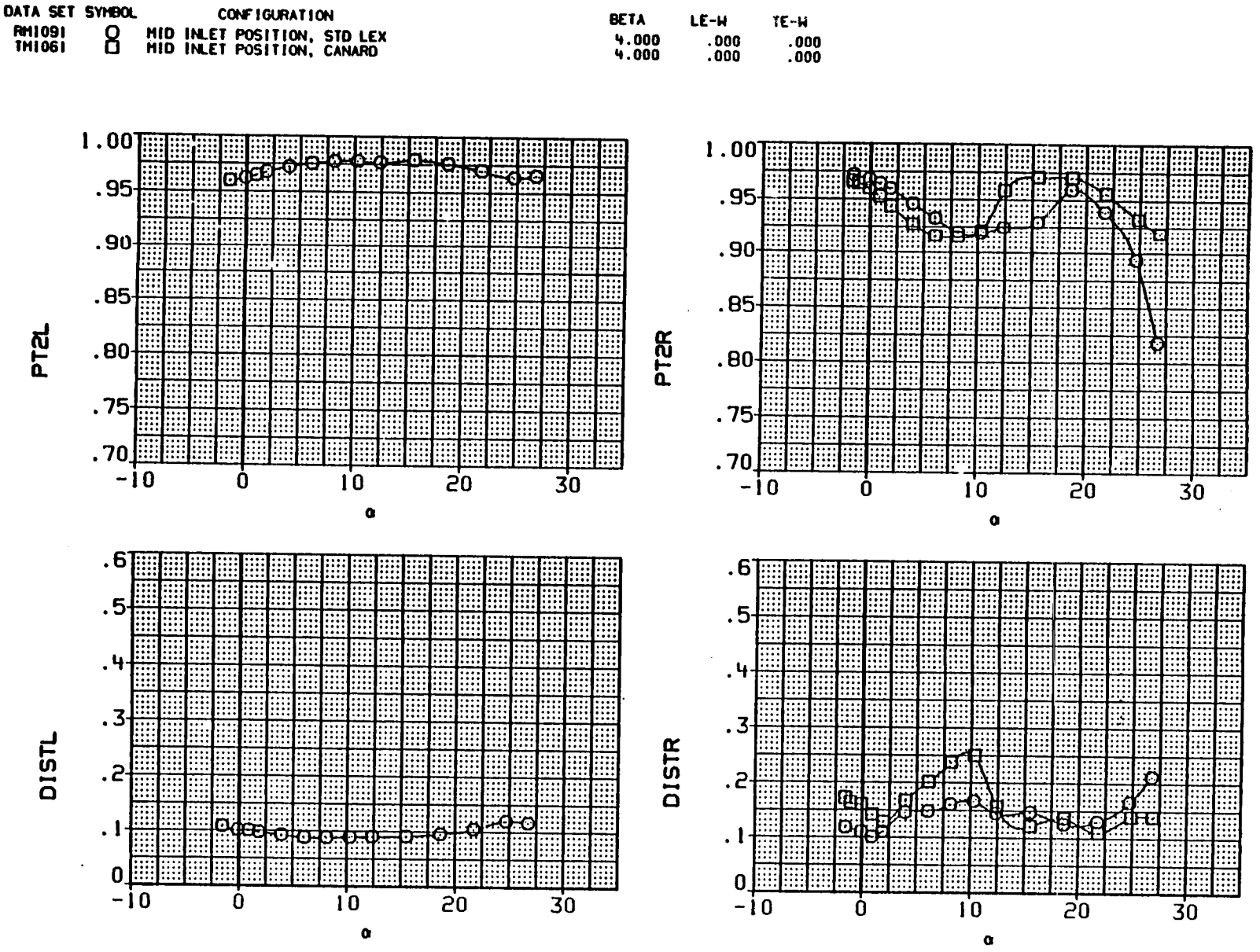

(w) Mach = 0.90.

Figure 10.- Continued.

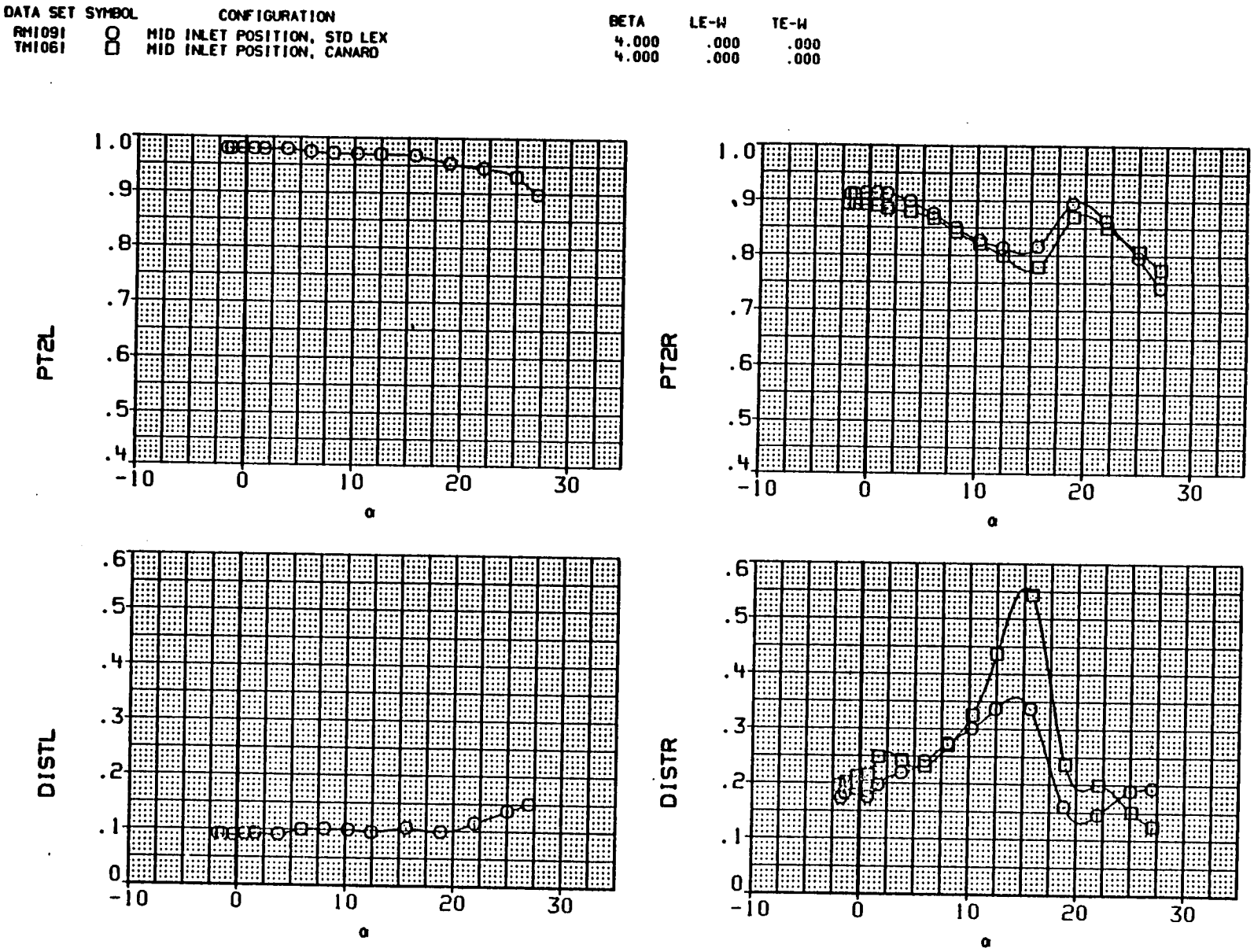

(x) Mach = 1.20.

Figure 10.- Continued.

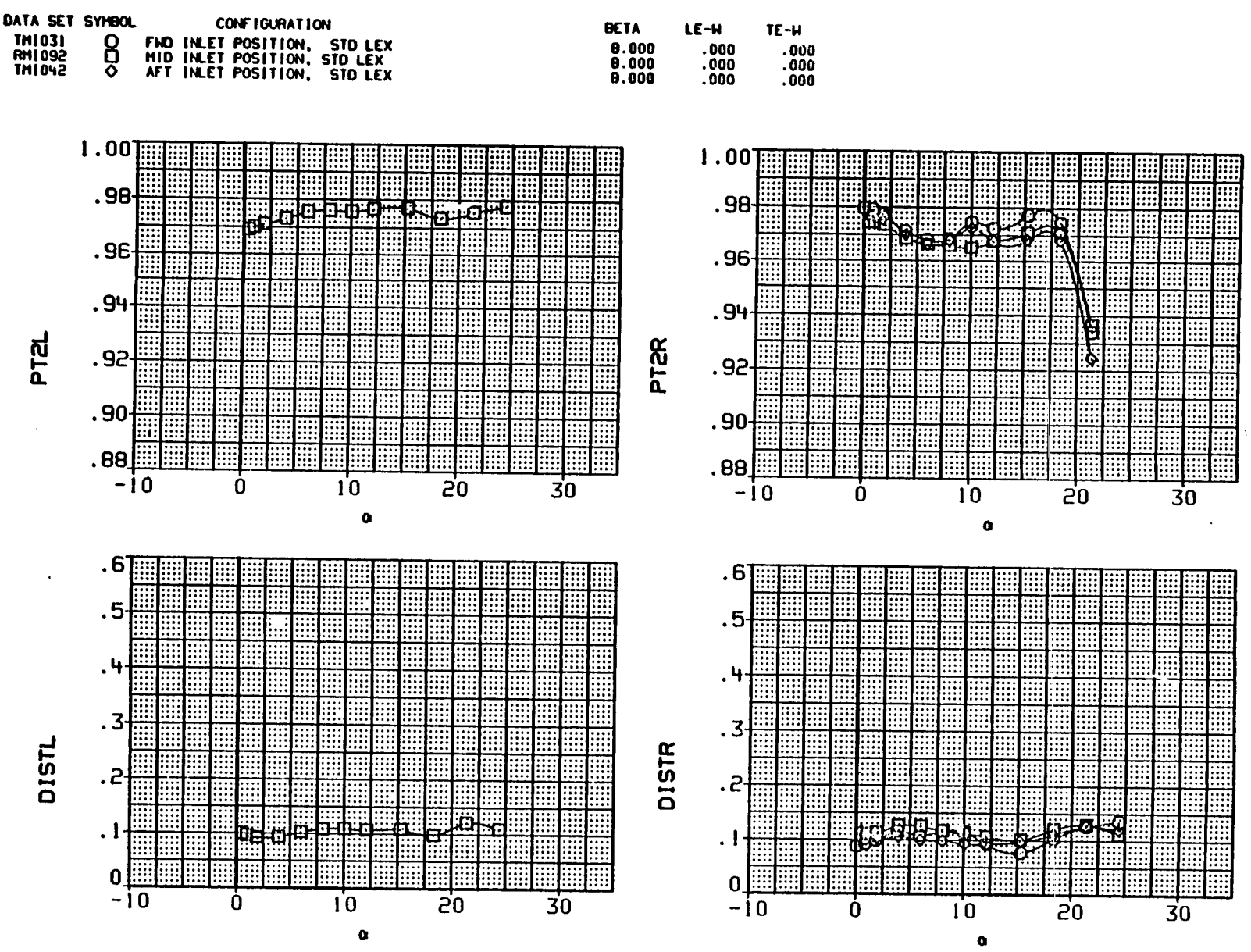

(y) Mach = 0.60.

Figure 10.- Continued.

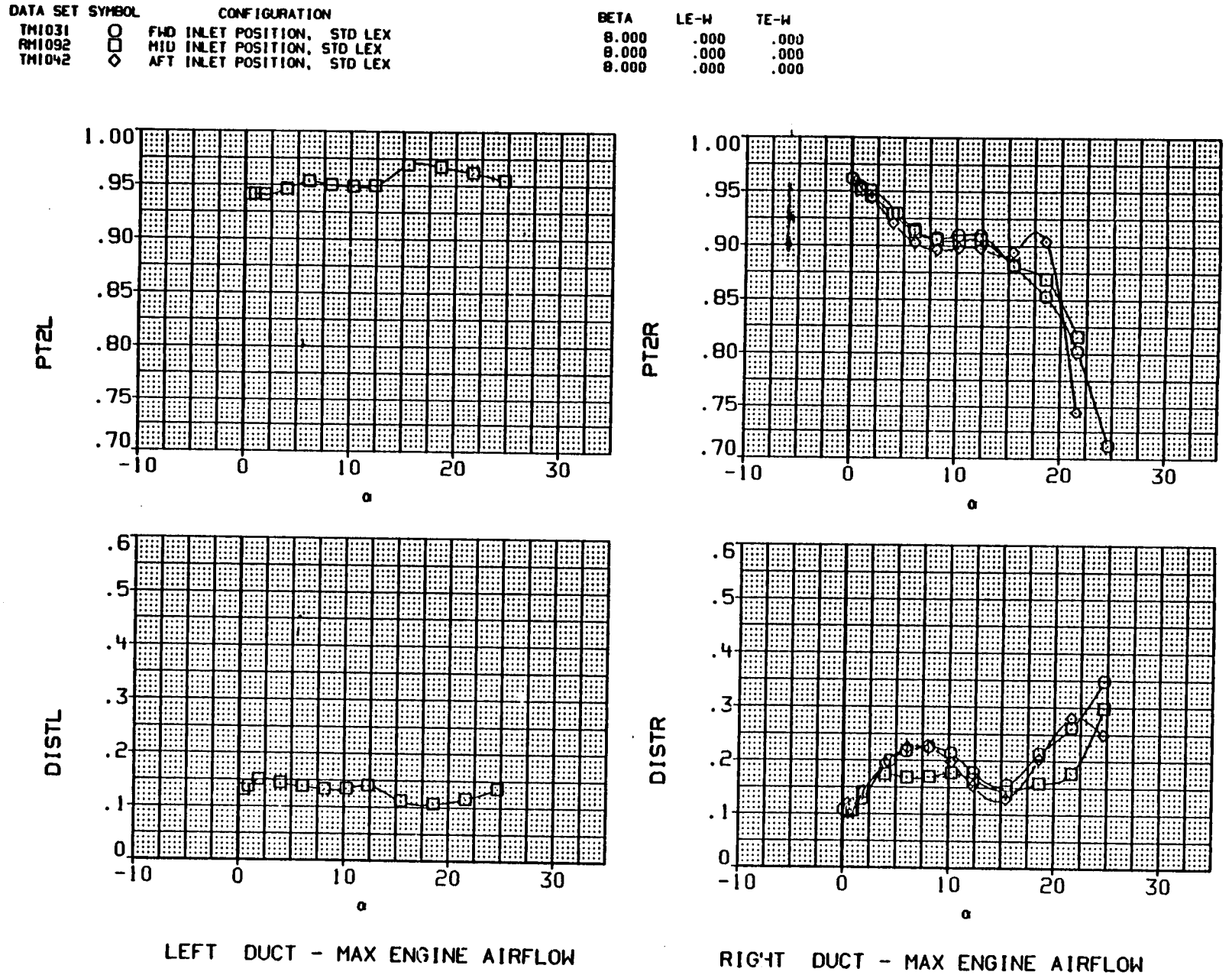

LEFT DUCT - MAX ENGINE AIRFLOW RIGHT DUCT - MAX ENGINE AIRFLOW

(z) Mach = 0.90.

Figure 10.- Continued.

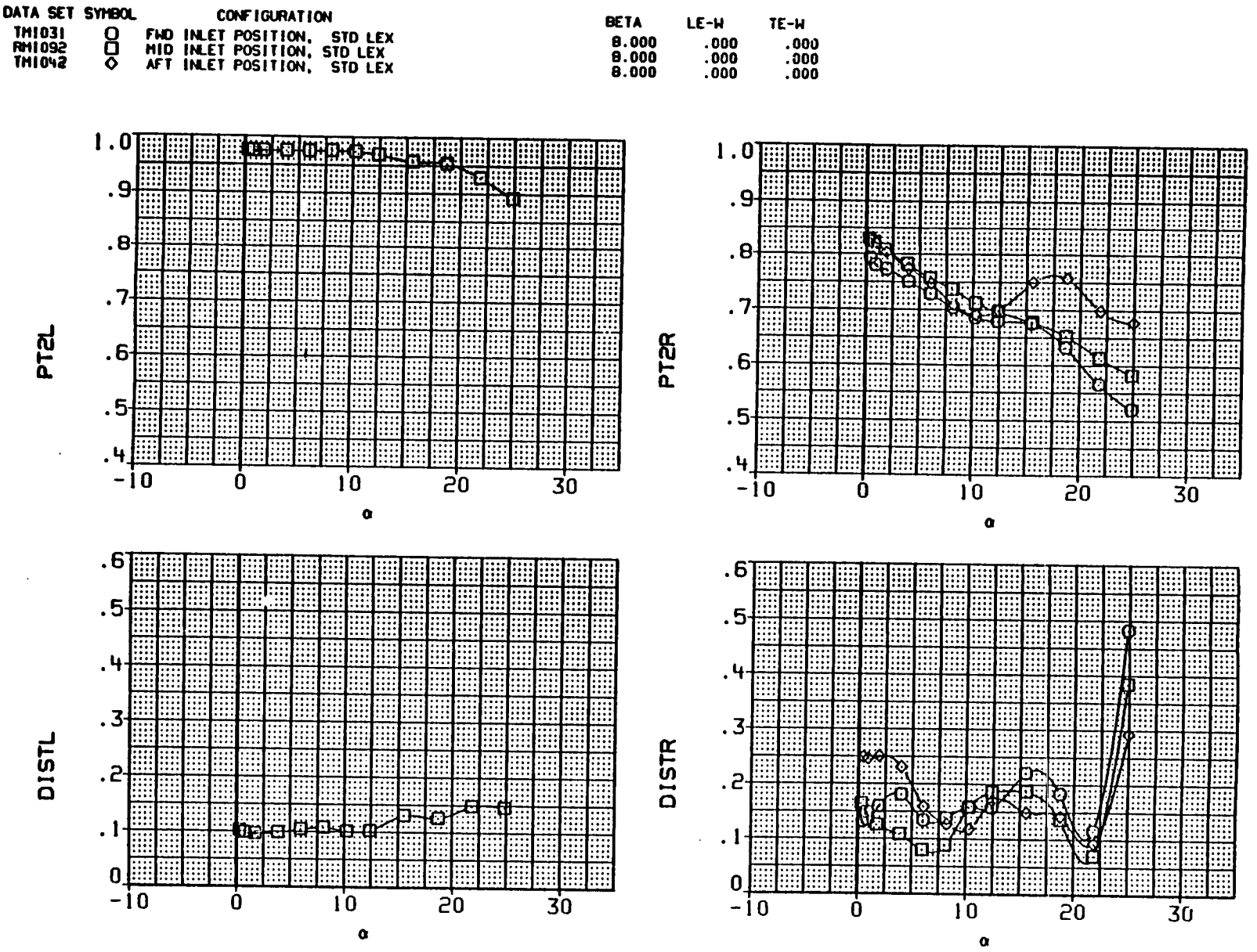

(aa) Mach = 1.20.

Figure 10.- Continued.

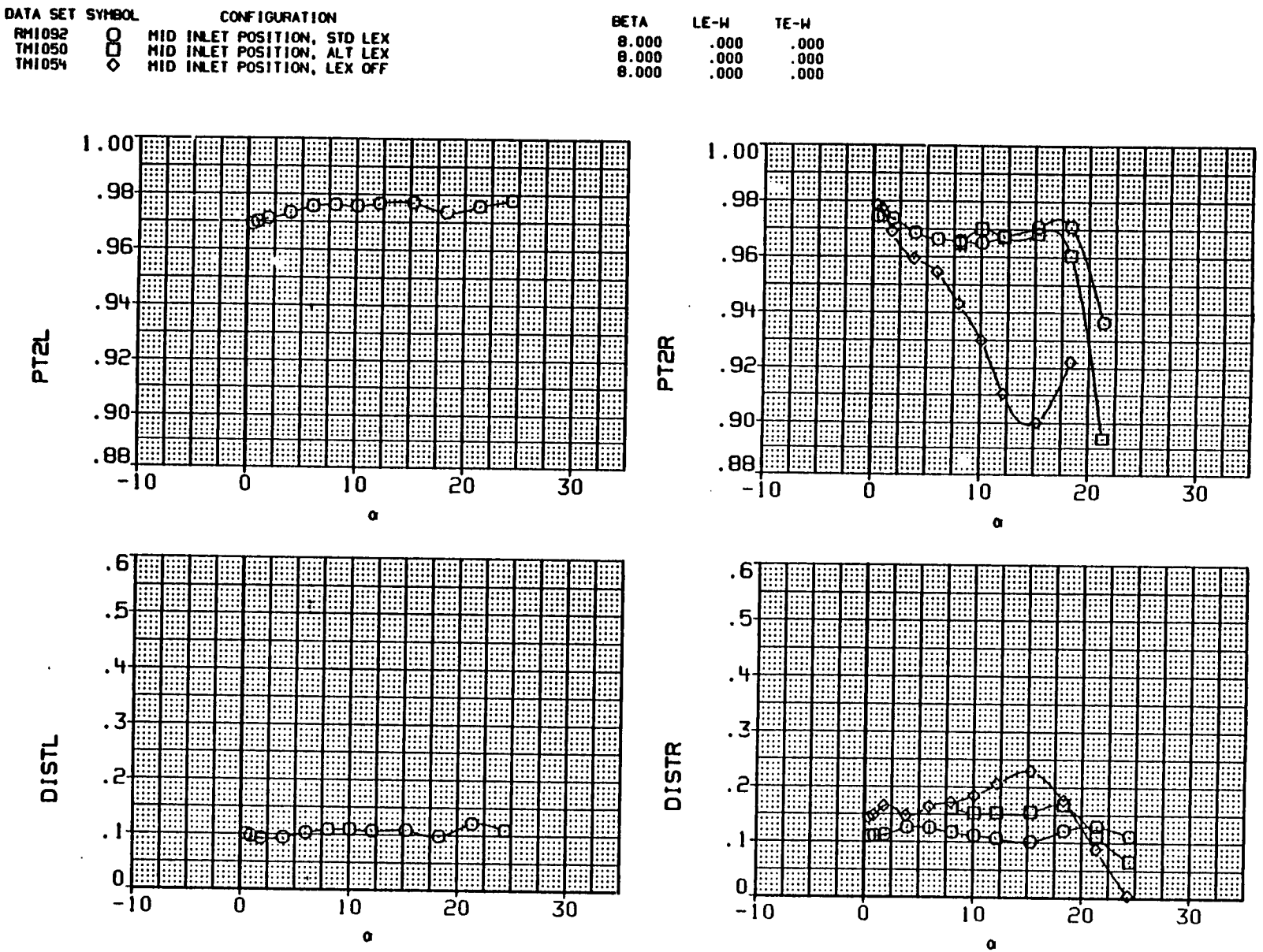

(bb) Mach = 0.60.

Figure 10.- Continued.

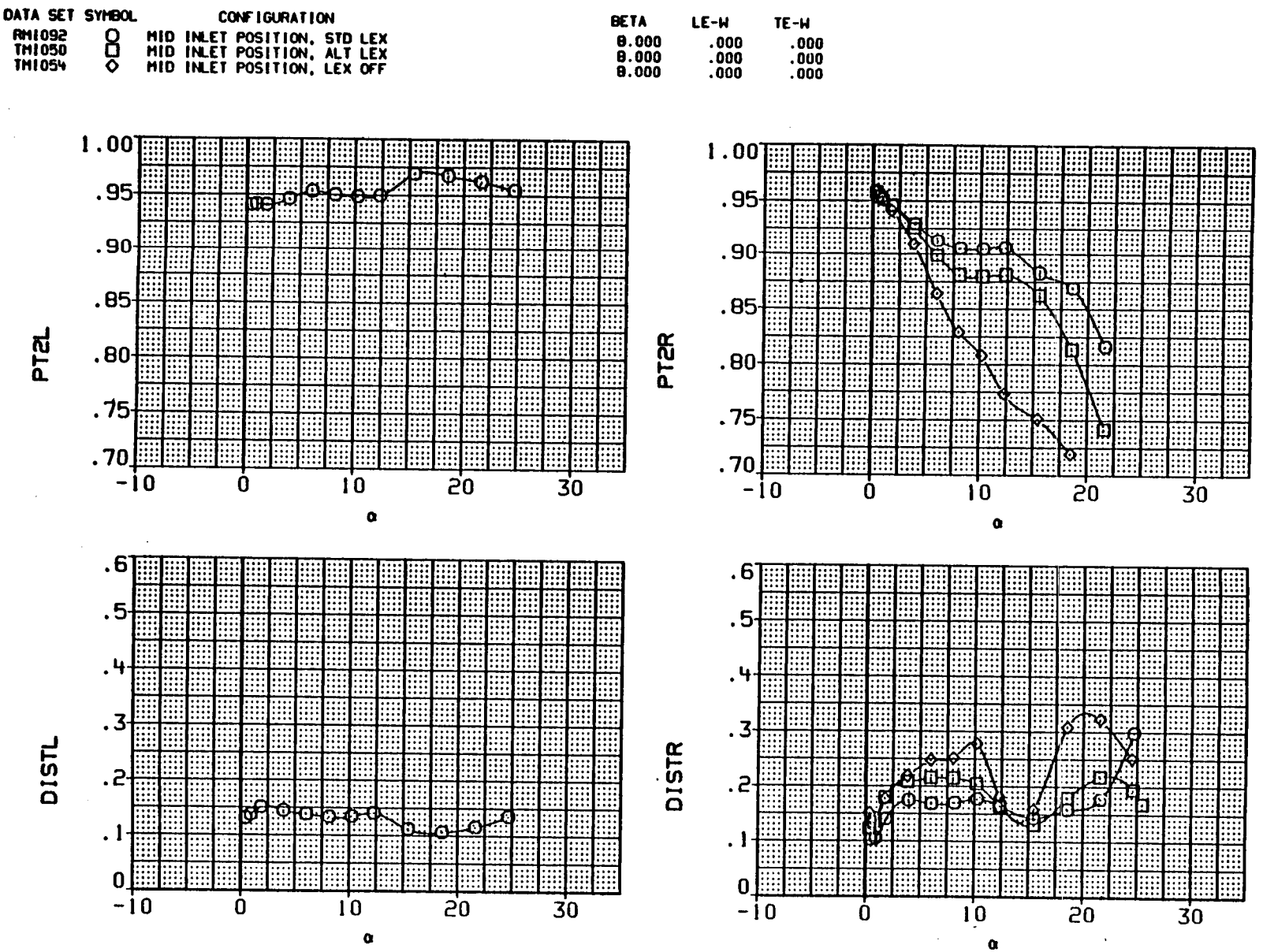

(cc) Mach = 0.90.

Figure 10.- Continued.

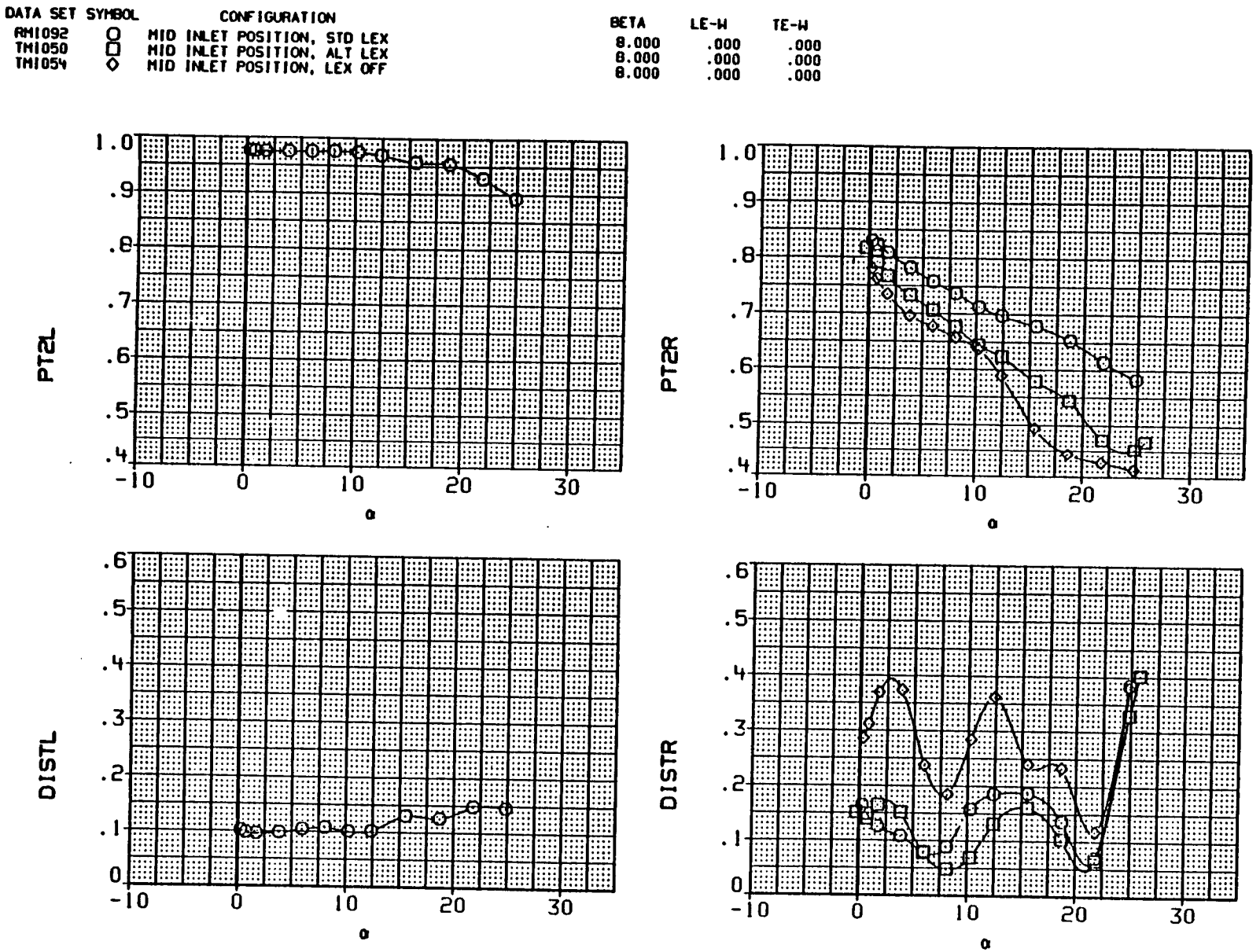

(dd) Mach = 1.20.

Figure 10.- Continued.

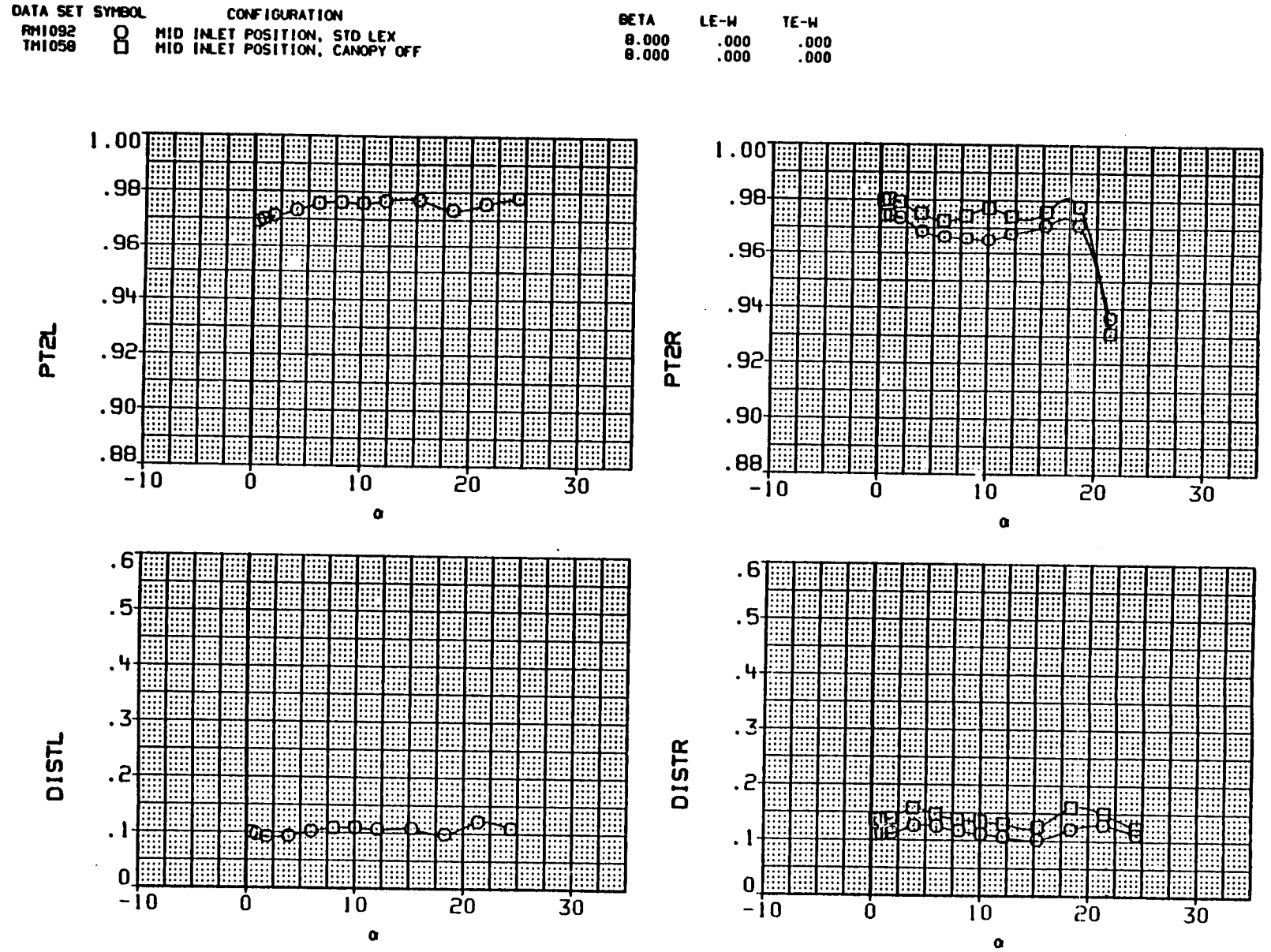

(ee) Mach = 0.60.

Figure 10.- Continued.

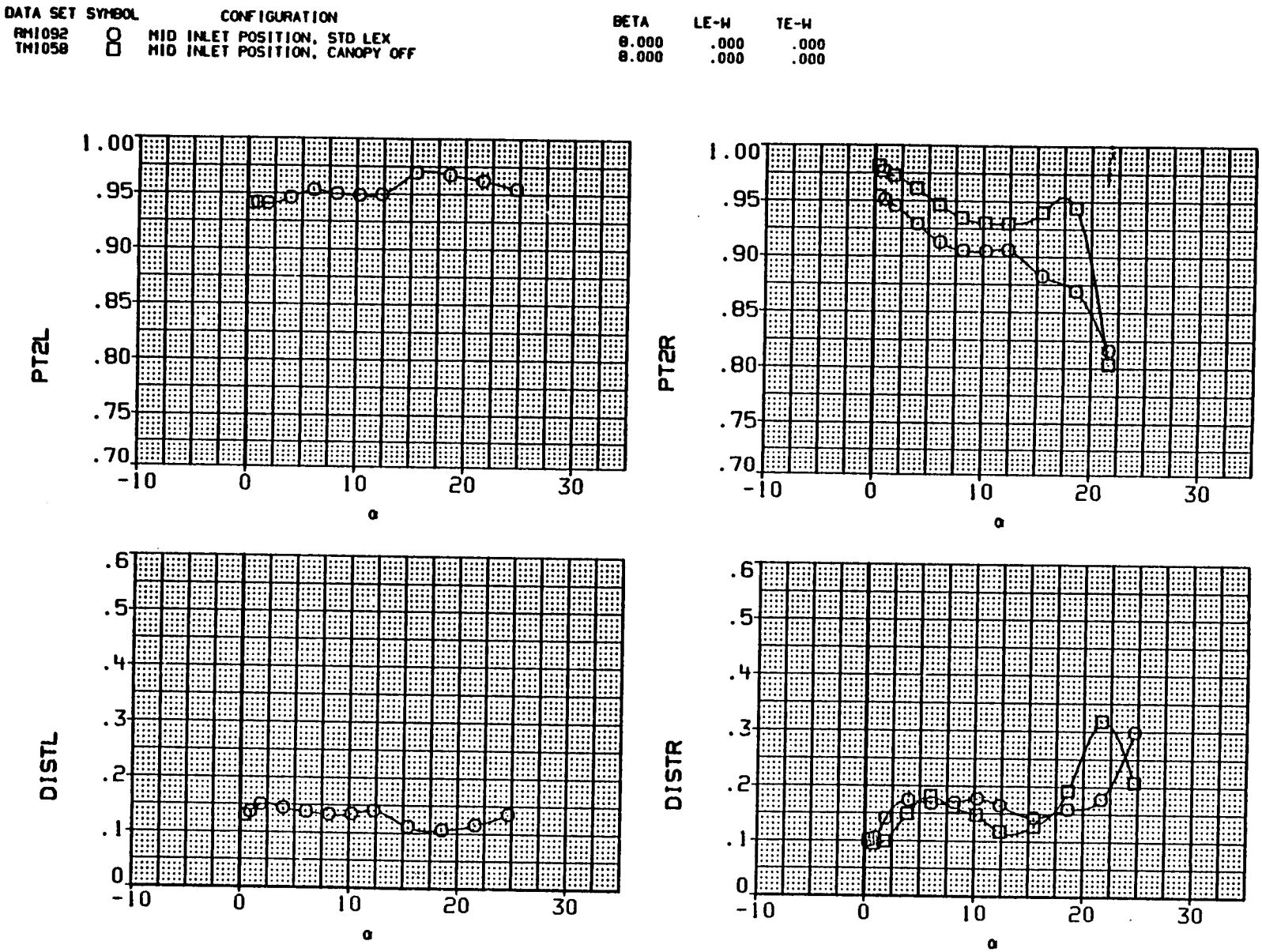

LEFT DUCT - MAX ENGINE AIRFLOW

RIGHT DUCT - MAX ENGINE AIRFLOW

(ff) Mach = 0.90.

Figure 10.- Continued.

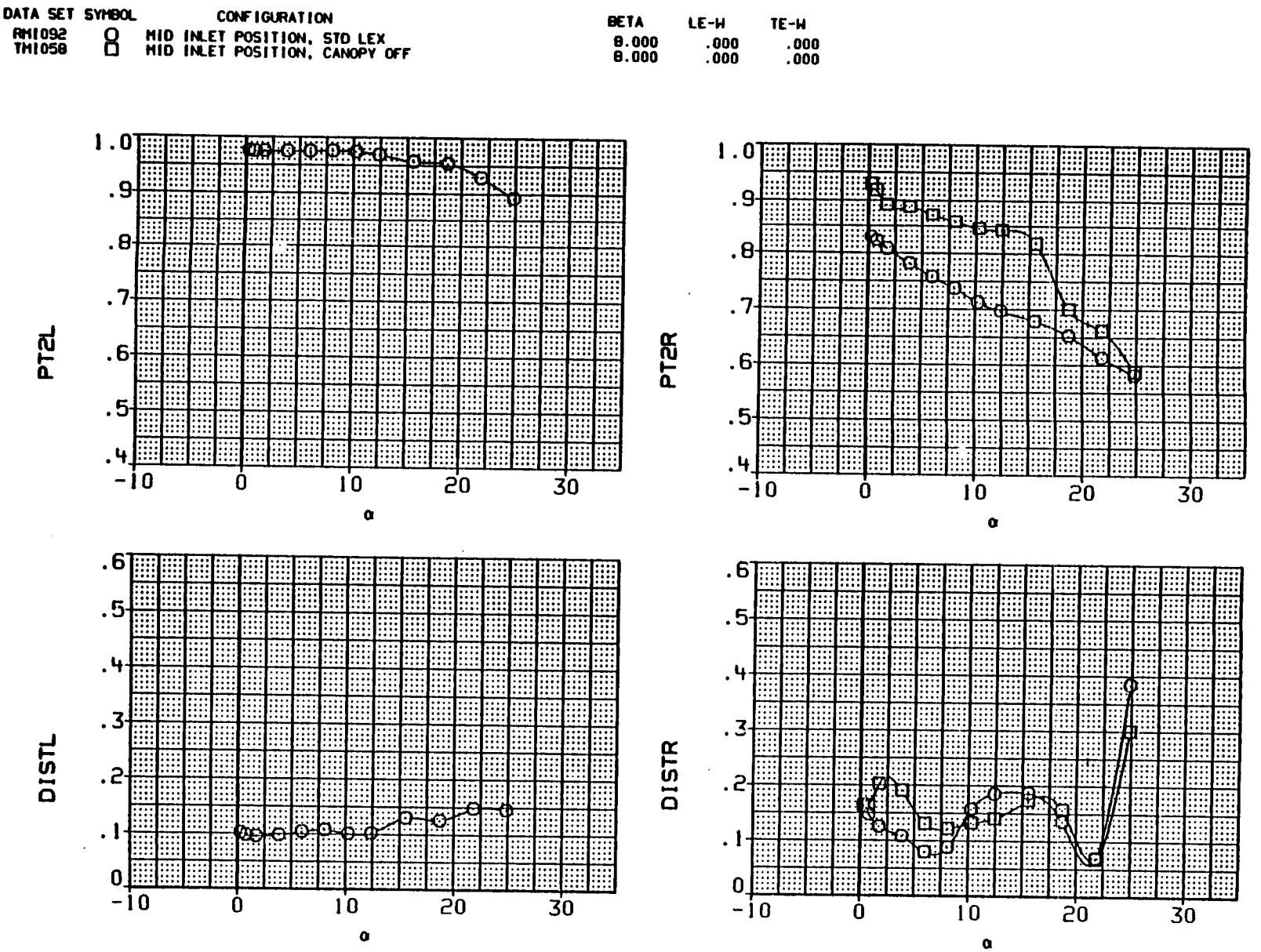

(gg) Mach = 1.20.

Figure 10.- Continued.

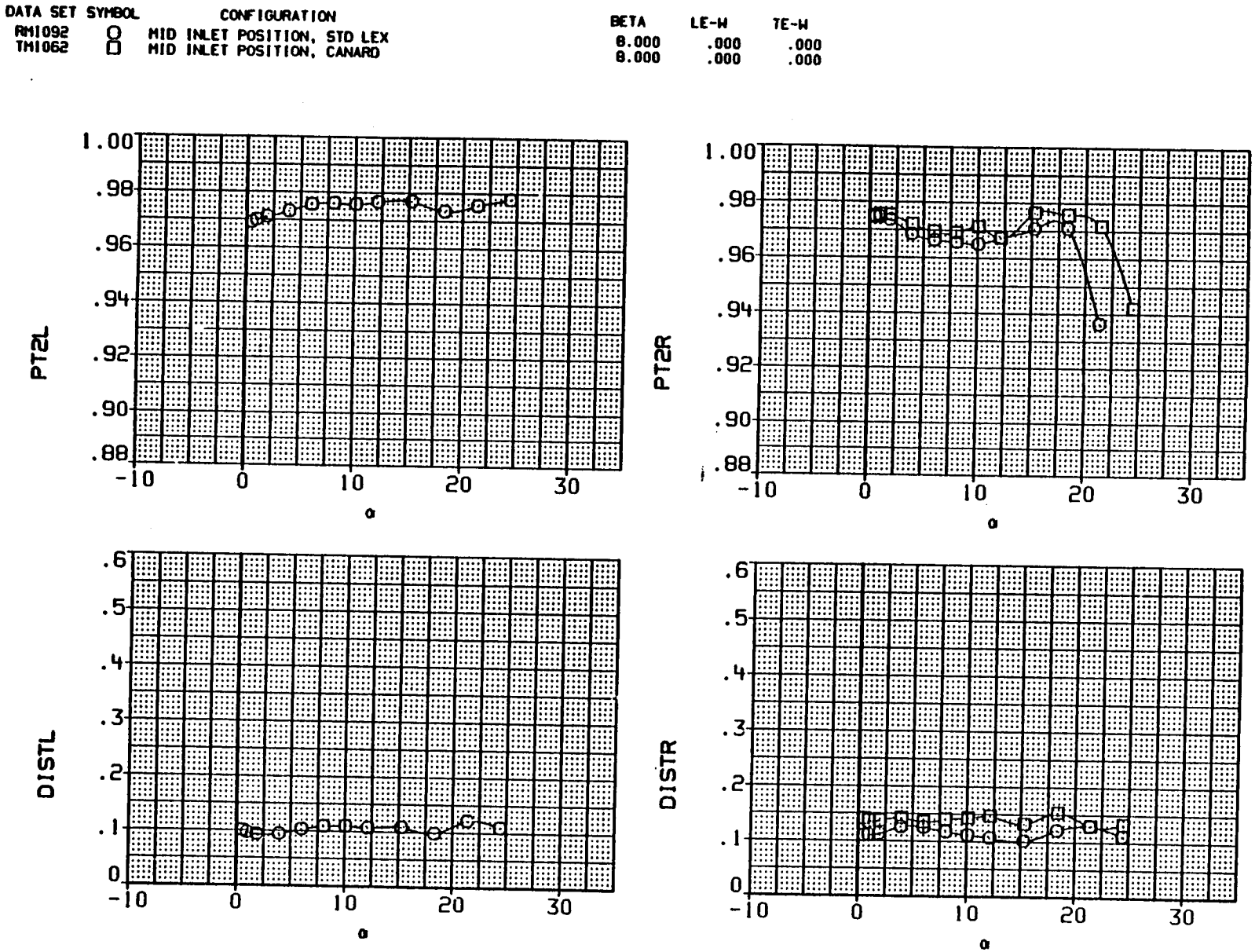

LEFT DUCT - MAX ENGINE AIRFLOW

RIGHT DUCT - MAX ENGINE AIRFLOW

(hh) Mach = 0.60.

Figure 10.- Continued.

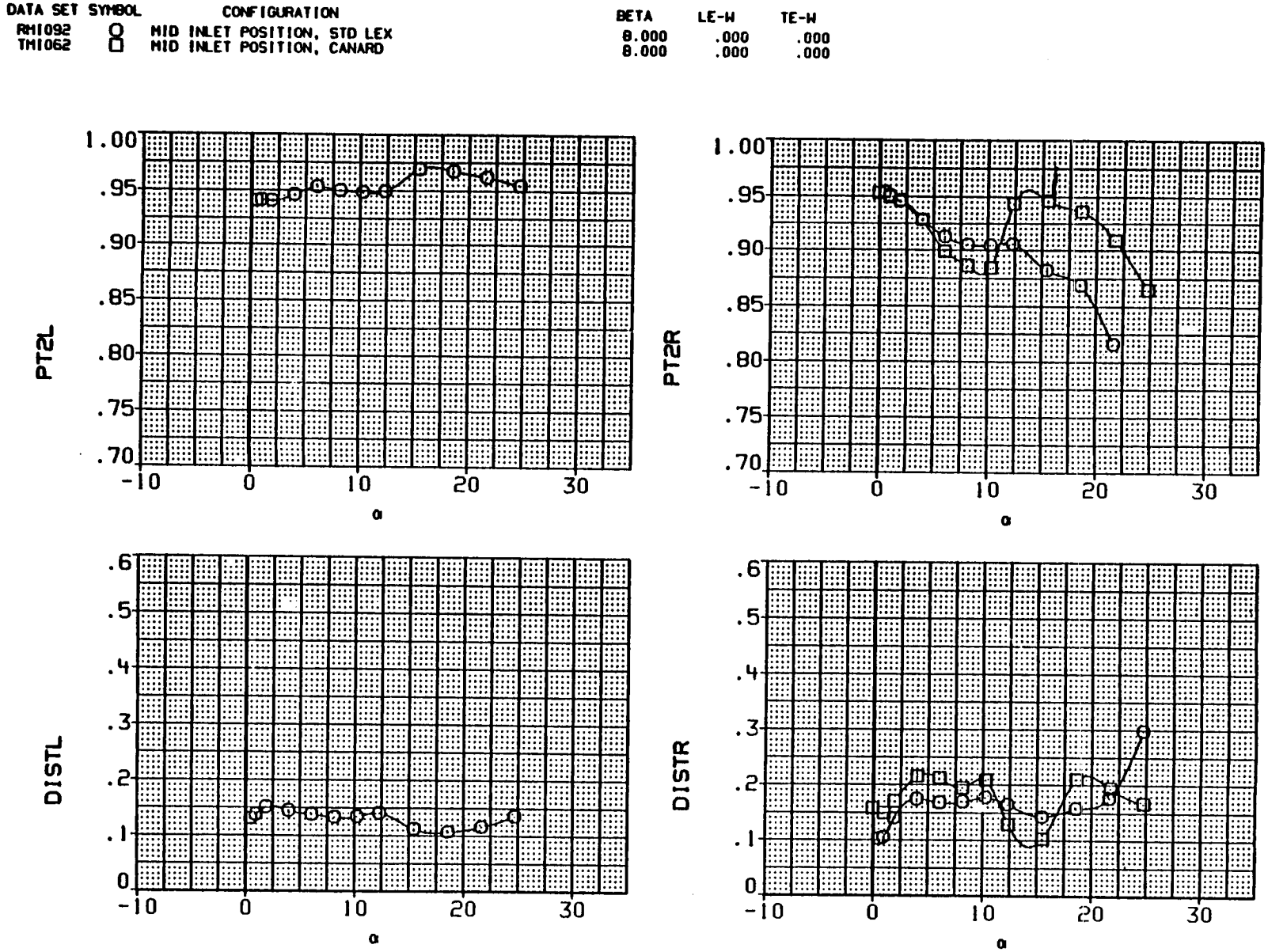

LEFT DUCT - MAX ENGINE AIRFLOW

RIGHT DUCT - MAX ENGINE AIRFLOW

(ii) Mach = 0.90.

Figure 10.- Continued.

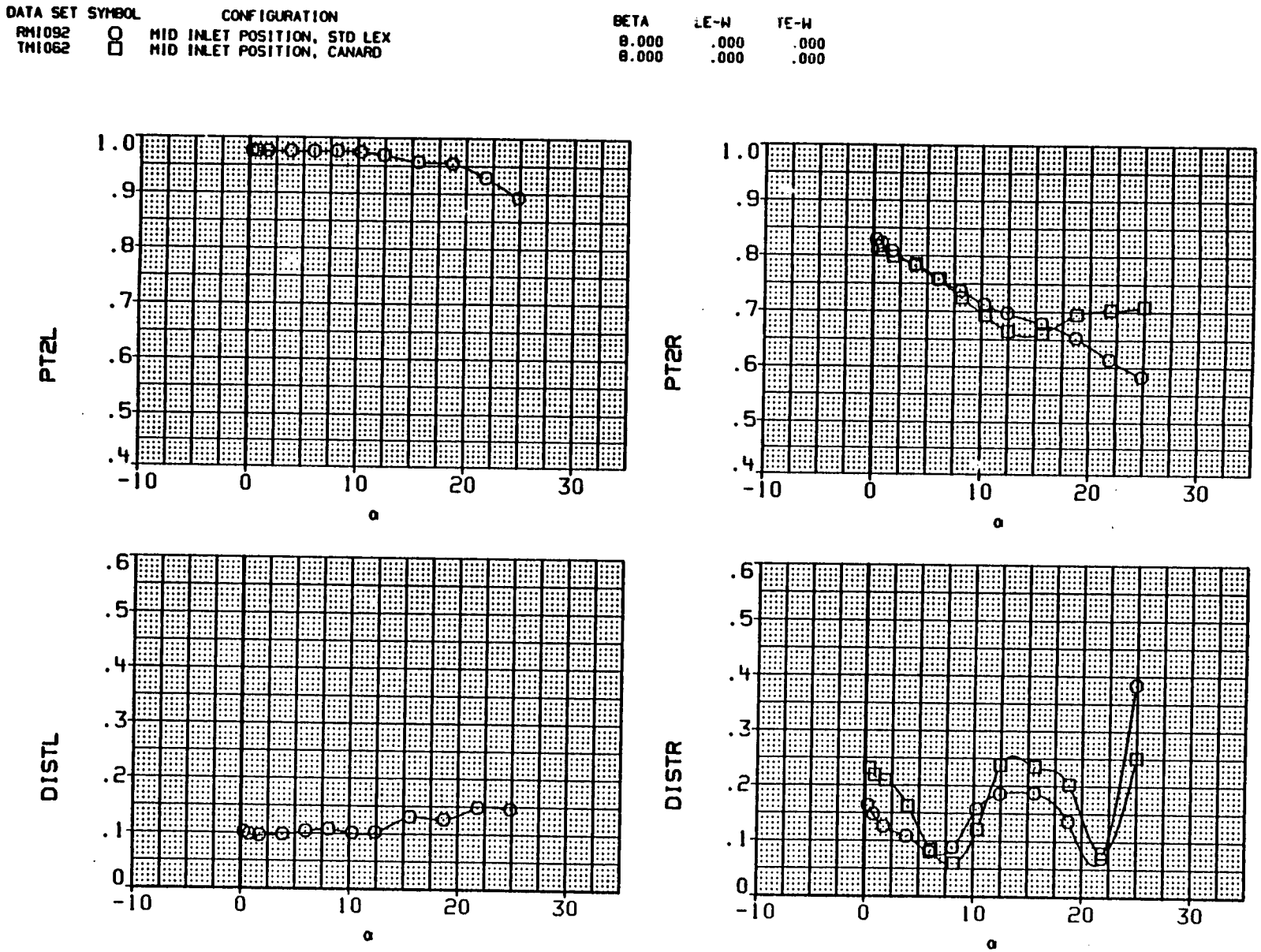

LEFT DUCT - MAX ENGINE AIRFLOW

RIGHT DUCT - MAX ENGINE AIRFLOW

(jj) Mach = 1.20.

Figure 10.- Continued.

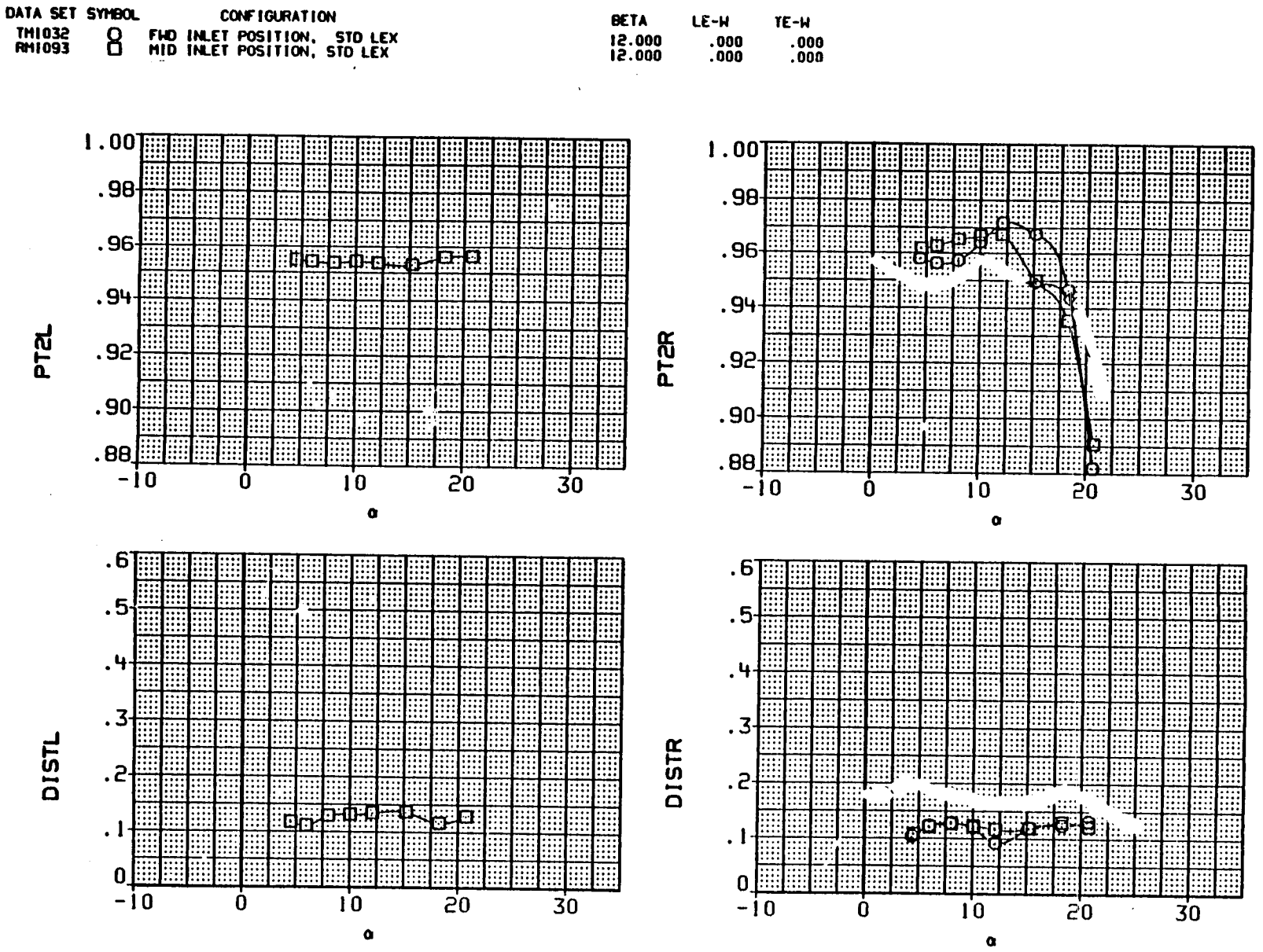

LEFT DUCT - MAX ENGINE AIRFLOW

RIGHT DUCT - MAX ENGINE AIRFLOW

(kk) Mach = 0.60.

Figure 10.- Continued.

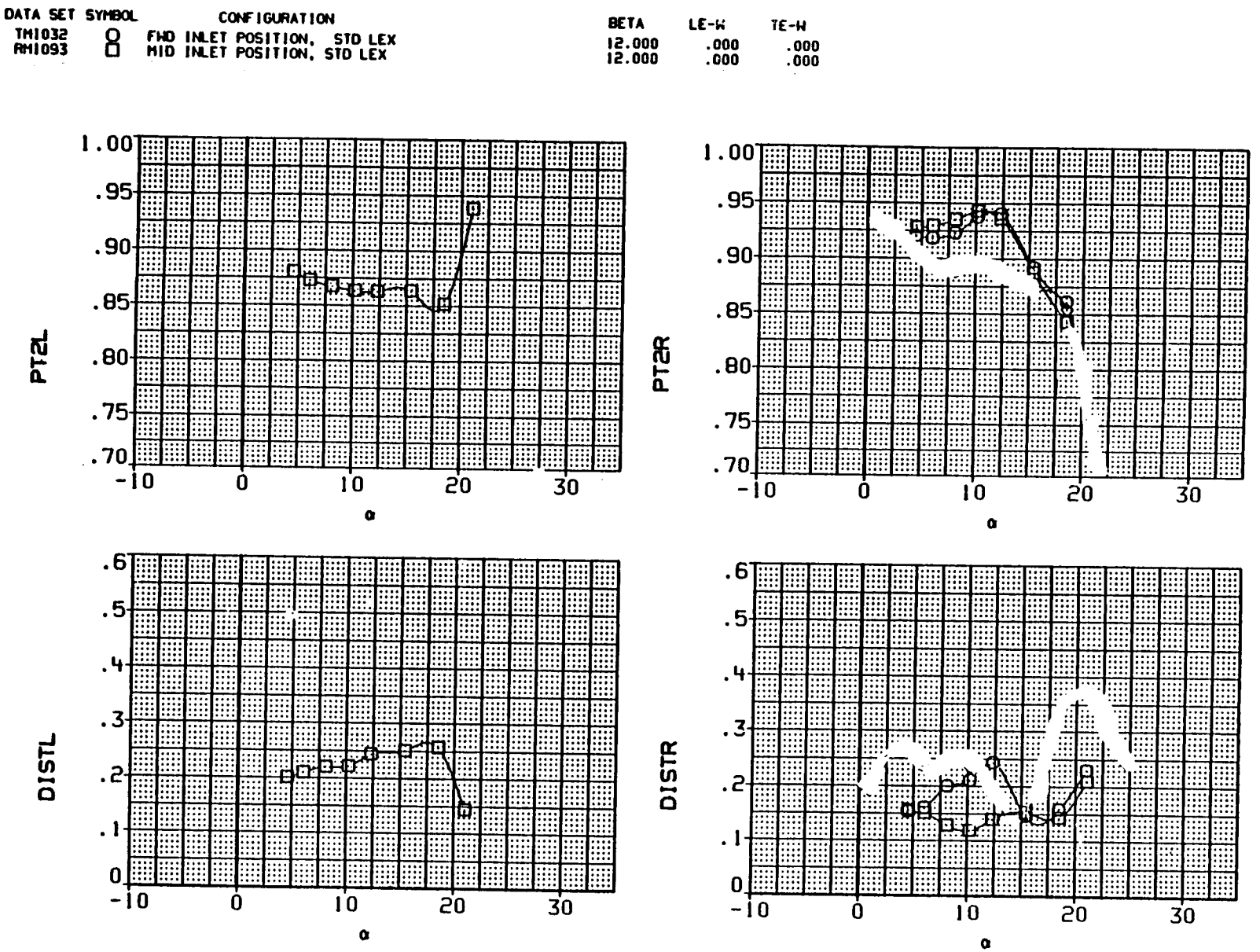

LEFT DUCT - MAX ENGINE AIRFLOW

RIGHT DUCT - MAX ENGINE AIRFLOW

(11) Mach = 0.90.

Figure 10.- Continued.

DATA SET	SYMBOL	CONFIGURATION	BETA	LE-H	TE-H
TM1032	○	FWD INLET POSITION, STD LEX	12.000	.000	.000
RM1093	□	MID INLET POSITION, STD LEX	12.000	.000	.000

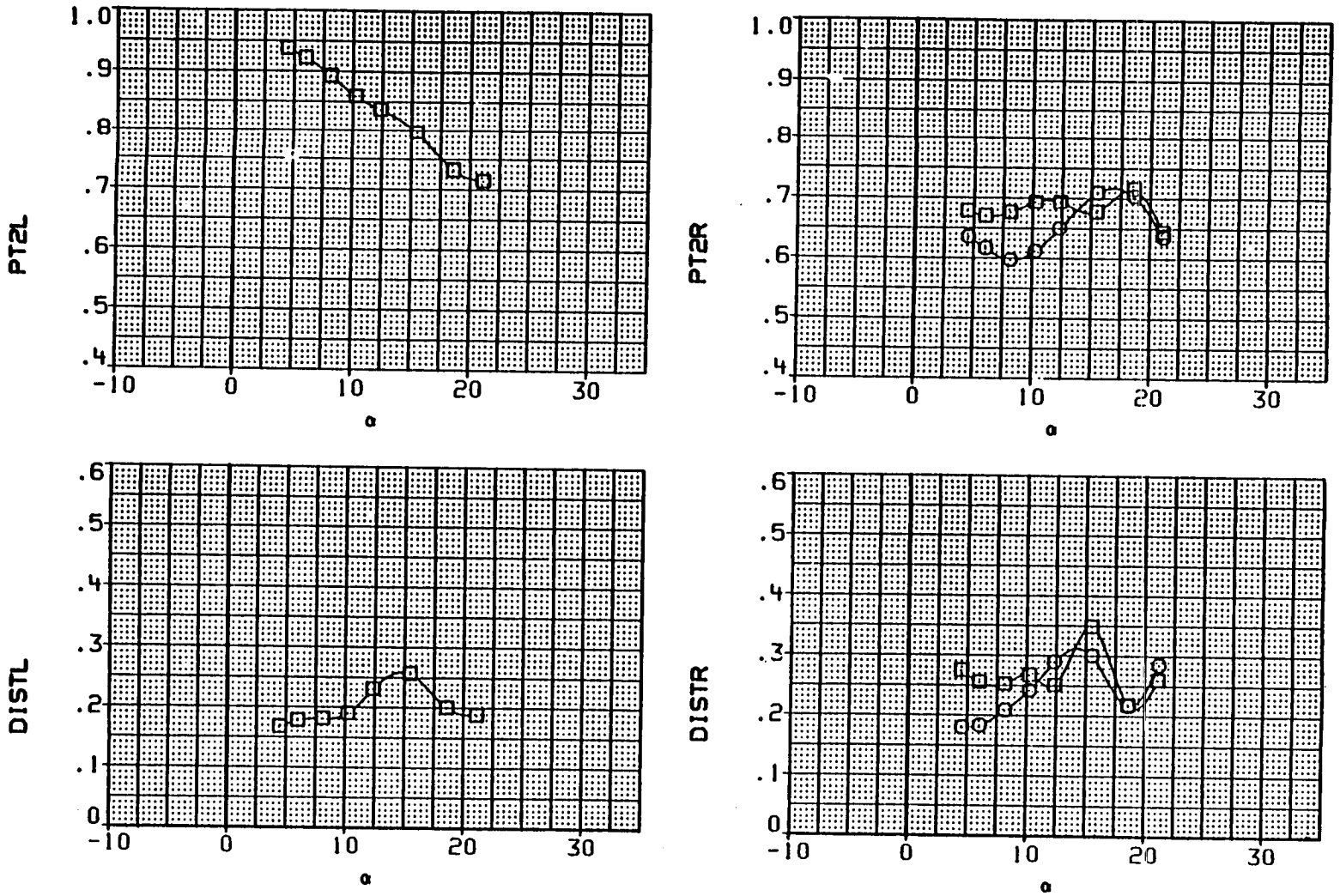

LEFT DUCT - MAX ENGINE AIRFLOW

RIGHT DUCT - MAX ENGINE AIRFLOW

(mm) Mach = 1.20.

Figure 10.- Continued.

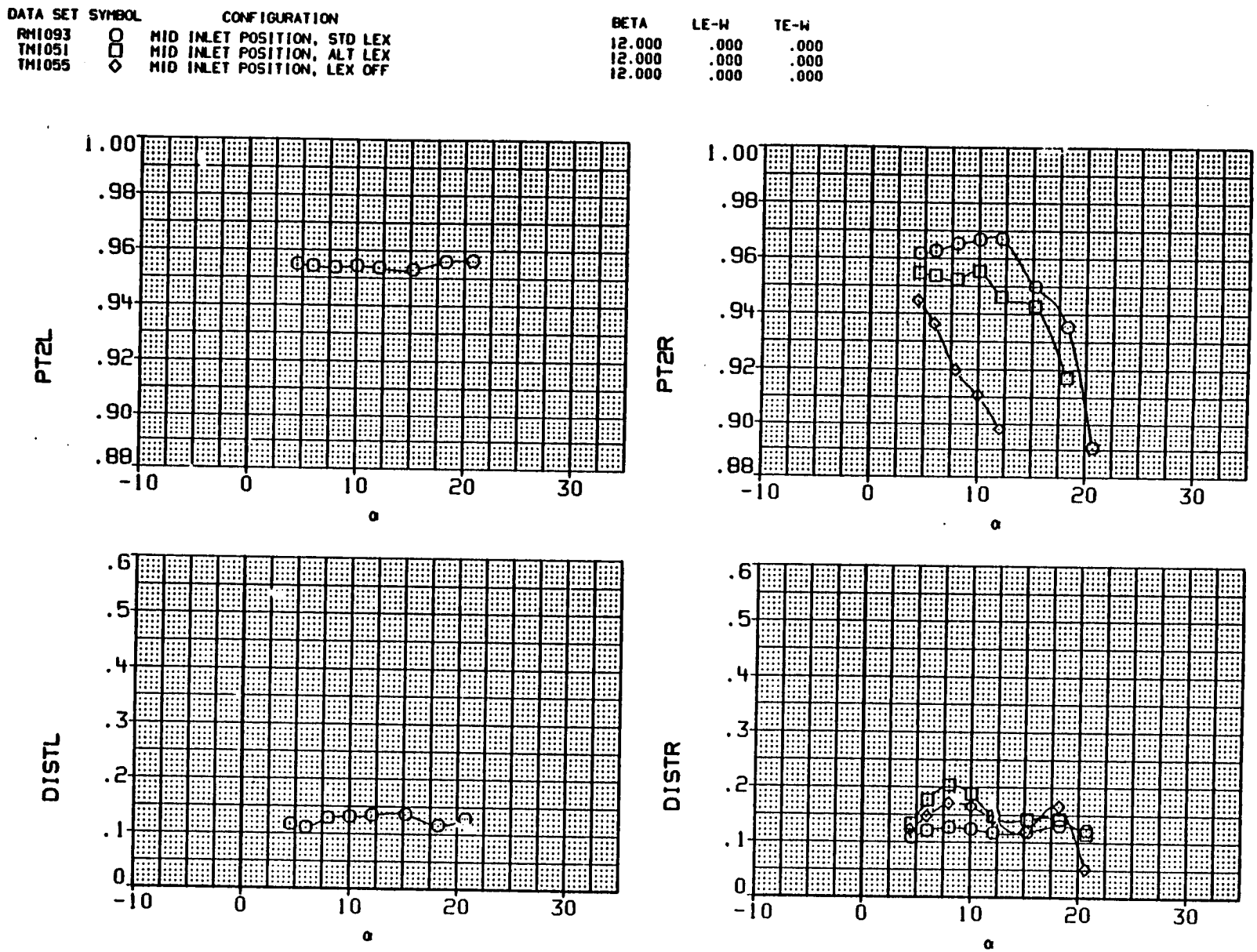

(nn) Mach = 0.60.

Figure 10.- Continued.

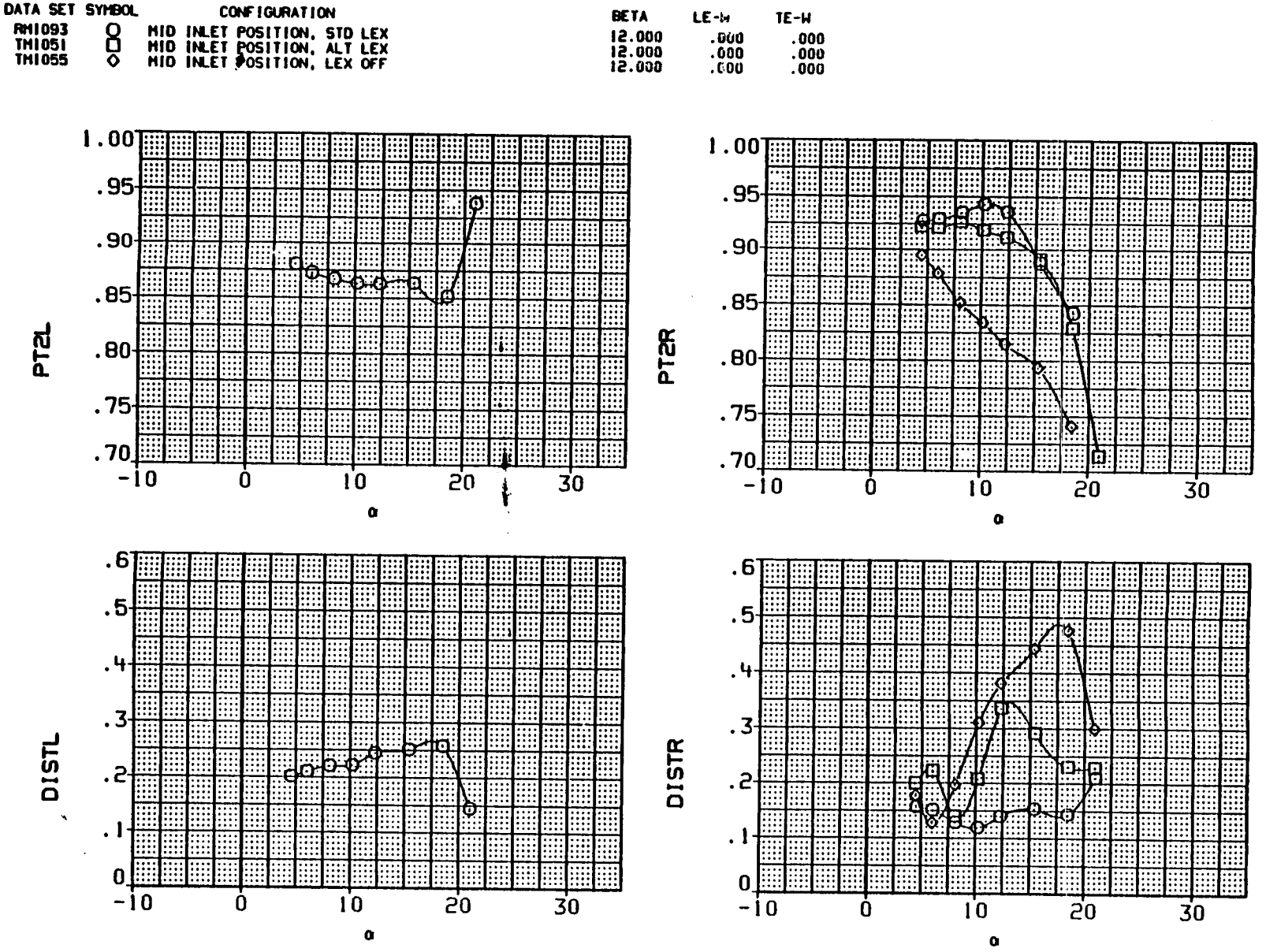

(oo) Mach = 0.90.

Figure 10.- Continued.

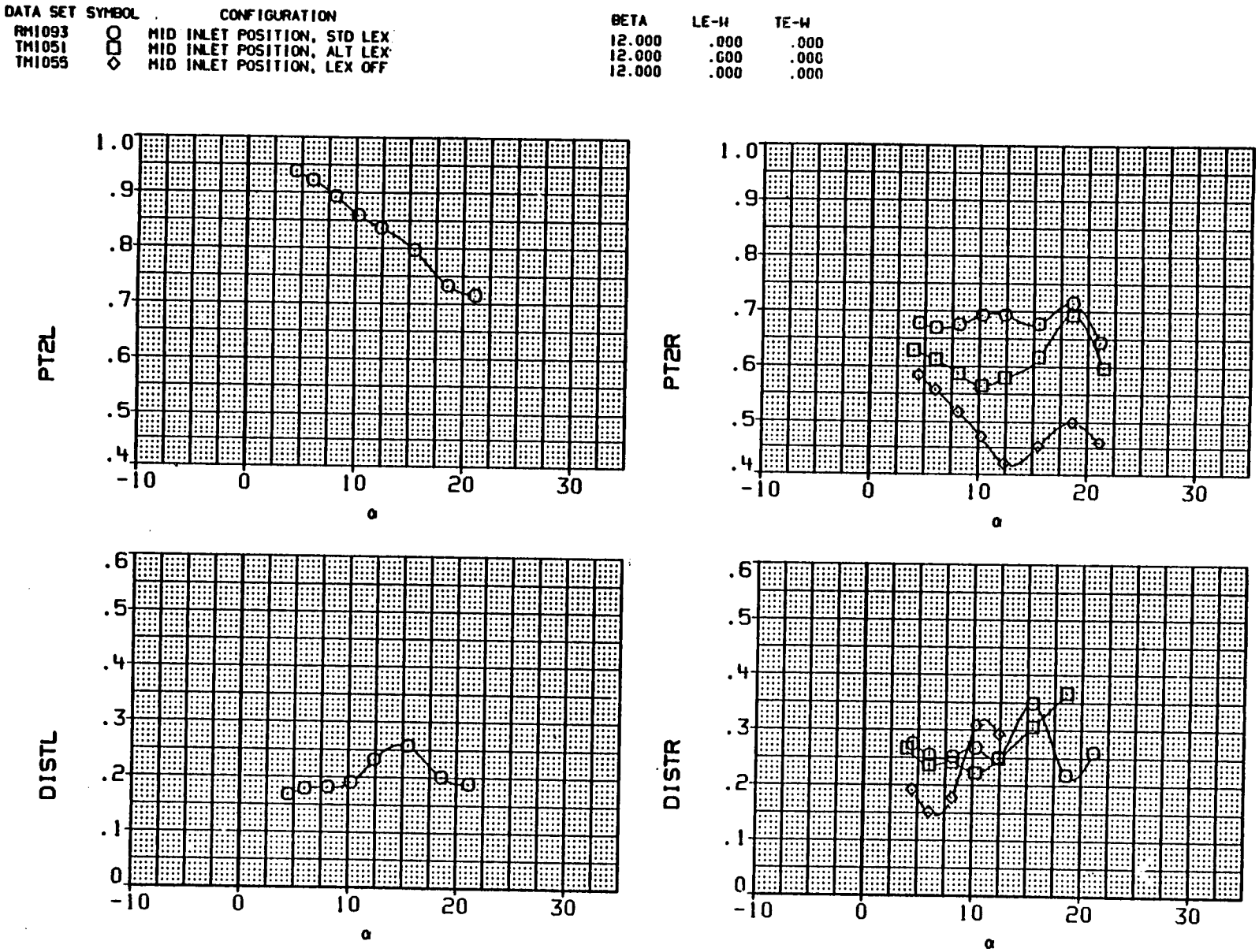

(pp) Mach = 1.20.

Figure 10.- Continued.

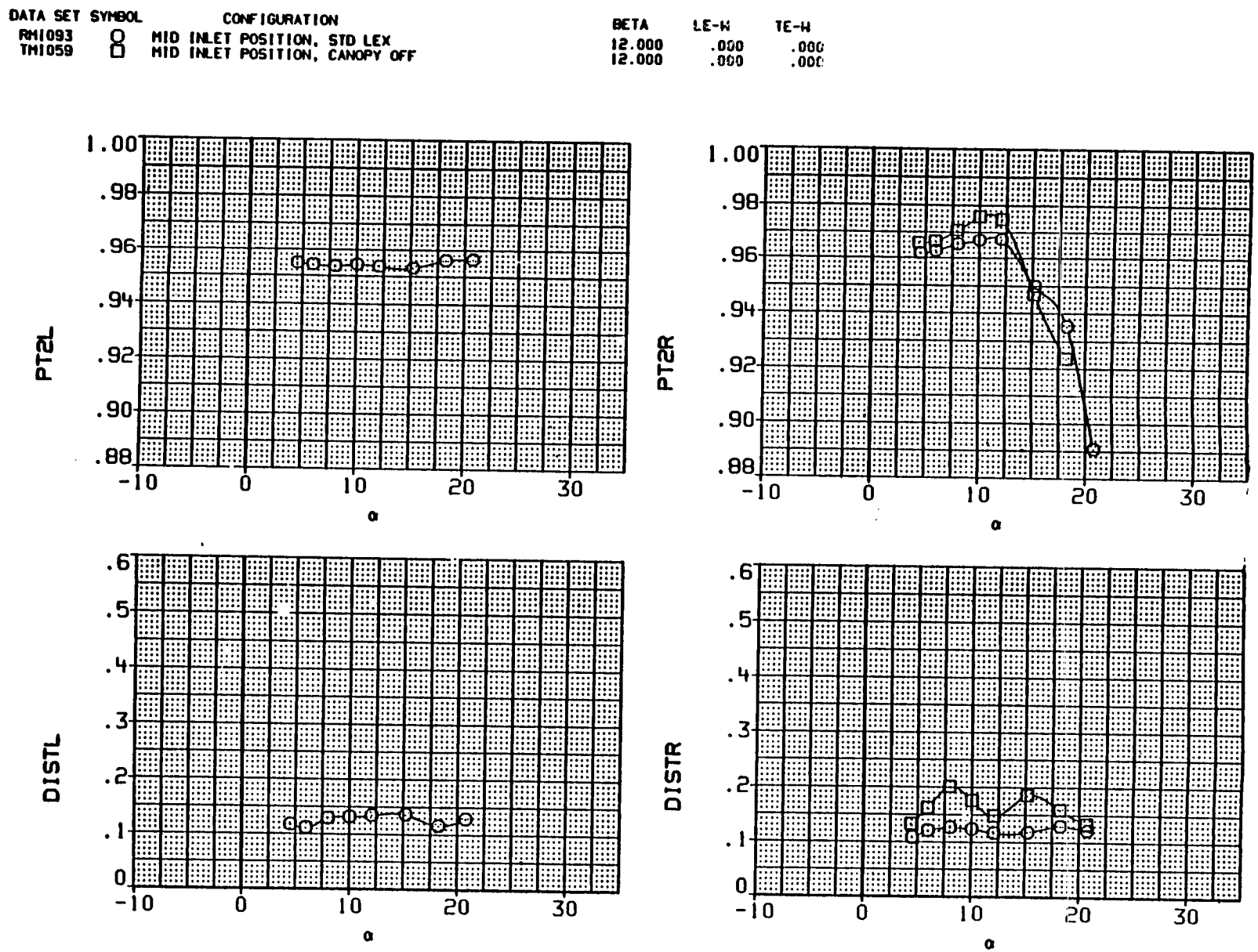

LEFT DUCT - MAX ENGINE AIRFLOW

RIGHT DUCT - MAX ENGINE AIRFLOW

(qq) Mach = 0.60.

Figure 10.- Continued.

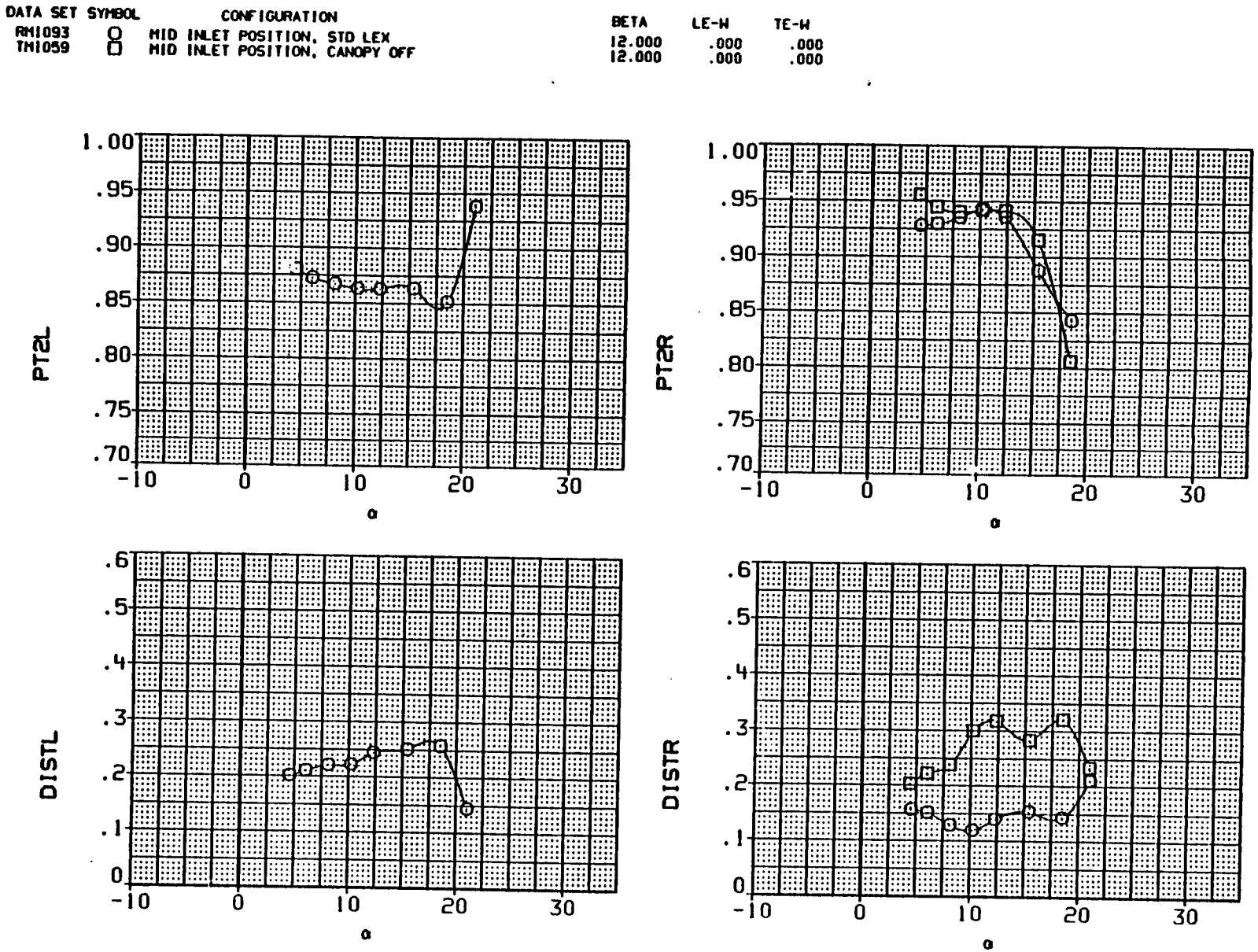

LEFT DUCT - MAX ENGINE AIRFLOW RIGHT DUCT - MAX ENGINE AIRFLOW

(rr) Mach = 0.90.

Figure 10.- Continued.

DATA SET	SYMBOL	CONFIGURATION	BETA	LE-W	TE-W
RM1093	○	MID INLET POSITION, STD LEX	12.000	.000	.000
TM1059	□	MID INLET POSITION, CANOPY OFF	12.000	.000	.000

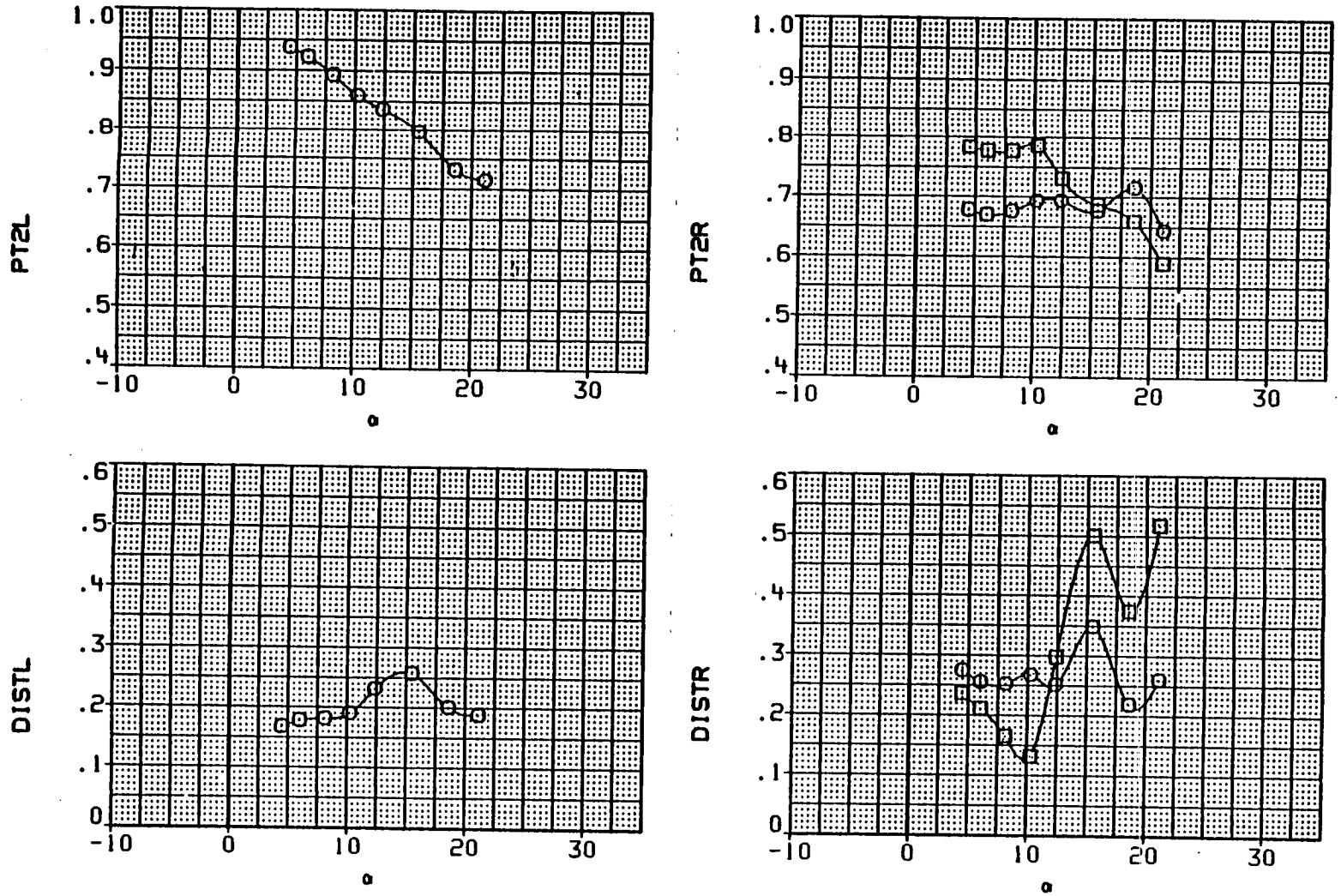

LEFT DUCT - MAX ENGINE AIRFLOW

RIGHT DUCT - MAX ENGINE AIRFLOW

(ss) Mach = 1.20.

Figure 10.- Continued.

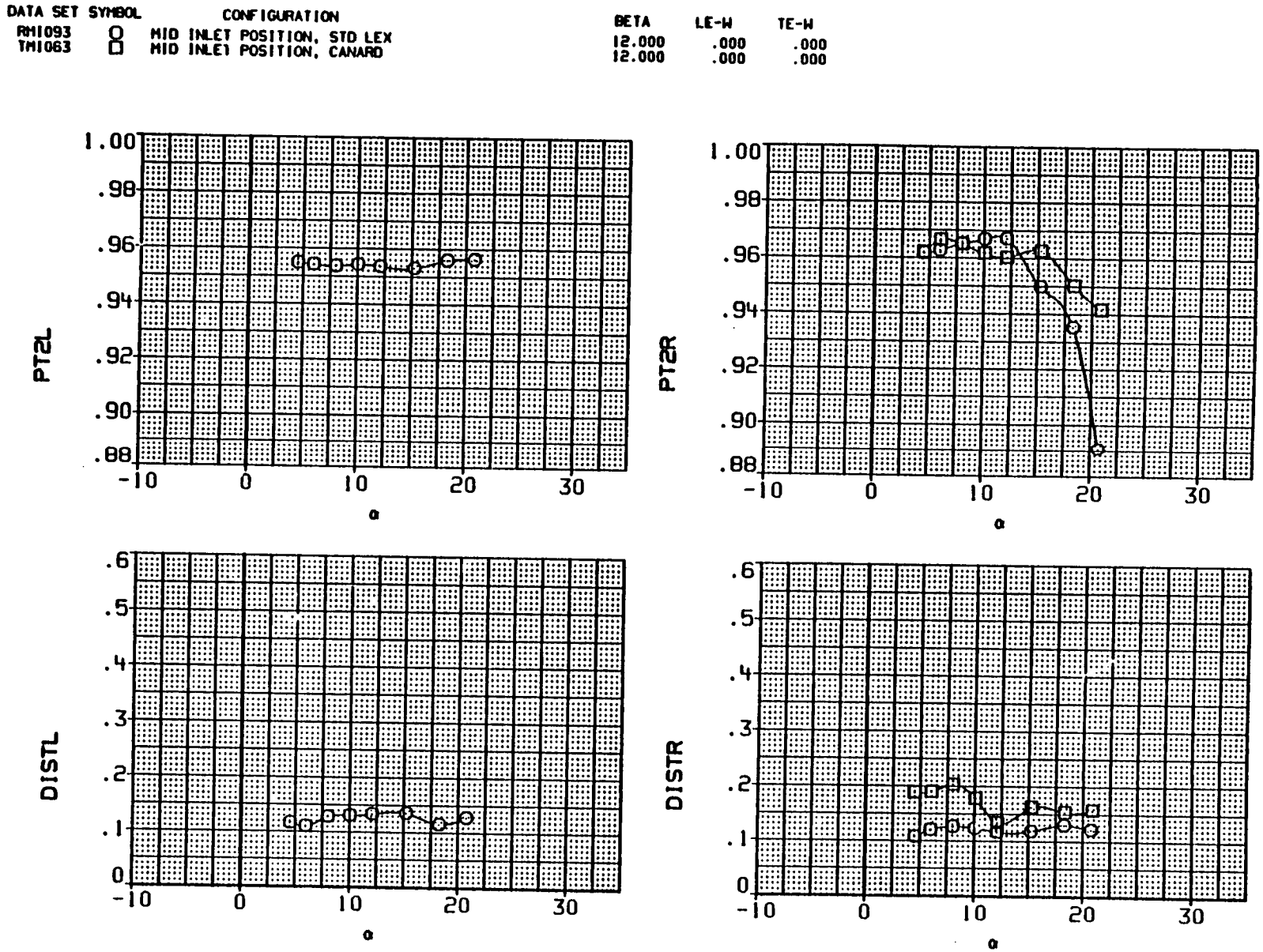

(tt) Mach = 0.60.

Figure 10.- Continued.

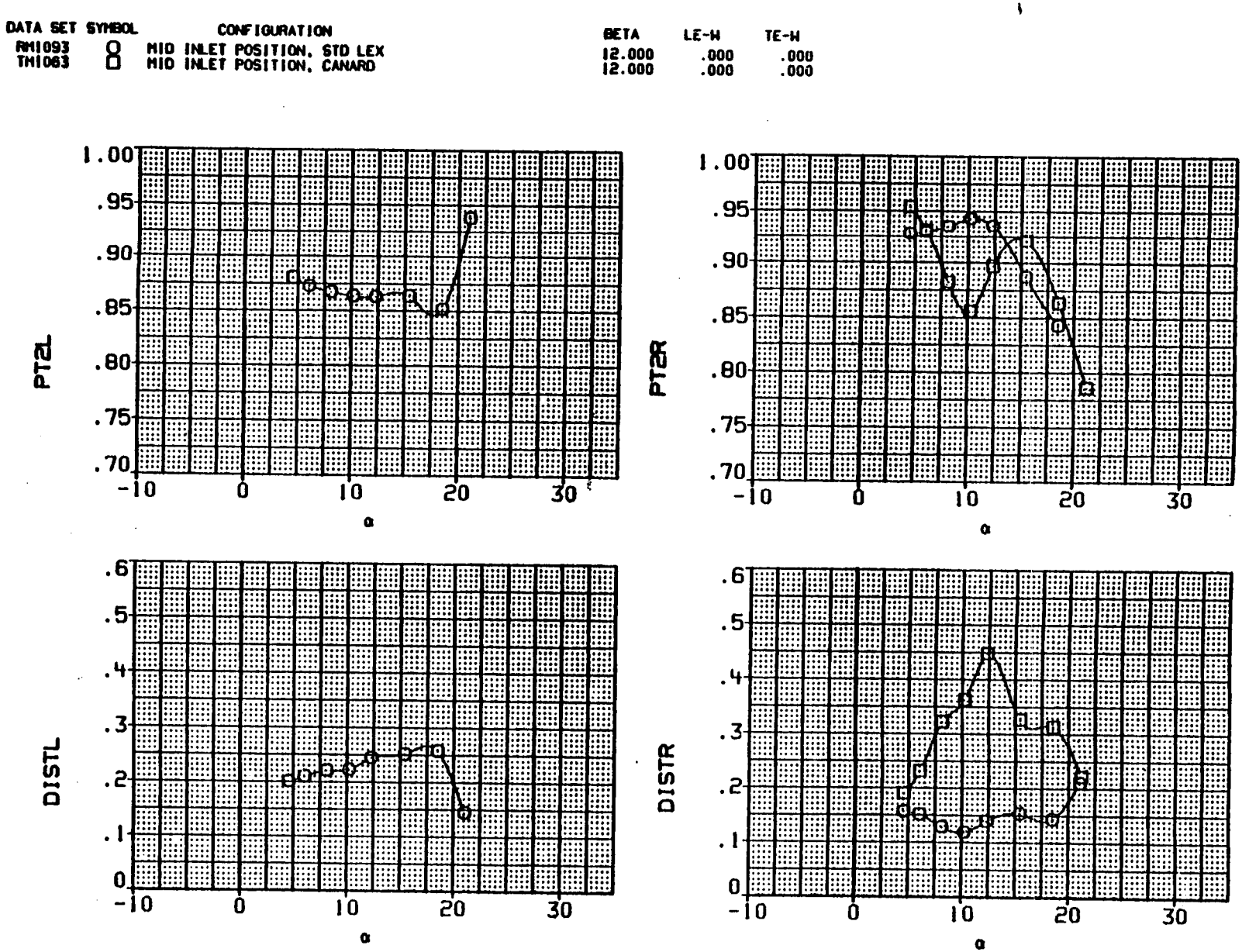

(uu) Mach = 0.90.

Figure 10.- Continued.

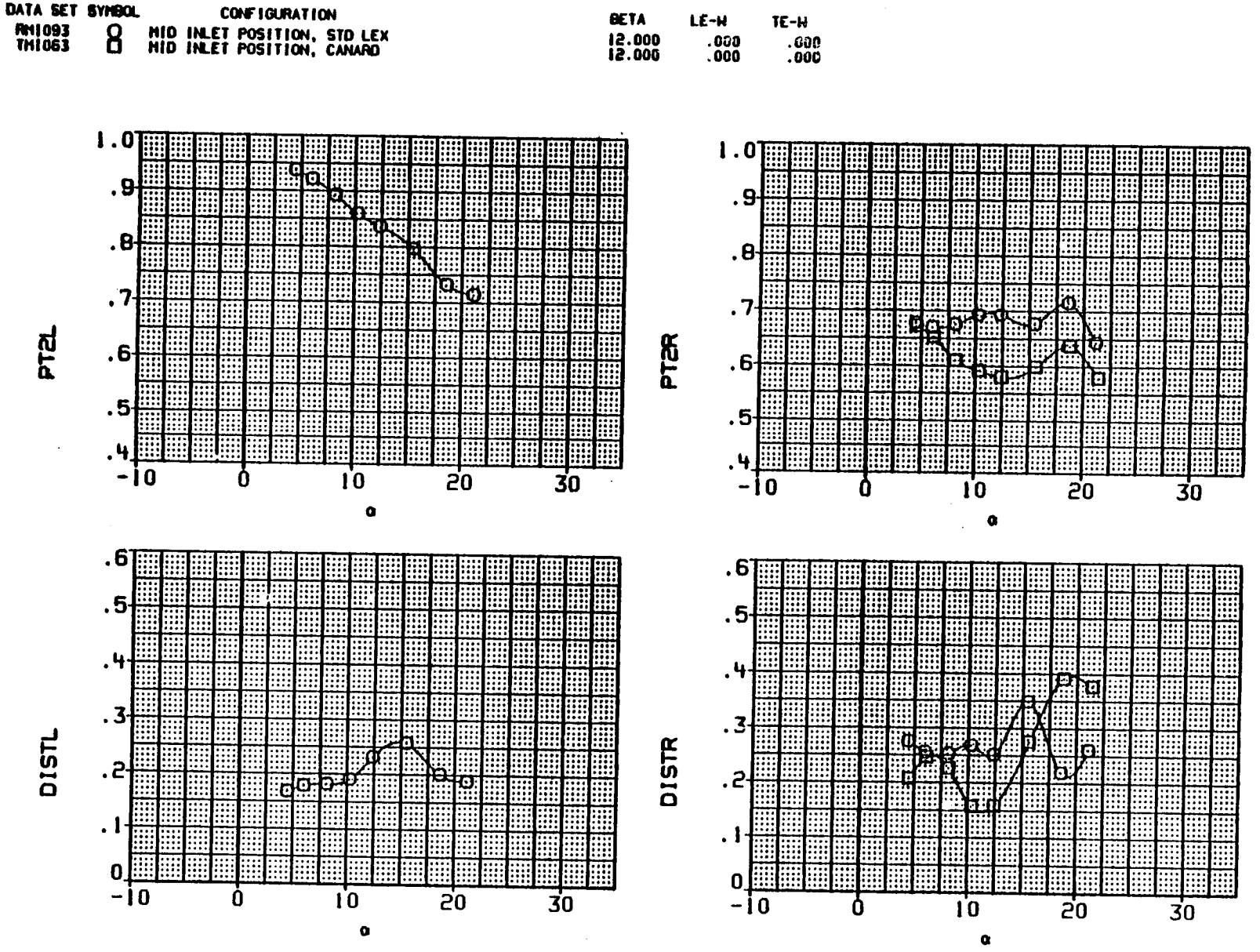

(vv) Mach = 1.20.

Figure 10.- Concluded.

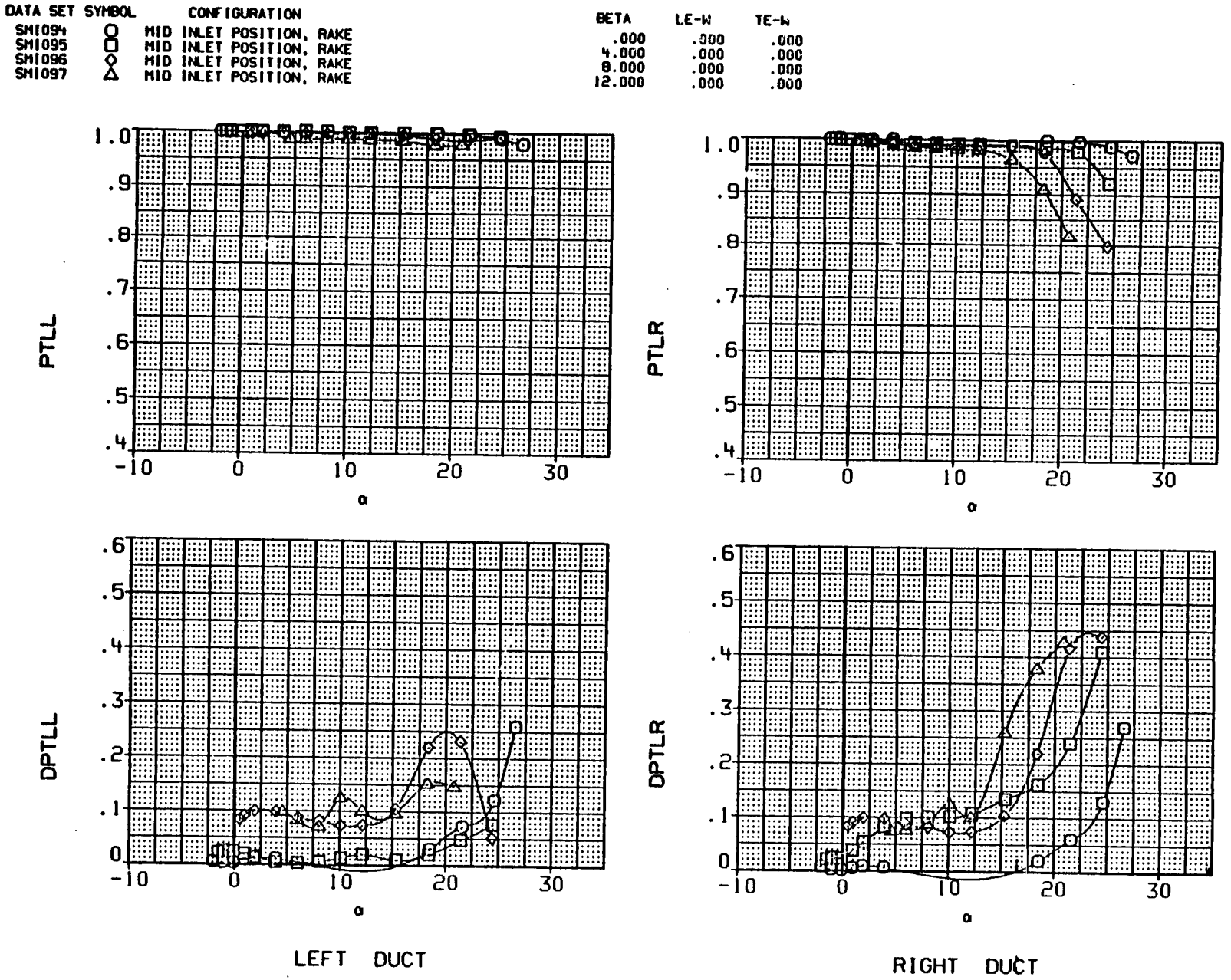

(a) Mach = Mach = 0.60.

Figure 11.- Flow field characteristics at the inlet entrance.

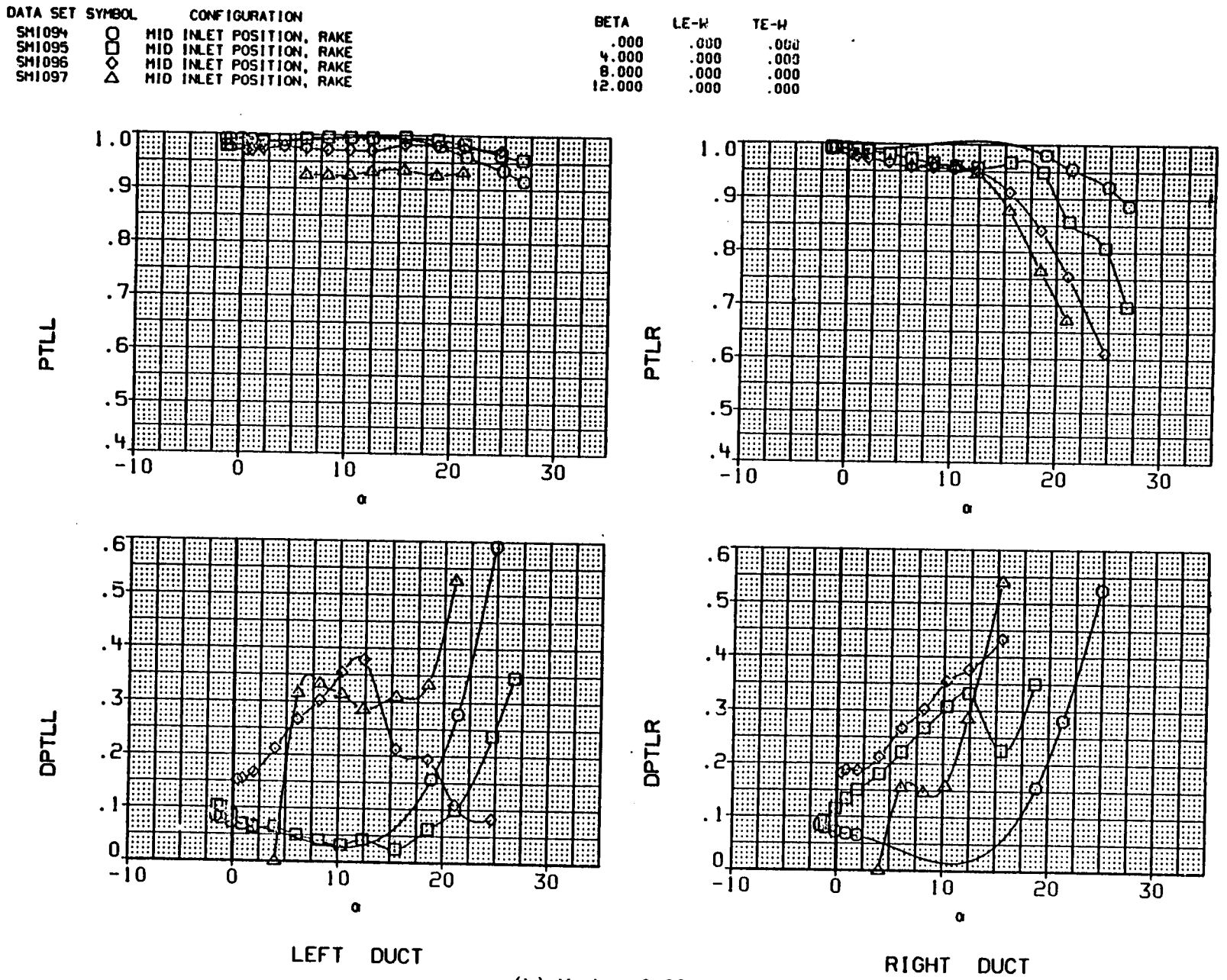

(b) Mach = 0.90.

Figure 11.- Continued.

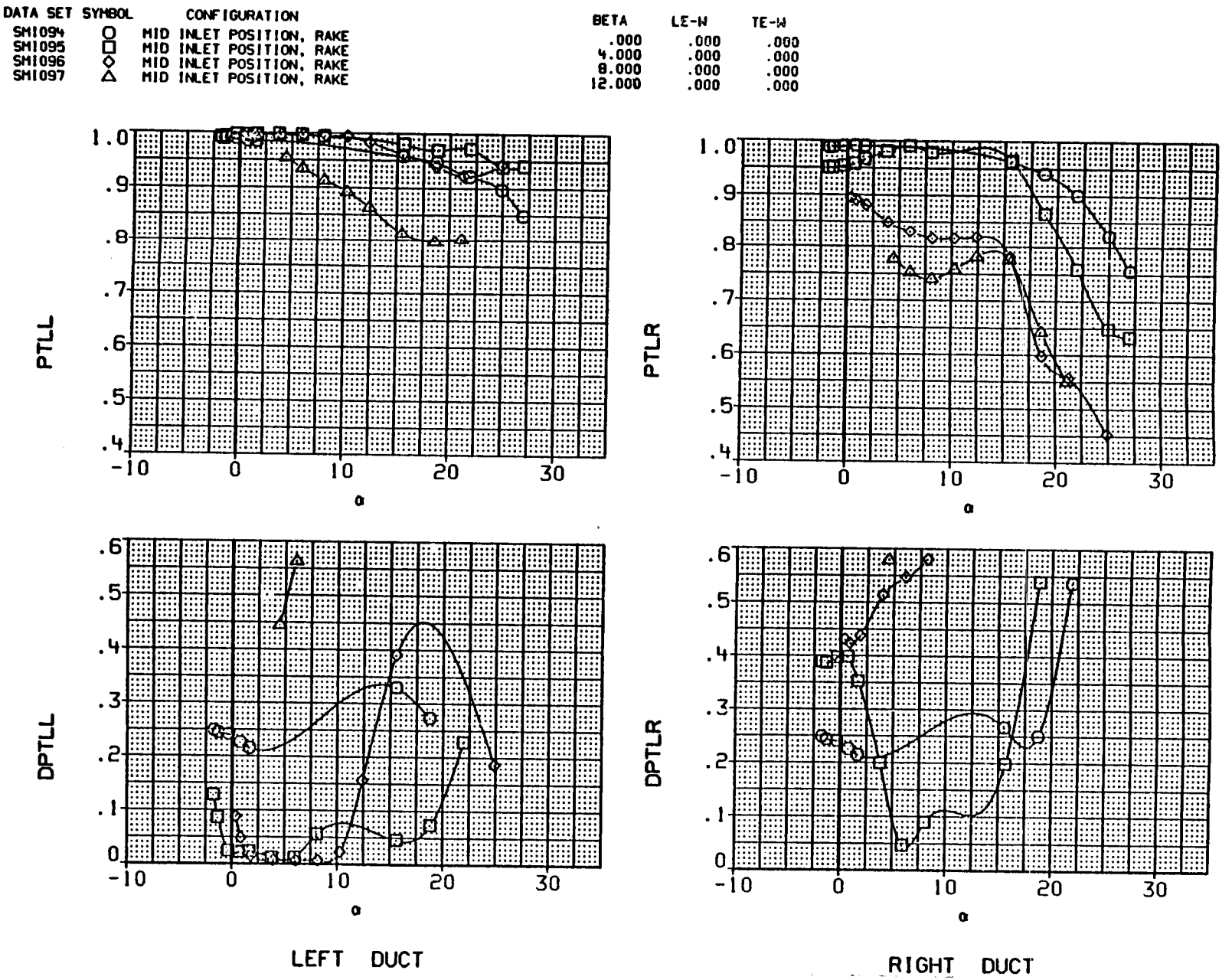

(c) Mach = 1.20.

Figure 11.- Continued.

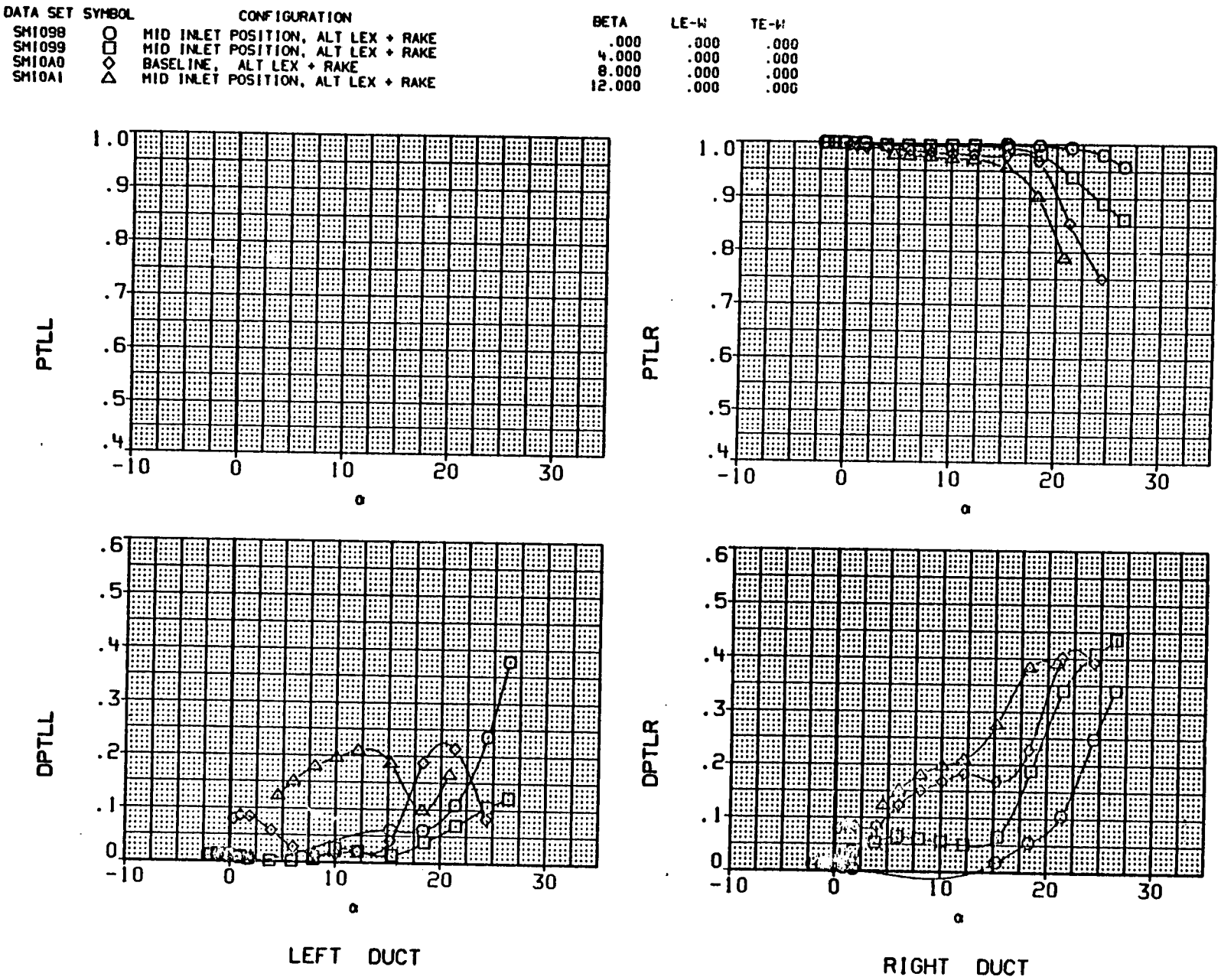

(d) Mach = 0.60.

Figure 11.- Continued.

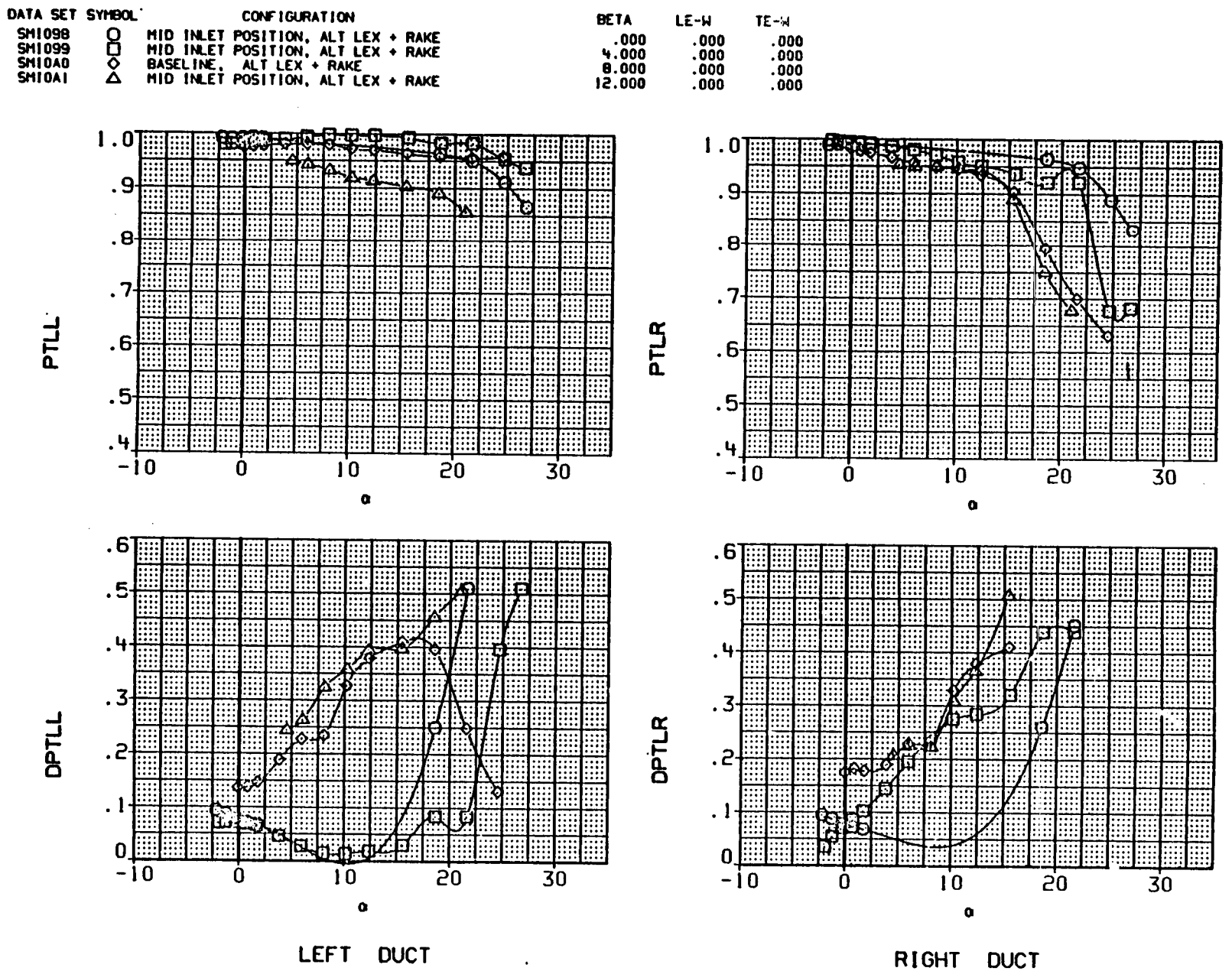

(e) Mach = 0.90.

Figure 11.- Continued.

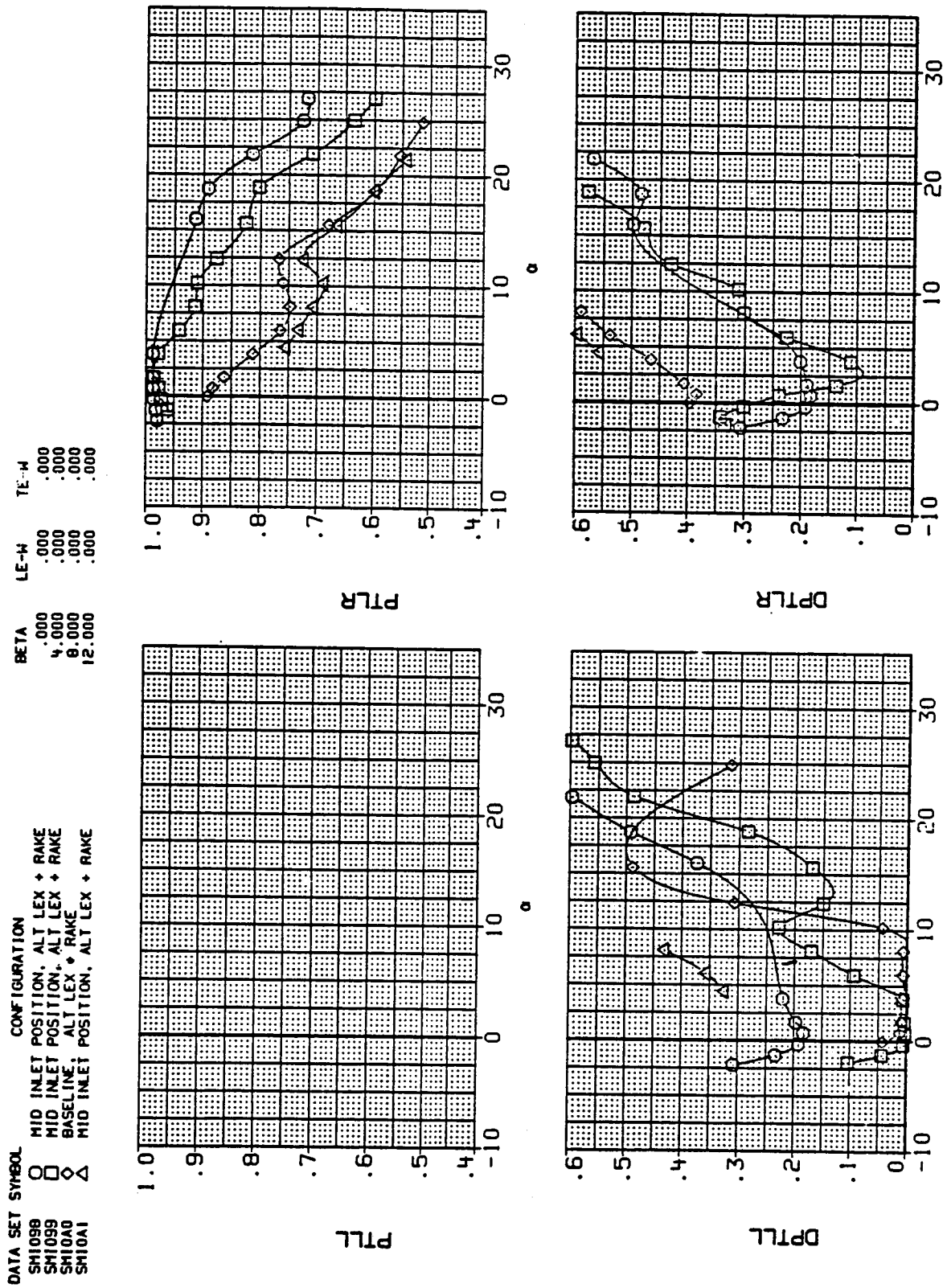

(f) Mach = 1.20.

Figure 11.- Continued.

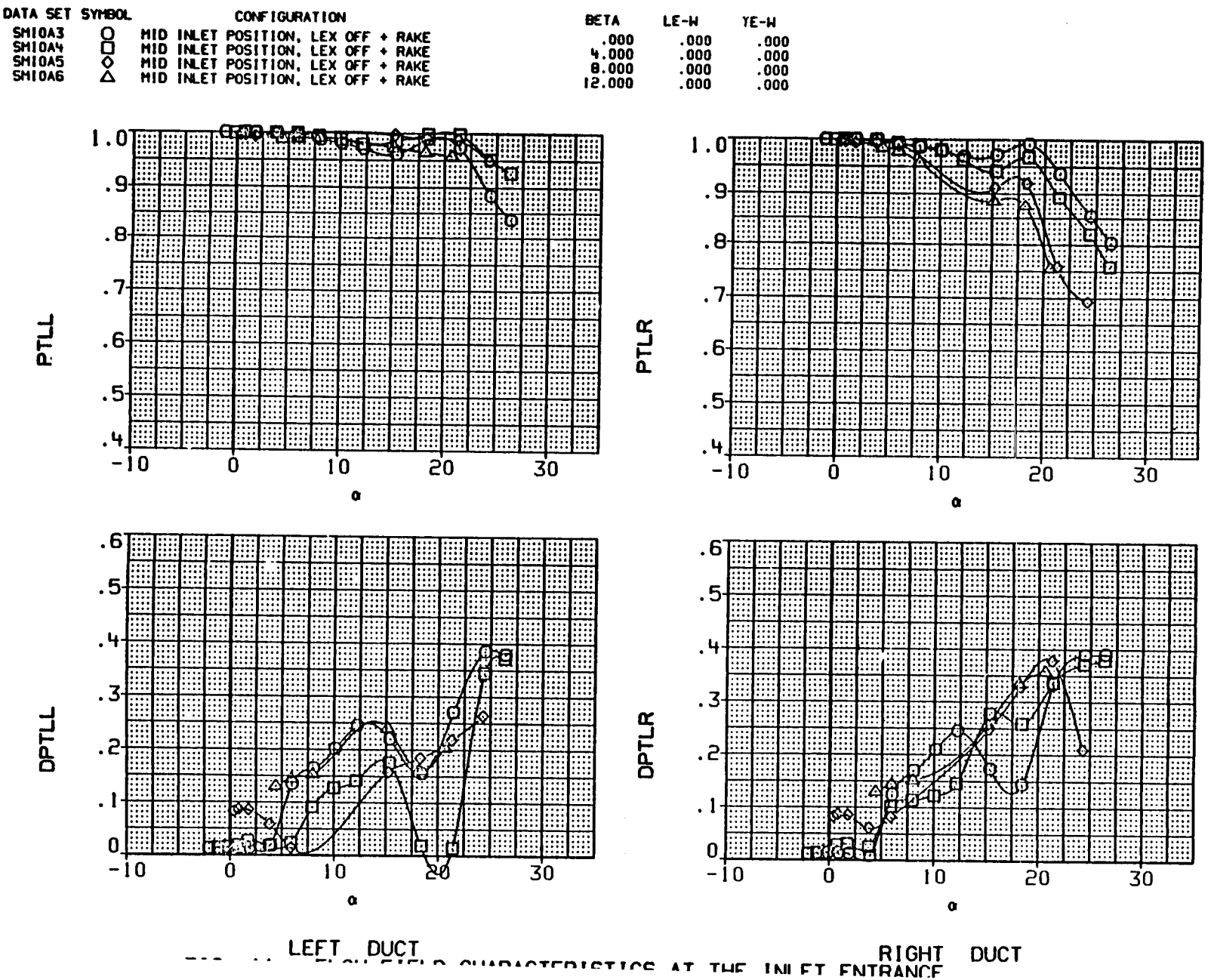

(g) Mach = 0.60.

Figure 11.- Continued.

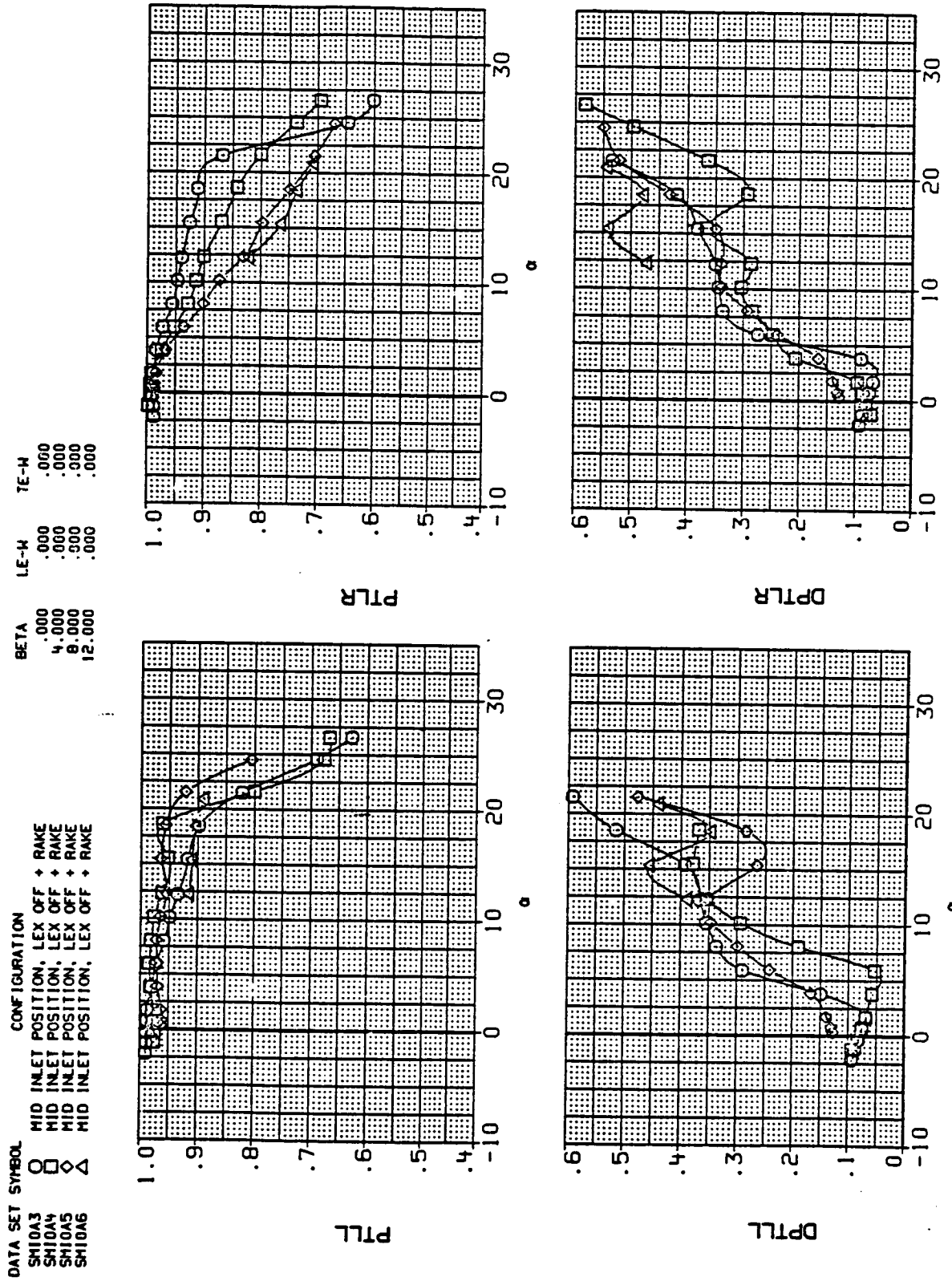

(h) Mach = 0.90.

Figure 11.- Continued.

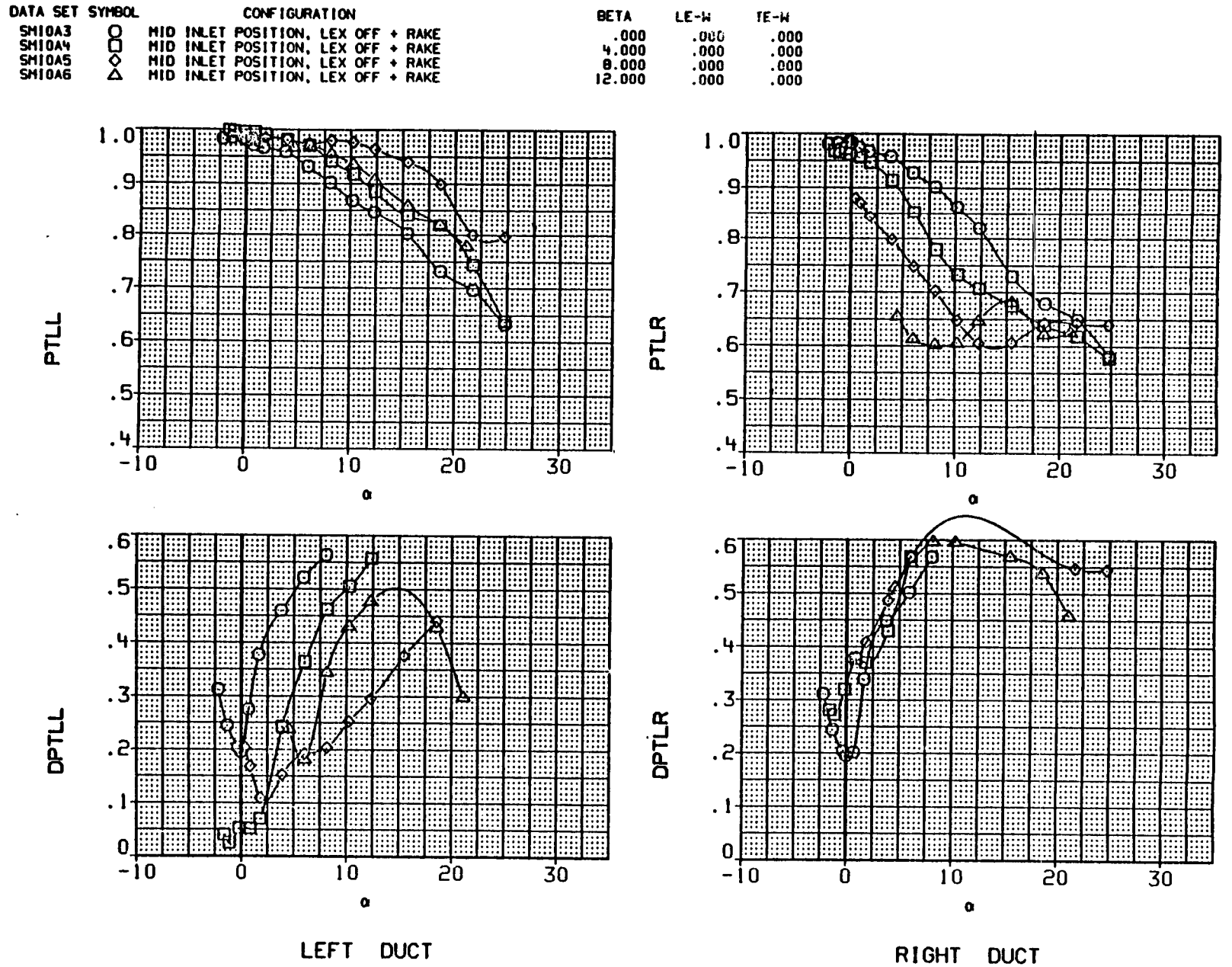

(i) Mach = 1.20.

Figure 11.- Continued.

DATA SET	SYMBOL	CONFIGURATION	BETA	LE-H	TE-H
SM10A7	○	MID INLET POSITION, CANOPY OFF + RAKE	.000	.000	.000
SM10A8	□	MID INLET POSITION, CANOPY OFF + RAKE	4.000	.000	.000
SM10A9	◇	MID INLET POSITION, CANOPY OFF + RAKE	8.000	.000	.000
SM10B0	△	MID INLET POSITION, CANOPY OFF + RAKE	12.000	.000	.000

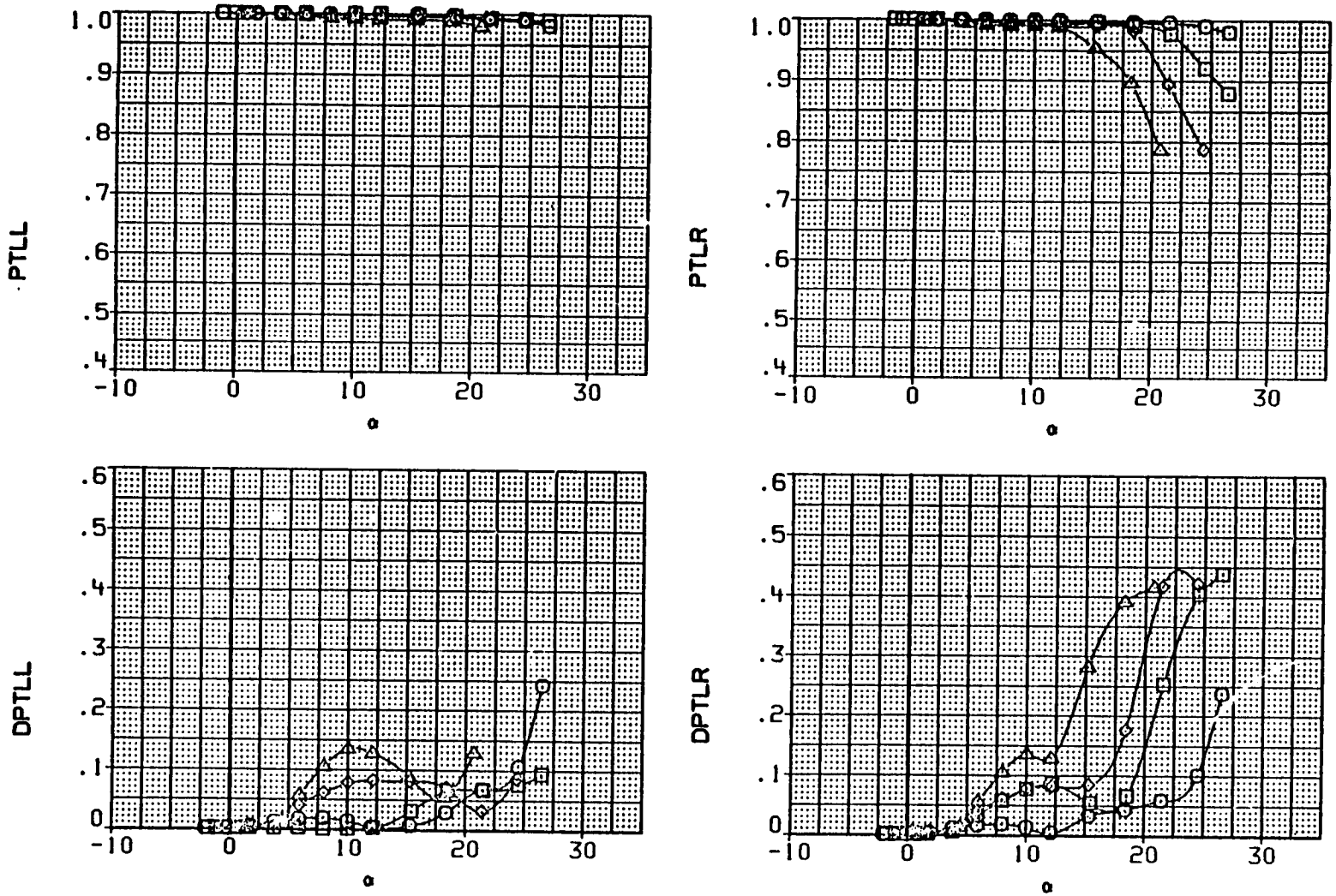

LEFT DUCT RIGHT DUCT

FLOW FIELD CHARACTERISTICS AT THE INLET ENTRANCE

(j) Mach = 0.60.

Figure 11.- Continued.

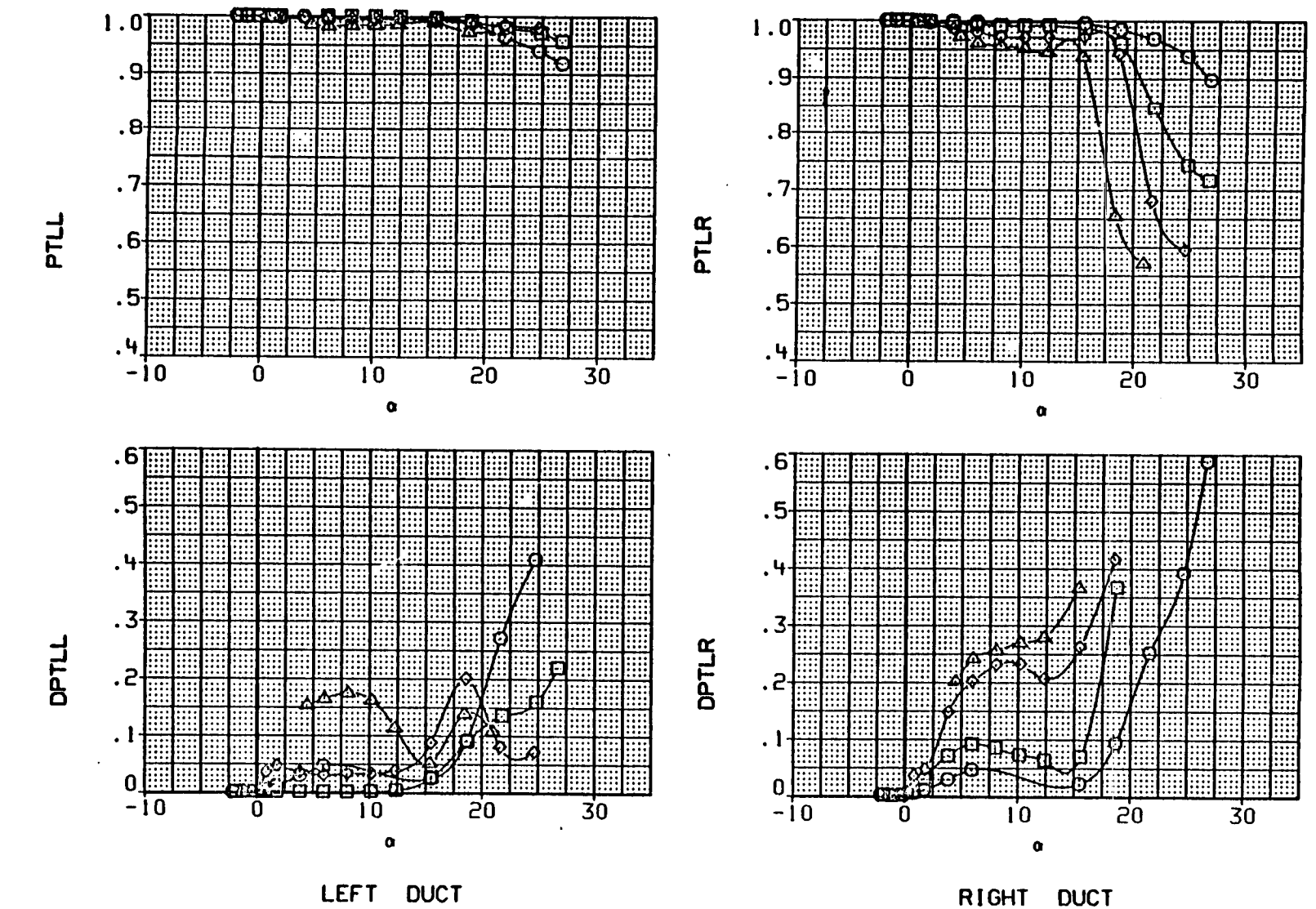

(k) Mach = 0.90.

Figure 11.- Continued.

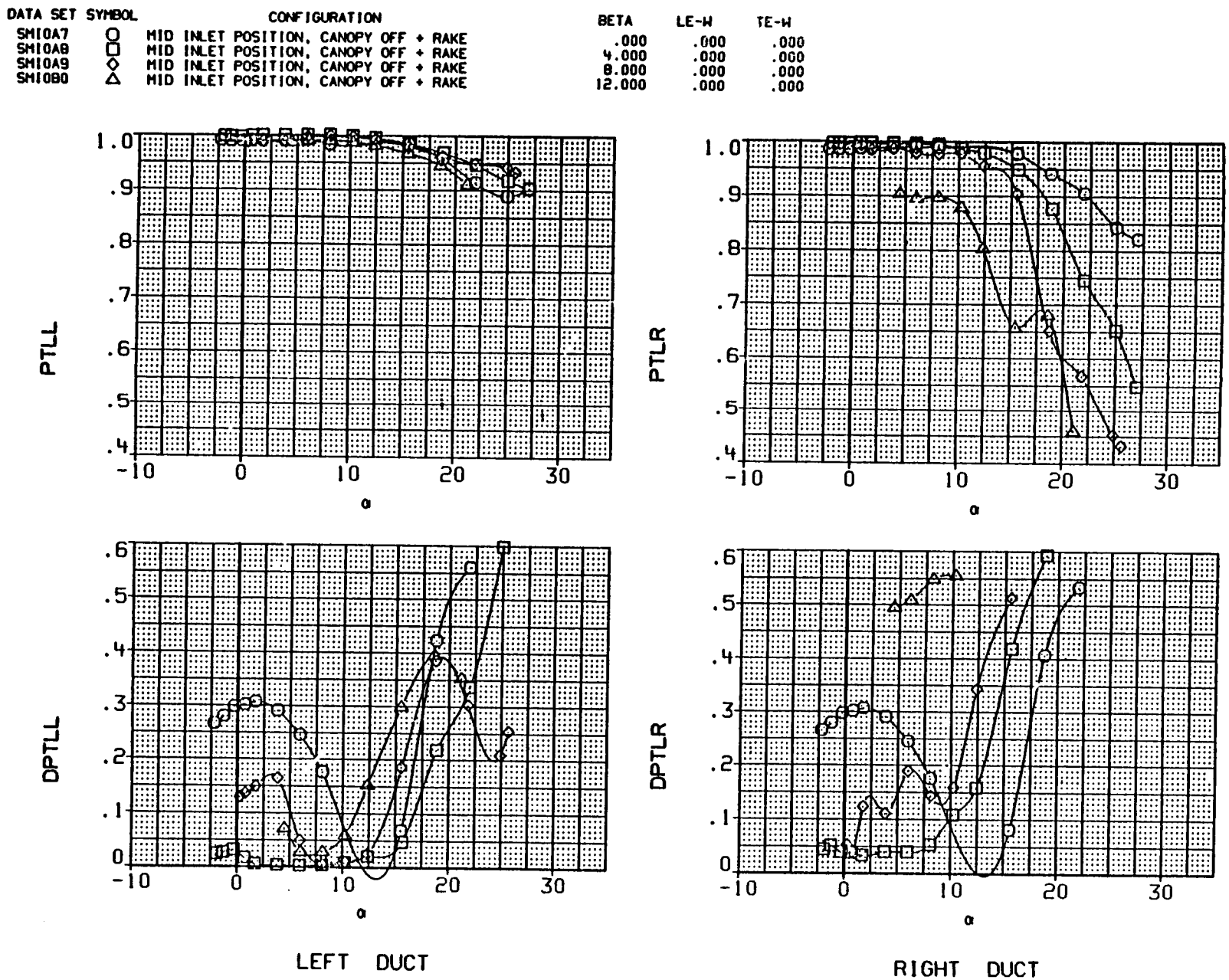

(1) Mach = 1.20.

Figure 11.- Continued.

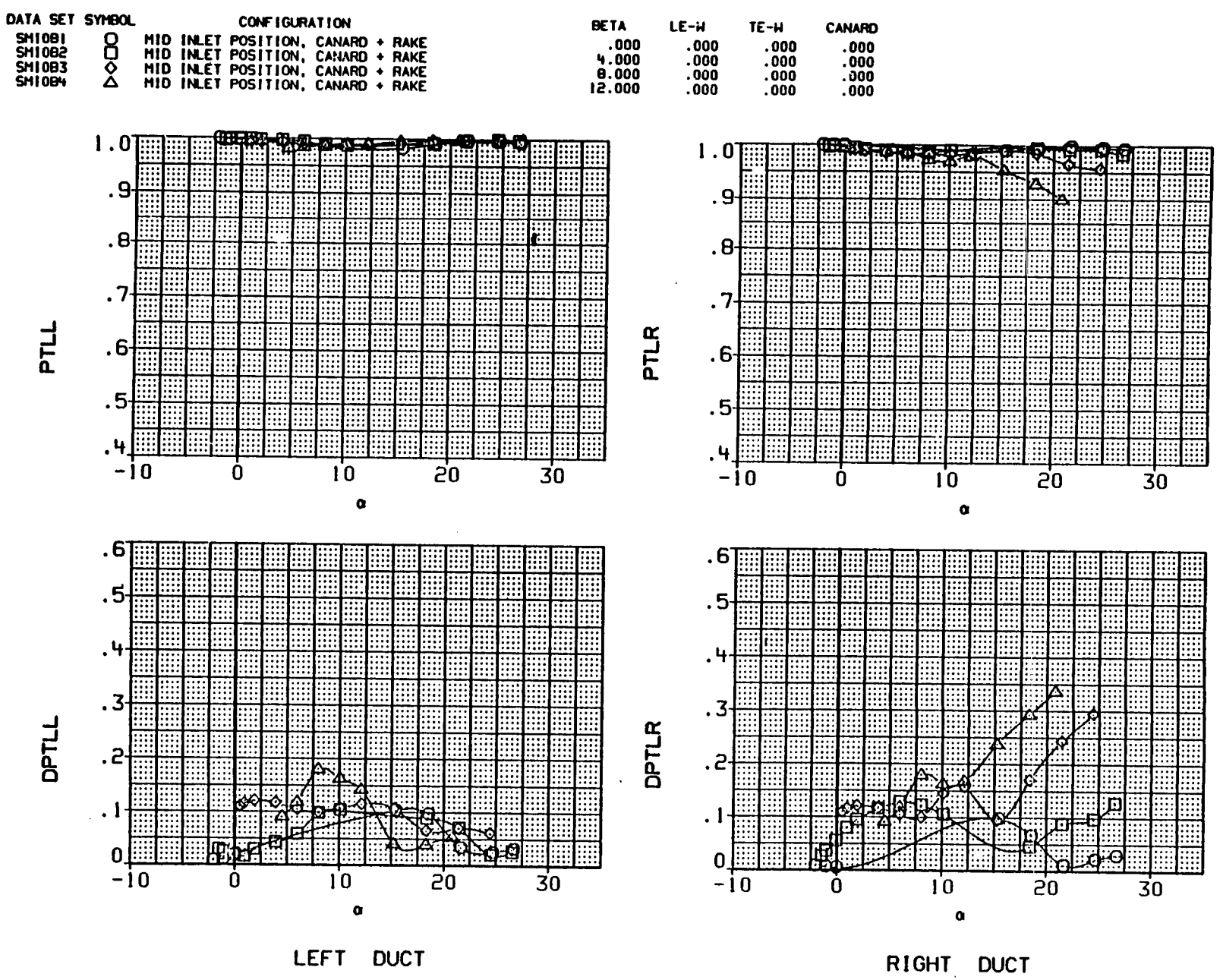

(m) Mach = 0.60.

Figure 11.- Continued.

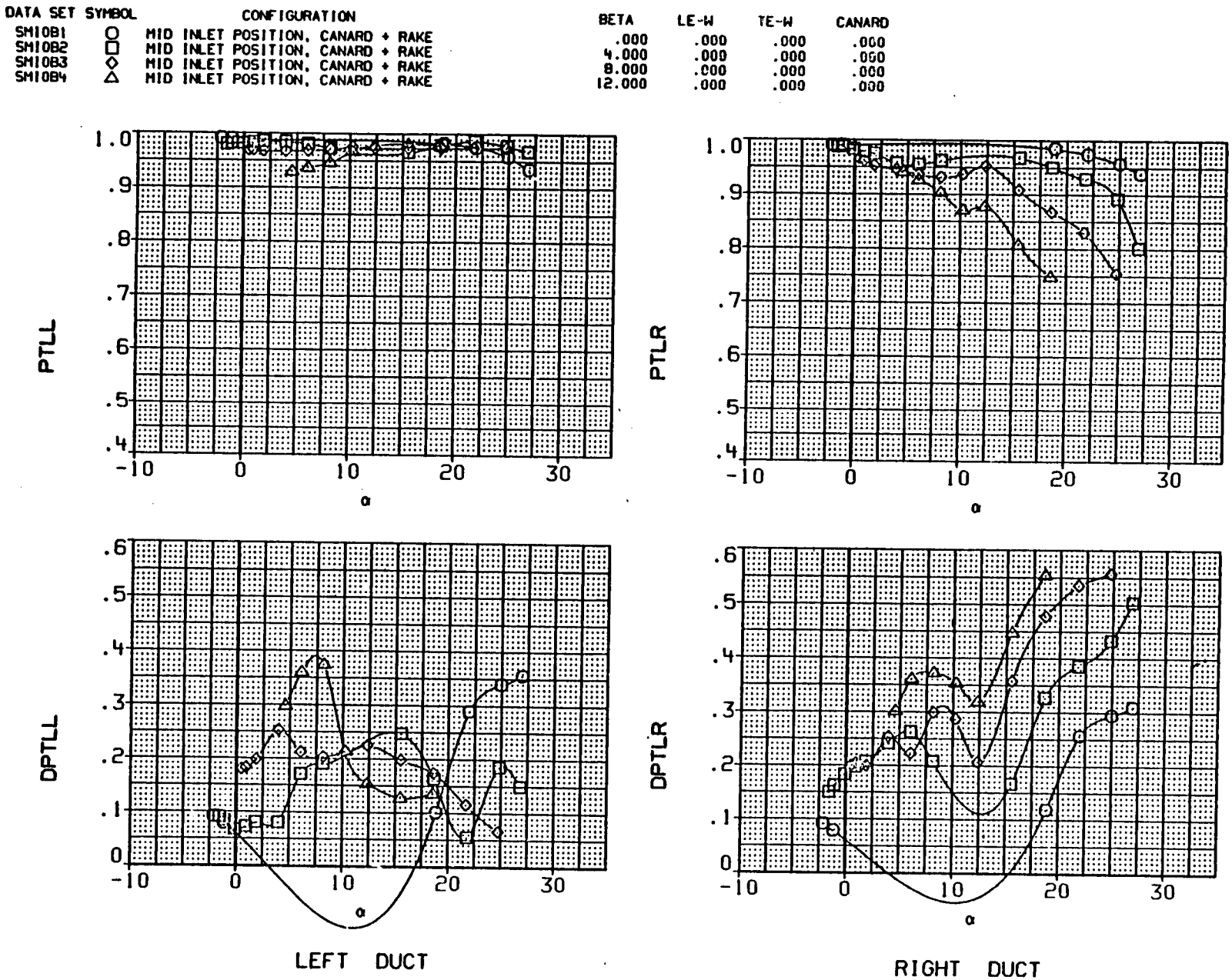

(n) Mach = 0.91.

Figure 11.- Continued.

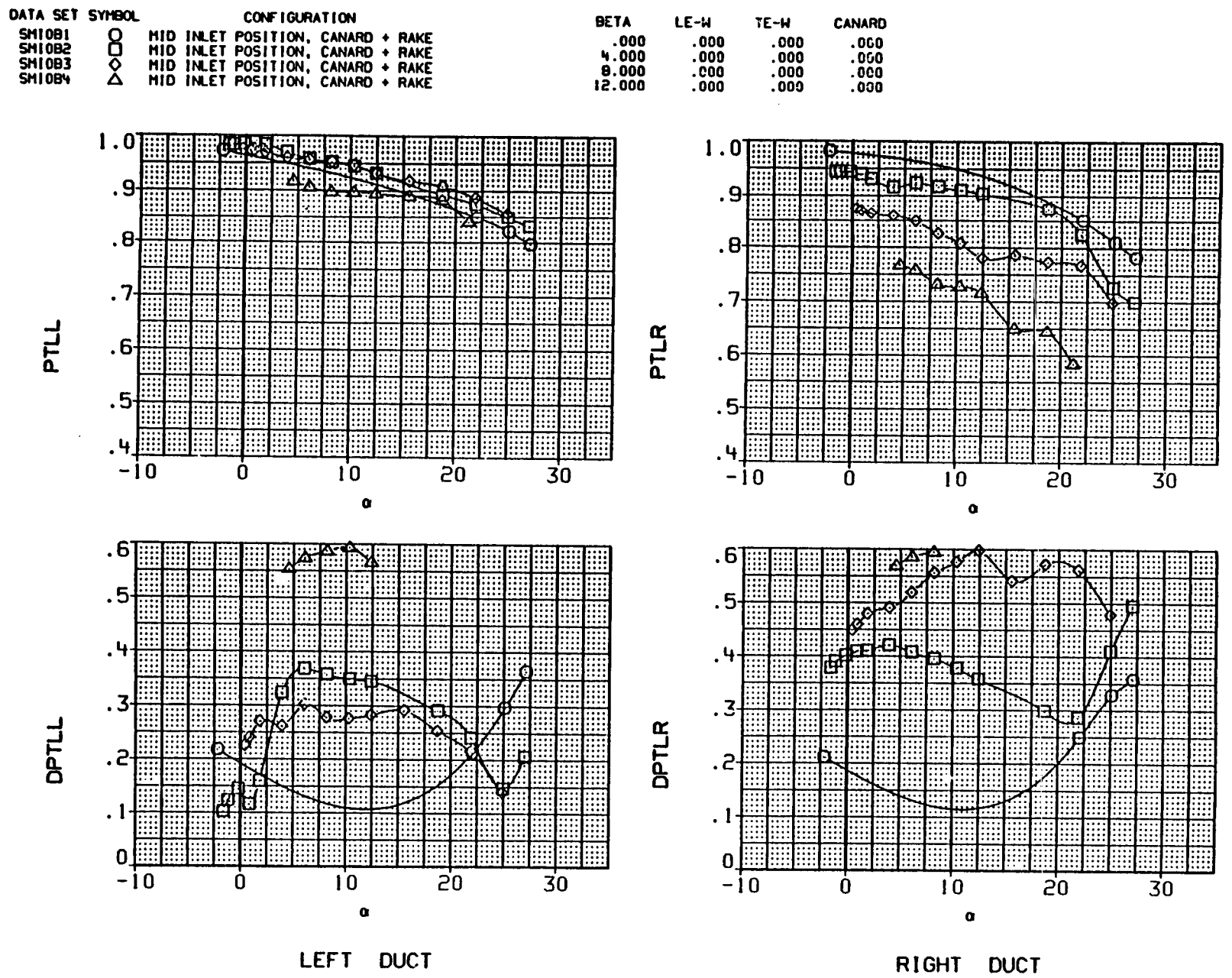

(o) Mach. = 1.19.

Figure 11.- Continued.

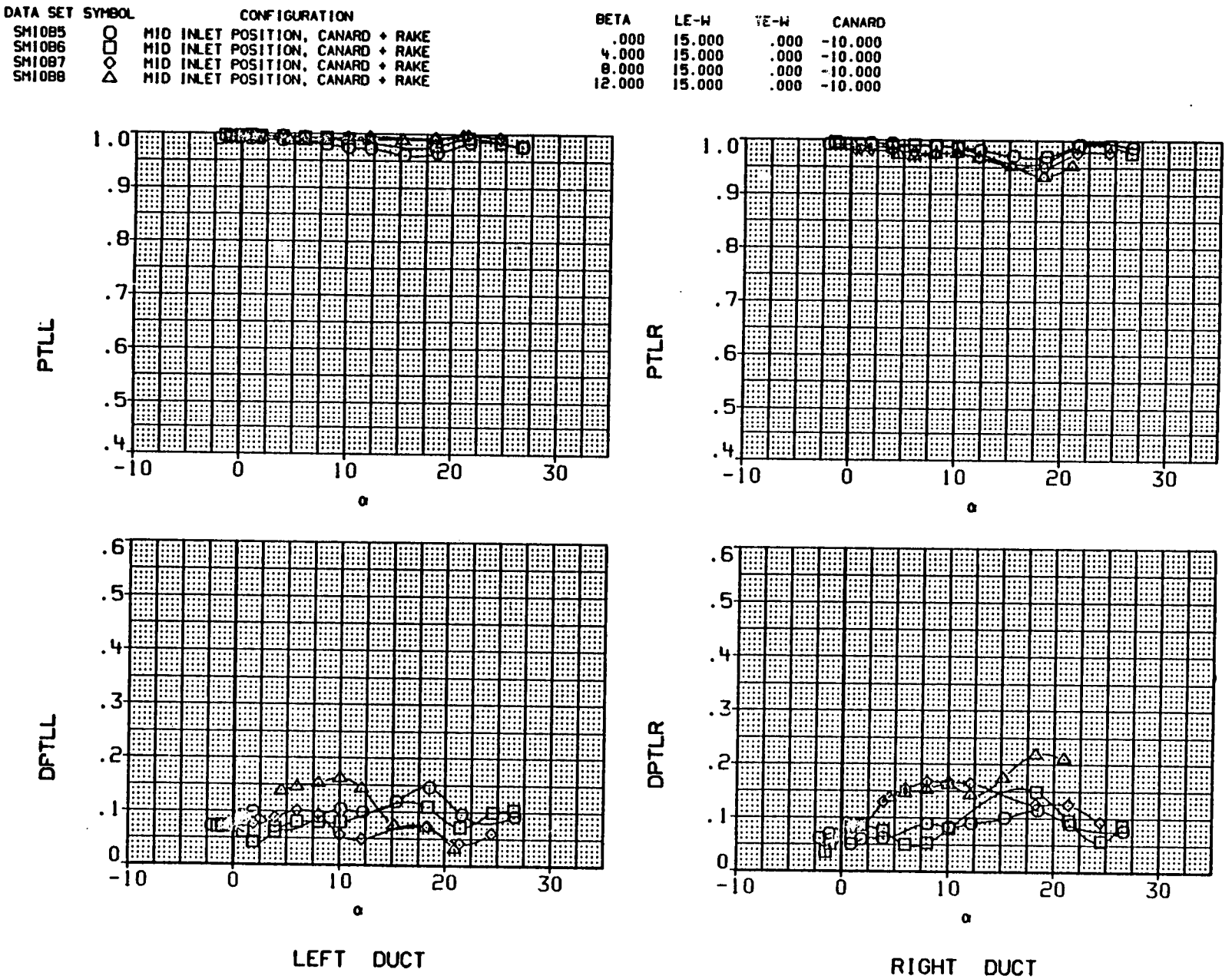

(p) Mach = 0.60.

Figure 11.- Continued.

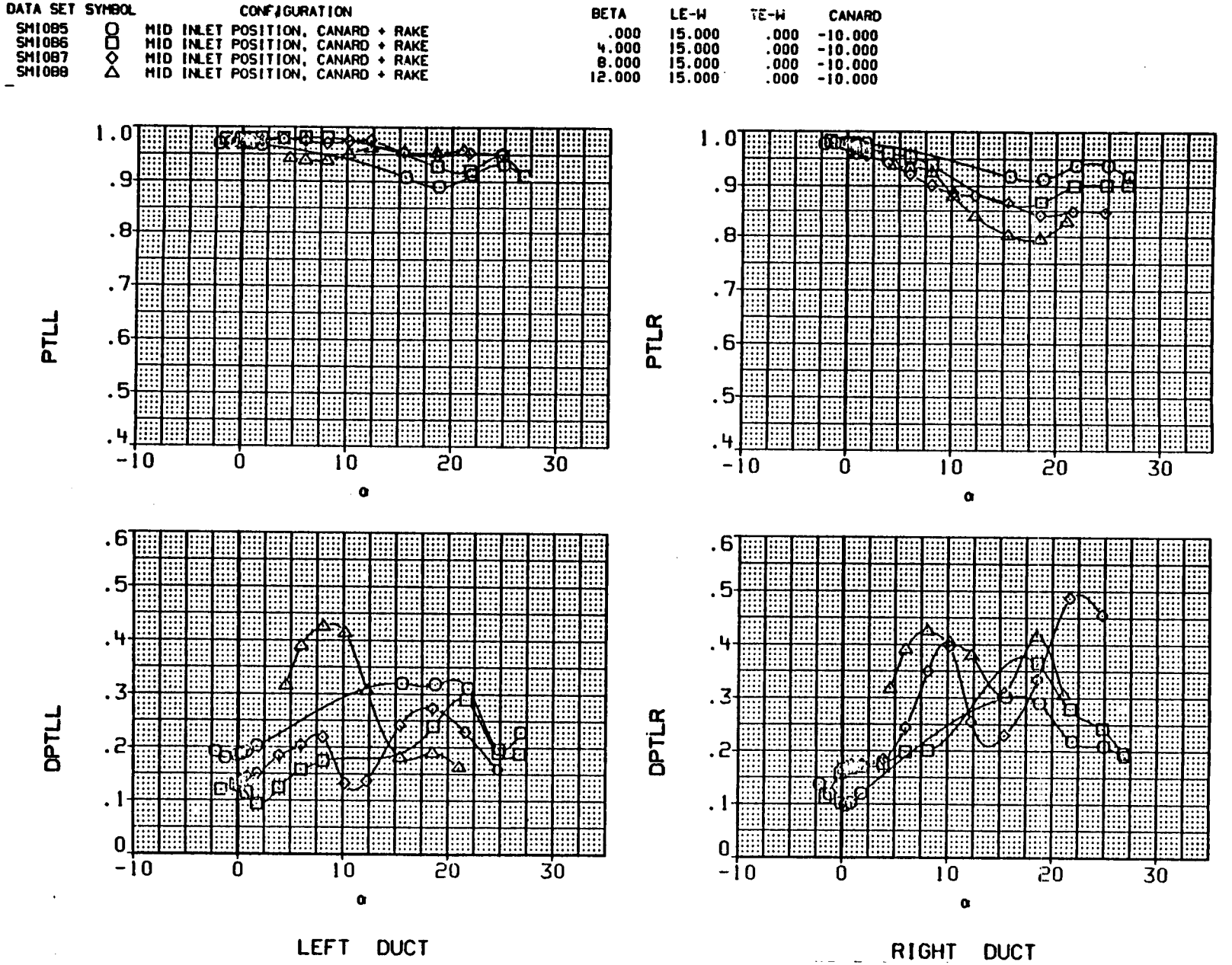

(q) Mach = 0.91.

Figure 11.- Continued.

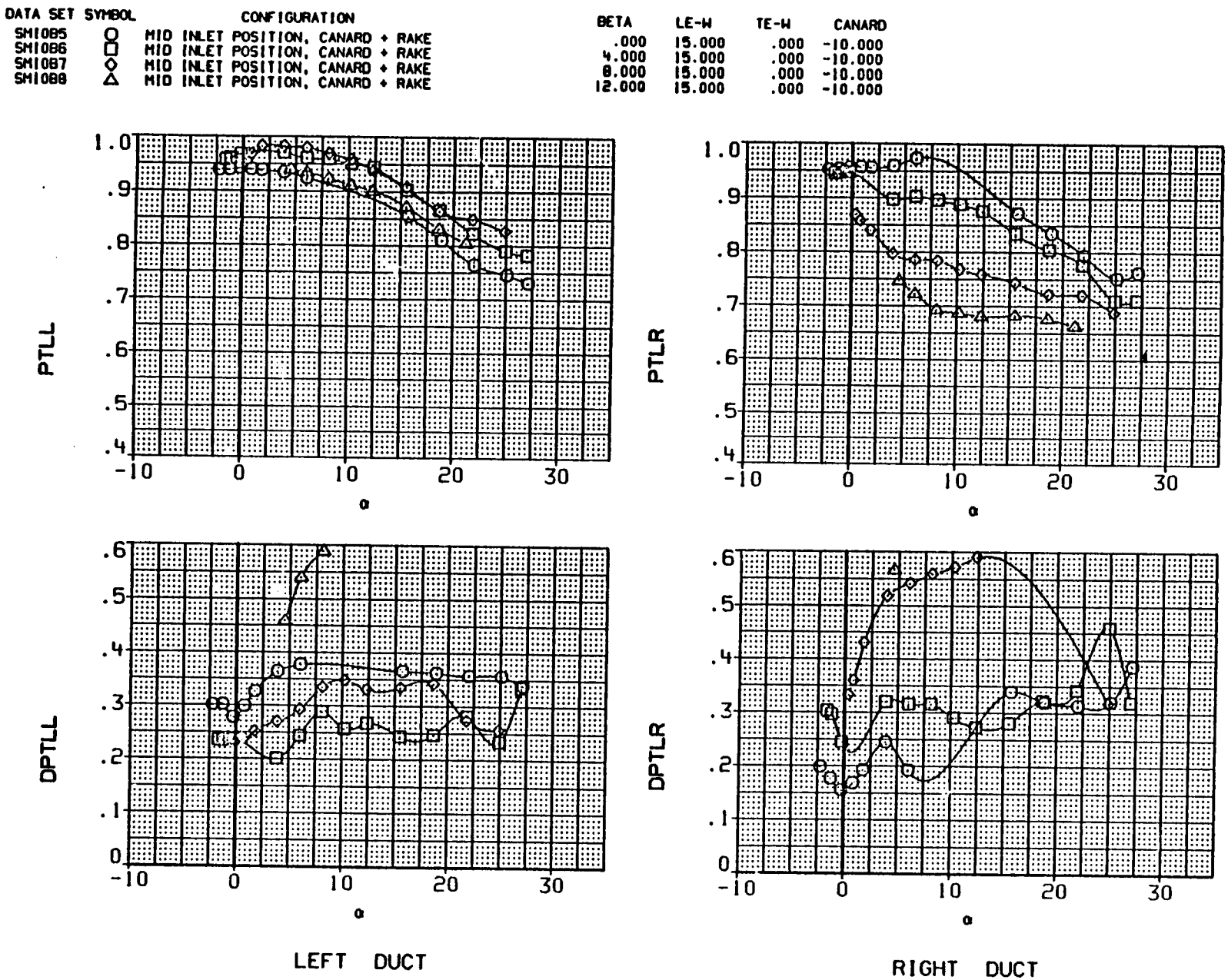

(r) Mach = 1.20.

Figure 11.- Continued.

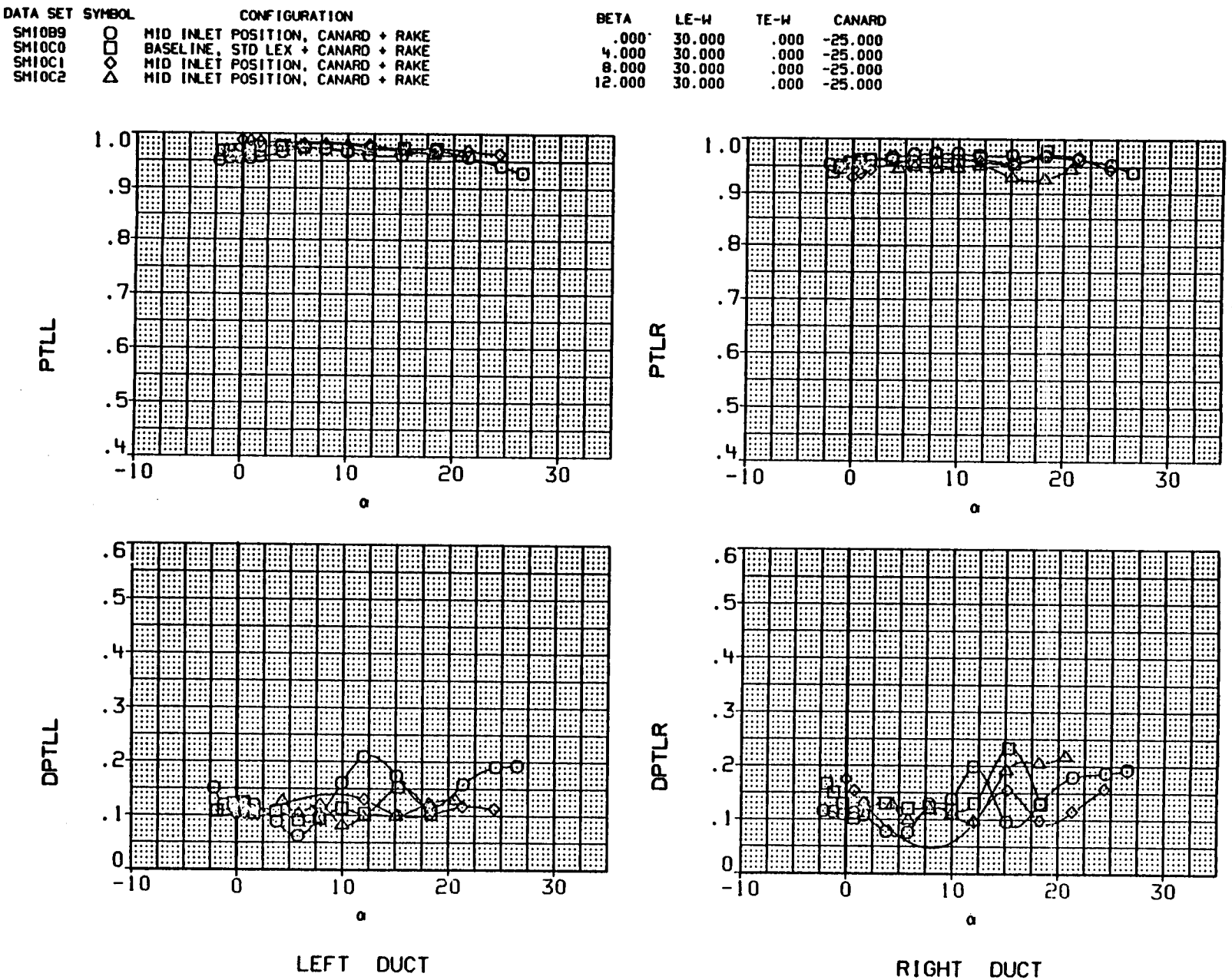

(s) Mach = 0.60.

Figure 11.- Continued.

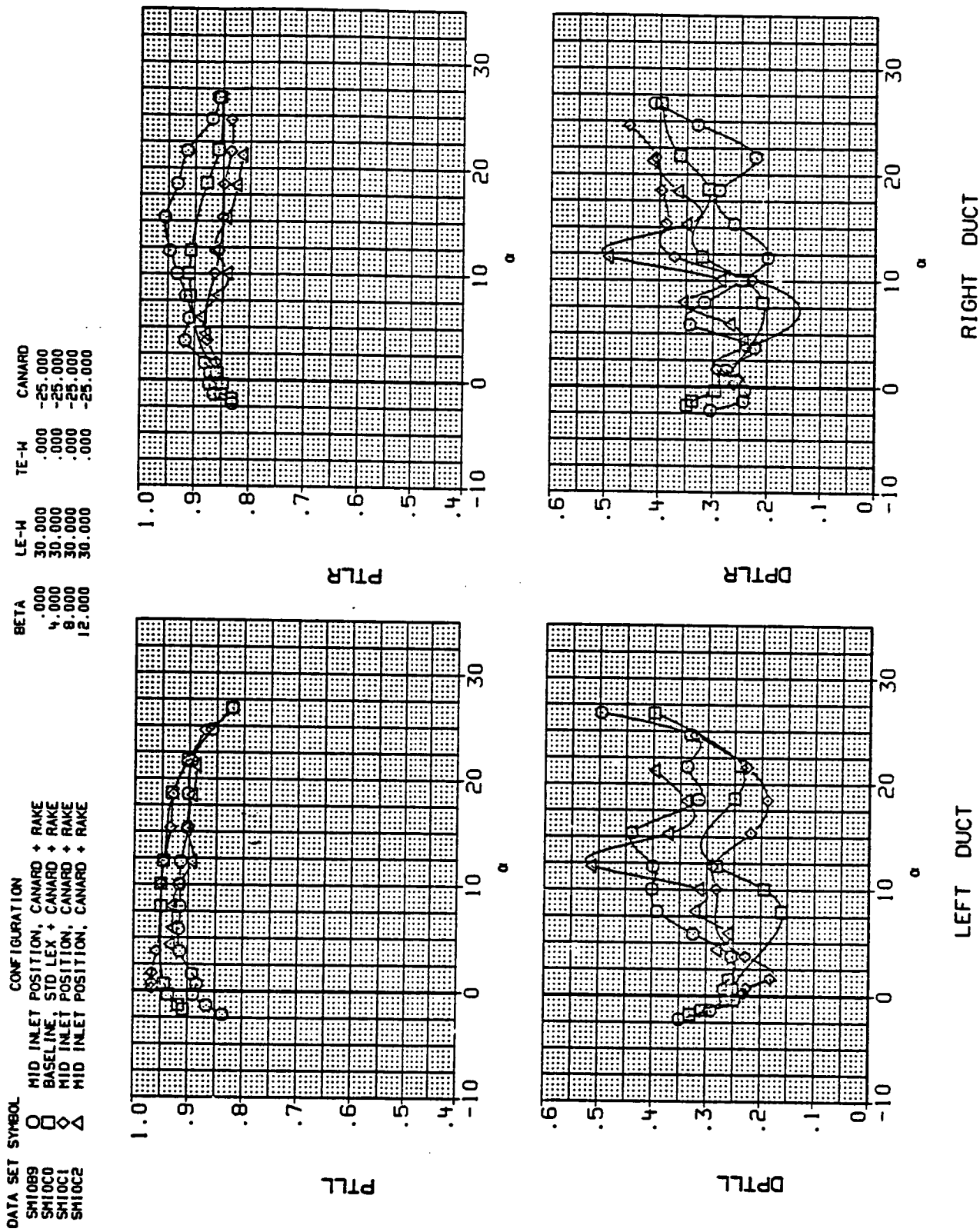

(t) Mach = 0.90.

Figure 11.- Continued.

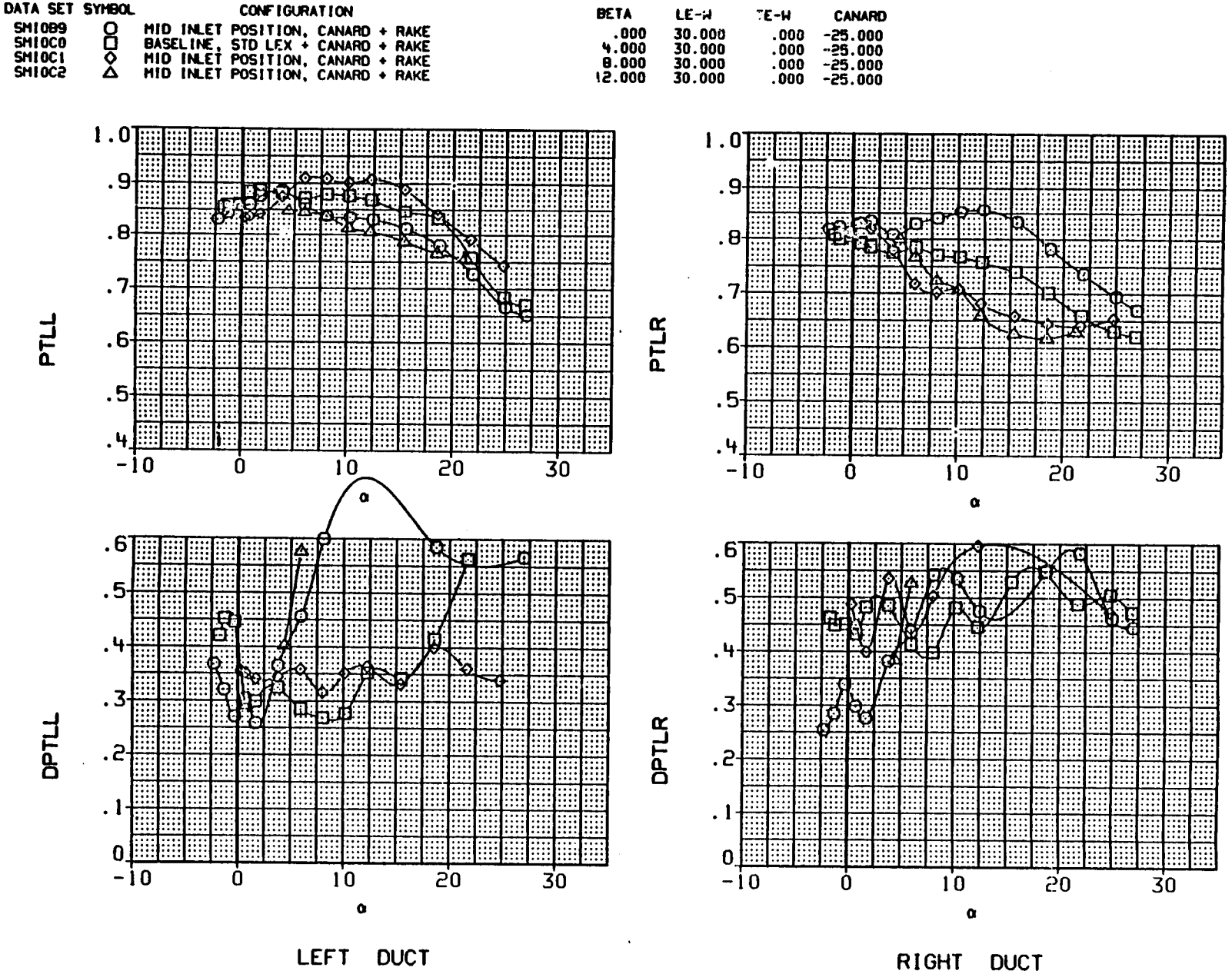

(u) Mach = 1.20.

Figure 11.- Continued.

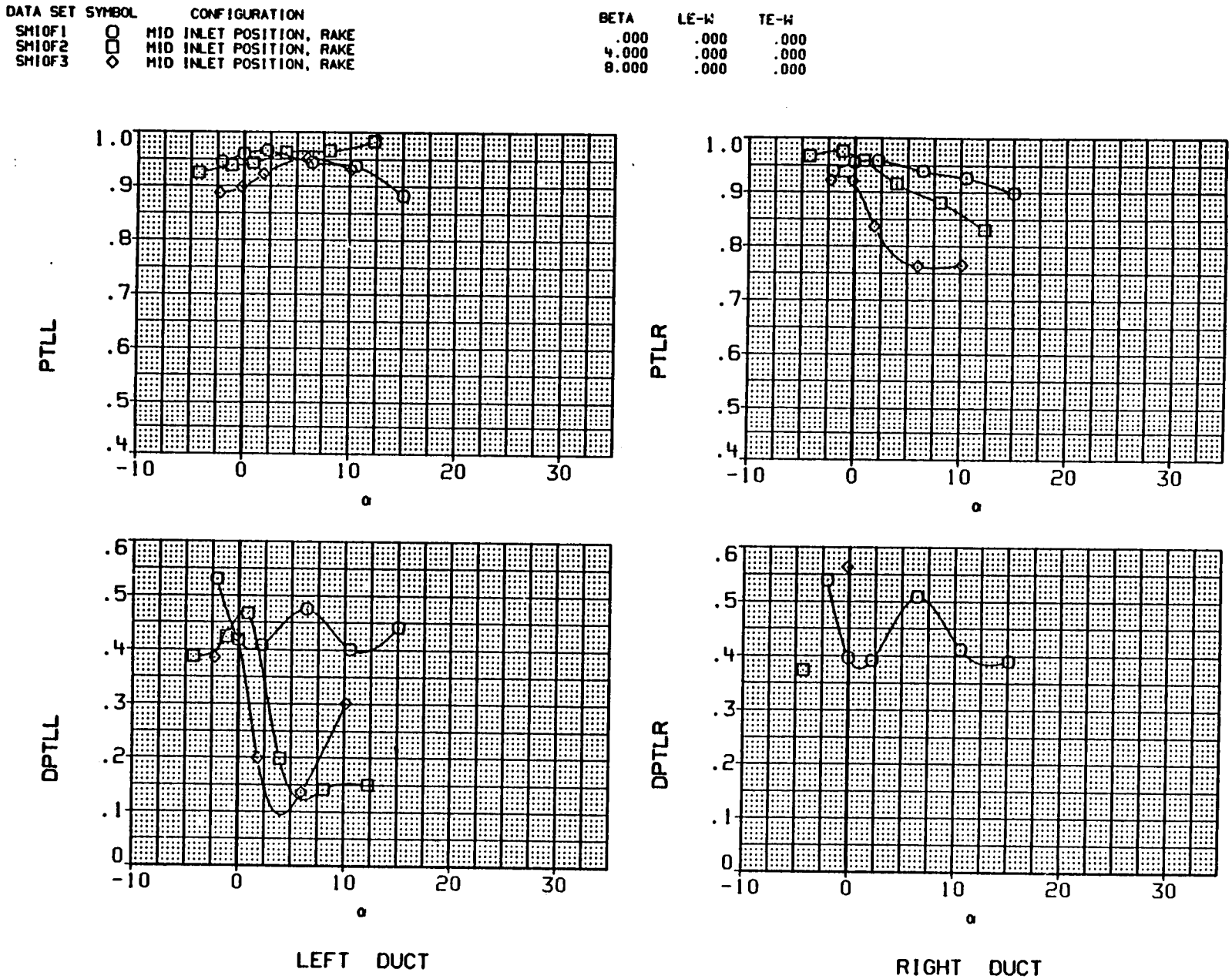

(v) Mach = 1.60.

Figure 11.- Continued.

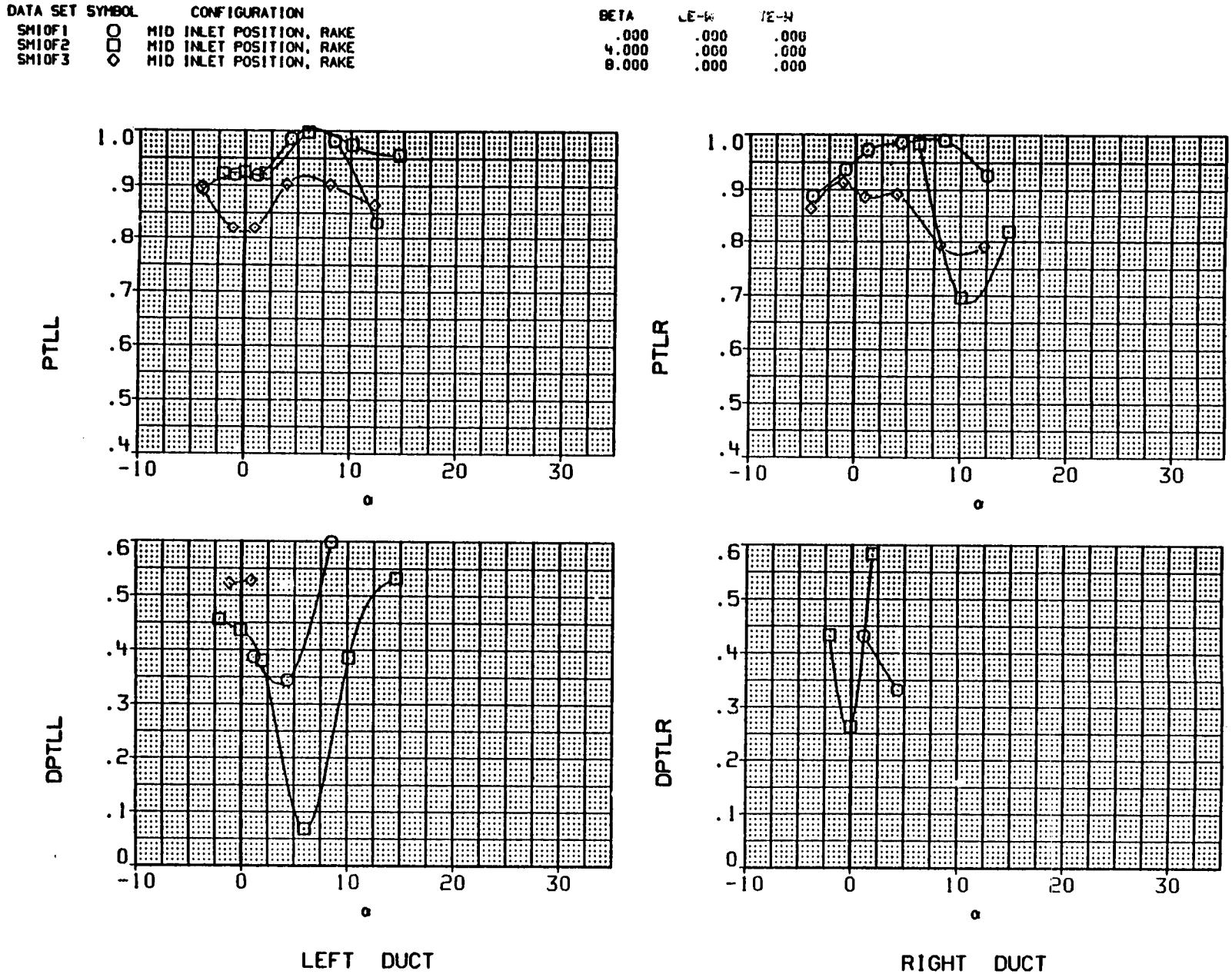

(w) Mach = 2.00.

Figure 11.- Continued.

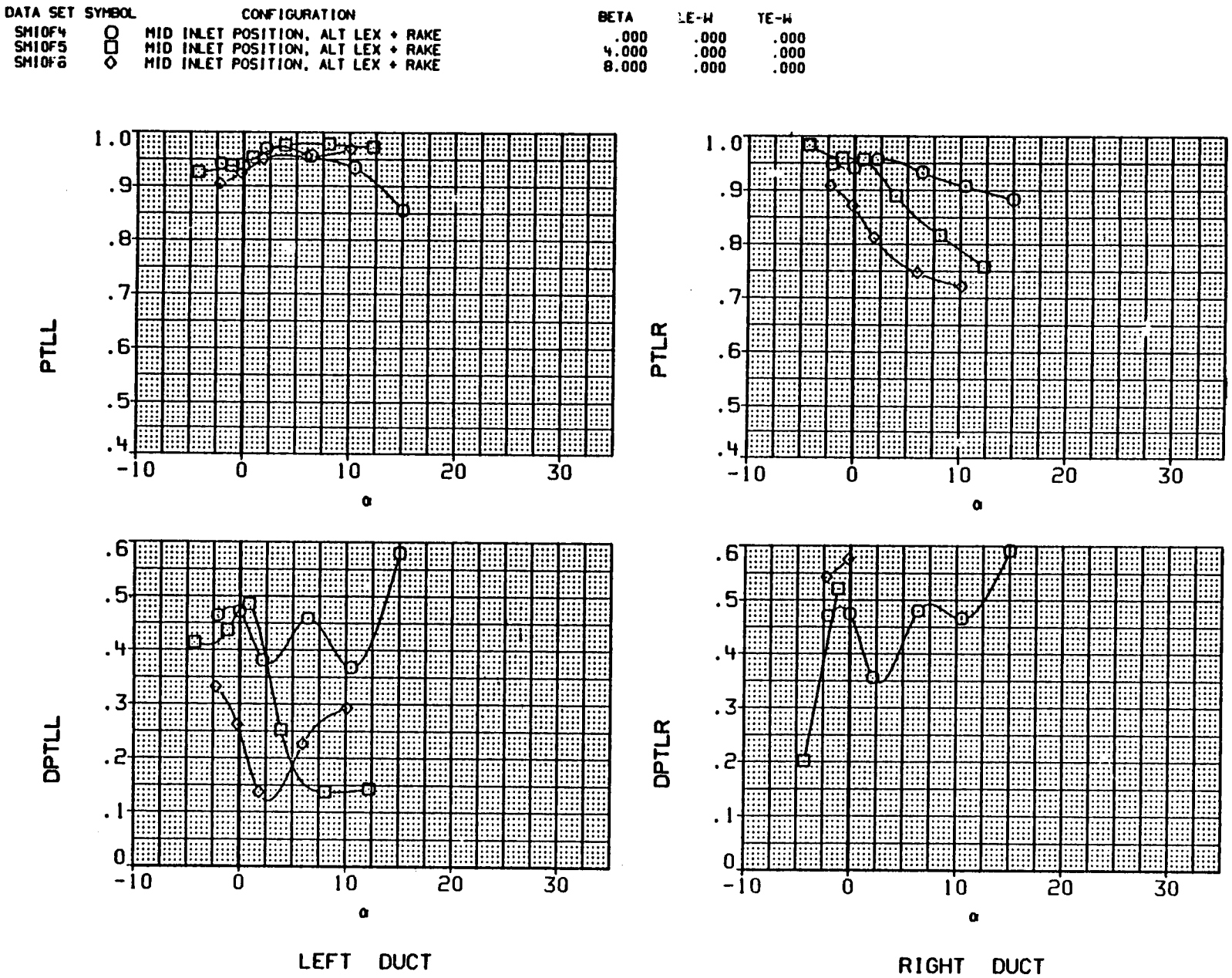

(x) Mach = 1.60.

Figure 11.- Continued.

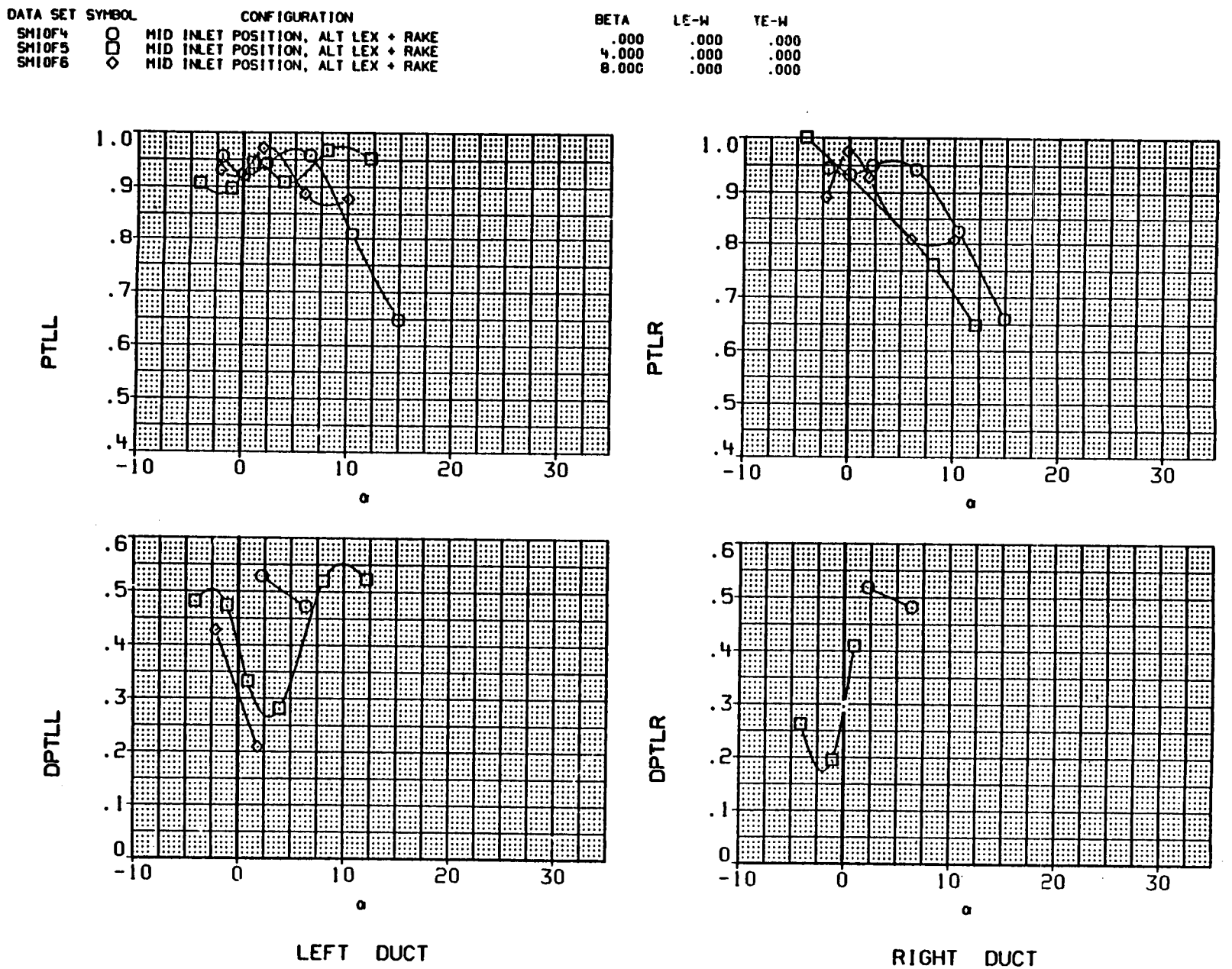

(y) Mach = 2.00.

Figure 11.- Continued.

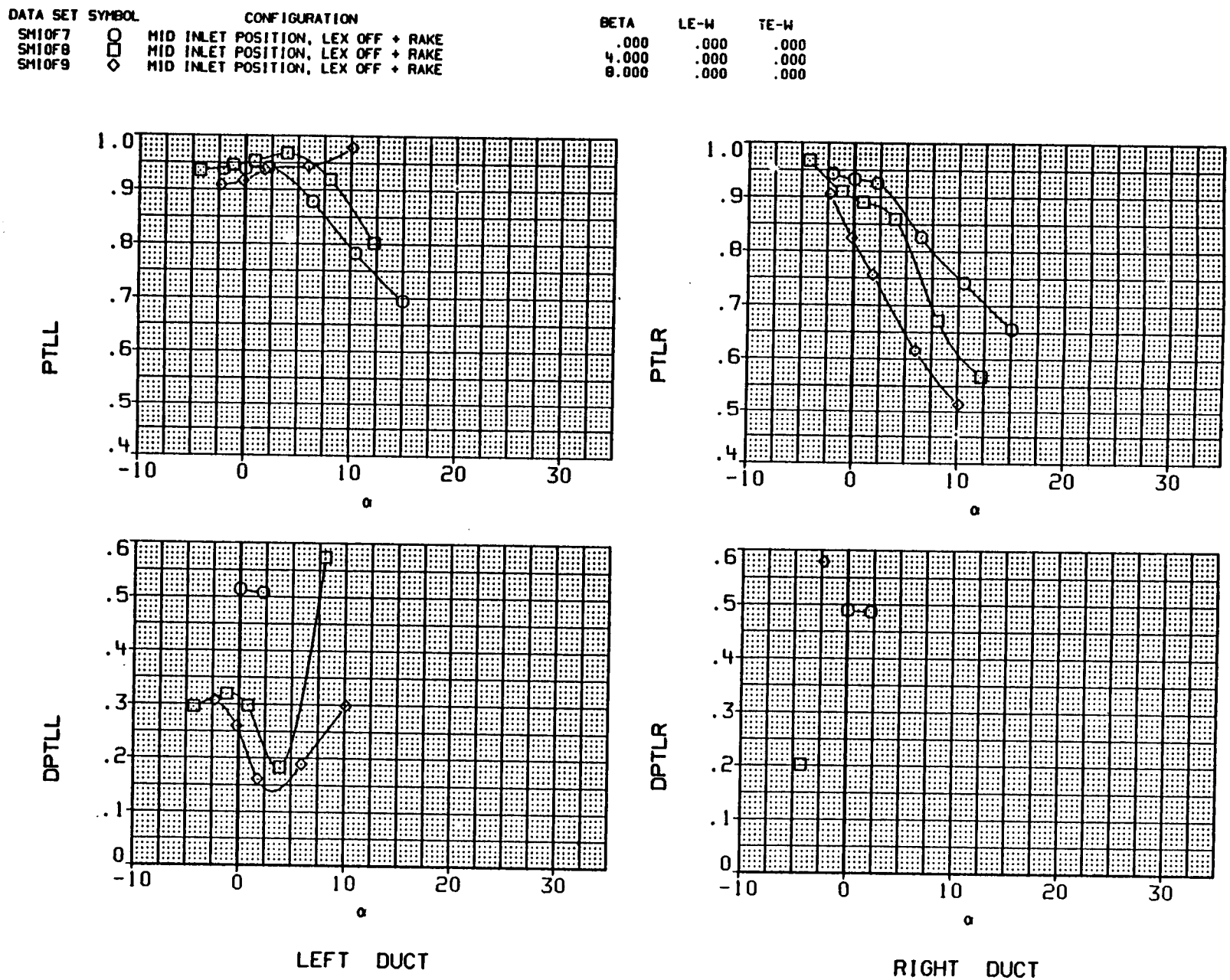

(z) Mach = 1.60.

Figure 11.- Continued.

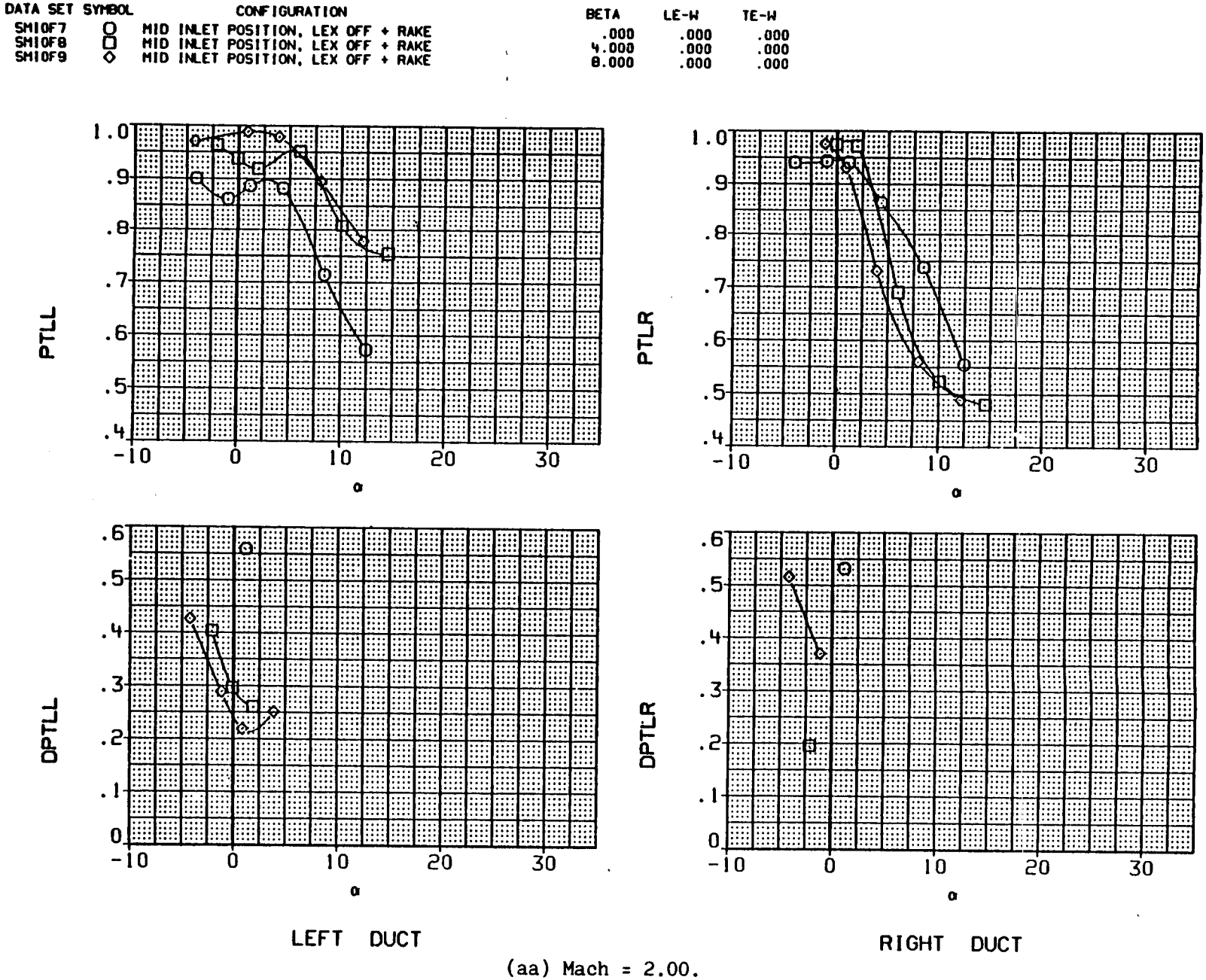

(aa) Mach = 2.00.

Figure 11.- Continued.

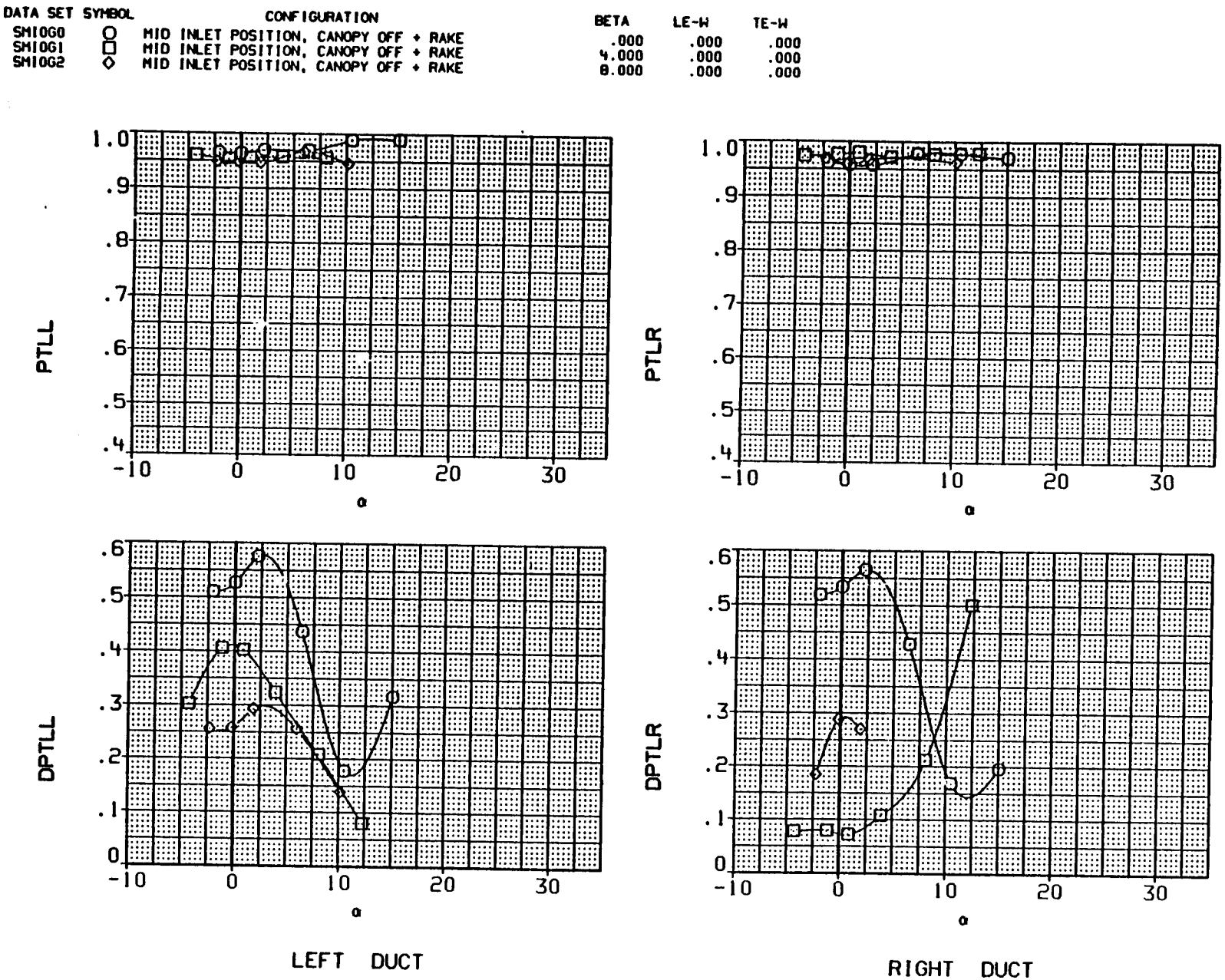

(bb) Mach = 1.60.

Figure 11.- Continued.

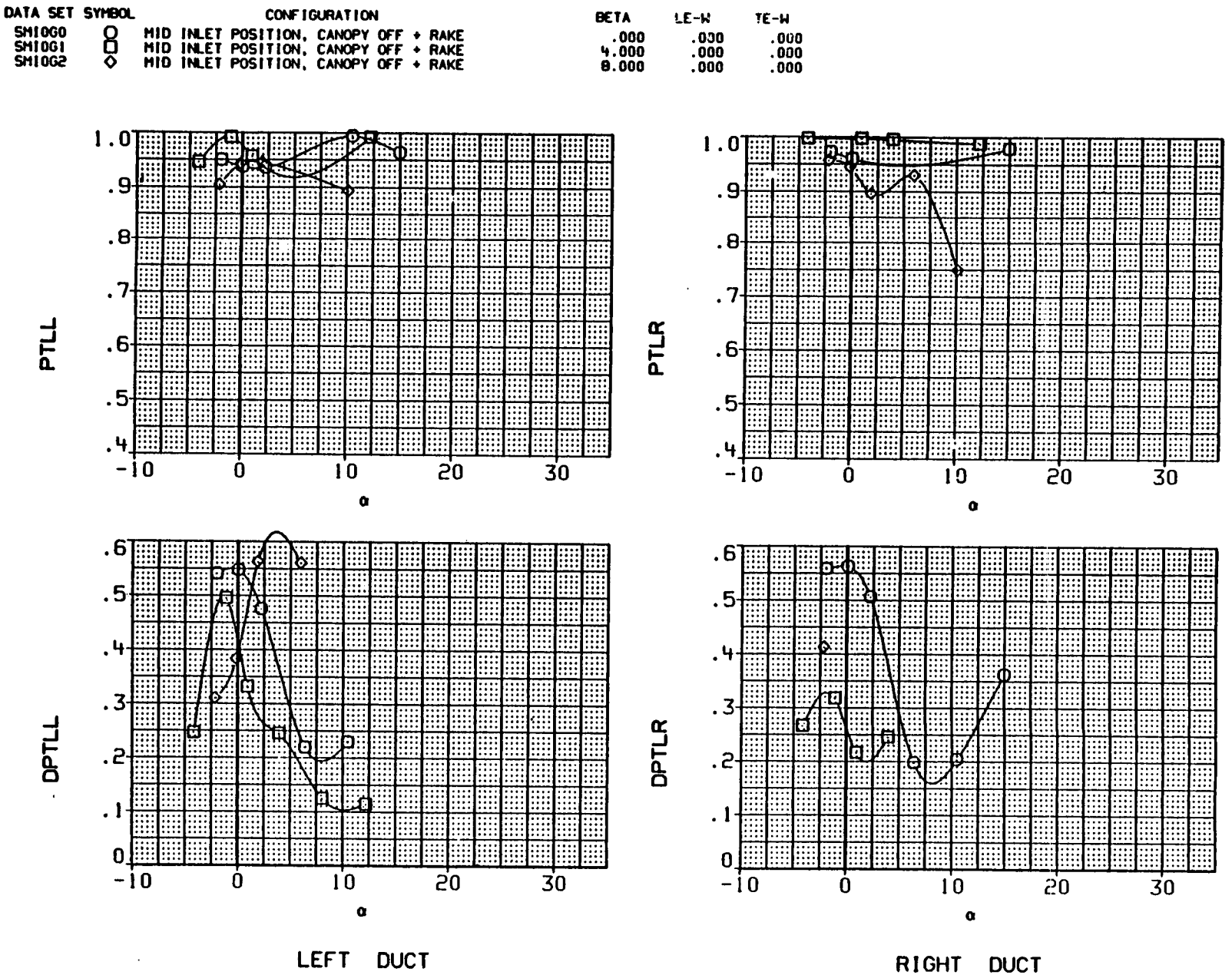

(cc) Mach = 2.00.

Figure 11.- Continued.

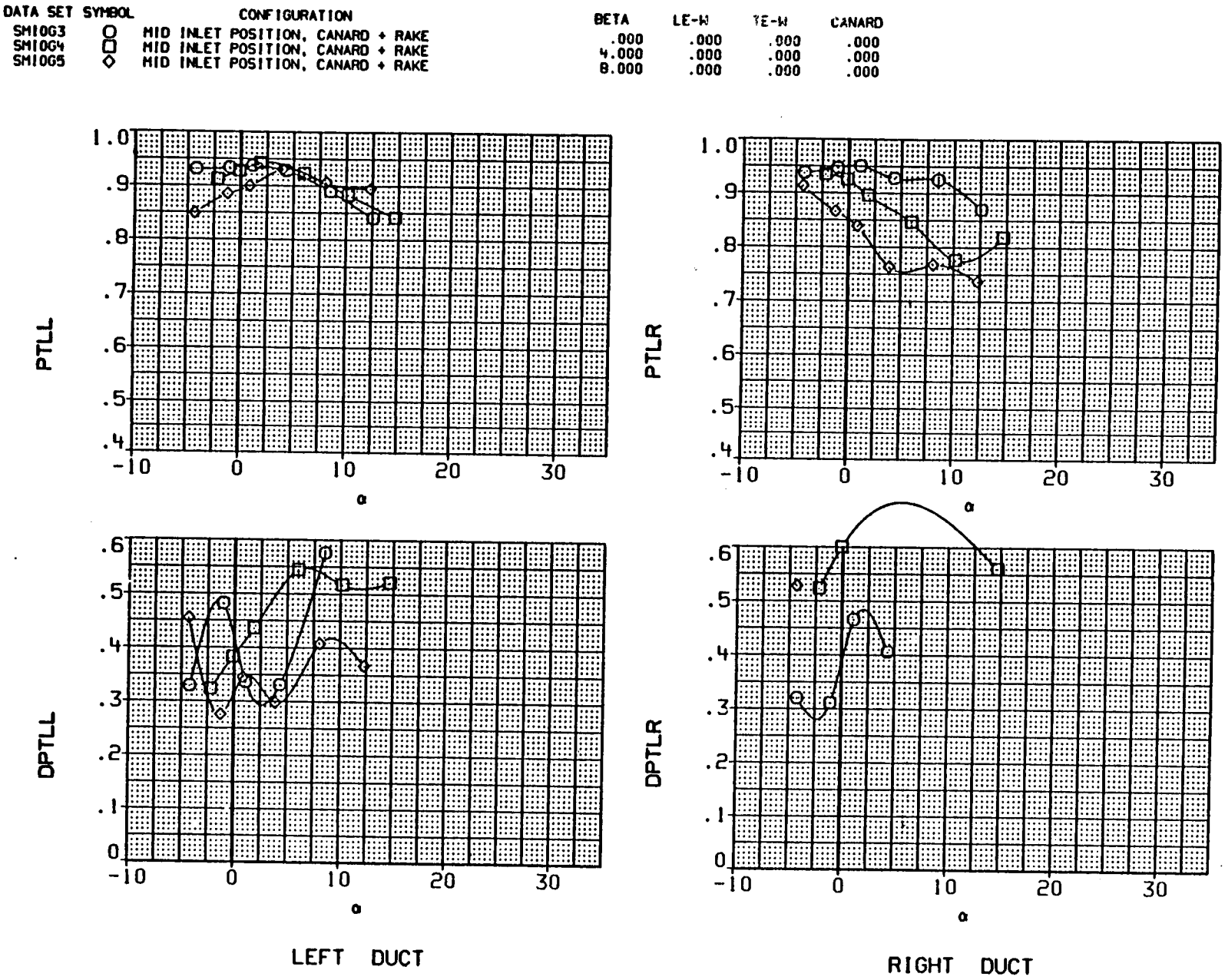

(dd) Mach = 1.60.

Figure 11.- Continued.

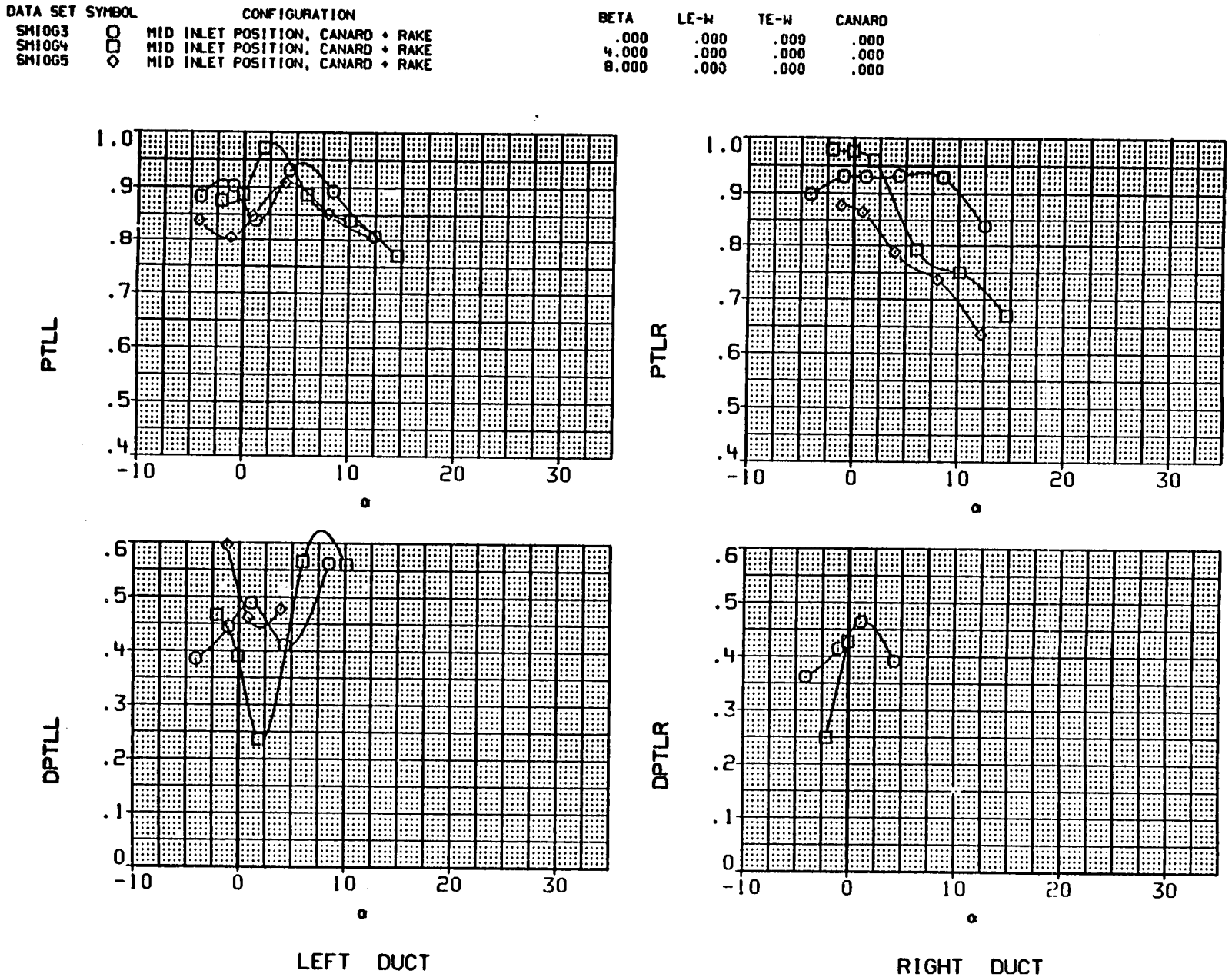

(ee) Mach = 2.00.

Figure 11.- Continued.

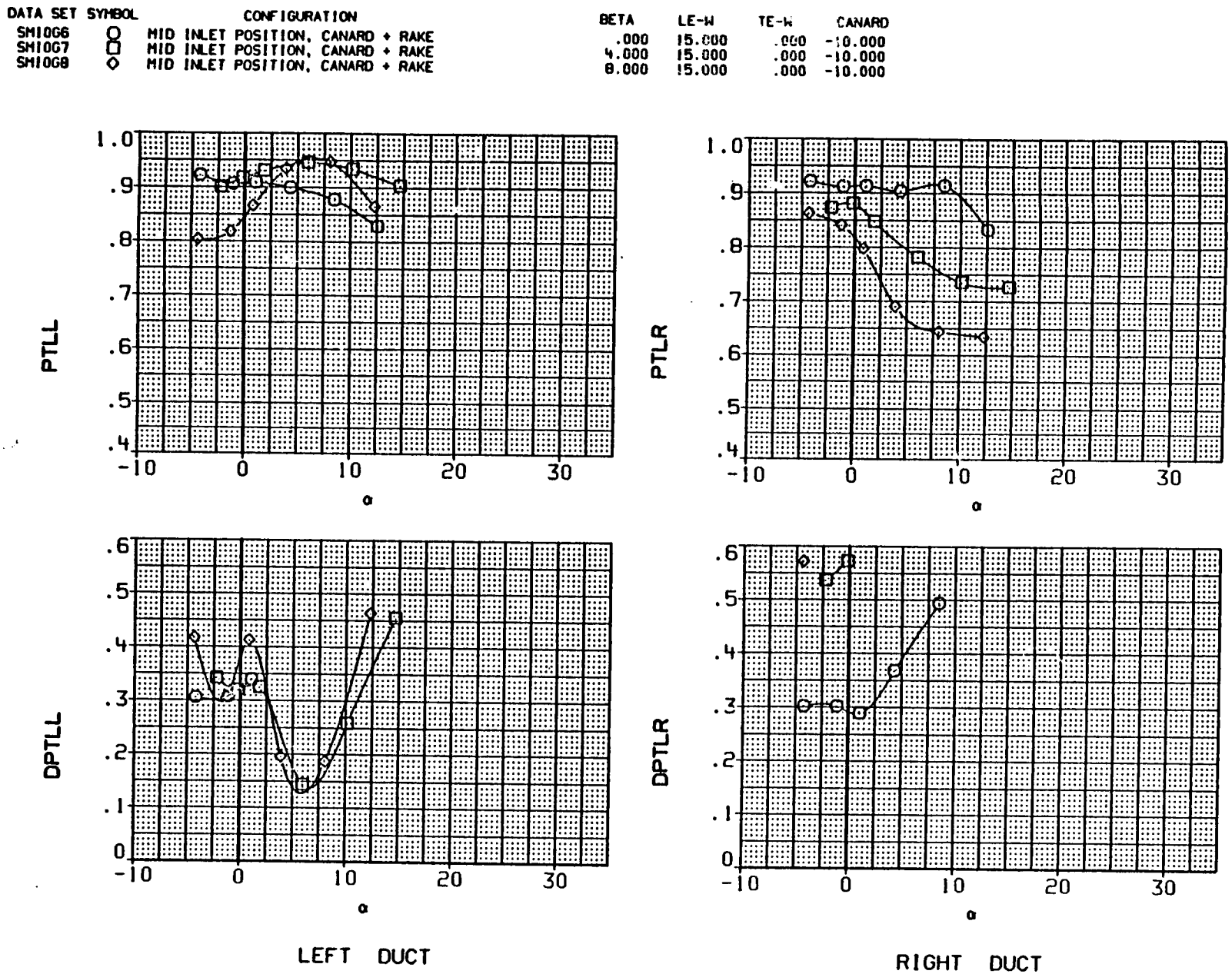

(ff) Mach = 1.60.

Figure 11.- Continued.

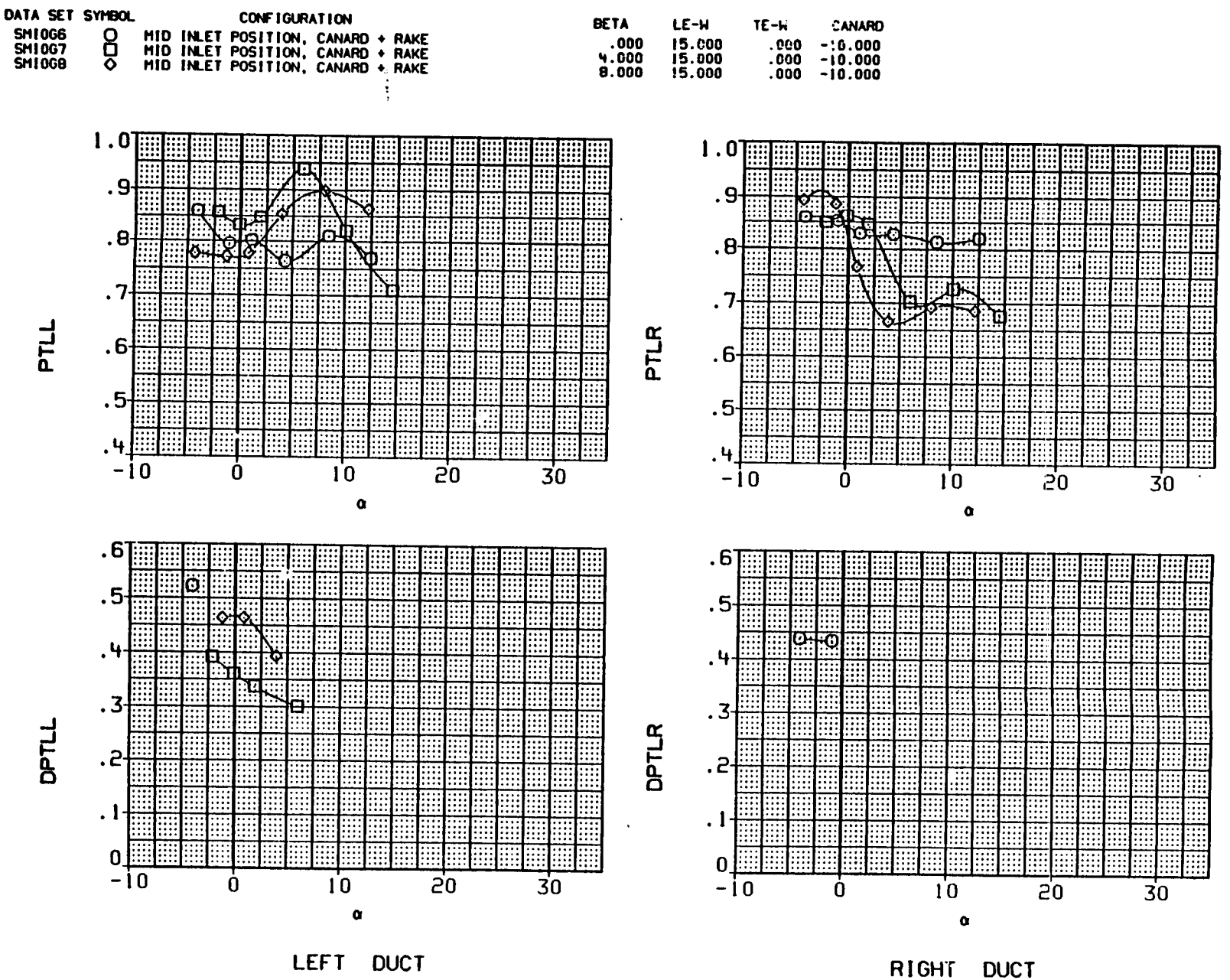

(gg) Mach = 2.00.

Figure 11.- Concluded.

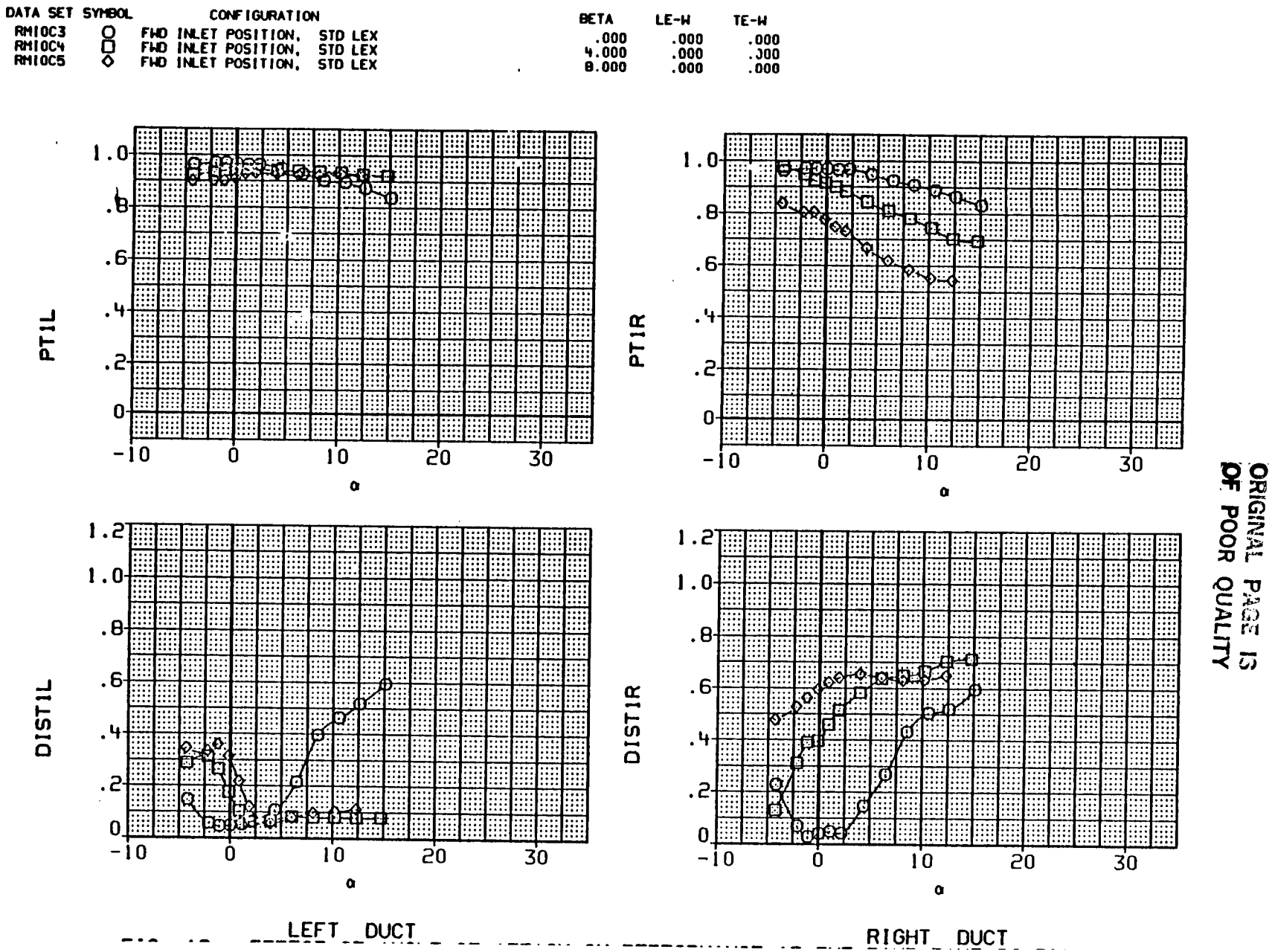

(a) Mach = 1.60.

Figure 12.- Effect of angle of attack on performance at the ramp rake station.

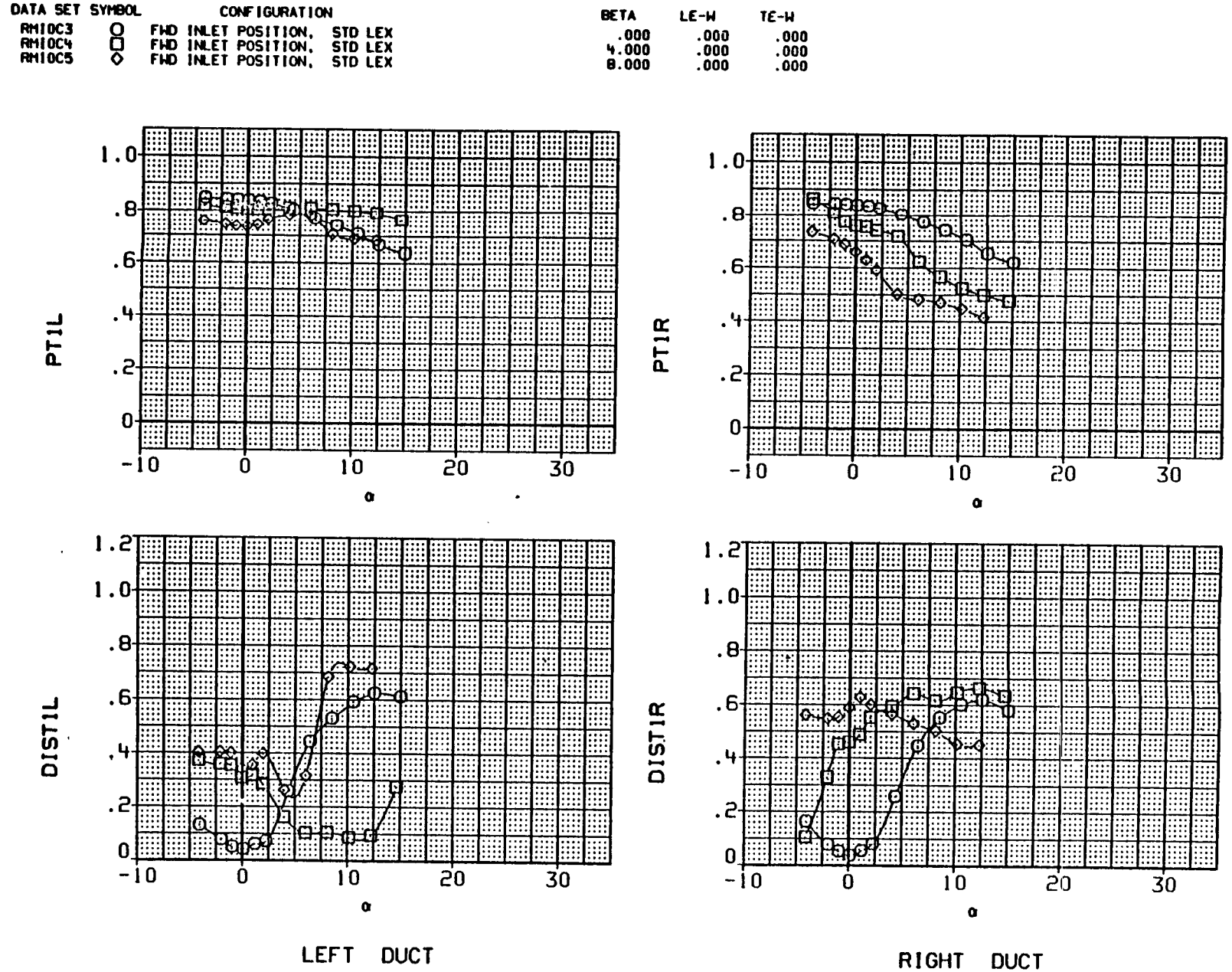

(b) Mach = 2.00.

Figure 12.- Continued.

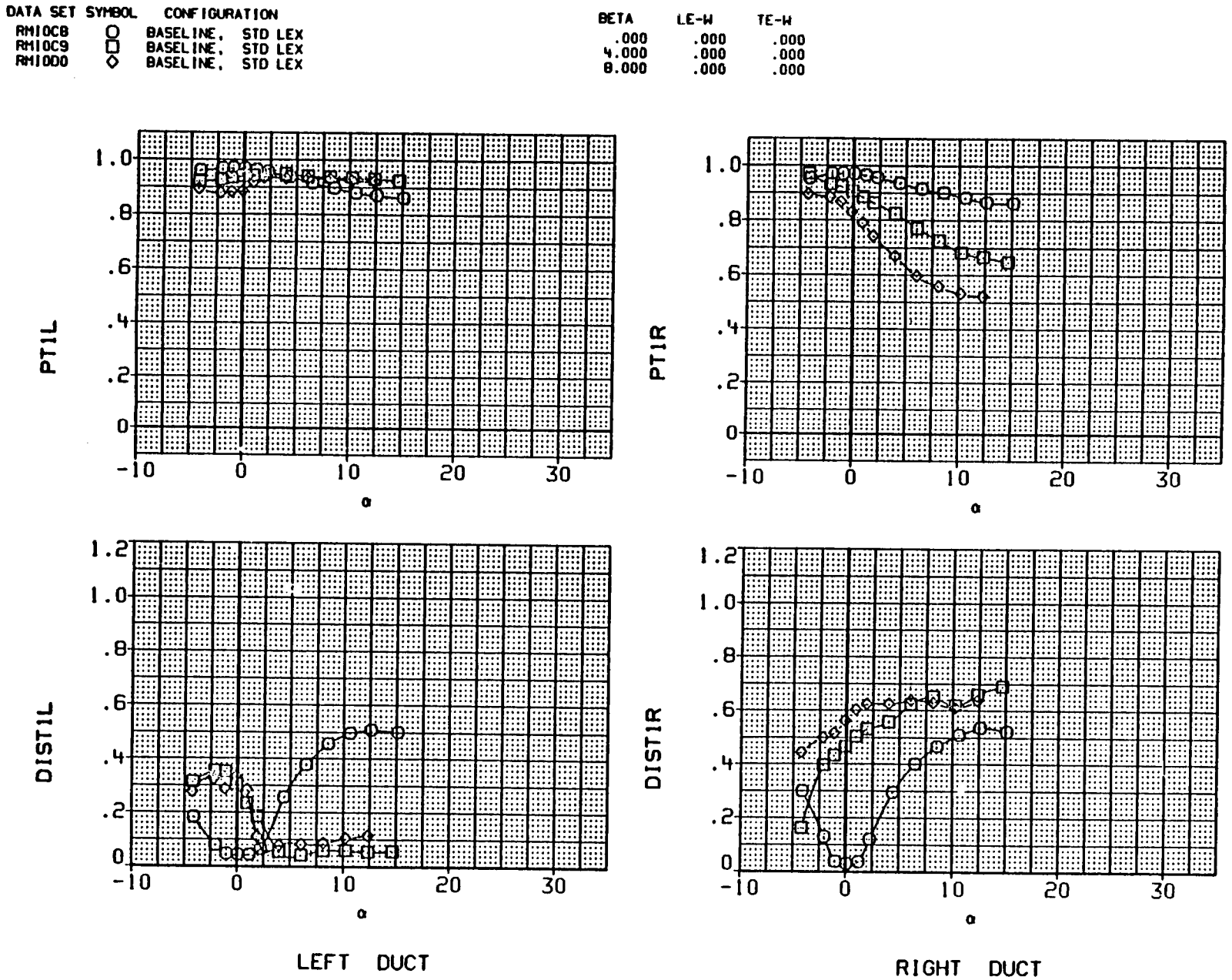

(c) Mach = 1.60.

Figure 12.- Continued.

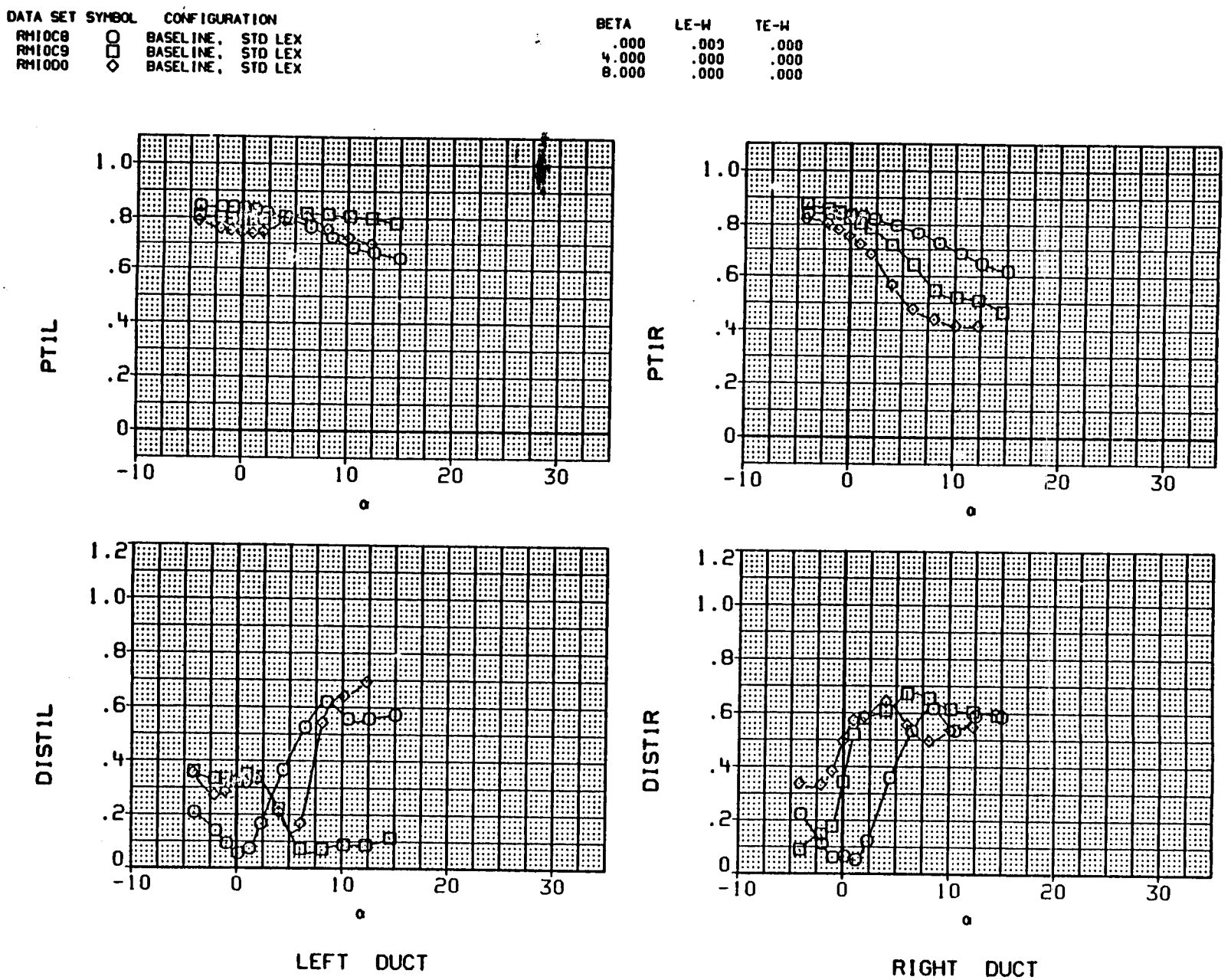

(d) Mach = 2.00.

Figure 12.- Continued.

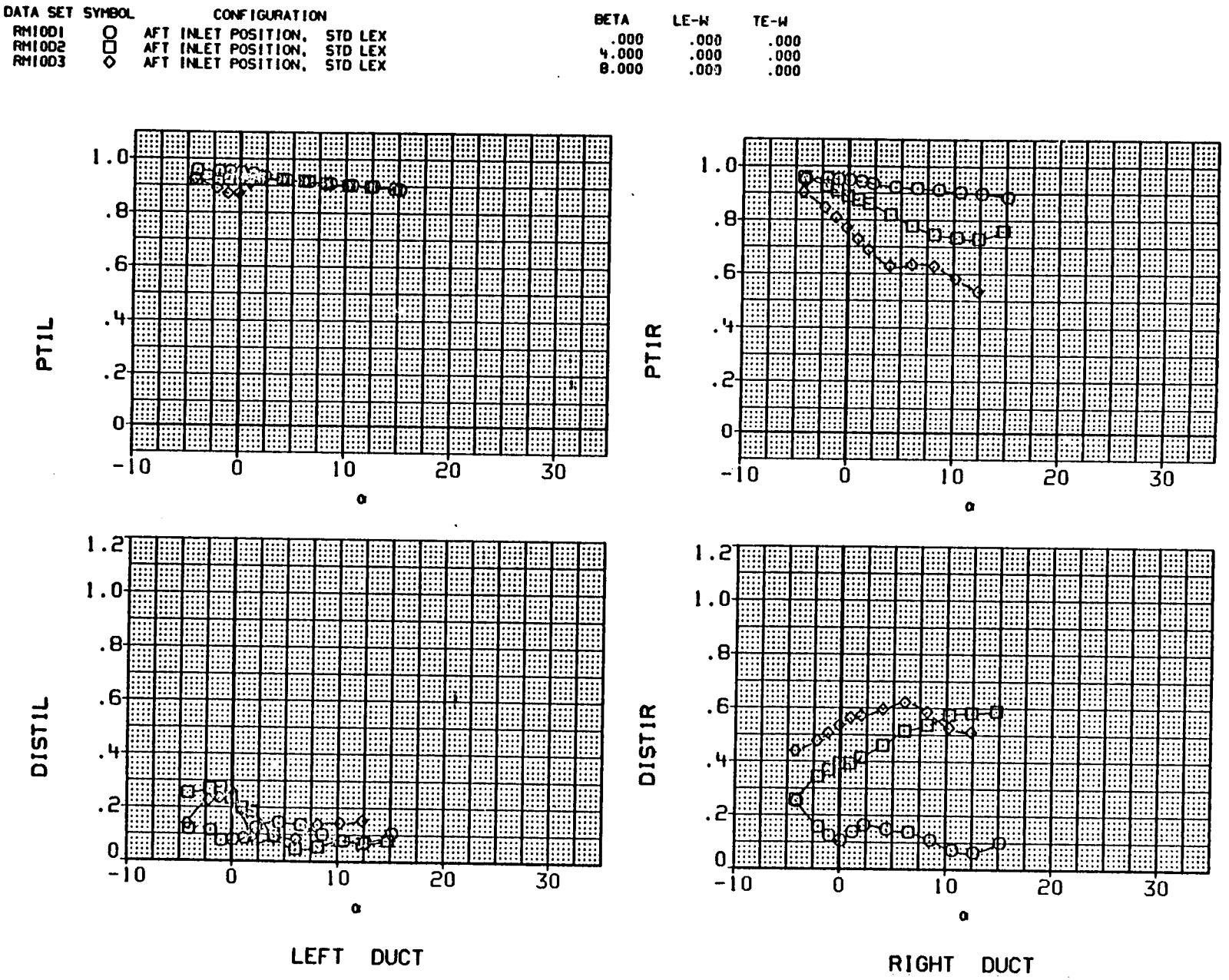

(e) Mach = 1.60.

Figure 12.- Continued.

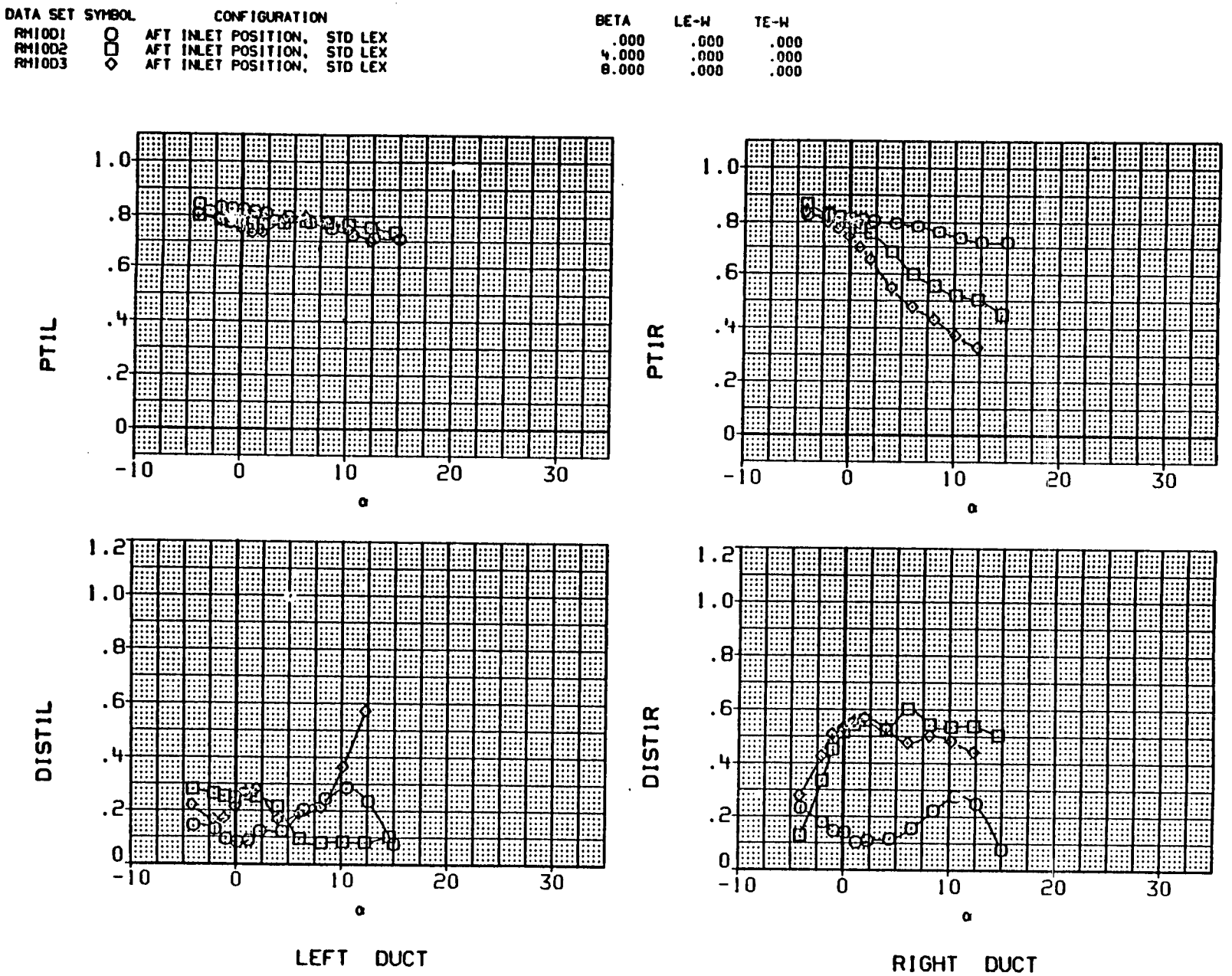

(f) Mach = 2.00.

Figure 12.- Continued.

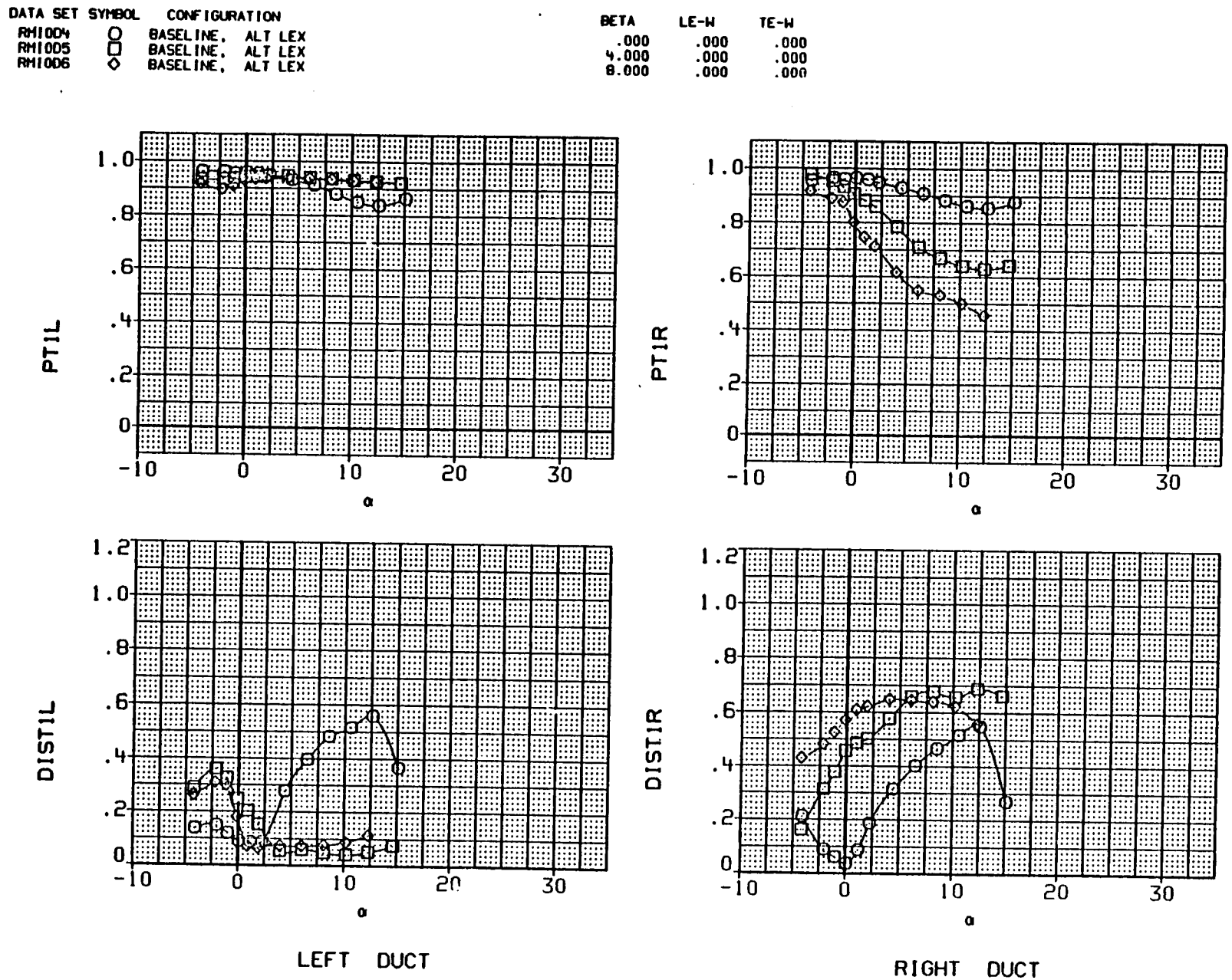

(g) Mach = 1.60.

Figure 12.- Continued.

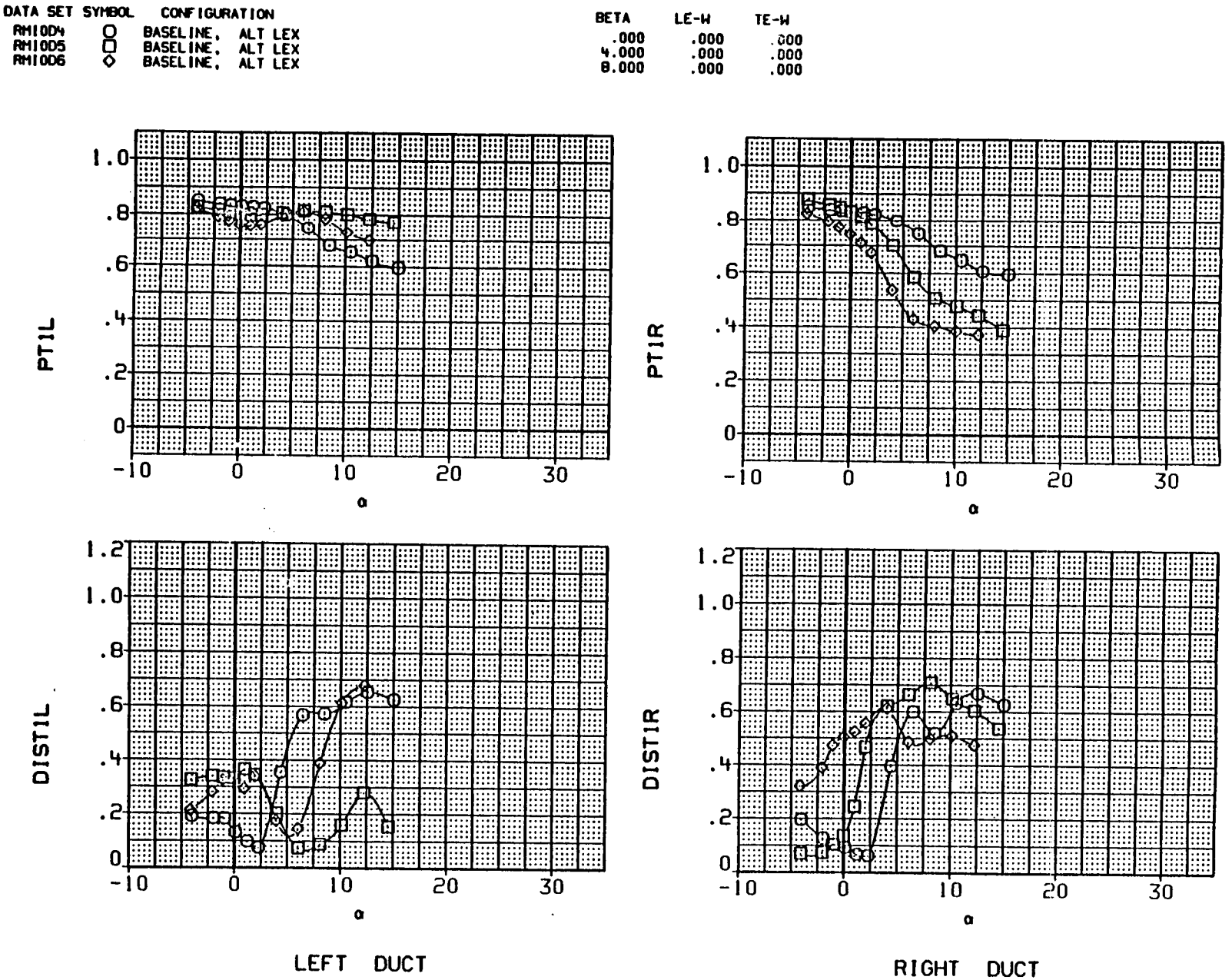

(h) Mach = 2.00.

Figure 12.- Continued.

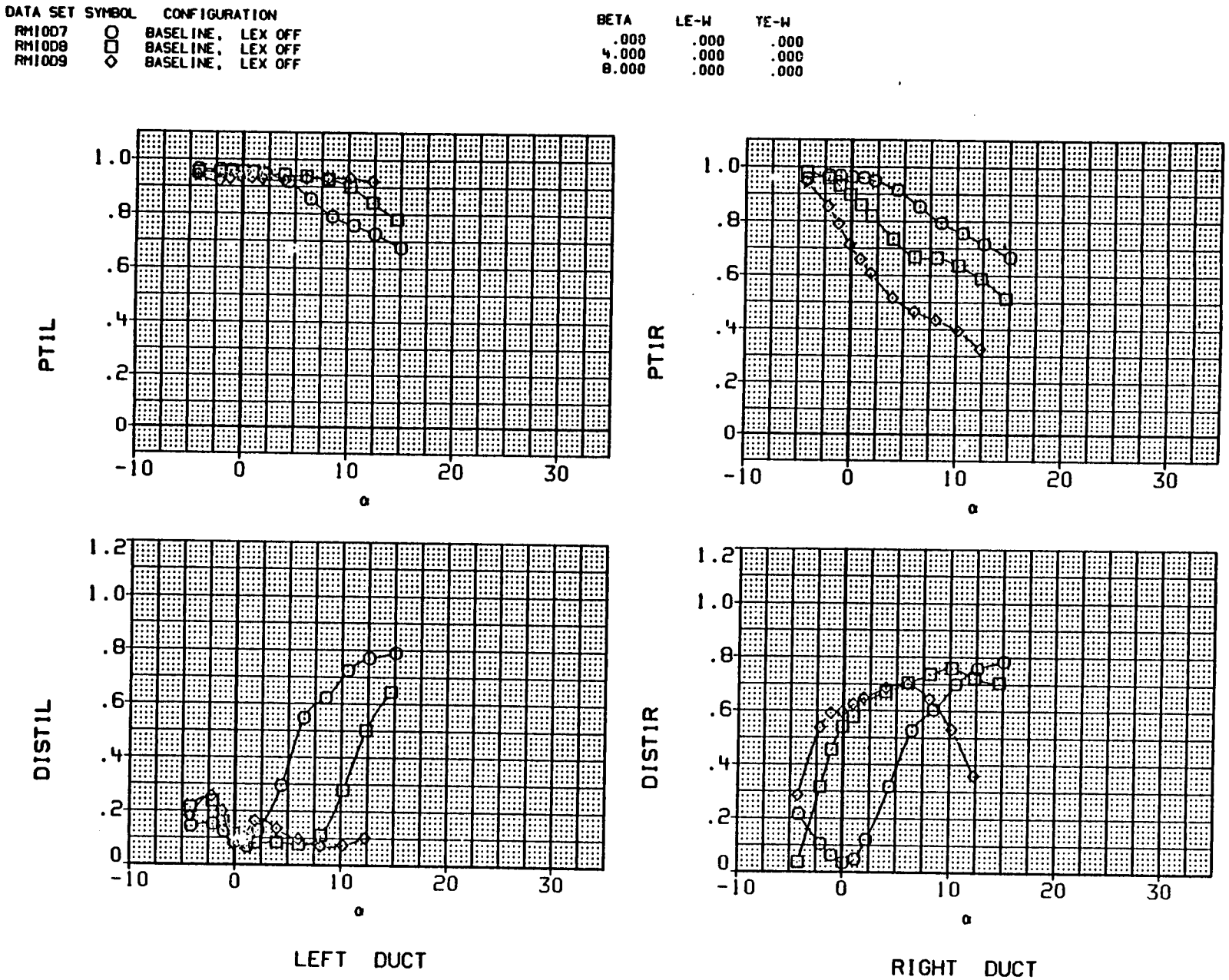

(i) Mach = 1.60.

Figure 12.- Continued.

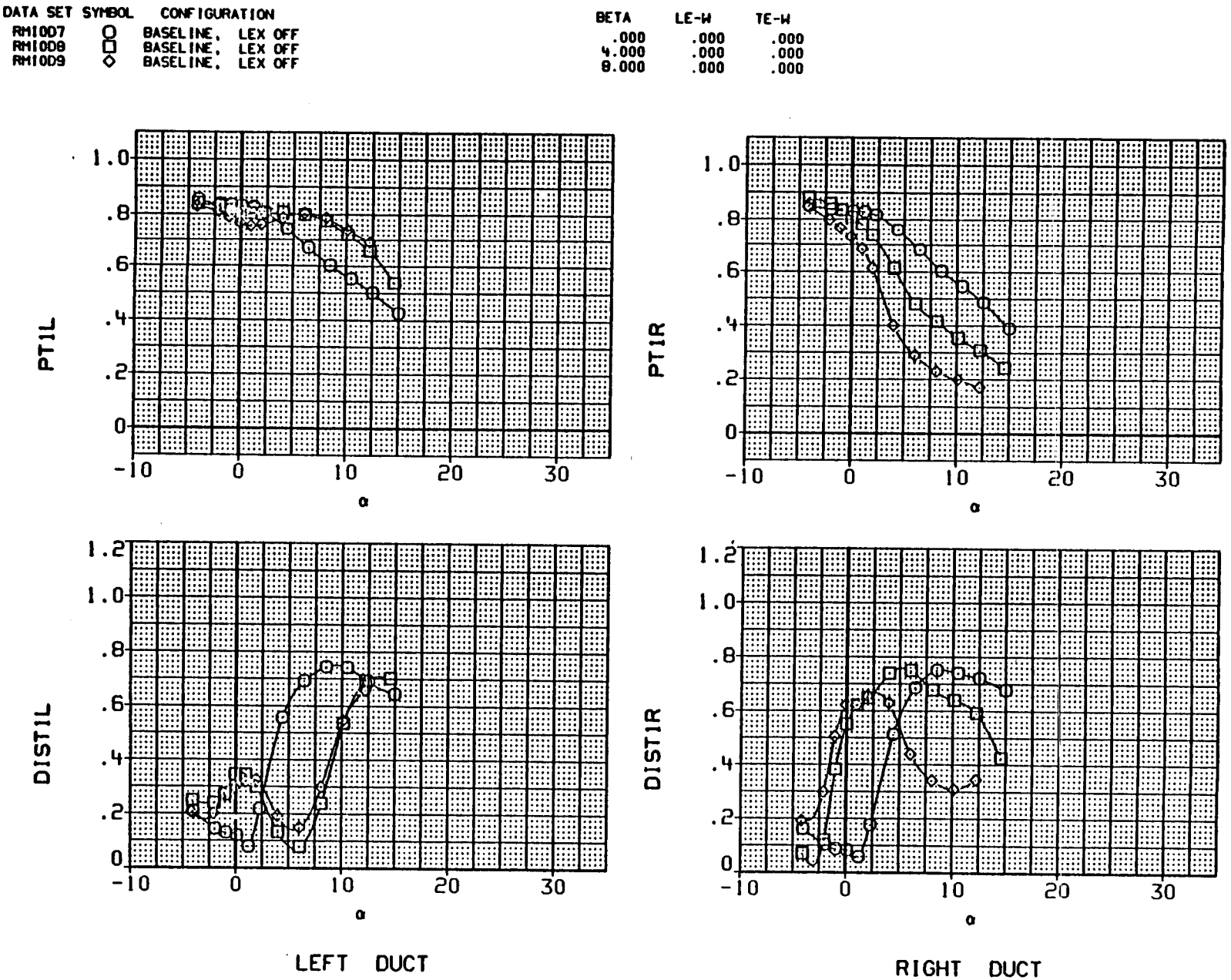

(j) Mach = 2.00.

Figure 12.- Continued.

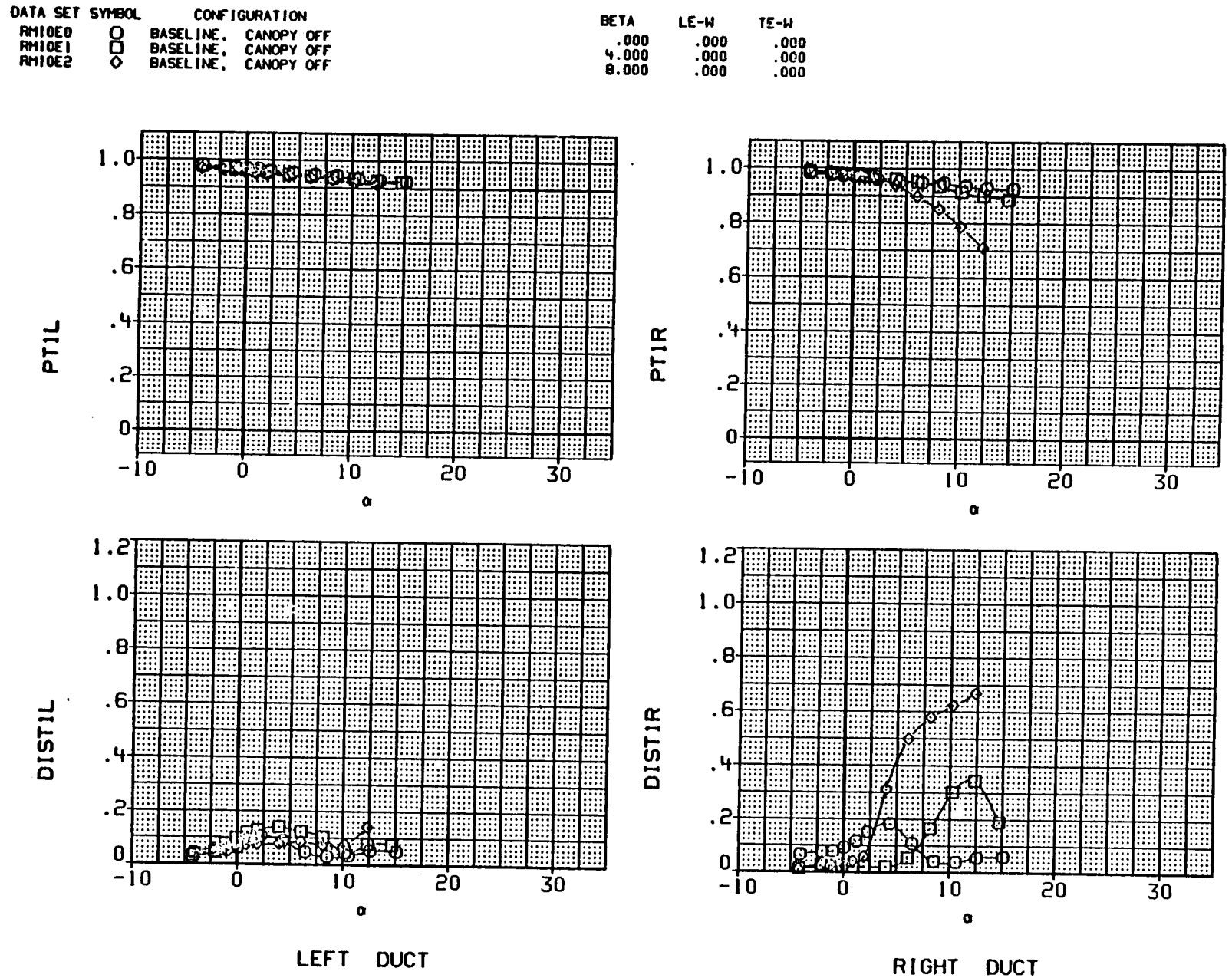

(k) Mach = 1.60.

Figure 12.- Continued.

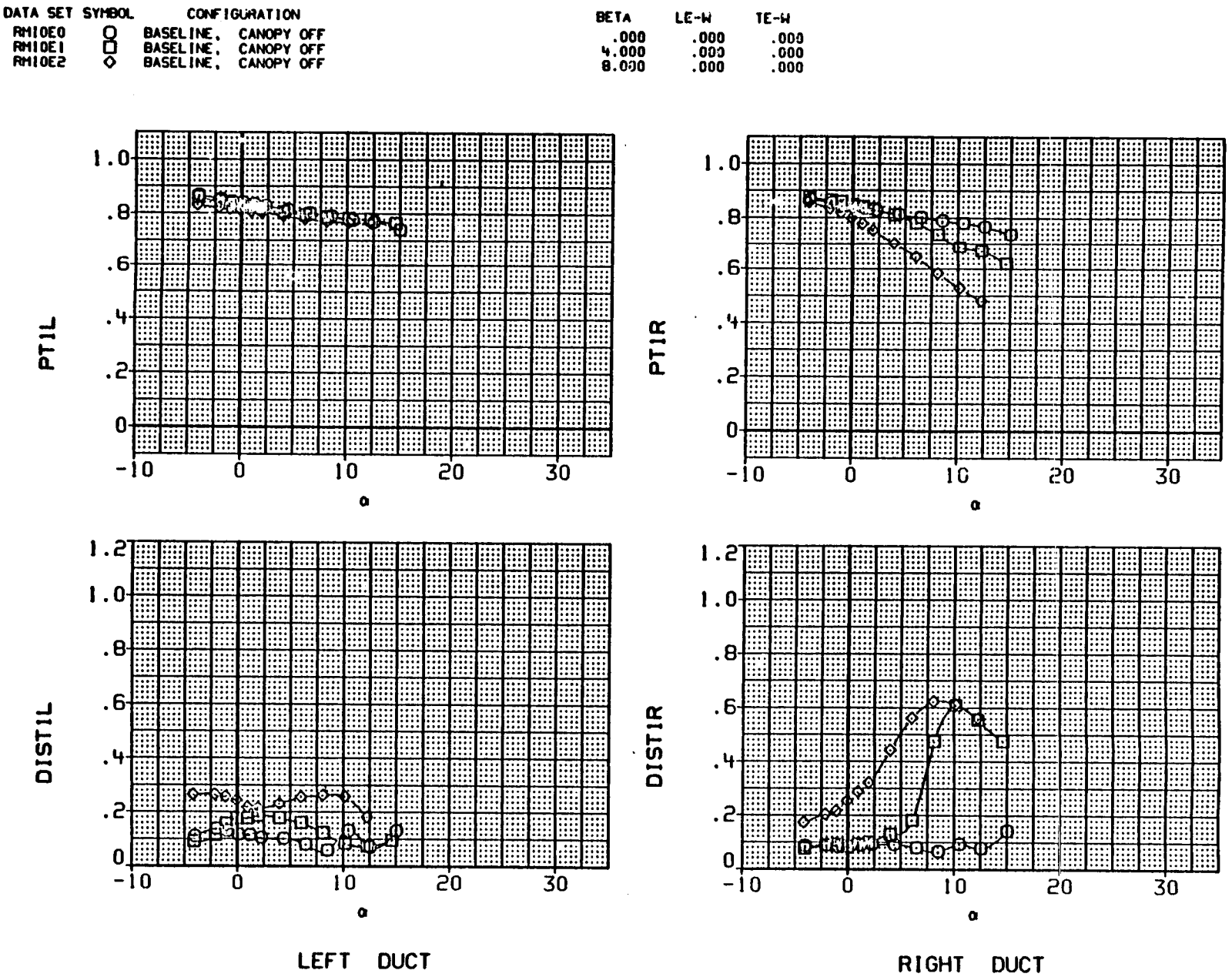

(1) Mach = 2.00.

Figure 12.- Continued.

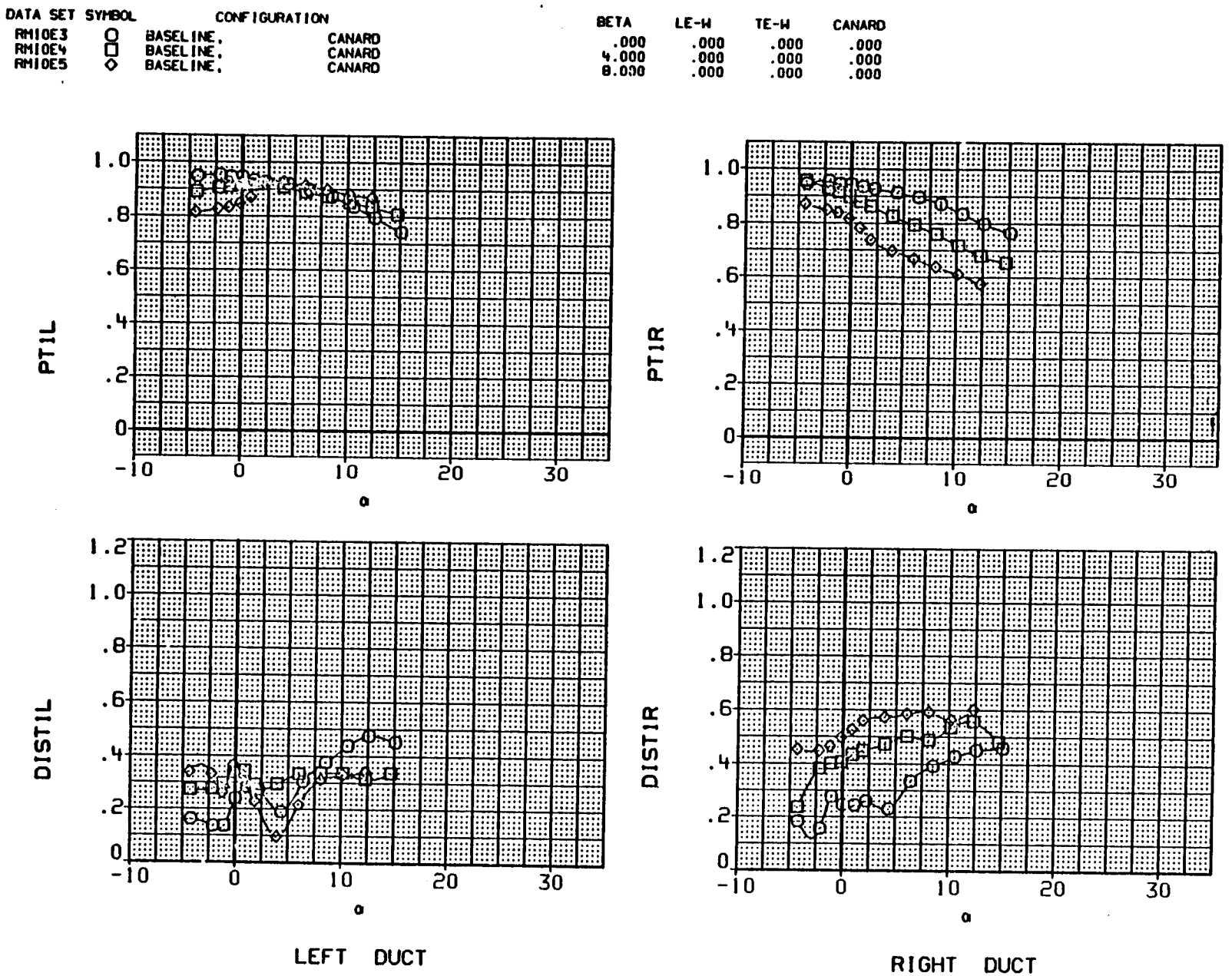

(m) Mach = 1.60.

Figure 12.- Continued.

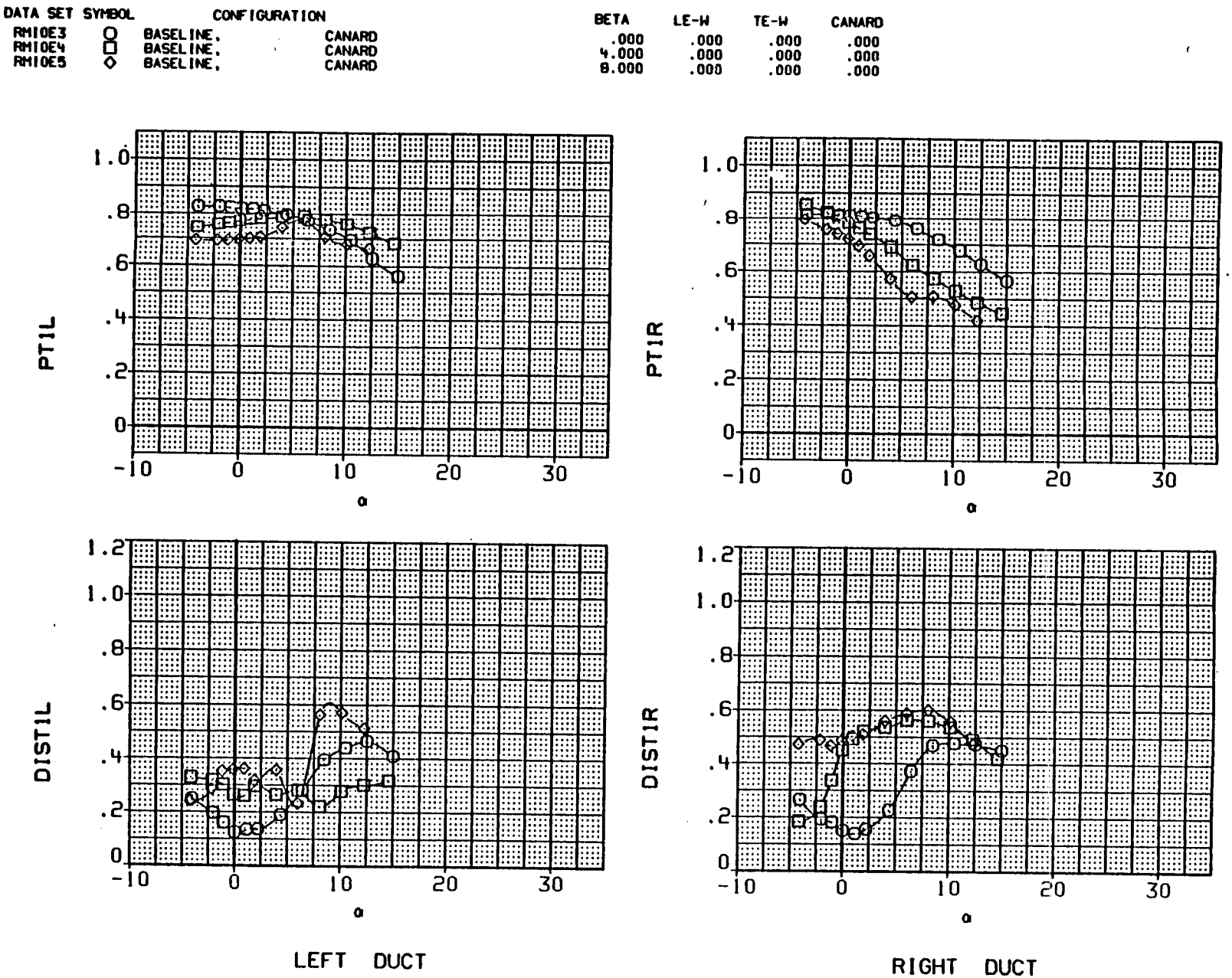

(n) Mach = 2.00.

Figure 12.- Continued.

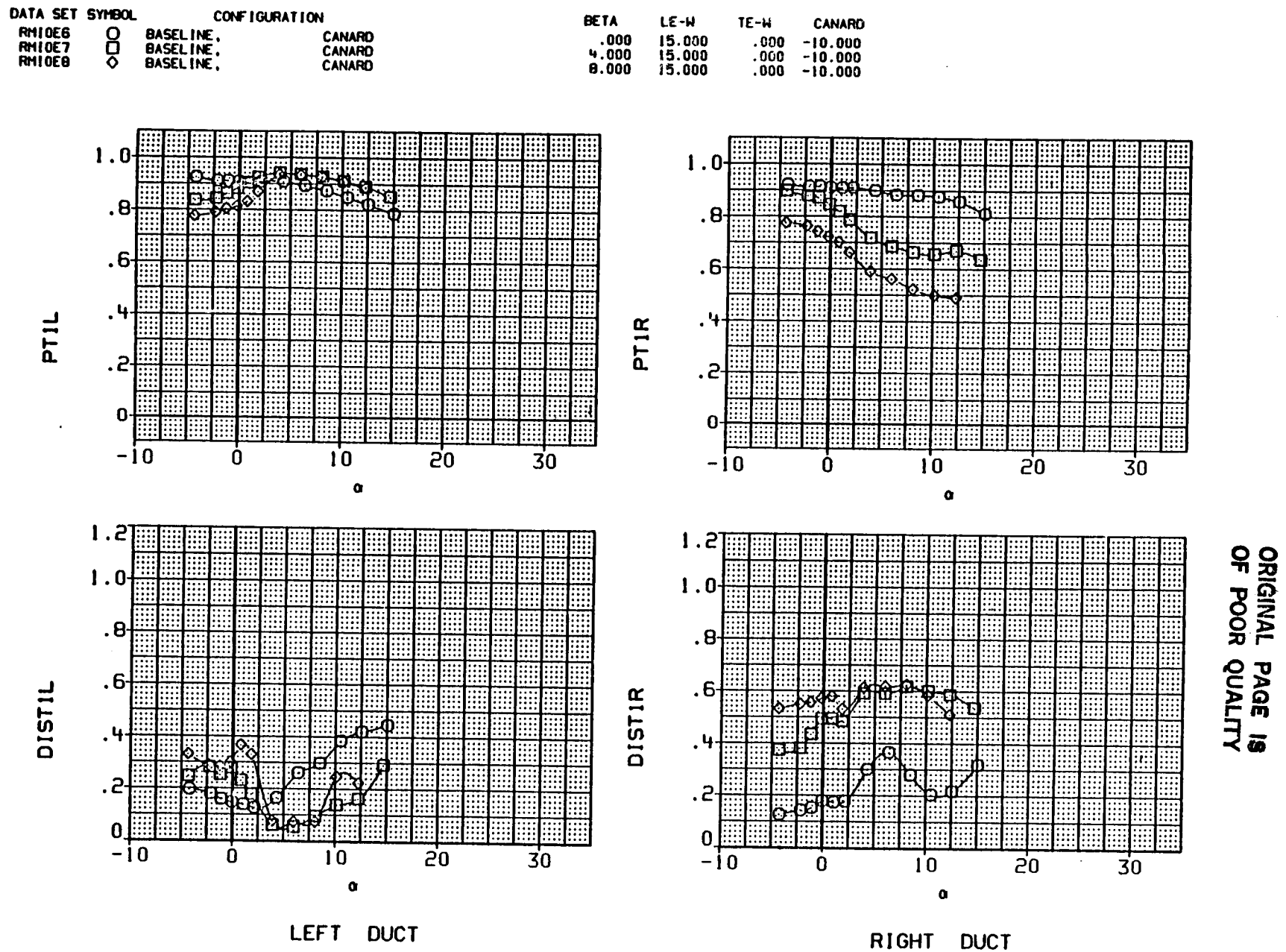

(o) Mach = 1.60.

Figure 12.- Continued.

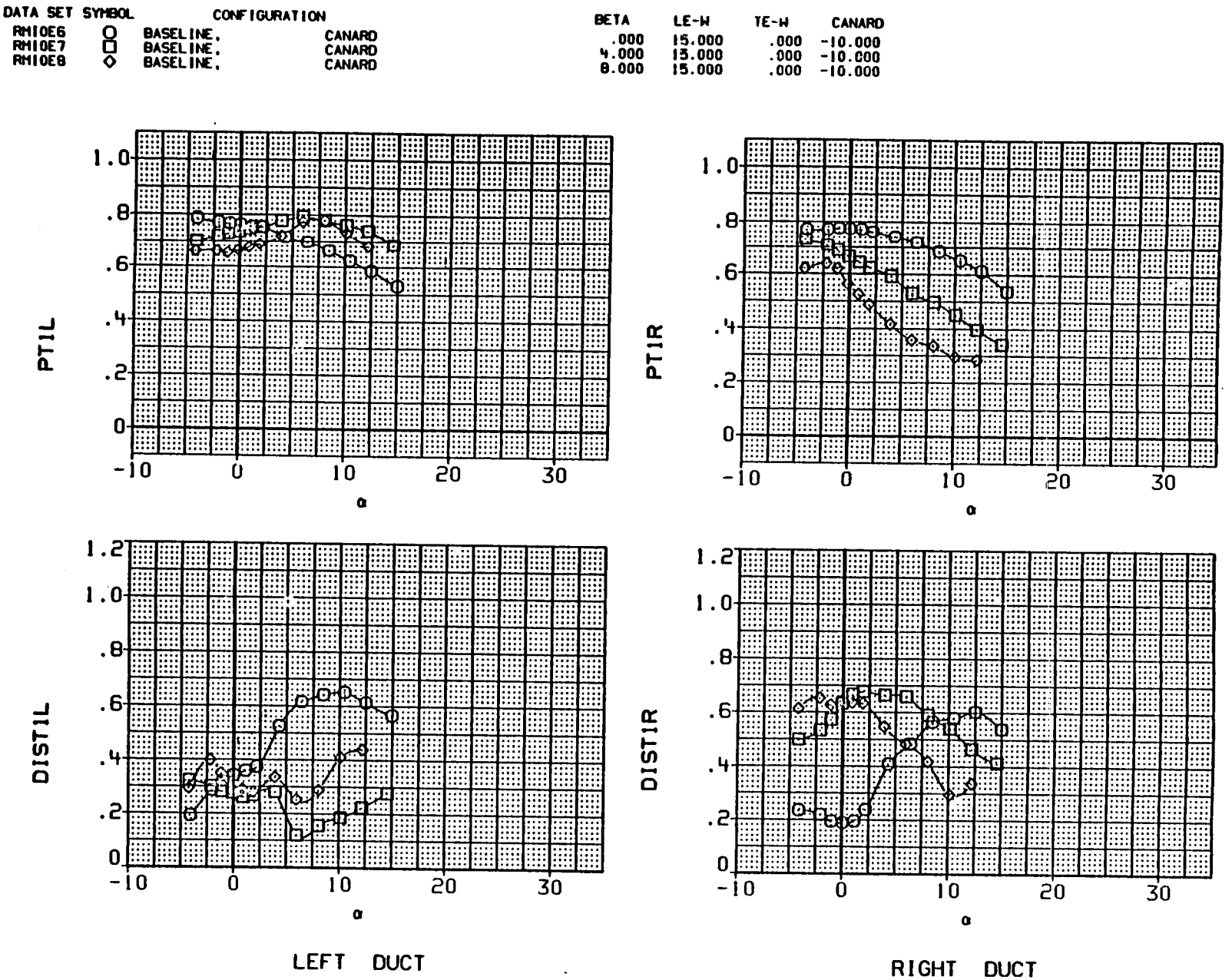

(p) Mach = 2.00.

Figure 12.- Concluded.

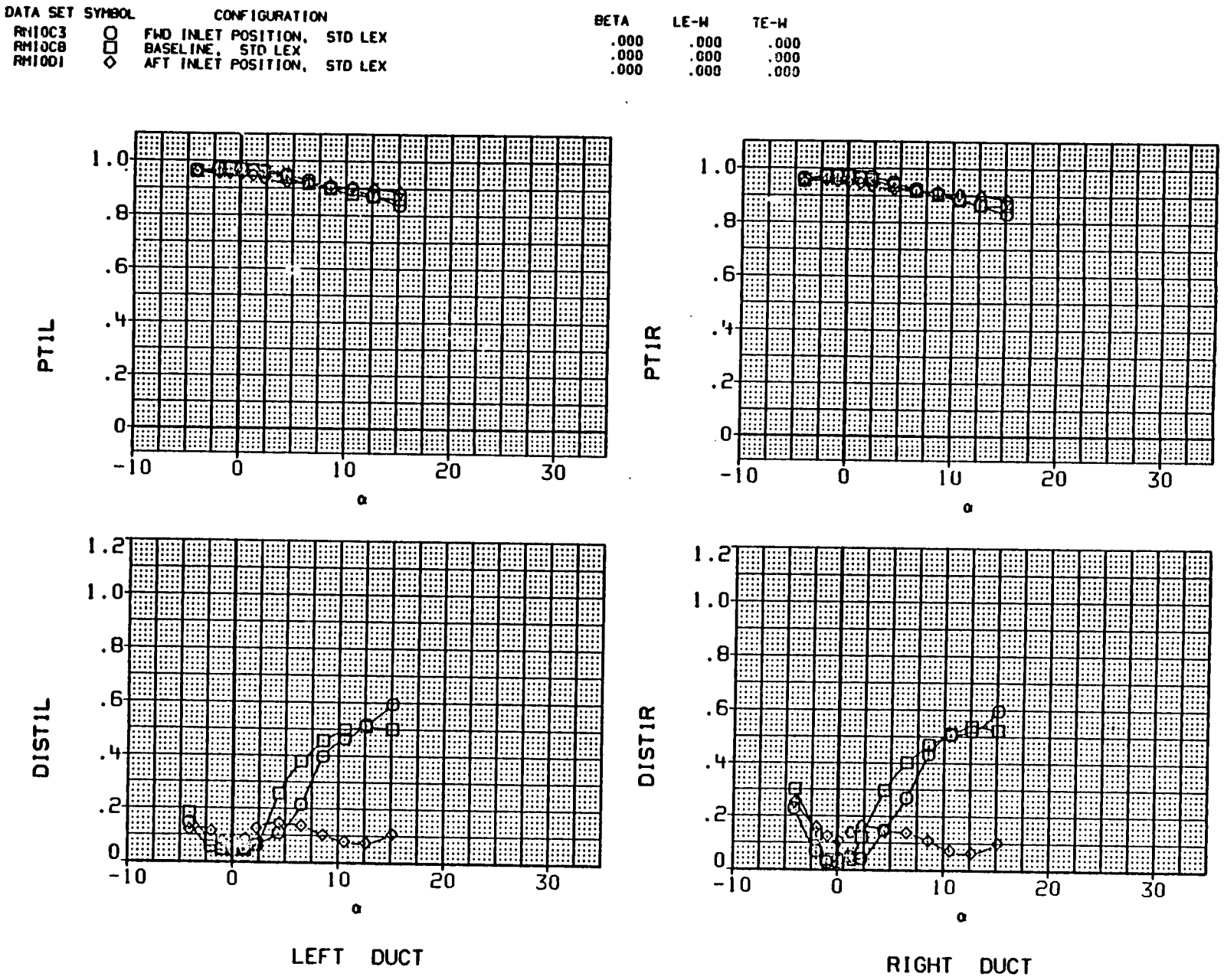

(a) Mach = 1.60.

Figure 13.- Effect of model configuration on performance at the ramp rake station.

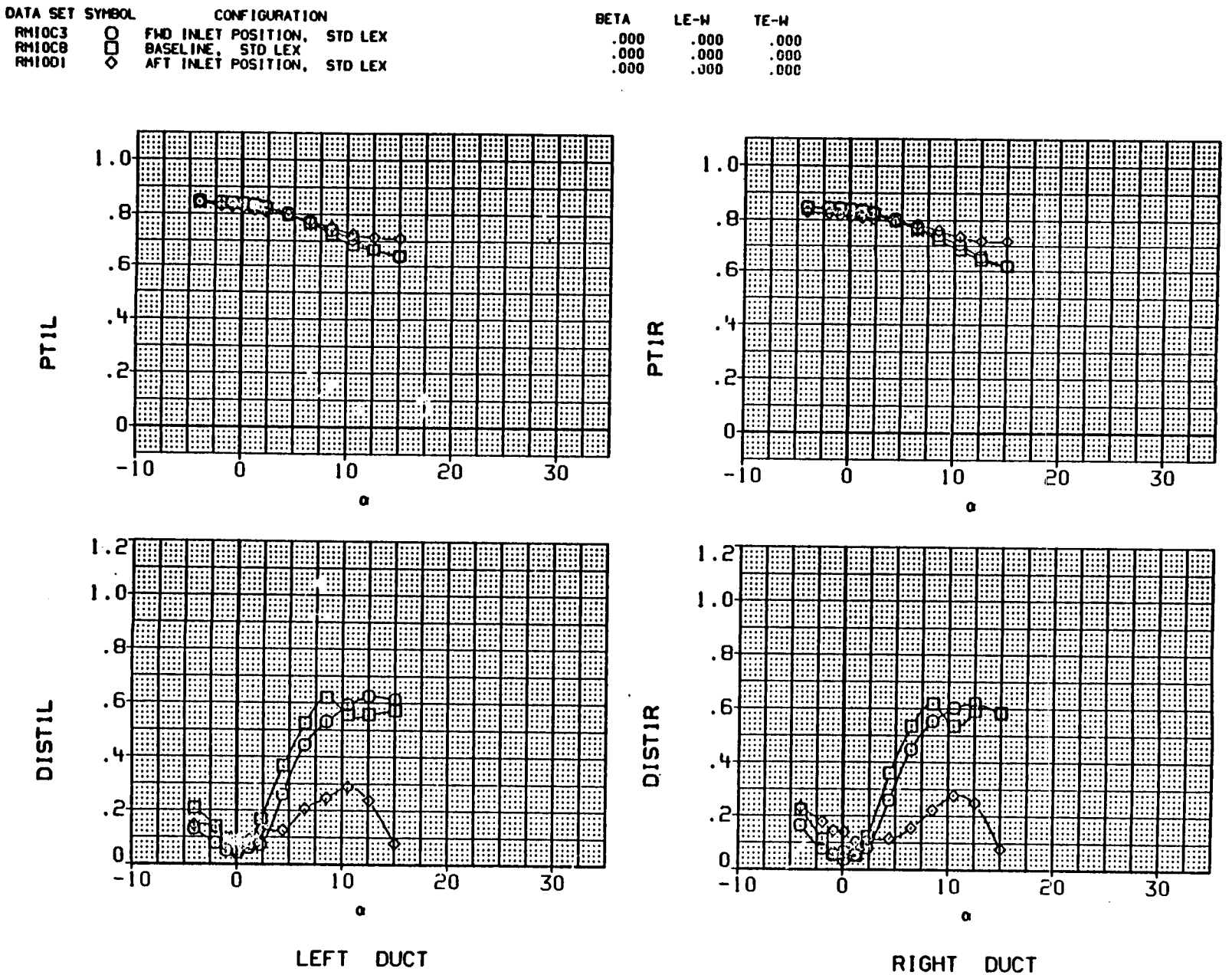

(b) Mach = 2.00.

Figure 13.- Continued.

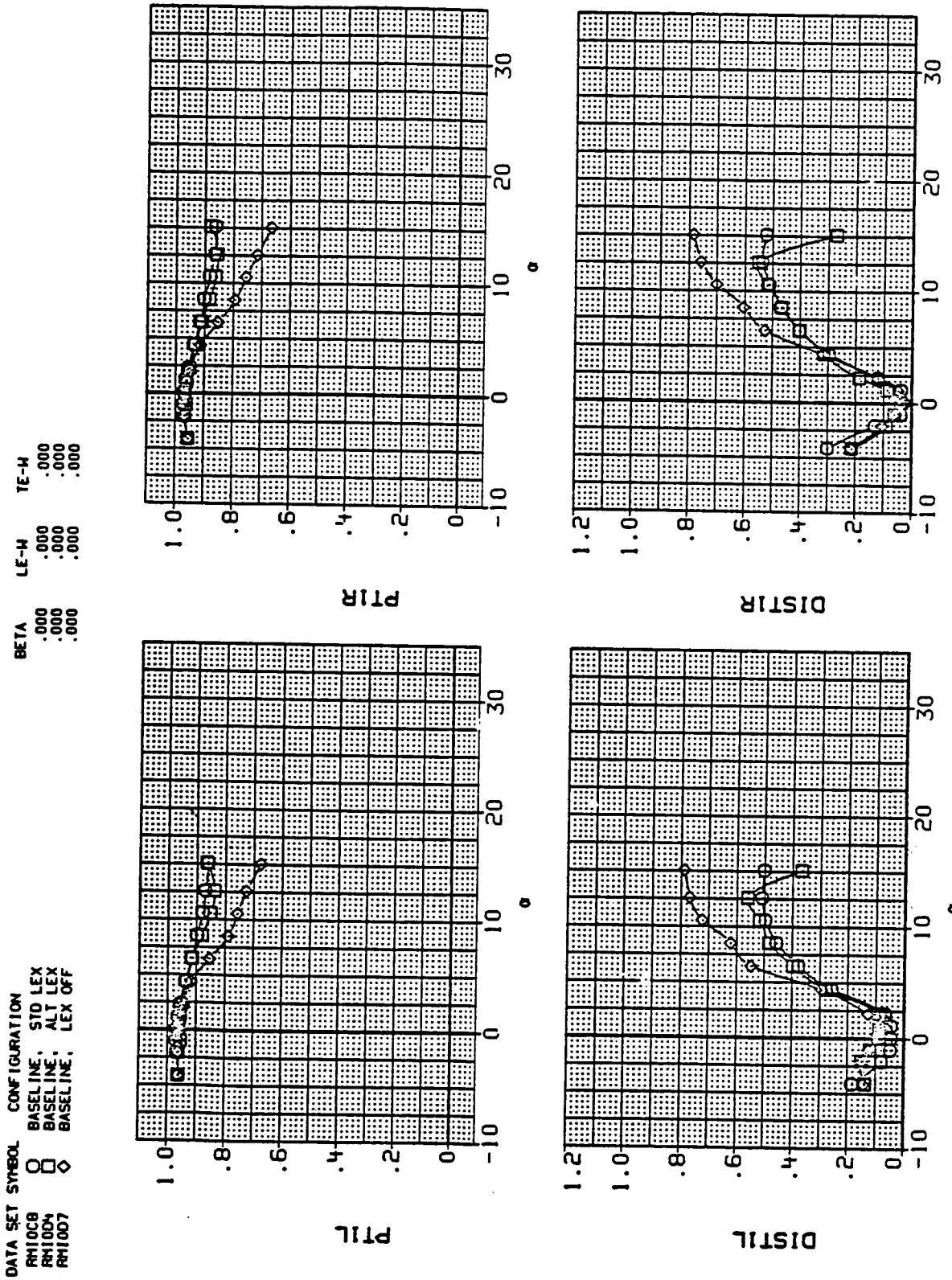

(c) Mach = 1.60.

Figure 13.- Continued.

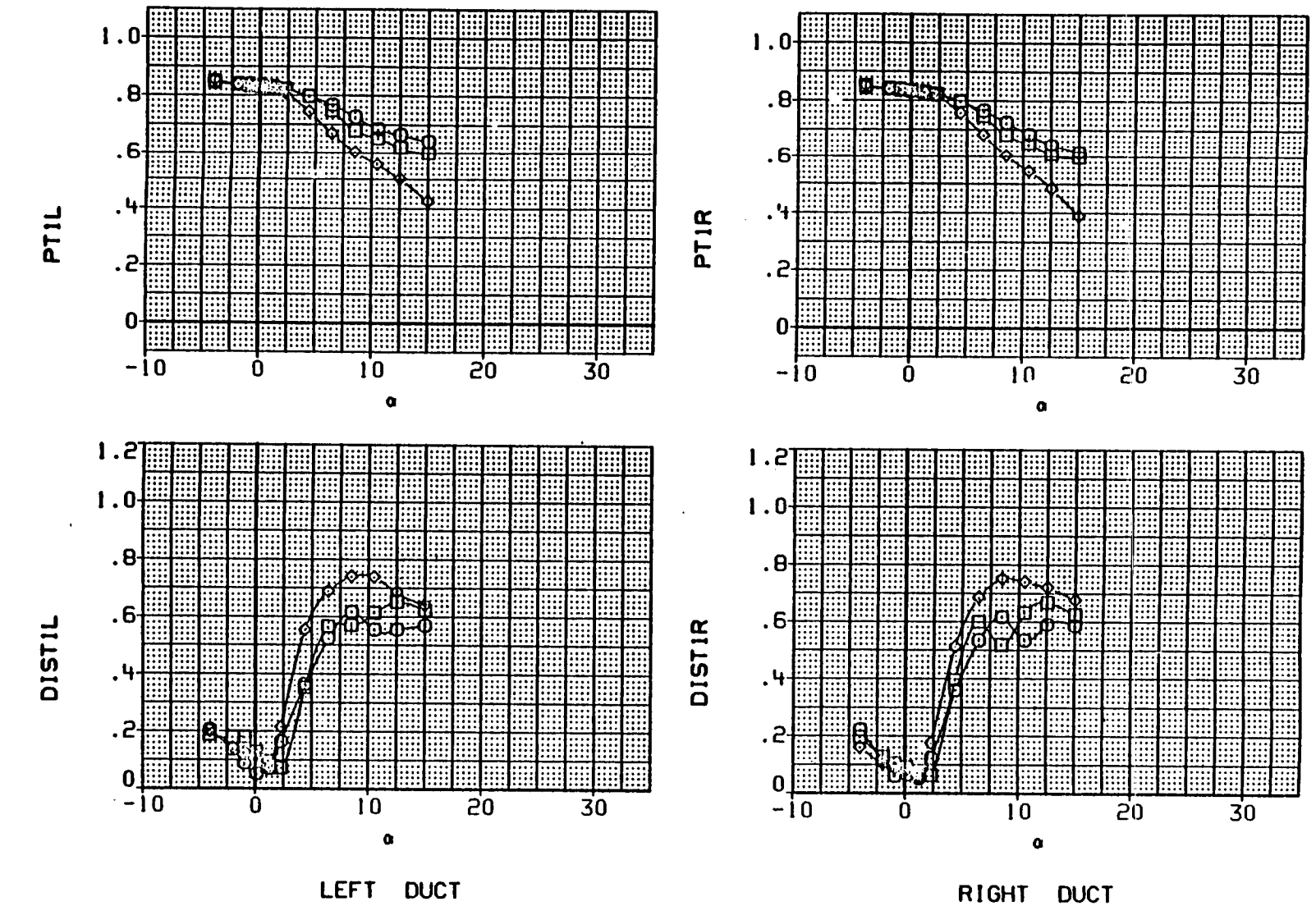

(d) Mach = 2.00.

Figure 13.- Continued.

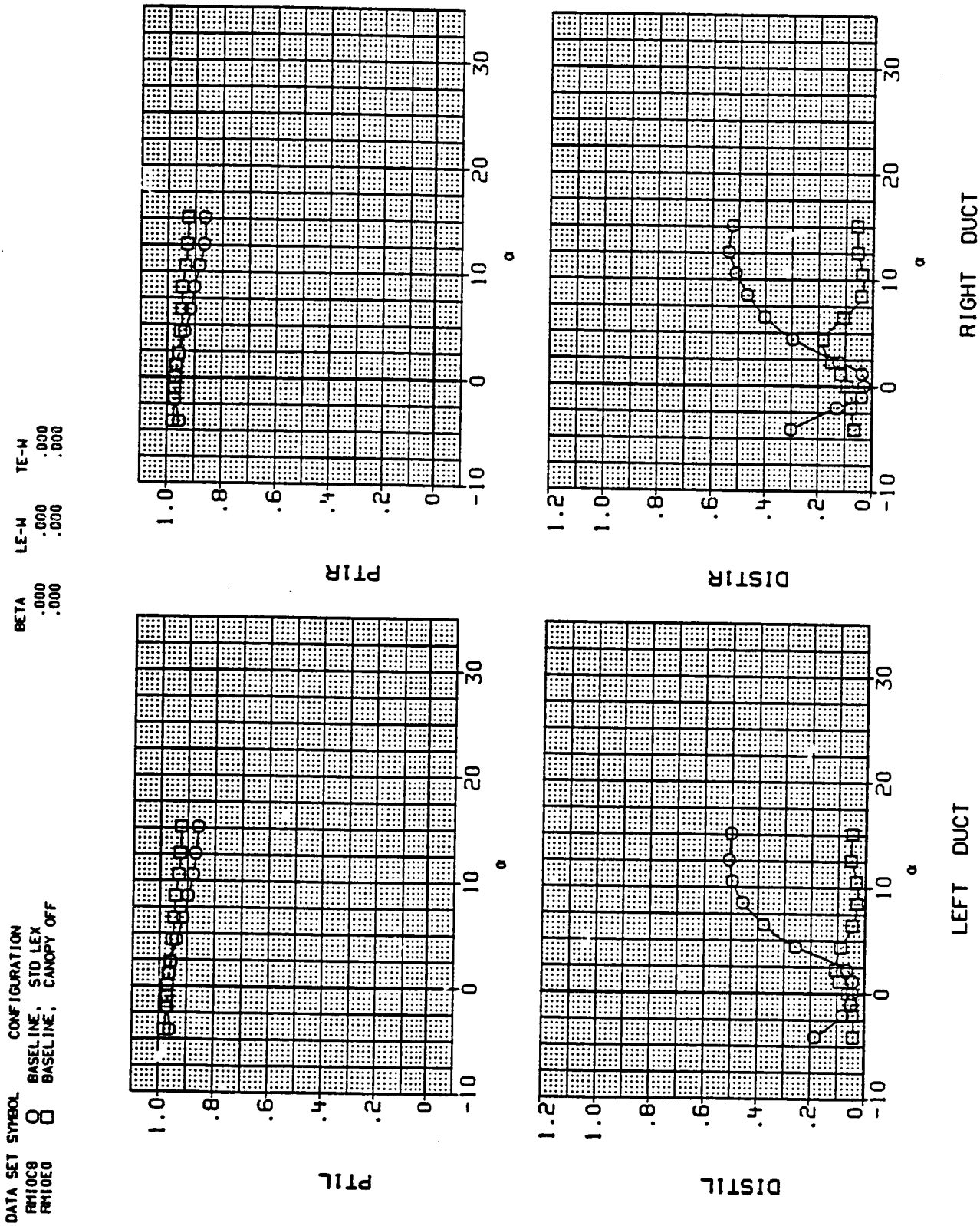

(e) Mach = 1.60.

Figure 13.- Continued.

C-3

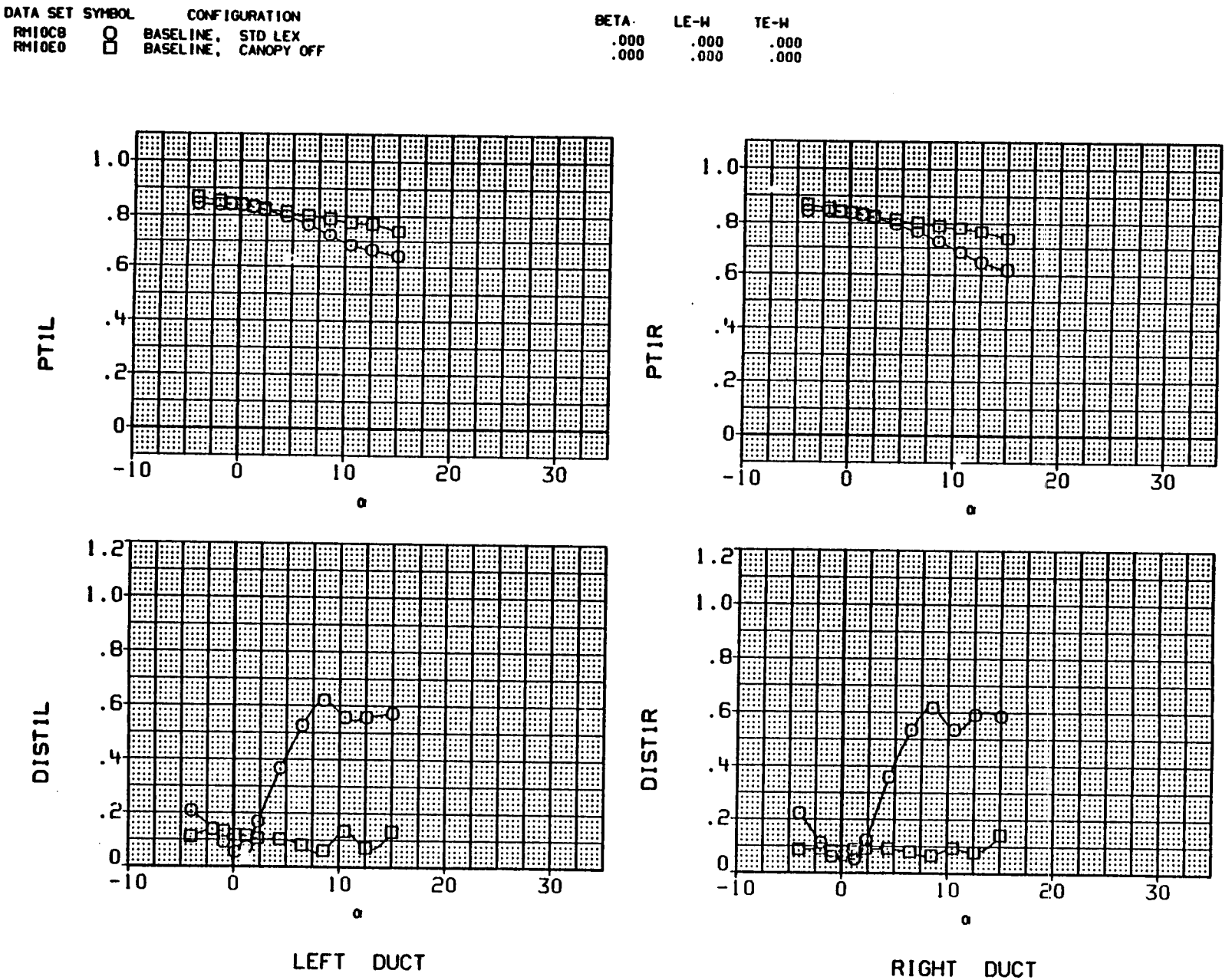

(f) Mach = 2.00.

Figure 13.- Continued.

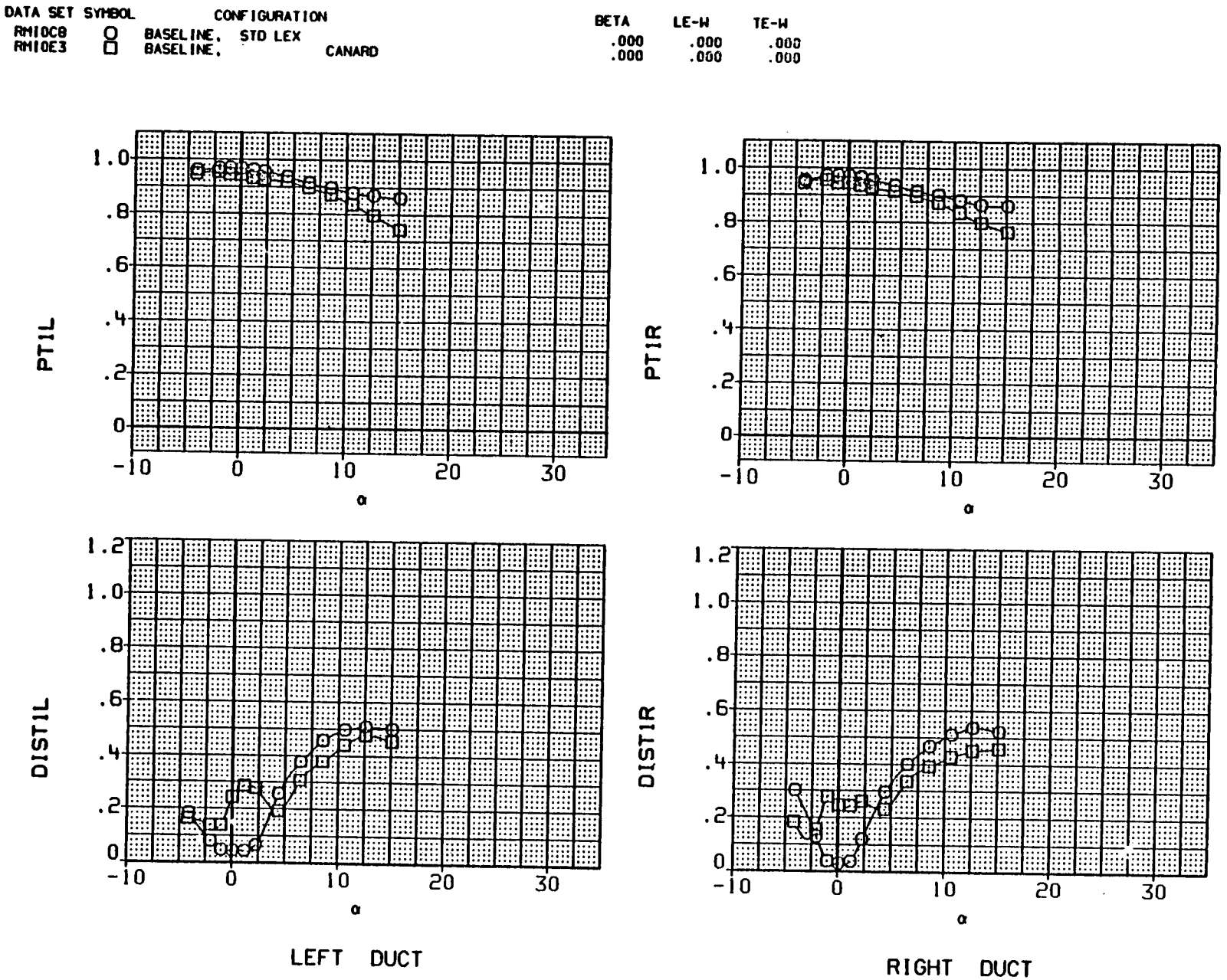

(g) Mach = 1.60.

Figure 13.- Continued.

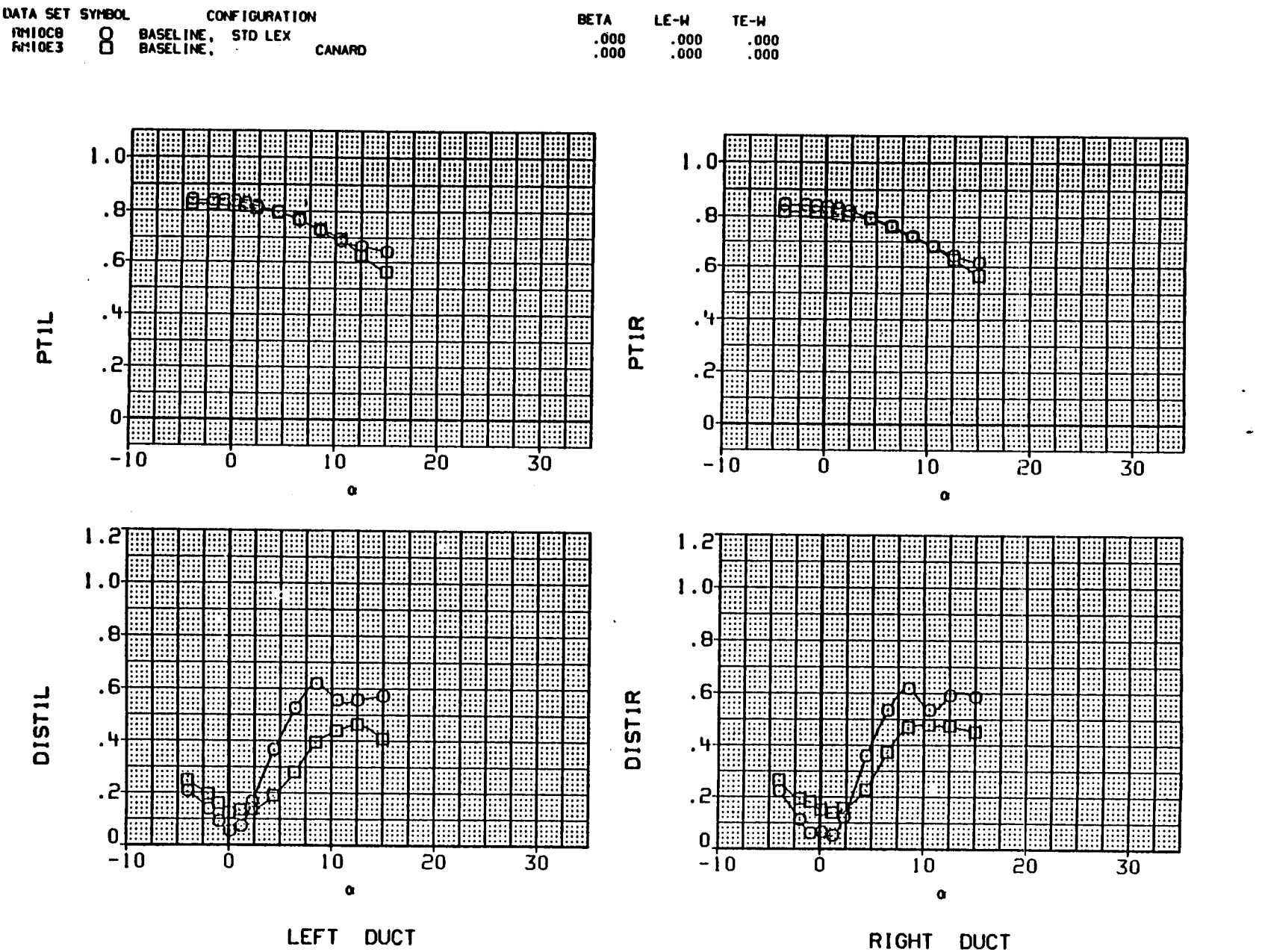

(h) Mach = 2.00.

Figure 13.- Continued.

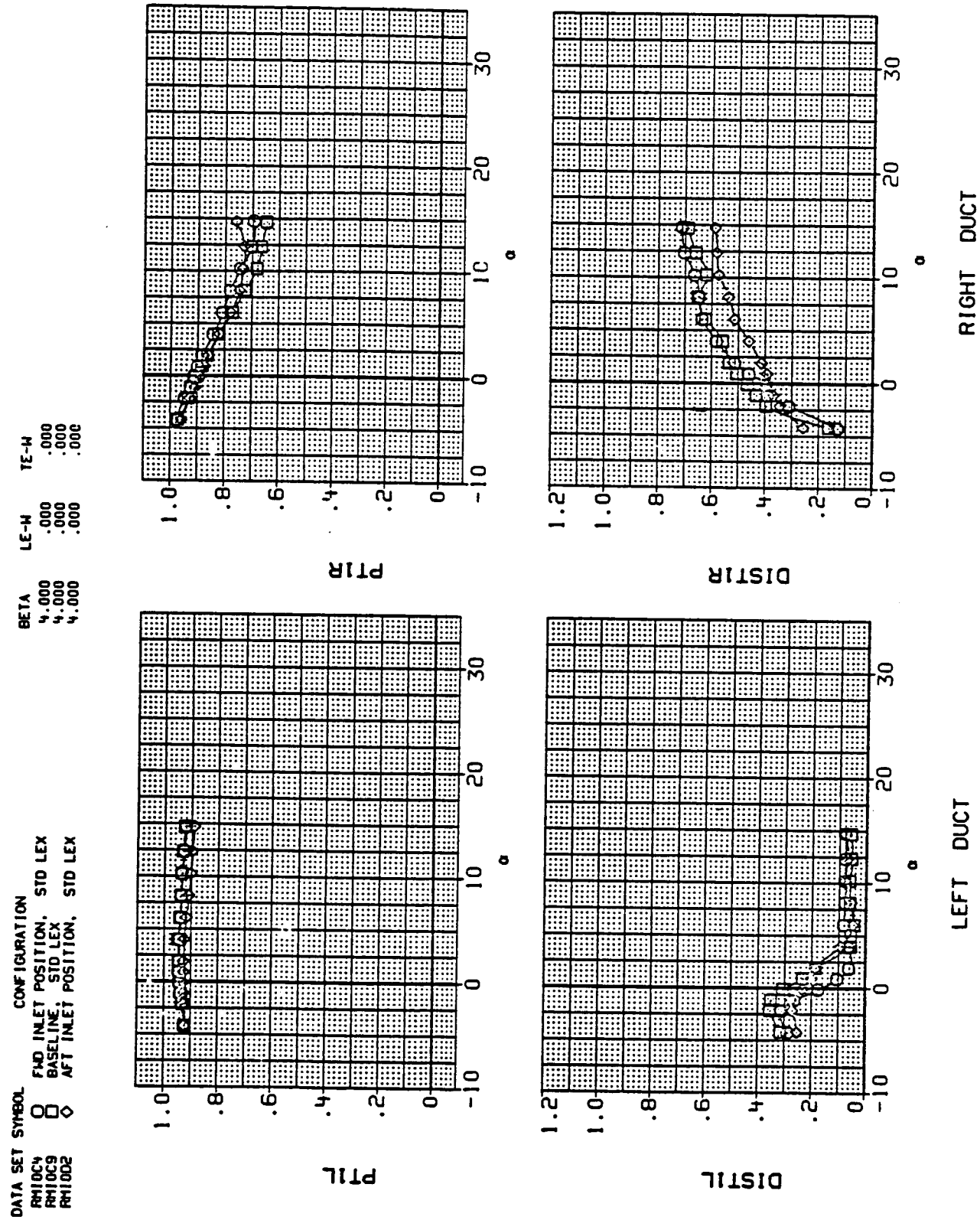

(i) Mach = 1.60.

Figure 13.- Continued.

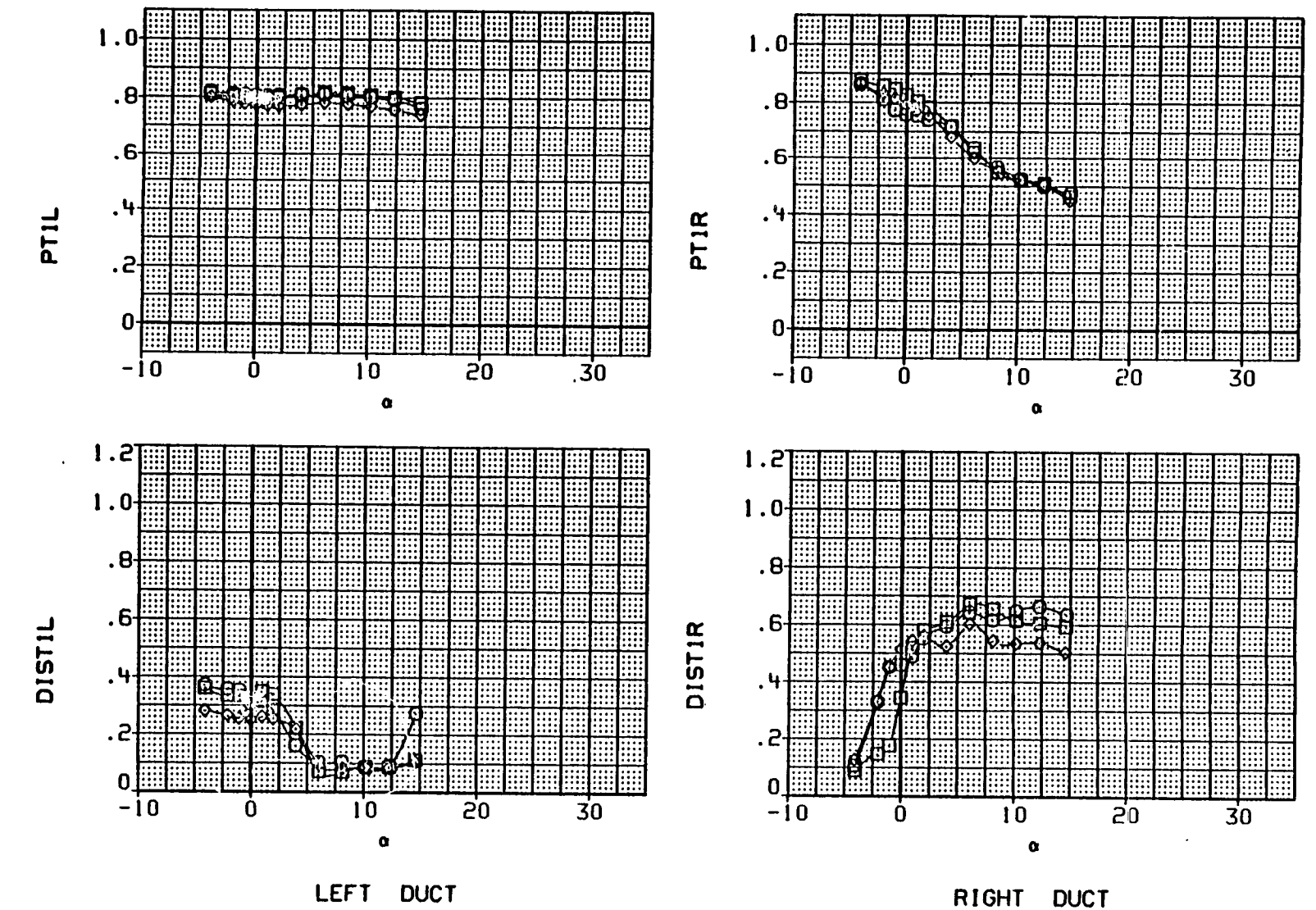

(j) Mach = 2.00.

Figure 13.- Continued.

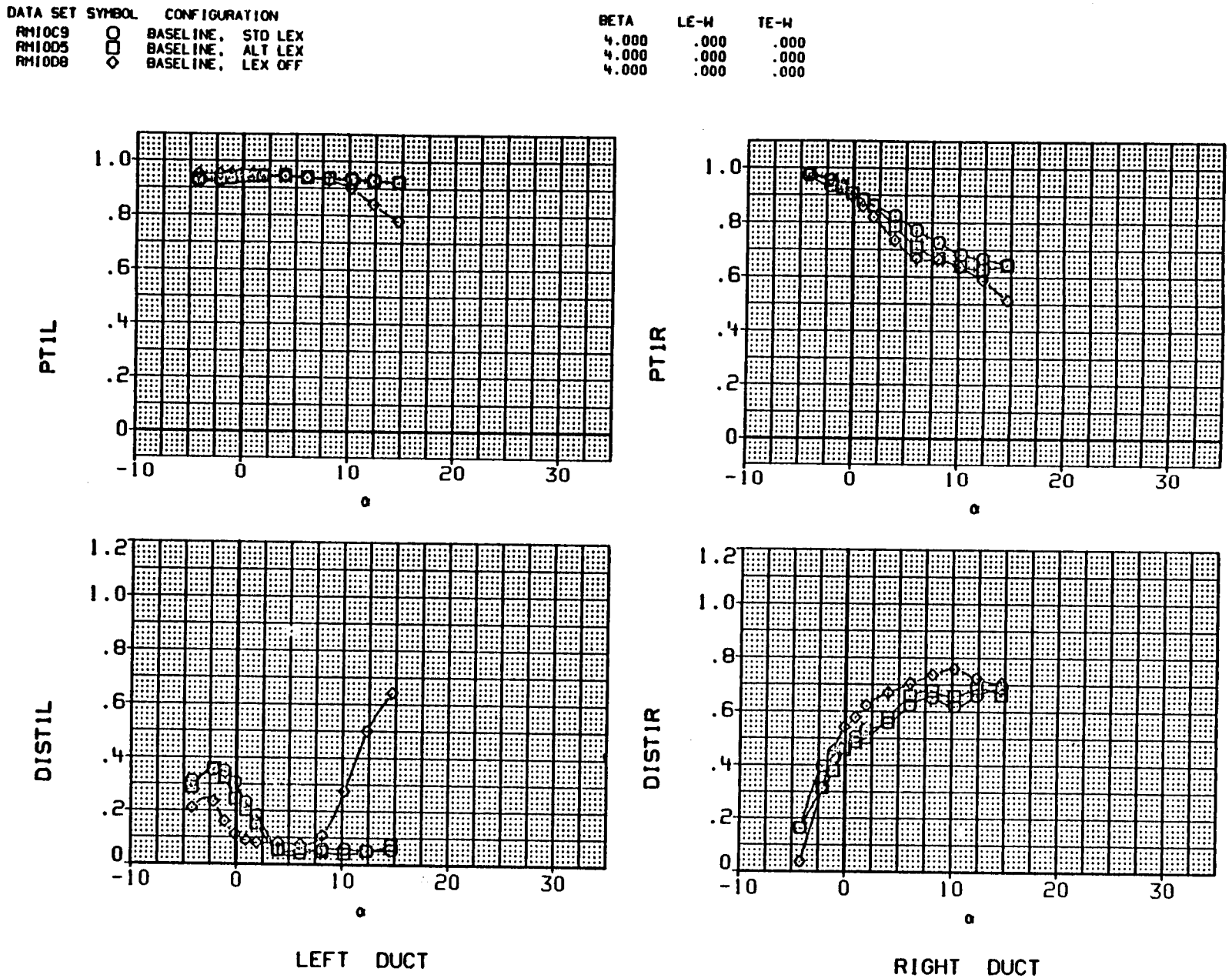

(k) Mach = 1.60.

Figure 13.- Continued.

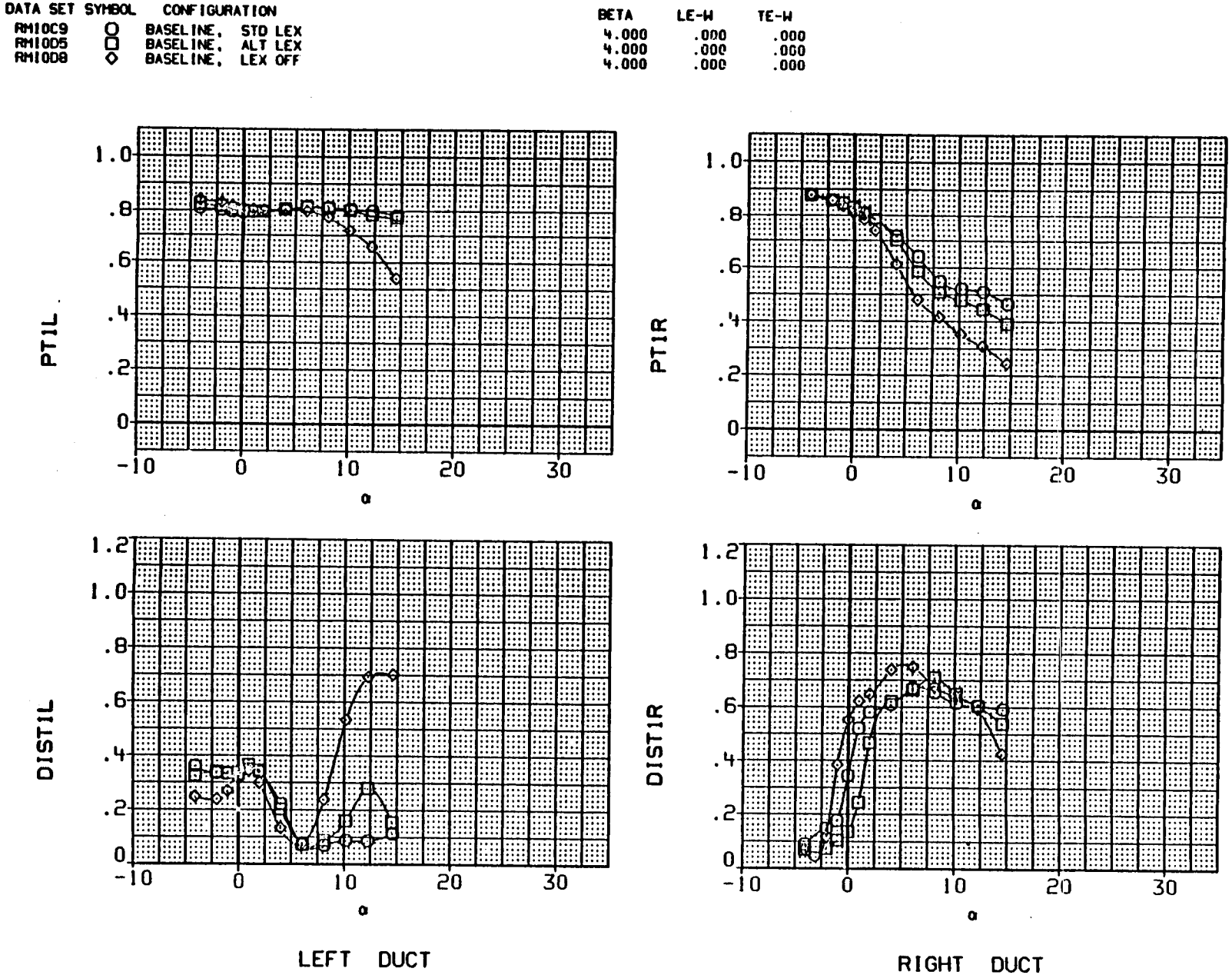

(1) Mach = 2.00.

Figure 13.- Continued.

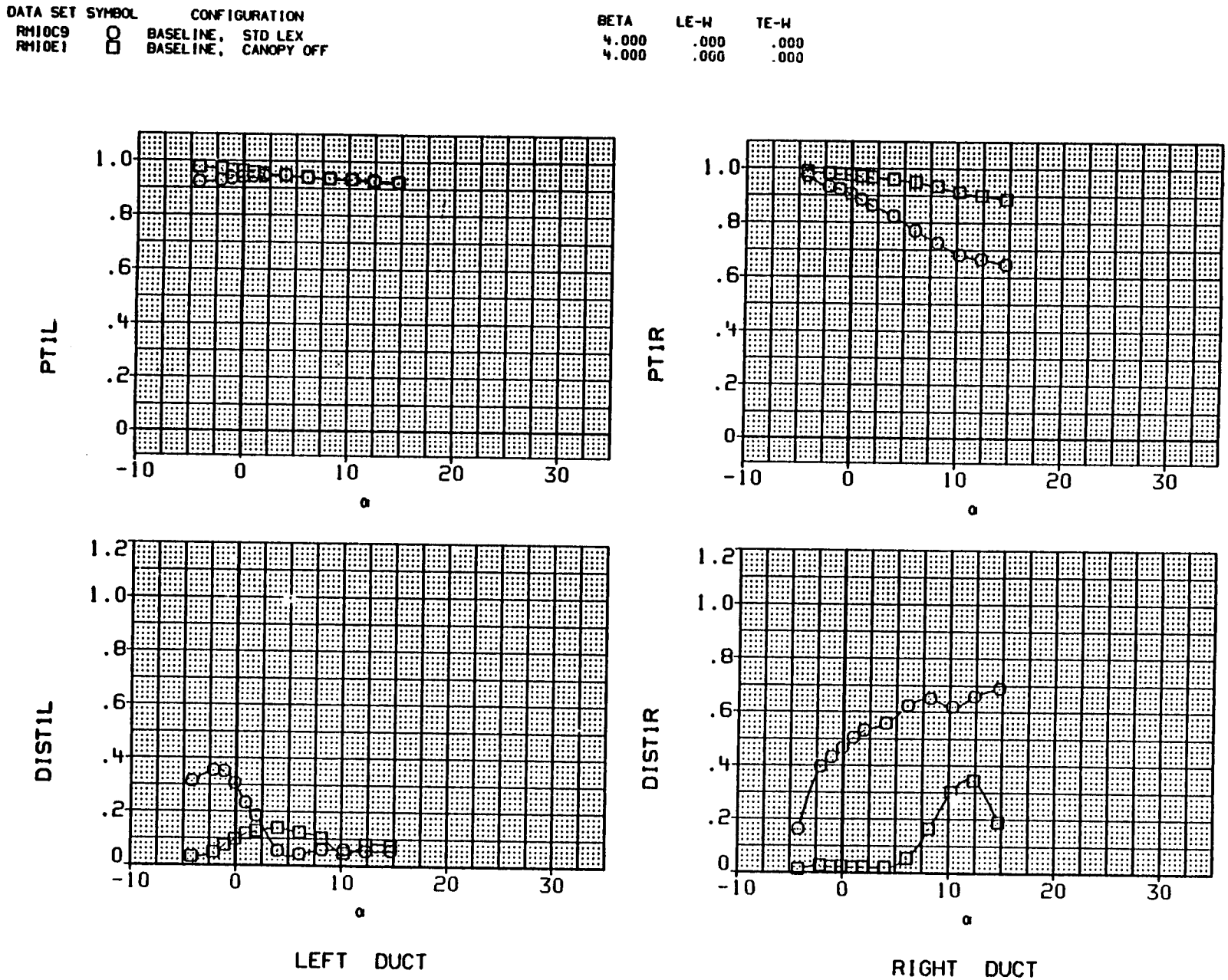

(m) Mach = 1.60.

Figure 13.- Continued.

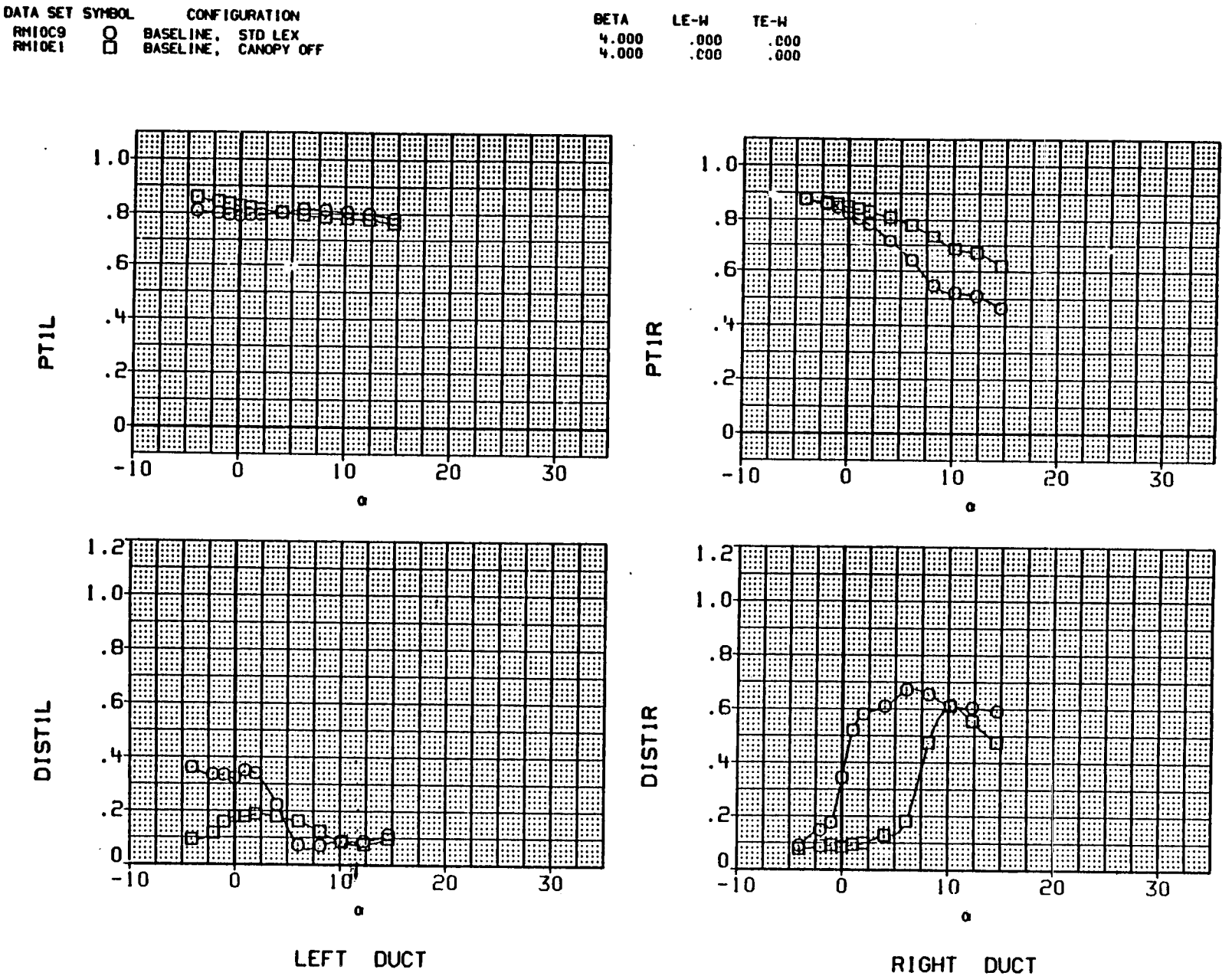

(n) Mach = 2.00.

Figure 13.- Continued.

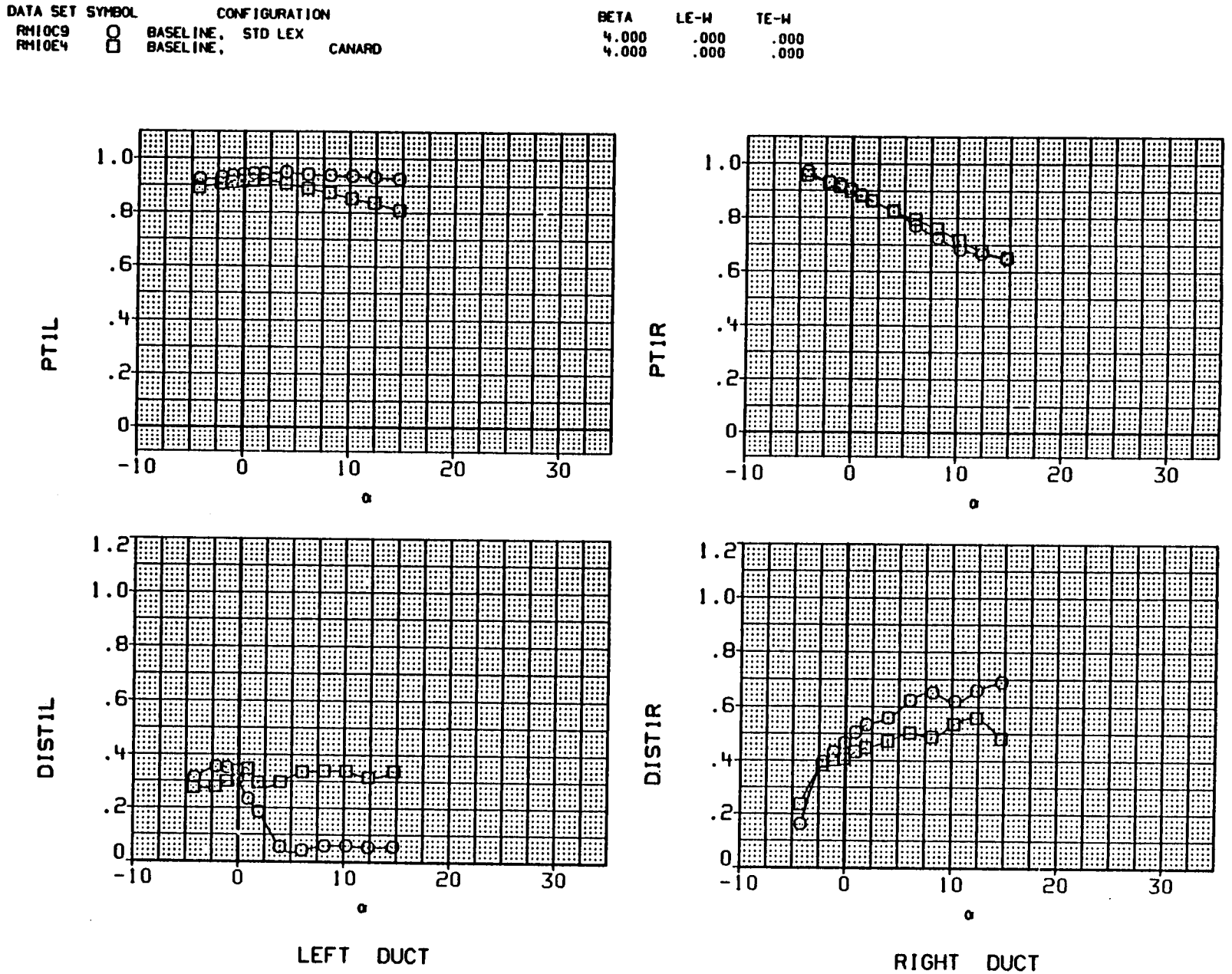

(o) Mach = 1.60.

Figure 13.- Continued.

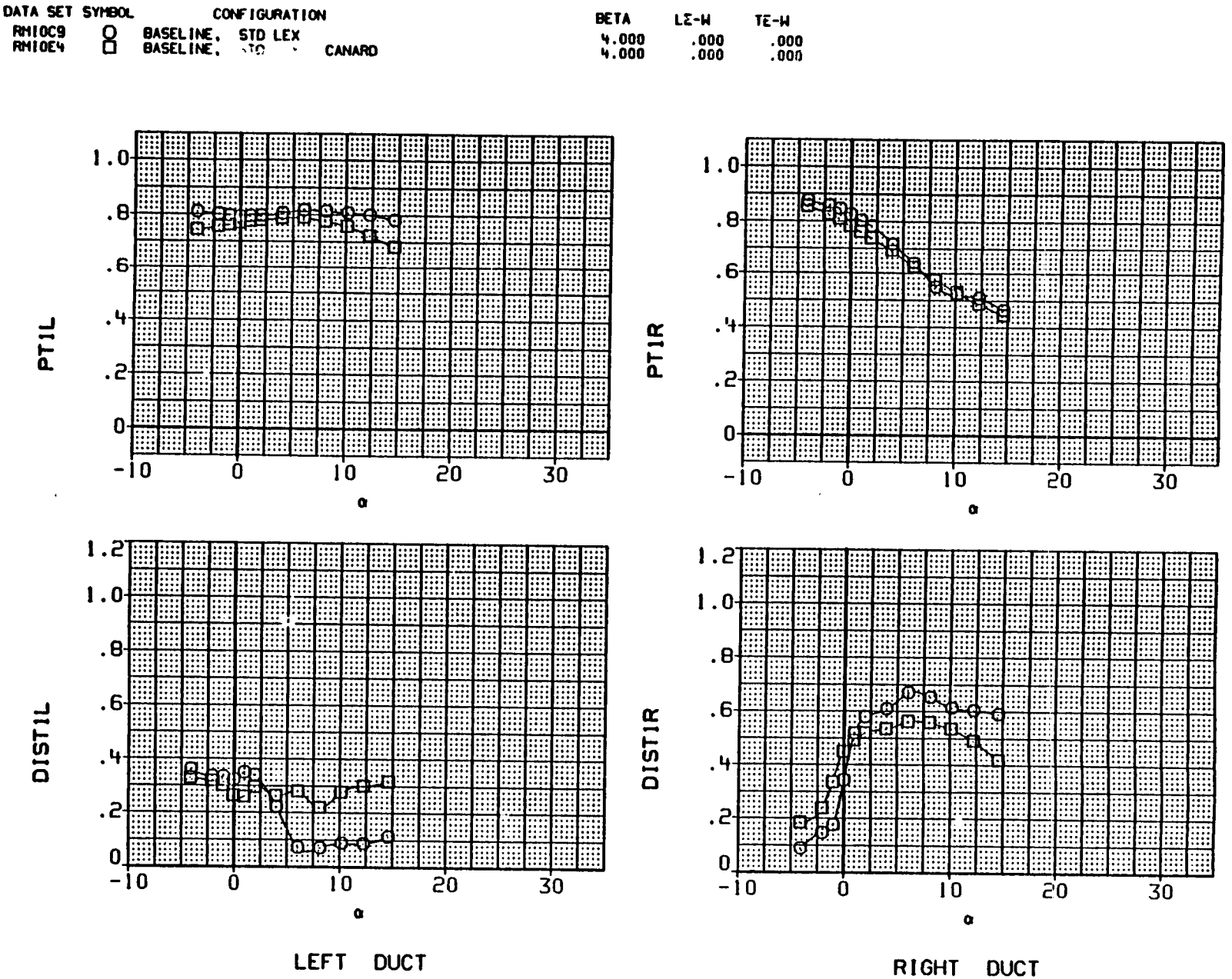

(p) Mach = 2.00.

Figure 13.- Continued.

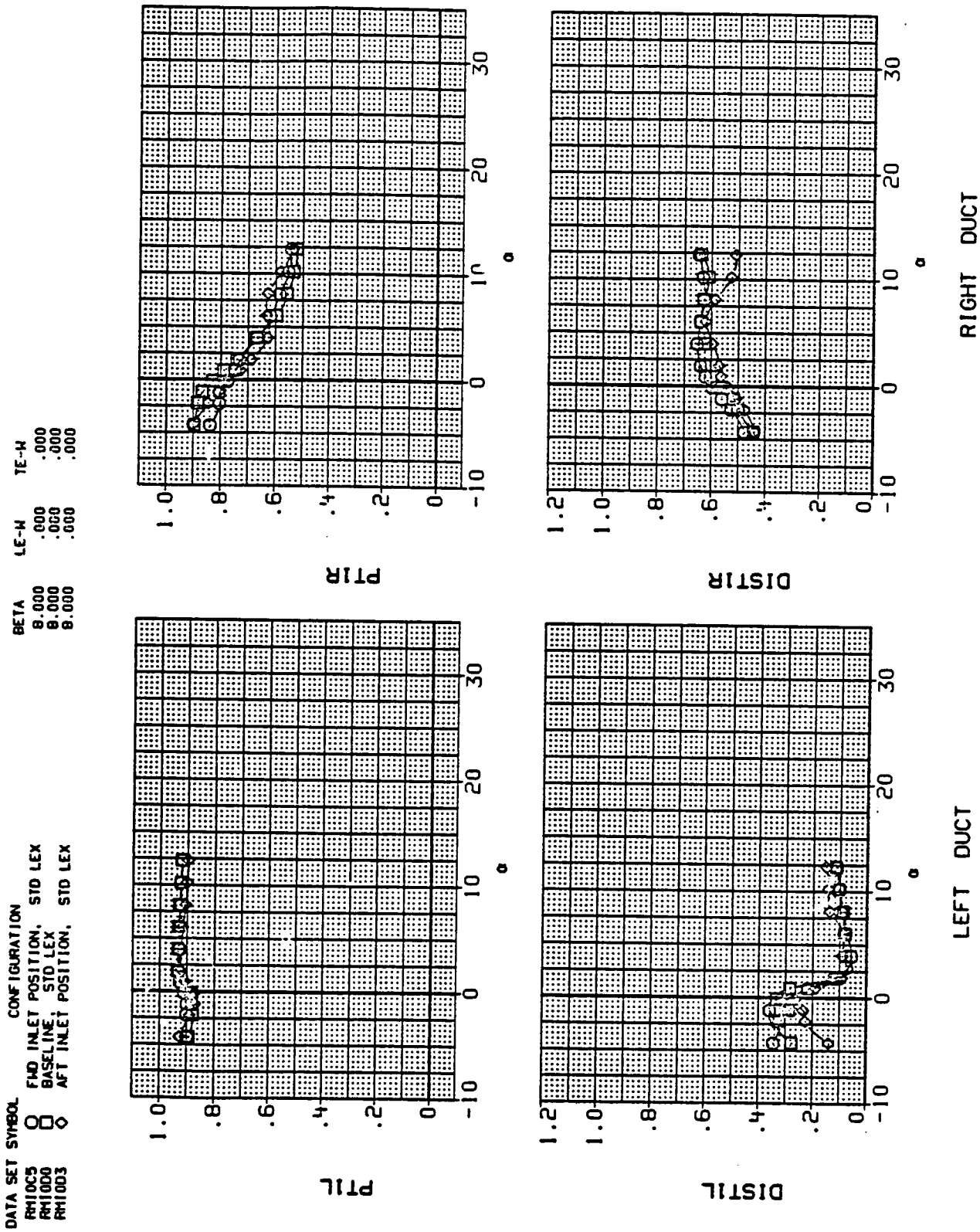

(q) Mach = 1.60.

Figure 13.- Continued.

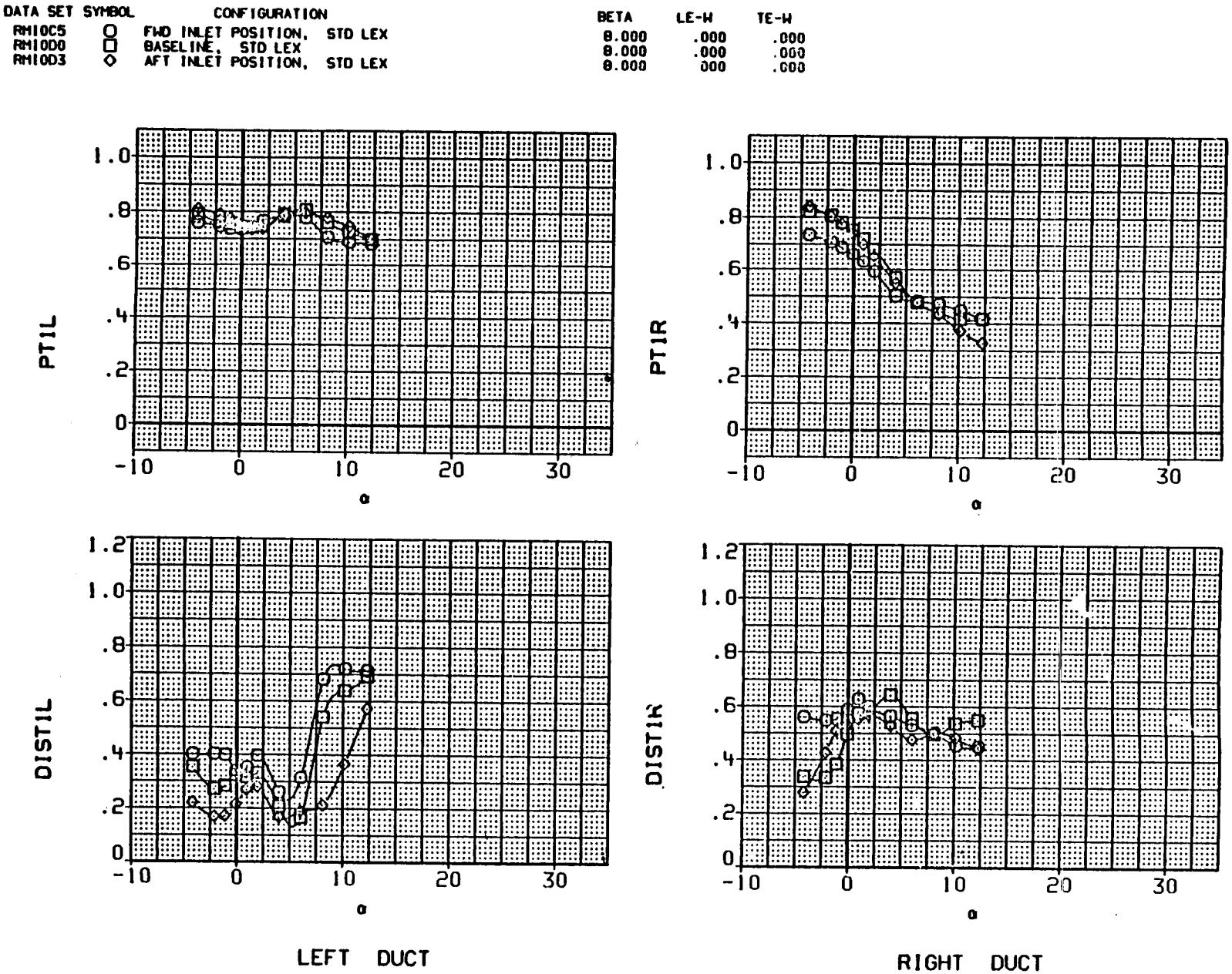

(r) Mach = 2.00.

Figure 13.- Continued.

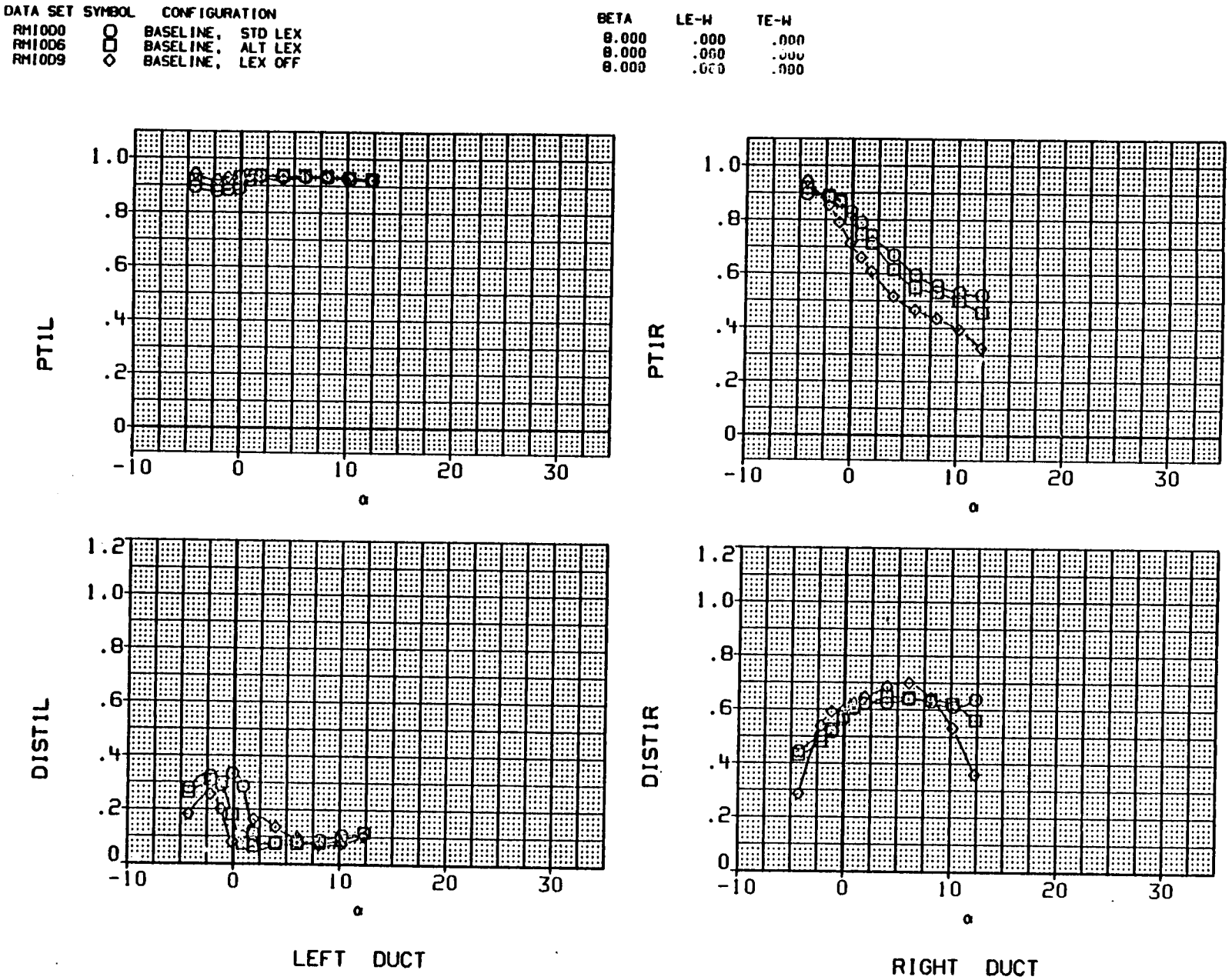

(s) Mach = 1.60.

Figure 13.- Continued.

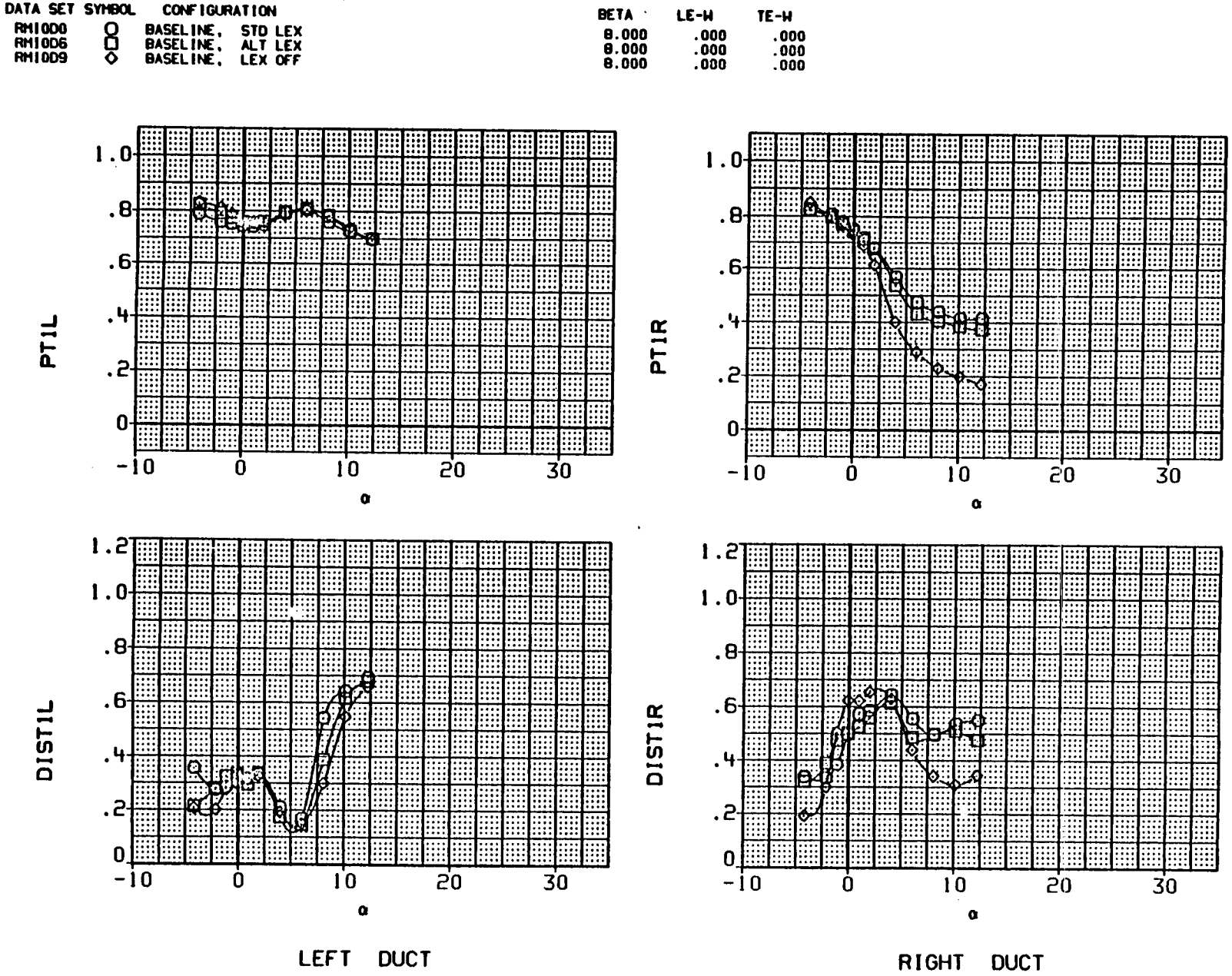

(t) Mach = 2.00.

Figure 13.- Continued.

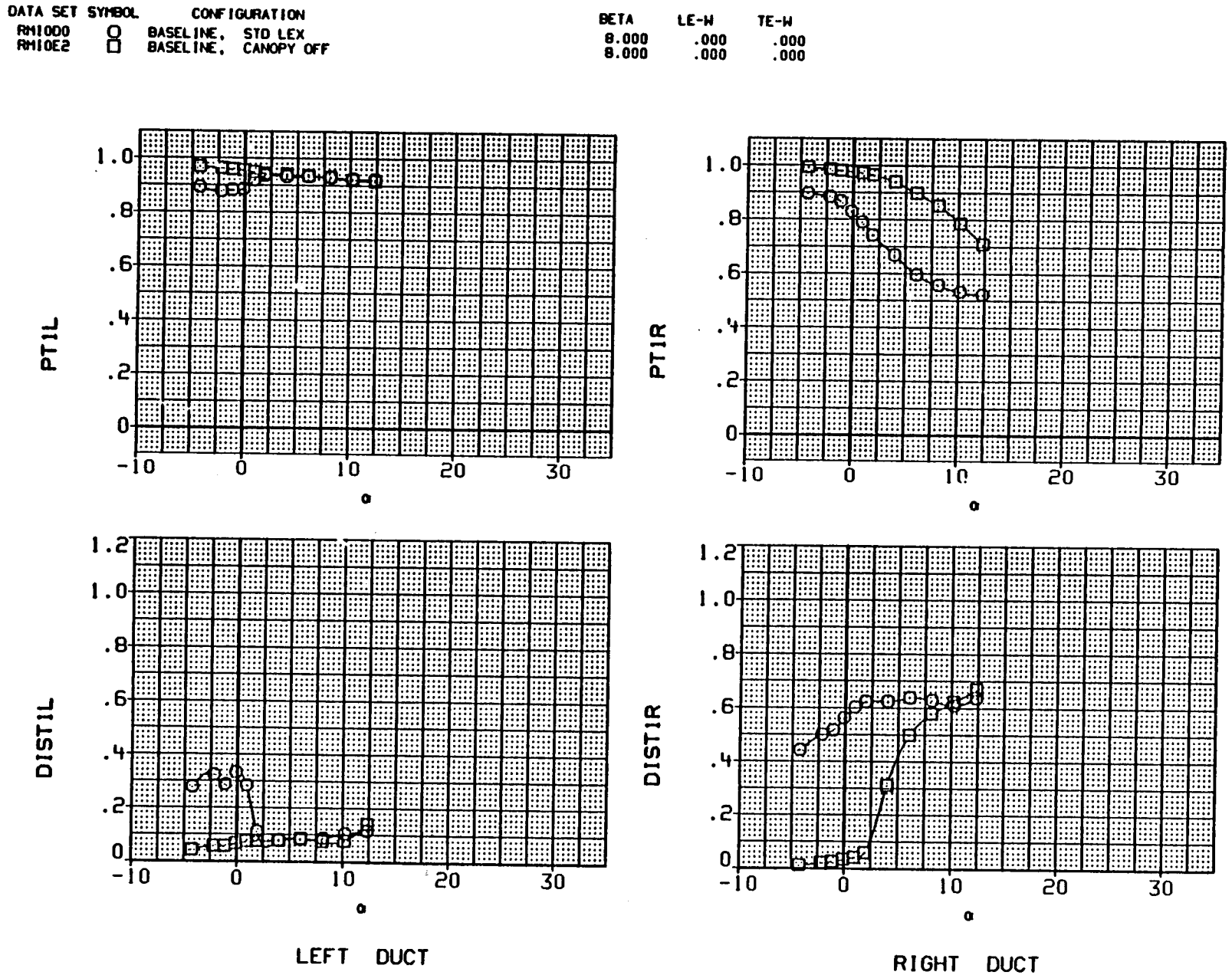

(u) Mach = 1.60.

Figure 13.- Continued.

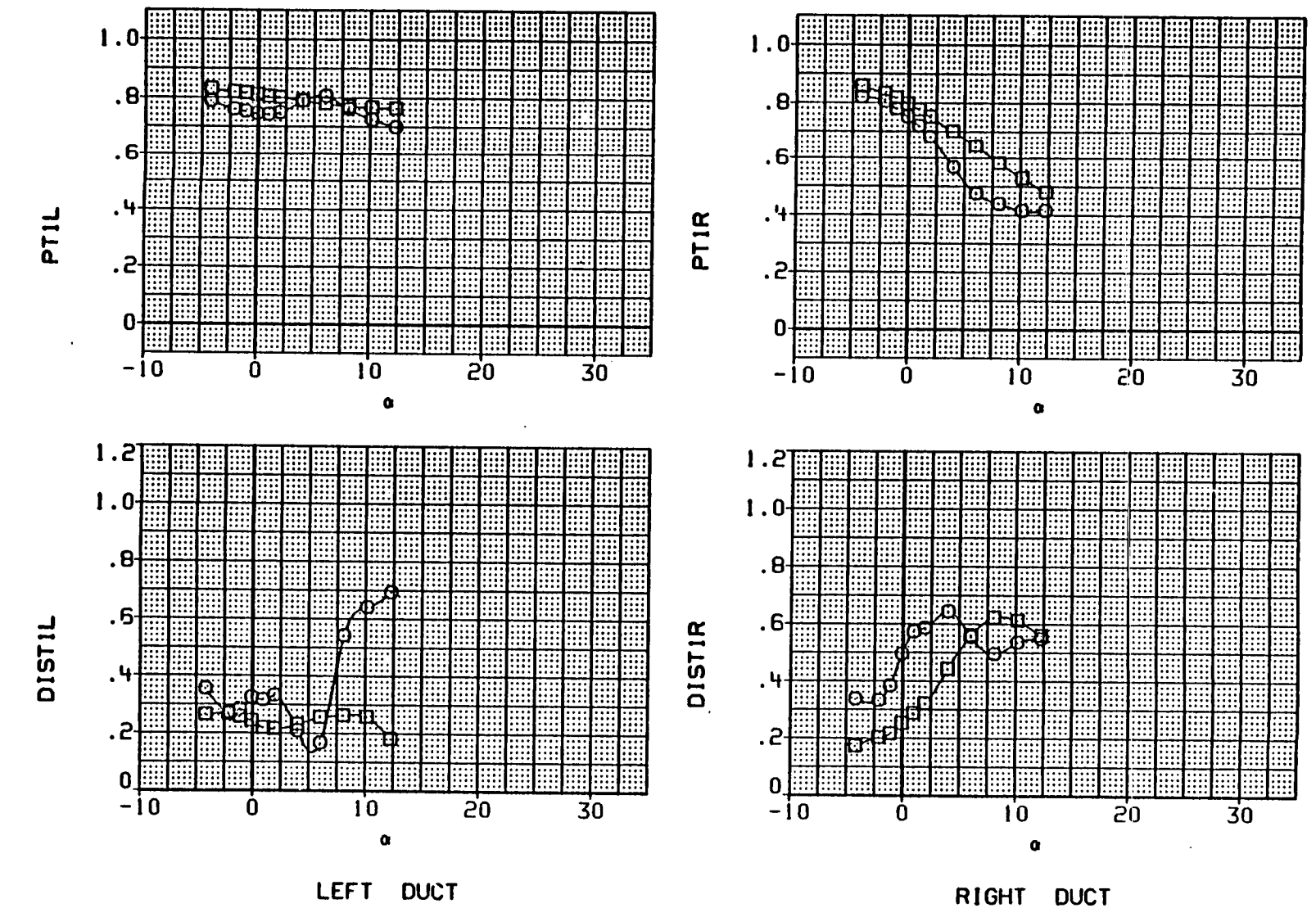

(v) Mach = 2.00.

Figure 13.- Continued.

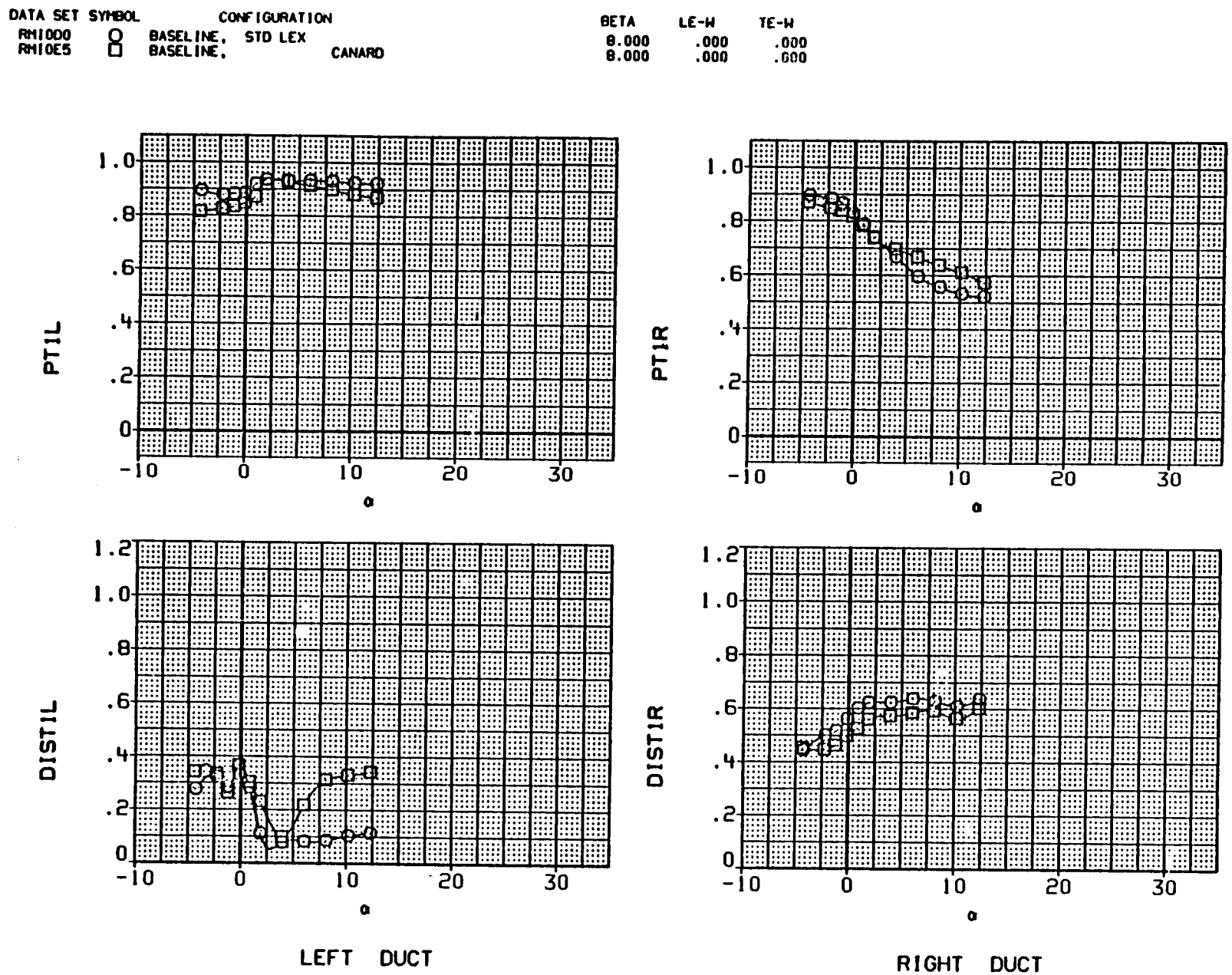

(w) Mach = 1.60.

Figure 13.- Continued.

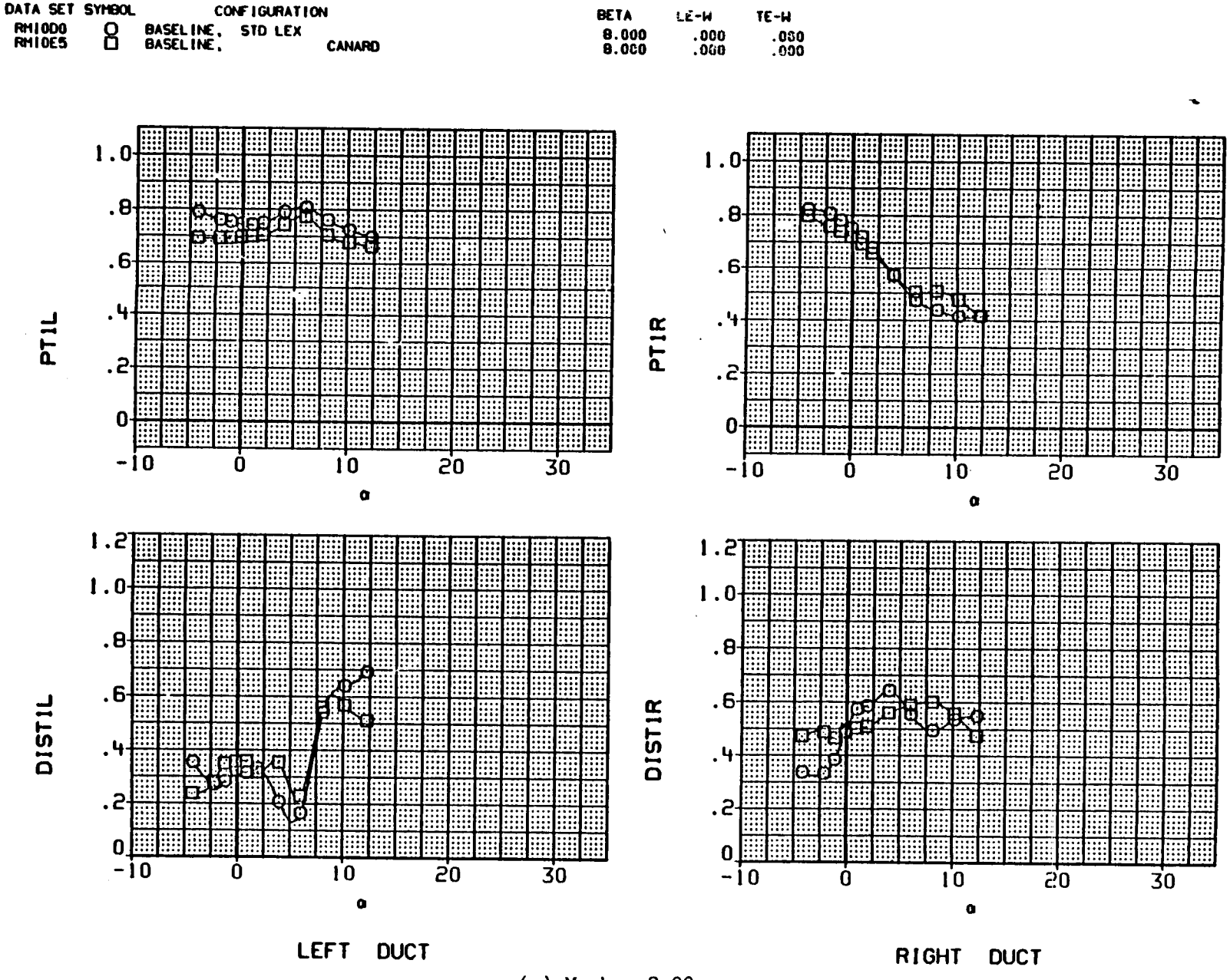

(x) Mach = 2.00.

Figure 13.- Concluded.

1. Report No.	2. Government Accession No.	3. Recipient's Catalog No.
NASA TM-88210		

4. Title and Subtitle	5. Report Date
TOP-MOUNTED INLET PERFORMANCE FOR A V/STOL FIGHTER/ATTACK AIRCRAFT CONFIGURATION	January 1987
	6. Performing Organization Code
7. Author(s)	8. Performing Organization Report No.
Donald B. Smeltzer	A-86110
	10. Work Unit No.
9. Performing Organization Name and Address	
Ames Research Center Moffett Field, CA 94035	11. Contract or Grant No.
	13. Type of Report and Period Covered
12. Sponsoring Agency Name and Address	Technical Memorandum
National Aeronautics and Space Administration Washington, DC 20546	14. Sponsoring Agency Code 505-43-01

15. Supplementary Notes

Point of Contact: Donald B. Smeltzer, Ames Research Center, M/S 227-6
Moffett Field, CA 94035 (415) 694-5858 or FTS 464-5858

16. Abstract

Inlet flow-field and compressor-face performance data were obtained for a 0.095-scale model of vertical/short take-off and landing (V/STOL) fighter/attack aircraft configuration with twin top-mounted inlets. Tests were conducted at Mach numbers from 0.6 to 2.0 and at angles of attack and sideslip up to 27° and 12°, respectively. Reynolds number was held constant at 9.8×10^6 per meter. The effects of inlet location, wing leading-edge extension (LEX) planform area, canopy-dorsal integration, variable incidence canards, and wing leading- and trailing-edge flap deflections were determined. The results show that at Mach numbers up to 0.9, distortion is relatively low (20% or less) at all angles of attack and sideslip. However, at Mach numbers of 1.2 and above, operation may be restricted because of either high distortion or low pressure recovery (80% or less), or both. These difficulties may be overcome with alterations to the LEX/canopy/body juncture.

17. Key Words (Suggested by Author(s))	18. Distribution Statement
Inlets Vertical/short take-off and landing (V/STOL)	Unclassified-Unlimited Subject Category - 02

19. Security Classif. (of this report)	20. Security Classif. (of this page)	21. No. of Pages	22. Price*
Unclassified	Unclassified	213	A10

*For sale by the National Technical Information Service, Springfield, Virginia 22161